

Doctoral Dissertation (Shinshu University)

**STUDY ON LINEAR SYNCHRONOUS  
MOTOR DESIGN FOR OIL PALM CUTTER**

March 2015

Fairul Azhar bin Abdul Shukor



---

## Table of Contents

Table of Contents .....	i
List of Figures .....	iii
List of Tables .....	vi
List of Abbreviations .....	vii
<b>Chapter 1: Introduction .....</b>	<b>1</b>
1.1 Problem Statement.....	4
1.2 Objective.....	5
1.3 Scope of Study .....	5
1.4 Thesis Layout.....	7
1.5 References of Chapter 1 .....	8
<b>Chapter 2: Basic Concept of E-Cutter's Actuator.....</b>	<b>11</b>
2.1 Mechanization of Oil Palm Harvesting Tool.....	11
2.2 Basic Concept and Current Status of the E-Cutter Development .....	13
2.3 Introduction to the Linear Motor .....	17
2.3.1 Switched Reluctance Linear Synchronous Motor .....	19
2.3.2 Permanent Magnet Linear Synchronous Motor .....	20
2.4 Design Target and Restriction of the E-Cutter's Actuator .....	21
2.5 Performance Index of the E-Cutter's Actuator .....	22
2.6 Introduction to Finite Element Method .....	25
2.7 References of Chapter 2.....	29
<b>Chapter 3: Design and Development of the Switched Reluctance Cylindrical Linear Synchronous Motor (SRCLSM).....</b>	<b>35</b>
3.1 Initial Structure Parameter of the SRCLSM .....	35
3.2 Effect of air gap's length and teeth pitch to the SRCLSM thrust .....	41
3.3 Estimation and comparison of the SRCLSM six phase performance .....	46
3.4 Manufactured of the SRCLSM .....	51
3.5 Static Characteristics Measurement of the SRCLSM.....	52
3.5.1 Static Thrust Characteristic.....	52
3.5.2 <i>RL</i> Characteristic .....	59
3.5.3 Electrical Time Constant Characteristic .....	65
3.5.4 Effect of Manufacturing Tolerance to Static Thrust Characteristic.....	67
3.6 Feasibility of the SRCLSM Implement as E-Cutter's Actuator .....	75
3.7 Summary.....	76
3.8 References of Chapter 3.....	76

---

<b>Chapter 4: Design and Development of the Permanent Magnet Cylindrical Linear Synchronous Motor .....</b>	<b>79</b>
4.1 Basic Structure Parameter of the PMCLSM.....	79
4.2 Design of the Structure Parameter of the PMCLSM.....	86
4.2.1 Effect of coil height and permanent magnet radius to the PMCLSM performance.....	87
4.2.2 Effect of permanent magnet height and shaft radius to the PMCLSM performance.....	91
4.2.3 Comparison of the PMCLSM performance with commercialize linear motor.....	95
4.3 Manufactured of the PMCLSM.....	96
4.4 Static Characteristics Performance of the PMCLSM.....	98
4.4.1 Static Thrust Characteristic.....	99
4.4.2 <i>RL</i> Characteristic.....	108
4.4.3 Electrical Time Constant Characteristic.....	113
4.5 Feasibility of the PMCLSM Implement as E-Cutter’s Actuator.....	116
4.6 Summary.....	116
4.7 References of Chapter 4.....	117
<b>Chapter 5: Conclusions and Recommendation for Future Work.....</b>	<b>121</b>
5.1 Conclusions.....	121
5.2 Recommendation for Future Work.....	123
<b>Appendices .....</b>	<b>125</b>
Appendix A List of publications.....	125
Appendix B Reprint of publications.....	127

---

## List of Figures

Figure		Page
<b><u>Chapter 1</u></b>		
Figure 1.1	Type of end product of palm oil.	2
<b><u>Chapter 2</u></b>		
Figure 2.1	<i>Cantas</i> <sup>TM</sup> structure.	12
Figure 2.2	E-Cutter structure.	14
Figure 2.3	Structure and construction of 1PhSTLOA.	16
Figure 2.4	Cutting evaluation of 1PhSTLOA.	16
Figure 2.5	Cross sectional view of oil palm frond.	21
Figure 2.6	Comparison of performance index between difference types of commercialized PMLM.	25
Figure 2.7	Design step of E-Cutter's actuator using FEM.	28
Figure 2.8	E-Cutter's actuator model.	28
Figure 2.9	E-Cutter's actuator mesh.	28
Figure 2.10	Magnetic flux density of the E-Cutter's actuator.	29
Figure 2.11	Flux lines of the E-Cutter's actuator.	29
<b><u>Chapter 3</u></b>		
Figure 3.1	Outline structure of the six phase SRCLSM (unit:mm).	36
Figure 3.2	6 phase structure topology.	36
Figure 3.3	6 phase thrust characteristic.	37
Figure 3.4	Comparison of single and double coil structure (unit:mm).	38
Figure 3.5	Comparison of thrust characteristics between single and double coil structure.	39
Figure 3.6	Teeth parameter of the SRCLSM.	39
Figure 3.7	Performance comparison of the SRCLSM with different teeth width, $t_w$ .	40
Figure 3.8	Initial structure parameter of the six phase SRCLSM (unit : mm).	40
Figure 3.9	Single phase SRCLSM with different teeth pitch, $\tau_p$ (unit : mm).	41
Figure 3.10	Comparison between material's <b>BH</b> curve.	42
Figure 3.11	Sample of single phase thrust characteristic of the SRCLSM.	43
Figure 3.12	Maximum thrust, $F_{max}$ of the SRCLSM.	45
Figure 3.13	Maximum thrust of all the SRCLSM models at $I = 0.7$ A.	46
Figure 3.14	Connection of the SRCLSM coils.	47
Figure 3.15	Pulse excitation sequence.	48
Figure 3.16	Single, three and six phase thrust characteristics of the SRCLSM.	49

Figure 3.17	Performance comparison of the SRCLSM with optimized teeth pitch, $\tau_p$ and difference air gap length, $\delta$ .	50
Figure 3.18	Performance comparison of the SRCLSM and commercialize PMLM.	51
Figure 3.19	Manufactured single phase SRCLSM.	52
Figure 3.20	Experiment setup for the thrust characteristic measurement of the single phase SRCLSM.	53
Figure 3.21	Schematic diagram for the thrust characteristic measurement of the single phase SRCLSM.	53
Figure 3.22	Thrust characteristic of the SRCLSM at current, $I = 0.7$ A.	54
Figure 3.23	Friction force of the SRCLSM at current, $I = 0.7$ A.	55
Figure 3.24	Comparison of thrust characteristic between simulation, measurement and mover type.	56
Figure 3.25	Effect of current, $I$ to maximum thrust, $F_{max}$ .	57
Figure 3.26	Thrust difference, $F_D$ of the SRCLSM	58
Figure 3.27	Friction force, $F_C$ of the SRCLSM at several current, $I$ .	59
Figure 3.28	Experiment setup for $RL$ characteristic measurement.	60
Figure 3.29	Schematic diagram for $RL$ characteristic measurement.	60
Figure 3.30	$RL$ characteristic of the SRCLSM .	63
Figure 3.31	$RL$ profile of the SRCLSM at several frequency, $f$ .	64
Figure 3.32	Electrical time constant, $\tau_e$ characteristic of the SRCLSM.	66
Figure 3.33	Electrical time constant, $\tau_e$ profile of the SRCLSM at several frequency, $f$ .	67
Figure 3.34	The SRCLSM structure with consideration of the manufacturing tolerance, $\Delta x$ .	69
Figure 3.35	The SRCLSM's model on several manufacturing tolerance, $\Delta x$ .	70
Figure 3.36	The SRCLSM's static thrust characteristics on several manufacturing tolerance, $\Delta x$ and current, $I = 0.5$ A.	71
Figure 3.37	Effect of manufacturing tolerance, $\Delta x$ to the maximum thrust, $F_{max}$ .	72
Figure 3.38	Thrust error, $\varepsilon_F$ by consideration of manufacturing tolerance, $\Delta x$ .	74

#### **Chapter 4**

Figure 4.1	Skeleton of 6 slot 8 pole PMCLSM.	80
Figure 4.2	Permanent magnet magnetization arrangement and pitch of magnetization, $\tau_{pm}$ .	81
Figure 4.3	Sample of dynamic thrust characteristics of the PMCLSM.	82
Figure 4.4	Performance comparison of the PMCLSM between difference stator types and magnetization direction arrangements.	84

---

Figure 4.5	Basic structure and structure parameter of the 6 slot 8 pole slot type PMCLSM.	88
Figure 4.6	Design procedure of first stage of PMCLSM design.	88
Figure 4.7	Average thrust $F_{ave}$ and total weight, $W_{tot}$ of the PMCLSM.	90
Figure 4.8	Structure parameters of the PMCLSM result from first stage of design (unit : mm).	91
Figure 4.9	Design procedure of second stage of design.	92
Figure 4.10	Effect of shaft radius, $r_s$ to average thrust, $F_{ave}$ of the PMCLSM.	93
Figure 4.11	Final structure parameter of the PMCLSM (unit : mm).	93
Figure 4.12	Effect of current to thrust of the PMCLSM.	94
Figure 4.13	Comparison between the PMCLSM and commercialized permanent magnet linear motor (PMLM) performance characteristics.	96
Figure 4.14	Manufactured PMCLSM.	98
Figure 4.15	Experiment setup for static thrust characteristic measurement.	100
Figure 4.16	Schematic diagram for static thrust characteristic measurement.	100
Figure 4.17	Sample of thrust and friction force of the PMCLSM.	101
Figure 4.18	Cogging force characteristic of the PMCLSM.	101
Figure 4.19	Thrust characteristic of the U phase.	104
Figure 4.20	Thrust characteristic of the V phase.	105
Figure 4.21	Thrust characteristic of the W phase.	106
Figure 4.22	Comparison of maximum and minimum thrust, $F_{max}$ and $F_{min}$ between measured and simulated result and measurement error, $\varepsilon$ .	107
Figure 4.23	Experiment setup for the $RL$ characteristic measurement.	110
Figure 4.24	Schematic diagram for the $RL$ characteristic measurement.	110
Figure 4.25	$RL$ profile characteristic of the PMCLSM for each phase at several frequencies.	111
Figure 4.26	$RL$ characteristic of the PMCLSM on each phase.	112
Figure 4.27	Electrical time constant, $\tau_e$ characteristic of the PMCLSM on each phase.	115

---

## List of Tables

Table		Page
<b><u>Chapter 2</u></b>		
Table 2.1	The 1PhSTLOA performance characteristics.	16
Table 2.2	Advantages and disadvantages of LIM and LSM.	19
<b><u>Chapter 3</u></b>		
Table 3.1	Simulation setting for SRCLSM.	38
Table 3.2	Coil settings for the SRCLSM.	41
Table 3.3	Mechanical properties comparison between SS400 and S45C materials.	42
Table 3.4	First and second order of maximum thrust, $F_{\max}$ for each air gap length, $\delta$ and corresponding teeth pitch, $\tau_p$ .	44
Table 3.5	Measurement setting for $RL$ characteristic.	61
Table 3.6	Summary of the SRCLSM design and develop results.	76
<b><u>Chapter 4</u></b>		
Table 4.1	The PMCLSM structure parameters.	81
Table 4.2	List of performance characteristics and it's equation.	83
Table 4.3	Comparison of best two model of slot-less and slot type PMCLSM.	86
Table 4.4	Highest average thrust, $F_{\text{ave}}$ model and its total weight, $W_{\text{tot}}$ on each $r_{\text{total}}$ .	91
Table 4.5	Specifications of the PMCLSM.	97
Table 4.6	Resistance, $R$ and inductance, $L$ at $f = 70$ Hz.	109
Table 4.7	The electrical time constant, $\tau_e$ at $f = 70$ Hz.	114
Table 4.8	Summary of the PMCLSM design and develop results.	117

---

## List of Abbreviations

### Abbreviations

1PhSTLOA	Single phase slot type linear oscillatory actuator
FEM	Finite Element Method
LIM	Linear induction motor
LSM	Linear synchronous motor
LSTM	Linear stepper motor
PMCLSM	Permanent magnet cylindrical linear synchronous motor
PMLM	Permanent magnet linear motor
PAM	Permeance analysis method
SRCLSM	Switched reluctance cylindrical linear synchronous motor
SRLSM	Switched reluctance linear synchronous motor

### Symbols

$a$	Copper wire cross sectional area	(m <sup>2</sup> )
$A_{DB}$	Gain	(dB)
$A$	Gain	
$\bar{B}$	Magnetic flux density	(T)
$\delta$	Air gap length	(m)
$\Delta F$	Thrust ripple	(%)
$\Delta x$	Manufacturing tolerance	( $\mu$ m)
$ \Delta x $	Absolute manufacturing tolerance	( $\mu$ m)
$E$	Young Modulus	(GPa)
$\bar{E}$	Electric field	(V)
$\varepsilon_F$	Thrust error	(%)
$f$	Frequency	(Hz)
$f_{osc}$	Oscillation frequency	(Hz)
$F$	Thrust	(N)
$F_{ave}$	Average thrust	(N)
$F_C$	Friction force	(N)
$F_{fwd}$	Forward direction force	(N)
$F_{rev}$	Reverse direction force	(N)
$F_{cog}$	Cogging force	(N)
$F_{annealing}$	Thrust of the SRCLSM with annealing mover	(N)
$F_{unannealing}$	Thrust of the SRCLSM with unannealing mover	(N)
$F_D$	Thrust difference	(%)
$F_{cutting}$	Cutting force	(N)
$F_{max}$	Maximum thrust	(N)
$F_{measured}$	Measured thrust	(N)

---

$F_{\text{simulated}}$	Simulated thrust	(N)
$F_{x=0}$	Starting thrust	(N)
$\theta_H$	Phase difference of two phase	( $^{\circ}$ )
$\xi$	Space factor equal to 0.6	
$G$	Motor constant square density	( $\text{N}^2/\text{Wm}^3$ )
$\overline{H}$	Magnetic field intensity	(kA/m)
$h_c$	Height of coil	(m)
$h_{\text{pm}}$	Height of permanent magnet	(m)
$I$	Current	(A)
$I_p$	Peak current	(A)
$I_{\phi}$	Phase current	(A)
Re {I}	Real parts of current expression	(A)
Im {I}	Imaginary parts of current expression	(A)
$i(t)$	Function current in time domain	(A)
$\overline{J}$	Current density	( $\text{A}/\text{m}^3$ )
$k_f$	Thrust constant	(N/A)
$k_m$	Motor constant	( $\text{N}/\sqrt{\text{W}}$ )
$l$	Copper wire length	(m)
$l_y$	Length of stator	(m)
$L$	Coil inductance	(H)
$L_{\text{max}}$	Maximum inductance	(H)
$L_{\text{min}}$	Minimum inductance	(H)
$m$	Mover's mass	(kg)
$N$	Coil turns	
$P_{\text{in}}$	Input power	(W)
$P_T$	Power consumption	(W)
$\phi$	Phase different	( $^{\circ}$ )
$\phi_C$	Copper wire diameter	(m)
$r_{\text{pm}}$	Radius of permanent magnet	(m)
$r_s$	Shaft radius	(m)
$r_{\text{total}}$	Total radius	(m)
$R$	Coil resistance	( $\Omega$ )
$R_S$	Standard resistance	( $\Omega$ )
$R_{\text{max}}$	Maximum resistance	( $\Omega$ )
$R_{\text{min}}$	Minimum resistance	( $\Omega$ )
$\rho_{\text{material}}$	Material density	( $\text{kg}/\text{m}^3$ )
$t_s$	Slot width	(m)
$t_w$	Teeth width	(m)
$t_y$	Yoke thickness	(m)
$THD_F$	Total harmonic distortion of thrust	(%)
$\sigma_t$	Tensile Strength	(MPa)
$\sigma_y$	Yield Strength	(MPa)

---

---

$\tau_c$	Coil pitch	(m)
$\tau_e$	Electrical time constant	(s)
$\tau_{e,max}$	Maximum electrical time constant	(s)
$\tau_{e,min}$	Minimum electrical time constant	(s)
$\tau_m$	Mechanical time constant	(s)
$\tau_p$	Teeth pitch	(m)
$\tau_{pm}$	Magnetic pole pitch	(m)
$v_m$	Mover speed	(m/s)
$V$	Volume	(m <sup>3</sup> )
$\nu$	Poisson ratio	
$v(t)$	Function of voltage in time domain	(V)
$V_{part}$	Volume of linear motor part	(m <sup>3</sup> )
$V_{mot}$	Motor volume	(m <sup>3</sup> )
$\text{Re}\{V\}$	Real parts of voltage expression	(V)
$\text{Im}\{V\}$	Imaginary parts of voltage expression	(V)
$W_{coil}, W_{pm}$ and $W_{yoke}$	Weight of the linear motor particular parts	(kg)
$W_c$	Coil width	(m)
$W_{tot}$	Total weight	(kg)
$\omega$	Angular Frequency	(rad/s)
$x$	Displacement	(m)
$x_T$	Total displacement	(m)
$+x$	Most positive displacement	(m)
$-x$	Most negative displacement	(m)



---

## Chapter 1: Introduction

Agricultural activity could be described as the science, art and business of cultivating soil, producing crops and raising livestock <sup>(1.1)</sup>. Even though agriculture activity is seen as uninteresting, low income and productivity of economic activity, but the contribution from this activity cannot be neglected especially in matters concerning food security. For example, in China, having only 7% of the world's total cultivated farmland, could support about 20% of the world's population's needs <sup>(1.2)</sup>. Moreover, agricultural sectors are also playing a role as a major economic contributor in several countries. In South Africa for instance, agricultural sectors provided 60% of employment opportunities and generated 27% of gross national product (GDP) in 2001 <sup>(1.3)</sup>. That same year, about 80% of Nepal's people were involved in agricultural economic activities yet contributed to about 40% of its GDP <sup>(1.4), (1.5)</sup>. For Nigeria, contribution of agricultural against its GDP has been shown increment pattern from about 51 % on 1970 to about 65 % on 2010 <sup>(1.6)</sup>. Even for USA, at New York State alone, agricultural contribute about USD 53,719 million to economic output with about 206,604 on employment contributions <sup>(1.7)</sup>.

Oil palm is the world's most fruit crop in the agricultural sector. It is caused by its unparalleled productivity and most productive oil plant in the world. The oil palm or its scientific name known as *Elaeis guineensis* is a tree without branches but with many wide leaves on its top or called as tree crown. The fruits are compactly packed in bunches which are hidden in the leaf axils in crowns <sup>(1.8)</sup>. The oil palm could live up to 30 years and could reaches height of 15 meters with a stem diameter about 45 cm <sup>(1.9)</sup>.

The palm oil could be found in numerous end products either in edible based and non-edible based product <sup>(1.10)</sup>. Figure 1.1 shows the product that could be derived from the palm oil <sup>(1.1), (1.10)</sup>. Despite of non-edible based product, the production of palm oil is most focus in edible product such as cooking oil and margarine <sup>(1.10)</sup>. Although ranked fourth in decades ago, awareness of the negative effects of Trans Fat on human health has caused palm oil becomes the most consumed vegetable oil in the world <sup>(1.8)</sup>. Conjunction with that, the production of palm oil is

expected to increase 3.47%/ year to support this demand. It will be estimated, in 2015, palm oil is set to become the most produced oil with total production of 37.41 million tonnes, surpassing soya bean oil <sup>(1.10)</sup>.

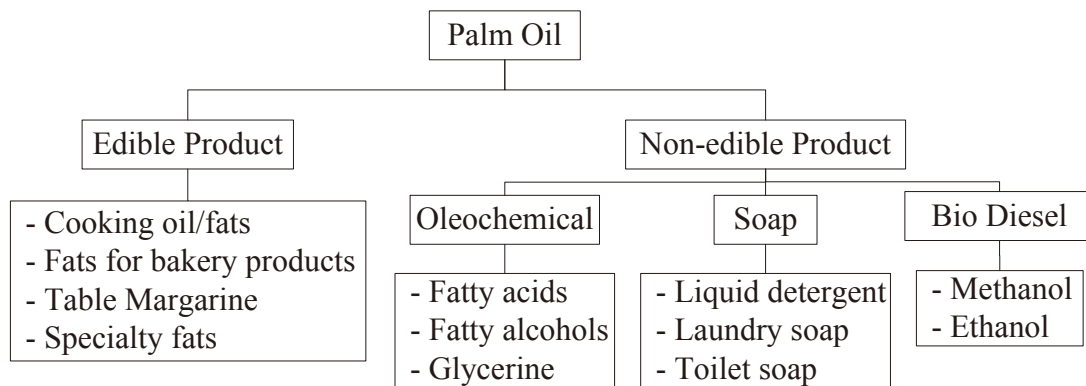


Figure 1.1 Type of end product of palm oil.

In order to support palm oil's demand, its productivity needs to be improved. There are several ways has been suggested to be implemented to increase the productivity of the agricultural product such as increase the labour productivity through improved service extension, reintroduction of the fertilizer, improved seed and enhance agricultural mechanization <sup>(1.11)</sup>. Therefore, in this research, improvement of the oil palm productivity through mechanization is focused.

Agricultural mechanization could be defined as an economic application of engineering technology to enhance the effectiveness and productivity of human labour <sup>(1.12)</sup>. The main objective of agricultural mechanization is reduce human drudgery, improve timeliness of operation, increase cultivation rate of an area of land and improve economy and standard of living of farmers through increased productivity <sup>(1.13)</sup>.

Mechanization has proven to enhance the agricultural activities and ensure sustainable agricultural production <sup>(1.14)</sup>. For example in the USA, farm mechanization allowed one farmer to feed from 5 people in 1880 to 80 people in 1982 <sup>(1.15)</sup>. In India, farm mechanization started in the 1970s. It shows that land productivity has increased drastically since the introduction of farm mechanization as a mechanical power source in India from about 0.80 kg/ha to 1.45 kg/ha <sup>(1.16)</sup>.

Agricultural mechanization also aims to reduce human energy along the cultivated activity. Nkakini *et al* (2006), has reported comparison of the energy used

---

to produce the same amount of cassava both manually and machine assisted. Based on the result, machine assisted operations have 83 times lower energy consumption compared to the manual operation of the same quantity of product <sup>(1.17)</sup>. On the other hand, in China, mechanization has become the latest economical source for the nation <sup>(1.2)</sup>.

Agricultural mechanization has been put in place during processing raw material to final product, land preparation, weeding, harvesting, pest control, irrigation and drainage, transportation and storage. The process cycle of oil palm based product starts with cultivation and harvesting activity <sup>(1.18)</sup>. Cultivation and harvesting involve seeding, fertilizing, weeding, cutting fronds and fruit bunches, collecting and transporting the fruit bunches to an industrial site for end product processing. Mechanization has considerable help to reduce the human effort to accomplish these activities. It also proven could improve the productivity of the palm oil production. For example, in weeding activities, through the mechanization has increased the ratio of labour to land hectare from 1 : 25 to 1 : 50. On the other hand, mechanization in fresh fruit bunch (FFB) collection has increased the earnings of the oil palm plantation company from about USD 4.96 per day to USD 14.52 per day <sup>(1.13)</sup>. Current technology has made further activity along the oil palm cultivation has been mechanized. WIW. Ismail *et al.*, 2000 & 2009 report regarding the vision system for prediction of fruit ripening development. It helps the harvester to harvest only the ripe fruit for palm oil quality guaranteed. However, the result of actual implementation of this technology has yet to be discovered. MS. Deraman *et al.*, 2007 discussed about the roller-type oil palm loose fruit picker development. It eases the harvester to pick loose fruit compares to before the introductory of this tools, the loose fruit was by hand collected.

In this research, mechanization of oil palm FFB harvesting tools was discussed. In Malaysia, efforts to develop mechanize oil palm FFB harvesting tools was initiated by the Malaysian Palm Oil Board (MPOB). The MPOB has introduced a mechanical based cutter known as *Cantas*<sup>TM</sup> <sup>(1.22) - (1.24)</sup>. The *Cantas*<sup>TM</sup> has demonstrated its capability to improve the oil palm FFB harvesting productivity through several fields testing sessions. It is found that, the *Cantas*<sup>TM</sup> could increase the oil palm FFB harvesting productivity more than twice compared to traditional technique. Despite of

---

it merits, due to weight of the top side of the *Cantas*<sup>TM</sup> made it become less efficient to harvest oil palm FFB located more than 8 meters in height <sup>(1.25)</sup>. At this height, the pole of *Cantas*<sup>TM</sup> starts to bends and made the mechanical system inside the *Cantas*<sup>TM</sup> stop working.

Due to the impressive performance of the *Cantas*<sup>TM</sup>, urge a solution needs to be discovered to at least bring the same performance to the higher oil palm. Therefore, an electrical based cutter or called as E-Cutter was introduced <sup>(1.25) - (1.27)</sup>. Through implementation of E-Cutter, the pole bending problem no longer disturb the function of harvesting tools by equipped this tool with flexible features.

## 1.1 Problem Statement

Development of *Cantas*<sup>TM</sup> by the MPOB is seen as a breakthrough to implementation of mechanization to oil palm FFB harvesting activity. Impressive performance has been shown by the *Cantas*<sup>TM</sup> through several field testing especially in term of cost and time performances. However, the operation of *Cantas*<sup>TM</sup> becomes less efficient at height of oil palm higher than 8 meters. At the height of the oil palm higher than 8 meters, the pole bending problem made the mechanical system of the *Cantas*<sup>TM</sup> was stopped and harvesting activity was unfeasible to accomplish.

The pole bending is caused by the weight of the top side of the *Cantas*<sup>TM</sup>. Since this factor could not be neglected, more flexible tools are required <sup>(1.26), (1.27)</sup>. Therefore, instead of mechanical based system employed in *Cantas*<sup>TM</sup>, an electrical based harvesting tool called as E-Cutter has been proposed <sup>(1.25) - (1.27)</sup>. The structure of E-Cutter will be similar as *Cantas*<sup>TM</sup>. An electrical generation system consist of 1.3 hp petrol engine coupled with an electrical generator will be placed on the bottom part of the E-Cutter. At the top side of the E-Cutter, a linear motor attached with a sickle will be placed to perform cutting operation. By using electrical based instead of mechanical based system, the pole bending problem will be no longer influence the operation of the harvesting tool.

In this research, the linear motor for the E-Cutter has been designed. Several prototypes of the linear motor comprise a single phase with slot and slotless stator type structure topology has been designed previously <sup>(1.28) - (1.31)</sup>. Despite of all the

---

linear motors have been designed and developed, the slot stator type linear motor as described in <sup>(1.31)</sup> is considered as the best model for the E-Cutter so far. The structure of the slot type linear motor has been designed in order to maximise its thrust while maintaining its restricted weight. It has thrust at mover displacement,  $x$  of 0 mm,  $F_{x=0}$  of 230 N and total weight,  $W_{tot}$  of 2.0 kg. The slot type of linear motor has been tested in laboratory before it could be confirmed to be implemented for E-Cutter actuator. Based on the testing result, it was confirmed that the thrust required by the E-Cutter has been fulfilled. However, it needs higher cutting time comparing to the *Cantas*<sup>TM</sup>. It only needs about 2 seconds to finish the cutting by using the *Cantas*<sup>TM</sup> compared to about 6 seconds by using E-Cutter with the slot type of linear motor <sup>(1.26)</sup>. Therefore, in this research, focus will be given to design and develop new linear motor to function as actuator for the E-Cutter. The new linear motor should have at least similar thrust,  $F$  and total weight,  $W_{tot}$  however the mover responses need to be improved to reduce cutting time.

## 1.2 Objective

The aim of this research is to develop the linear motor to work as the E-Cutter's actuator. The linear motor should have high thrust characteristic within its restricted weight. Two types of linear motor have been designed and developed which are switched reluctance cylindrical linear synchronous motor (SRCLSM) and permanent magnet cylindrical linear synchronous motor (PMCLSM). As a guide line along the design stage, the design target are listed below :-

1. Thrust,  $F$  :  $> 200$  N
2. Total weight,  $W_{tot}$  :  $\leq 2.0$  kg

## 1.3 Scope of Study

In this research, the E-Cutter's actuator was designed and developed. Furthermore, the aim of this research is to find appropriate linear motor type to be implemented as E-Cutter's actuator. There are two types of linear motor were considered which are switched reluctance cylindrical linear synchronous motor (SRCLSM) and permanent magnet cylindrical linear synchronous motor (PMCLSM).

---

Both types of linear motor were model using SolidWorks 2011 x64 Edition CAD software. Once the models of the linear motor have been established, it's were simulated using JMAG Designer (x64) version 13.0.02I. Each types of linear motor's structure were undergone structure design in order to maximize it performance. Once the appropriate parameters have been obtained, each types of linear motor were manufactured to validate the simulation result.

For the SRCLSM, the design stage start with a specific outline dimension. Three structure parameters have been varied to determine appropriate structure parameters. The structure parameters are air gap length,  $\delta$ , teeth pitch,  $\tau_p$  and ratio between teeth width,  $t_w$  and slot width,  $t_s$ . Each models of the SRCLSM was evaluated using thrust,  $F$ . The SRCLSM was intended to be designed in 6 phase. However, through the design and measurement stage, only single phase structure of the SRCLSM was considered. Based on the single phase performance, the 6 phase performance of the SRCLSM was estimated. Based on the estimated 6 phase performance, implementation feasibility of the SRCLSM to the E-Cutter actuator was observed.

For the PMCLSM, a 6 slot 8 pole structure topology was chose. The permanent magnet pitch,  $\tau_{pm}$ , coil pitch,  $\tau_c$  and air gap length,  $\delta$  were fixed. Three structural parameters have been varied along the structural design. The structural parameters are shaft radius,  $r_s$ , height of permanent magnet,  $h_{pm}$  and height of coil,  $h_c$ . The structural parameters were varied within fixed of total radius,  $r_{total}$ . The total radius,  $r_{total}$  was fixed at 20 mm, 25 mm and 30 mm. A model of the PMCLSM with complies with targeted thrust,  $F$  and total weight,  $W_{tot}$  was observed and chose as the PMCLSM for the E-Cutter's actuator. Based on its performance characteristics, implementation feasibility of the PMCLSM to the E-Cutter's actuator was observed.

The design model of the SRCLSM and PMCLSM were then compared to commercialize permanent magnet linear motor. Three type of commercialize permanent magnet linear motor has been selected which are slot type linear motor, slot less type linear motor and shaft motor. Around 200 models of linear motor have been picked and performances of them were compared to the SRCLSM and PMCLSM performance. Four performance characteristics were used which are thrust,  $F$ , thrust constant,  $k_f$ , motor constant,  $k_m$  and motor constant square density,  $G$ .

---

## 1.4 Thesis Layout

The thesis consists of five chapters. Chapter one gives an overview and discusses the purpose of this study. The motivations of this study are addressed in the problem statement and the objectives of research also listed in this chapter. Chapter two presents the basic concept of E-Cutter's actuator. This chapter start with introduction to the basic concept and operation of *Cantas*<sup>TM</sup> and E-Cutter. On top of that, brief of the *Cantas*<sup>TM</sup>'s performance and it draw back as well as current status of E-Cutter development also were explained. Furthermore, introduction to both linear motor types which are the SRCLSM and the PMCLSM also being covered. The method to determine the design target for the linear motor also was discussed.

Chapter three describe the design and develop the SRCLSM. This chapter start with initial consideration of SRCLSM structure topology. After that, the structure of the SRCLSM was finalized by considering several parameters such as air gap length,  $\delta$ , teeth pitch,  $\tau_p$  and teeth width,  $t_w$ . The SRCLSM has been manufactured based on its final structure parameters. The performance characteristics of the SRCLSM were then measured and decision on feasibility to implement the SRCLSM as E-Cutter actuator was decided.

Chapter four covers the design and develop the PMCLSM. The design stage was started from selection of 6 slot 8 pole permanent magnet linear motor structure topology. The stator of the PMCLSM was set to slot type and slotless. Meanwhile several arrangements of permanent magnet magnetization were tested to select the appropriate permanent magnet magnetization direction for the PMCLSM's mover. In this chapter as well, measurement result of the PMCLSM characteristics was covered. The decision on feasibility to implement the PMCLSM as E-Cutter actuator also decided. Chapter Five presents a conclusion of the overall study and recommendations for future work.

---

## 1.5 References of Chapter 1

- (1.1) R. Ghazali, M. Yusof and S. Ahmad, Non-Food Applications of Palm-Based Products – Market Opportunities and Environmental Benefits, *Palm Oil Developments* 44, 8 -12, 2006.
- (1.2) J. Yuan, The Status of China’s Agricultural Machinery Industry and the Prospects for International Cooperation, *Agricultural Engineering International: the CIGR Journal of Scientific Research and Development*. Invited Overview Paper. Vol. 7, ISSN 1682-1130, 2005.
- (1.3) DFID, Better livelihoods for poor people: The role of agriculture, Department for International Development, UK, 2002.
- (1.4) KB. Shrestha, Selected country reports: Nepal, agricultural diversification and international competitiveness, Asian Productivity Organization, 2003.
- (1.5) R. Nepal and B. Gopal Thapa, Determinants of agricultural commercialization and mechanization in the hinterland of a city in Nepal, *Applied Geography* 29, 377–389, 2009.
- (1.6) OT. Olajide, BH. Akinlabi and AA. Tijani, Agriculture resource and economic growth in Nigeria, *European Scientific Journal* October Edition Vol. 8, No.22 ISSN: 1857 – 7881 (Print) e - ISSN 1857- 7431, pp. 103 - 115, 2012.
- (1.7) MS. Todd, The contribution of agriculture to the New York Economy, *Research & Policy Brief Series*, Issue Number 61, August 2014.
- (1.8) DA. Adetan, LO. Adekoya and KA. Oladejo, An Improved Pole-and-Knife Method of Harvesting Oil Palms. *Agricultural Engineering International: CIGR E-Journal*, Manuscript PM 06 027. Vol. IX., ISSN 1682-1130, 2007.
- (1.9) S. Khozirah, KC. Khoo and MA. Abd. Razak, Oil palm stem utilization. *Research Pamphlet No.107*. Kepong. Forest Research Institute Malaysia, p. 120, ISSN 0126-8198, 1991.
- (1.10) Y. Basiron and MA. Simeh, Vision 2020 – The Palm Oil Phenomenon, *Oil Palm Industry Economic Journal* Vol. 5(2), pp. 1 – 10, 2005.
- (1.11) P. Wobst and R. Mhamba, Towards Agricultural Development and Poverty Alleviation in Tanzania: Some Policy Options. Trade and Macroeconomics Division, International Food Policy Research Institute, Washington D.C, 2000.
- (1.12) FF. Mathias, Agricultural mechanization in Mali and Ghana: strategies, experiences and lessons for sustained impacts *Agricultural and Food Engineering Working Document*, Food and Agriculture Organization of the United Nations, FAO, 2010.
- (1.13) L. Teo, Mechanization in Oil Palm Plantations: Achievement and Challenges, *Malaysian Oil Science and Technology* 2002 Vol. 11 No. 2, pp. 70-77, 2002.
- (1.14) SN. Asoegwu and AO. Asoegwu, An overview of agricultural mechanization and its environmental management in Nigeria. *Agricultural Engineering International: the CIGR Journal* vol. 9(6), pp. 1-22, 2007.
- (1.15) AO. Ani and AP Onwualu, Agricultural mechanization: A Pre-requisite for food security in West Africa. 1<sup>st</sup> International Conference of the West African

- 
- Society of Agricultural Engineering, Abuja, Nigeria, pp. 24-28, 2002.
- (1.16) G. Singh, Agricultural Machinery Industry in India (Manufacturing, marketing and mechanization promotion). Status of Farm Mechanization in India, pp. 154-174, 2006.
- (1.17) SO. Nkakini, MJ. Ayotamuno, SOT. Ogaji, and SD. Probert, Farm mechanization leading to more effective energy-utilizations for cassava and yam cultivations in Rivers State, Nigeria. Applied energy 83(12), pp. 1317-1322, 2006.
- (1.18) N. Nazir, D. Setyaningsih, Life Cycle Assessment of Biodiesel Production from Palm Oil and Jatropha Oil in Indonesia, 7th Biomass Asia Workshop, Jakarta, Indonesia, pp. 1 – 6, 2010.
- (1.19) WIW. Ismail, MZ. Bardaie and AM. Abdul Hamid, Optical Properties for Mechanical Harvesting of Oil Palm FFB, Journal of Oil Palm Research Vol. 12 No. 2, pp. 38-45, 2000.
- (1.20) WIW. Ismail, MH. Razali, AR. Ramli, MN. Sulaiman and MHB. Harun, Development of Imaging Application for Oil Palm Fruit Maturity Prediction, Engineering e-Transaction (ISSN 1823-6379), Vol. 4, No. 2, pp 56-63, 2009.
- (1.21) MS. Deraman, AR. Shuib and MS. Jaafar, Roller-Type Oil Palm Loose Fruit Picker, MPOB Information Series, MPOB TT No. 419, ISSN 1511-7871, 2007.
- (1.22) J. Abdul Razak, S. Abdul Rahim, H. Ahmad, J. Johari and M. Mohd Noor, Hand-Held Cutter, MPOB Information Series, MPOB TT No. 180, ISSN 1511-7871, 2003.
- (1.23) J. Abdul Razak, S. Abdul Rahim, H. Ahmad, J. Johari and M. Mohd Noor, High Reach Oil Palm Motorized Cutter, MPOB Information Series, MPOB TT No. 349, ISSN 1511-7871, 2007.
- (1.24) J. Abdul Razak, H. Ahmad, J. Johari, M. Noor, Y. Gono and O. Ariffin, *Cantas*<sup>TM</sup> - A tool for the efficient harvesting of oil palm fresh fruit bunches, Journal of Oil Palm Research, Vol. 20, pp. 548 – 558, 2008.
- (1.25) F. Azhar, Design of a linear oscillatory actuator for oil palm mechanical cutter, MSc. Thesis, University Putra Malaysia, 2009.
- (1.26) F. Azhar, M. Norhisam, H. Wakiwaka, K. Tashiro, M. Nirei, Current Achievement and Future Plan for Improvement for E Cutter Development, The 24<sup>th</sup> Symposium on Electromagnetics and Dynamics, SEAD 24, Toyama, Japan, pp. 459-464, 2012.
- (1.27) F. Azhar, M. Norhisam, H. Wakiwaka, K. Tashiro, M. Nirei, Initial Progress and Possible Improvement of E-Cutter Linear Actuator Development, IEEE International Conference on Power and Energy (PECon 2012), Sabah, Malaysia, pp. 933-938, 2012.
- (1.28) M. Norhisam, K. Alias, RN. Firdaus, S. Mahmud and N. Mariun, Comparison on Thrust Characteristic of Linear of Actuators, IEEE International Conference on Power and Energy Conference, 2006. PECon '06. pp. 470 –

- 
- 475, 2006.
- (1.29) M. Norhisam, F. Azhar, R.N. Firdaus, H. Hashim, M. Nirei, H. Wakiwaka and J. Abdul Razak, Effect of Spring Constant and Thrust Constant to Displacement Characteristics of LOA, *Journal of the Japan Society of Applied Electromagnetics and Mechanics (JSAEM)*, Vol.17 No.3, pp. 437 – 440, 2009.
- (1.30) M. Norhisam, RN. Firdaus, F. Azhar, N. Mariun, I. Aris, J. Abdul Razak and H. Wakiwaka, Analysis of Thrust Constant, Electrical and Mechanical Time Constant for Slot-Less Moving Magnet Linear Oscillatory Actuator, *Journal of the Japan Society of Applied Electromagnetics and Mechanics (JSAEM)*, Vol.17, Supplement, pp. S41 – S44, 2009.
- (1.31) F. Azhar, M. Norhisam, NF. Mailah, MR. Zare, H. Wakiwaka and M. Nirei, Thrust Optimization of Linear Oscillatory Actuator Using Permeance Analysis Method, *International Review of Electrical Engineering (I.R.E.E.)*, Vol. 6, No. 7, pp. 2929 – 2938, 2011.

---

## Chapter 2: Basic Concept of E-Cutter's Actuator

### 2.1 Mechanization of Oil Palm Harvesting Tool

Traditionally, the oil palm fruit fresh fruit bunches were harvested using a sickle. The sickle is attached to an aluminium pole. The length of the aluminium pole depends on the average height of the palm oil in the harvesting area. The sickle is placed at the base point of the bunch and the harvester will pull the aluminium pole several times to accomplish the cutting process. It took about 386 seconds to complete one cycle of harvesting activity <sup>(2.1)</sup>. By using traditional harvesting technique, it was recorded that the ratio of worker to the area of land (ha) was 1:18 and oil palm productivity was 11.60 tonnes/day <sup>(2.2)</sup>. However, the traditional harvesting technique consumes a lot of time of the harvester and could reduce the rate of harvester <sup>(2.3) - (2.5)</sup>.

Over the years, numerous of researchers has been working out to introduce mechanizes harvester for various fruits. It was started about 1970s when human start to improve the productivity and encountering the shortage of the number of labor in the agricultural sector <sup>(2.6)</sup>. In 1983, A. M. Ramsay has discussed on the mechanization of raspberries in Scotland. Base on his findings, by applying mechanization at the raspberries plantation could improve the productivity over 10% compared to hand pickers harvesting <sup>(2.6)</sup>. G. Gianmetta and G. Zimmelatti, 1997, discussed a mechanical pruning system for Olive-Groves <sup>(2.7)</sup>. Based on this paper finding, the mechanical pruning could reduce the labour requirement from 128 man h/100 trees on hand pruning and 21 man h/100 trees for half mechanical pruning to 4 man h/100 trees. A mechanical system for apricots harvesting was designed and tested in <sup>(2.8)</sup>. Base on the test that has been conducted, the mechanical pruner could harvest about 1500 kg apricots compared to 450 kg and 22.50 kg by using traditional tools and hand picker respectively within 1 hour harvesting time. It is also increasing the number of trees harvested per minute up to 400 tree compared to 20 trees and 6 trees by using traditional tools and handpicked. A. Torregrosa *et al.*, 2009 through their paper has discussed the application of two type mechanizations to citrus harvesting in Spain.

---

There are tractor shaker and trunk shaker using hand held pruner. The tractor shaker was most effective (72 % detachment) than hand-held shakers (57 %) <sup>(2.9)</sup>.

By taking the inspire by the various mechanize harvesting system mentioned above, mechanization harvesting system for oil palm fruit system is come to idea to be realized. Before the harvesting system for oil palm fruit could be designed, the features of the fruit itself need to be studied. The oil palm fruits are normally compactly packed in a bunch. It is also hidden in the leaf axils in crowns and about 12 m height above the ground. Stalk of frond that underlying a bunch need to be cut first before the bunch could be harvested and fall freely on the ground <sup>(2.1)</sup>. The previous discussed mechanize of the harvesting system is implementing shake-catch mechanism <sup>(2.6) - (2.9)</sup>. All the fruits mention is having non-similarity with the oil palm fruit especially when the location and bunch type fruit are considered. The limited space between the fronds and bunches also made the shake-catch mechanism is unrealistic. Furthermore, implementing this technique made loose fruit numbers become higher hence increase the harvesting time especially during the time of collecting the loose fruit. Therefore, the bunch-harvested style is suggested to use in order to design and develop mechanize harvesting system for oil palm fruit <sup>(2.1), (2.10)</sup>.

The Malaysian Palm Oil Board (MPOB) has initiated the mechanization of oil palm fruit harvester tools called as *Cantas*<sup>TM</sup>. Figure 2.1 shows the structure of the *Cantas*<sup>TM</sup>. The structure and mechanism of the *Cantas*<sup>TM</sup> is similar to sickle tools since it proven to be efficient enough so far in harvesting activities <sup>(2.2), (2.11), (2.12)</sup>.



Figure 2.1 *Cantas*<sup>TM</sup> structure.

The *Cantas*<sup>TM</sup> consists of a 1.3 hp petrol engine located at the bottom of a telescopic aluminium pole. At the top, a sickle or a chisel will be attached and use as a cutting head. The telescopic aluminium length could be adjusted suit with the oil palm height made it suitable to be used in various height of oil palm. The rotational motion of the engine is transmitted through a transmission shaft located inside the telescopic

---

aluminium pole to a pair of gears where the sickle is connected. These gears convert the rotational motion to linear oscillatory motion in order to vibrate the sickle. A con-rod mechanism activates the sickle to move up-down in its longitudinal direction, thus performing the cutting. The engine of *Cantas*<sup>TM</sup> has a working speed in the range between 3000 to 5000 rpm. With the engine speed, the sickle of *Cantas*<sup>TM</sup> has a maximum cutting displacement of 16 mm at 80 Hz of maximum cutting frequency<sup>(2.2), (2.11), (2.12)</sup>. The MPOB has setup several field testing session on the *Cantas*<sup>TM</sup> in commercial estates with the objectives of evaluating its performance and providing recommendations to the industry. As indicated in<sup>(2.2)</sup>, the field testing has been done in Tereh Selatan Estate, located in Johor, Malaysia. Two teams of workers have been established during the testing session where one team was used sickle tool and the other used the *Cantas*<sup>TM</sup>. Based on the field testing, by using the *Cantas*<sup>TM</sup>, productivity of oil palm increased from 4.19 tonnes/day to 11.60 tonnes/day as compared to the manual sickles. Worker to land ratio (ha) also increased from 1:18 to 1:37. Despite of a good achievement by the *Cantas*<sup>TM</sup>, this tool is found less efficient for height of oil palm more than 8 m. At this height of oil palm, the telescopic aluminium pole will start bends and making transmission of motion from the shaft to the cutting head ineffective<sup>(2.2), (2.13)</sup>.

## **2.2 Basic Concept and Current Status of the E-Cutter Development**

The mechanized oil palm fresh fruit bunch harvesting tools should be easy to handle, efficient enough and should improve the harvesting productivity. So far, the *Cantas*<sup>TM</sup> has proven its capability of improving the FFB harvesting activity based on the finding in<sup>(2.2)</sup>. However, the same productivity is only competent to maintain at height of oil palm up to 8 meters due to bending problem occurs in the *Cantas*<sup>TM</sup>. Nevertheless, mechanized tools similar to the *Cantas*<sup>TM</sup> still could be considered as the best structure for higher oil palm. The farmer needs to engage the sickle to the base point of bunches before the harvesting activity could be accomplished. However, a flexible system should be designed so that the performance of the mechanized tools is not affected by the bending occurrence.

---

Harvesting activity done in horizontally could reduce the total thrust needed. Therefore, in the *Cantas*<sup>TM</sup>, the MPOB adopted the vibrating mechanism that is transferred to a horizontal direction so that harvesting can be performed horizontally. Thus, a vibrating mechanism has therefore been designed and developed for the harvesting sickle which causes it to vibrate at high speed in the longitudinal direction of the pole's axis. Therefore, similar structure of harvesting tool as *Cantas*<sup>TM</sup> was proposed. In the new tool, at least comparable performance of the *Cantas*<sup>TM</sup> but more flexible was aimed. Instead of mechanical based tool in the *Cantas*<sup>TM</sup>, the new tool was designed in electrical based tool. The new tool is called as E-Cutter<sup>(2.13) - (2.15)</sup>. The basic structure of the E-Cutter is as shown in Figure 2.2. Since the structure of *Cantas*<sup>TM</sup> provides with several advantages especially on easiness to engage with the base of frond during the harvesting activity, the E-Cutter also maintain a similar structure of the *Cantas*<sup>TM</sup>.



Figure 2.2 E-Cutter structure.

The 2 stroke engine used in the *Cantas*<sup>TM</sup> will still be used in the E-Cutter. However, the engine is attached to an electrical generator in order to convert the mechanical energy to electrical energy. On the top side of the E-Cutter, a linear motor is used in order to provide direct linear vibration motion to the sickle in order to accomplish the harvesting activity. A copper wire will be utilized to replace the shaft inside the aluminum pole in order to transmit the electrical energy provided by the electric generator to the linear actuator. Therefore, this tool will keep operating efficiently even though the pole is bending caused by the height increments due to the copper is more flexible to compare to the shaft in the *Cantas*<sup>TM</sup><sup>(2.13) - (2.15)</sup>.

The E-Cutter development progress depends on the development of the electrical generator and the linear motor. The development of the electrical generator seems to be established through several types of permanent magnet generator with different performance characteristics have been designed and developed<sup>(2.16) - (2.19)</sup>. On

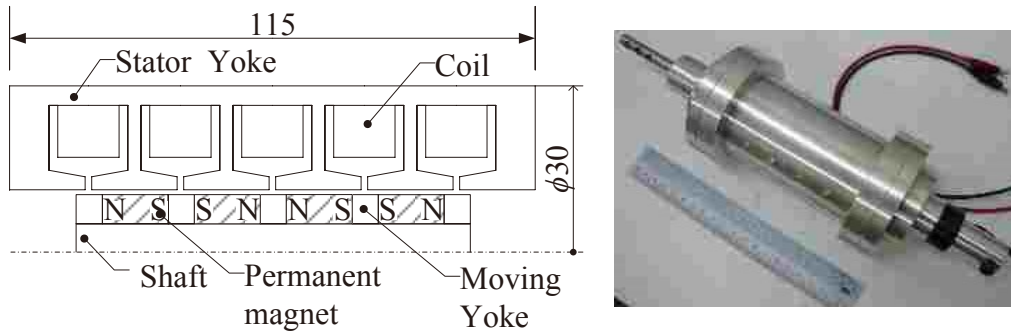
---

the other hand, the progress of linear motor development is still requiring significant improvement. Therefore, in this research, the design of linear motor for the E-Cutter's actuator was focused on.

Previously, four prototype of linear motor for E-Cutter's actuator has been designed and developed. The entire previous prototype has been design as single phase topology. Two type of stator types has been used which are slot less type <sup>(2.20)-(2.22)</sup> and slot type <sup>(2.13), (2.20), (2.23), (2.24)</sup>. The detail comparison of these linear motors performance is as discussed in <sup>(2.14), (2.15)</sup>. Despite of all the linear motor has been developed, the slot type linear motor as discussed in <sup>(2.13), (2.23), (2.25)</sup> could be considered as the best linear motor for E-Cutter actuator so far. In order to easy reference, this linear motor is referred as 1PhSTLOA.

The structure and construction of the 1PhSTLOA is as shown in Figure 2.3. The structure parameters of the 1PhSTLOA have been optimized in order to made the 1PhSTLOA having starter thrust,  $F_{x=0}$  is higher than 200 N and total weight,  $W_{tot}$  lower than 2.0 kg. Detail of the 1PhSTLOA performance characteristics is as listed in Table 2.1. Based on several session of laboratory testing, it is found that the 1PhSTLOA is feasible to accomplished frond and bunch cutting. The testing session is shown in Figure 2.4. Several fresh oil palm fronds with different size have been brought to laboratory during testing session. Even though the cutting frond and bunch is feasible by the 1PhSTLOA, it is found that the cutting time is slightly longer compared to the *Cantas*<sup>TM</sup>. It tooks only 2 seconds to finish cutting cycle by using *Cantas*<sup>TM</sup> compare to about 6 seconds by using the 1PhSTLOA.

The main drawback of the 1PhSTLOA comparing with the *Cantas*<sup>TM</sup> is the displacement,  $x$  and oscillation frequency,  $f_{osc}$ . Based on the observation, the *Cantas*<sup>TM</sup> could provide constant displacement,  $x$  of 16 mm at oscillation frequency,  $f_{osc}$  in the range of 50 – 80 Hz <sup>(2.2), (2.11), (2.12)</sup>. However, the 1PhSTLOA only could operate at displacement,  $x$  of 10 mm and oscillation frequency,  $f_{osc}$  of 68 Hz <sup>(2.13)</sup>. It is shown that, the 1PhSTLOA has an adequate cutting force, however lack on the dynamic performance especially in term of displacement,  $x$  and oscillation frequency,  $f_{osc}$ . Therefore, a new linear motor is needed to be designed to increase the reliability of the E-Cutter especially in terms of it dynamic performance.



(a) The 1PhSTLOA structure (unit in mm). (b) Construction of 1PhSTLOA.  
Figure 2.3 Structure and construction of 1PhSTLOA.

Table 2.1 The 1PhSTLOA performance characteristics.

Performance characteristics	Value
Starting thrust, $F_{x=0}$ (N)	222
Outer dimension, $\phi \times l$ (mm)	$\phi 60 \times 115$
Total weight, $W_{tot}$ (kg)	2.0
Thrust constant, $k_f$ (N/A)	58.15
Motor constant, $k_m$ (N/ $\sqrt{W}$ )	32.5
Motor constant square density, $G$ ( $\times 10^6$ N <sup>2</sup> /Wm <sup>3</sup> )	3.40
Displacement, $x$ (mm)	9.39
Oscillation frequency, $f_{osc}$ (Hz)	68



(a) Equipment setup for cutting evaluation.

(b) During cutting evaluation.



(c) Cutting process successfully done.

Figure 2.4 Cutting evaluation of 1PhSTLOA.

---

### 2.3 Introduction to the Linear Motor

Generally, a linear motion is produced by a combination of rotational motor and motion translator. Motion translator such as ball screws, gears, belts and etc. will be attached to the rotational motor shaft to convert rotational motion to linear motion. Despite of vast applications of this linear motion system, it inherent several drawbacks such as low acceleration performance, mechanical complexity and limitation, backlash and low impact load capacity<sup>(2.26)</sup>.

As an alternative, a linear motor is used to provide a linear motion with the absence of all above mentioned motion translators. By eliminating the motion translation parts, the system can work with no worries of backlash and compliance. The total parts can be reduced, hence increase the system reliability, make the system simpler and offer high flexibility to the system in terms of size and space. Furthermore, linear motors provide the system with low friction and wear and increase response, speed and acceleration of the moving parts<sup>(2.27), (2.28)</sup>. However, cost of the linear motor is relatively higher compared to the traditional system. Linear motor development's cost is proportional to it stroke and length. It is due to the increment of the permanent magnet price<sup>(2.29)</sup> and a fact of the linear encoder cost is length dependence<sup>(2.30)</sup>.

The linear motor can be dividing into three major types. There are linear induction motor (LIM), linear synchronous motor (LSM) and linear stepper motor (LSTM). The thrust of the LIM is produced by interaction of the magnetic field induced by the primary alternating magnetic field in stator and the induced current on the mover's conductor. The LSM produces thrust by interaction between alternating magnetic field induced by excited stator coil winding and an array of magnetic poles or a variable reluctance ferromagnetic rail. On the other hand, the LSTM created thrust by interaction of magnetic field produced by a step excitation style of stator coil and an array of magnetic poles or a variable reluctance ferromagnetic rail<sup>(2.31), (2.32)</sup>.

Despite of the LSTM, either the LIM or the LSM are suitable to be implemented as the E-Cutter's actuator. It is due to the ability of continues the movement of the mover part provided by the LIM and the LSM compared to the LSTM based on it thrust production process. Table 2.2 shows advantages and

---

disadvantages of the LIM and the LSM. One of key performance of the E-Cutter's actuator is high thrust density. Therefore, based on the comparison of advantages and disadvantages between the LIM and the LSM, the LSM is seen as the best candidate to be implemented as the E-Cutter's actuator. It is caused by higher thrust density capability offer by the LSM. However, position information to determine excitation sequence, a hall sensor can be used in the LSM driving system.

The LSM can be divided into two types. There are switched reluctance linear synchronous motor (SRLSM) and permanent magnet linear synchronous motor (PMLSM). The switched reluctance linear motor (SRLSM) converts reluctance thrust into mechanical power. The stator parts of the SRLSM consist of teeth stator yoke and coils while the mover parts consist of teeth ferromagnetic structure. The thrust of the SRLSM is produced by the tendency of the mover teeth to align with the stator teeth. Only an unidirectional pulse is required to produce thrust and made the mover moved from unaligned teeth to align condition teeth condition <sup>(2.33), (2.34)</sup>. On the other hand, the permanent magnet linear synchronous motor (PMLSM) adds a permanent magnet on the mover part. Depending on the magnetization direction arrangement of the permanent magnet, either ferromagnetic or non-ferromagnetic moving yoke will be used to rest the permanent magnet. The thrust of the PMLSM also produced by interaction between primary travelling magnetic field induced by the exciting coil and the magnetic field produced by the permanent magnet <sup>(2.23), (2.25)</sup>. Due to two sources of magnetic field exist, the thrust density of the PMLSM is relatively higher compared to the SRLSM.

The LSM can be designed either in rectangular/flat shape or cylindrical/tubular shape <sup>(2.35)</sup>. However, in this research, the cylindrical shape of the LSM was choosing based on several advantages opposed to the rectangular. The cylindrical shape of the LSM does not need end winding as the rectangular shape. All coils in the cylindrical shape are actively participating to the magnetic field and thrust production <sup>(2.36)</sup>. This condition increases coil efficiency and power to weight ratio. Furthermore, the cylindrical shape of LSM is comprised of ring shape of the coil winding. The ring shape coil winding is easy to manufacture and suit to industrially produce. The cylindrical shape of the LSM also has features of self-neutralization of normal force <sup>(2.37)</sup> and reduces support mechanism requirement <sup>(2.38)</sup>. On top of that, the cylindrical

shape of the LSM has a compact structure and high force density <sup>(2.38) - (2.40)</sup>. However, the cylindrical shape of the LSM limits the maximum stroke. Exceeding the limit stroke may cause vibrations and mechanical damage to the LSM <sup>(2.37)</sup>.

Table 2.2 Advantages and disadvantages of LIM and LSM.

	Linear induction motor (LIM)	Linear synchronous motor (LSM)
Advantages (2.31), (2.32)	<ul style="list-style-type: none"> <li>- Simple structure.</li> <li>- Low cost and easy manufacturing.</li> <li>- Low maintenance.</li> <li>- Robust.</li> </ul>	<ul style="list-style-type: none"> <li>- Higher efficiency.</li> <li>- Higher thrust density.</li> <li>- Better dynamic response.</li> </ul>
Disadvantages (2.31), (2.32)	<ul style="list-style-type: none"> <li>- Lower efficiency.</li> <li>- Lower power factor.</li> <li>- Lower thrust density.</li> </ul>	<ul style="list-style-type: none"> <li>- Expensive manufacturing cost due to magnet cost.</li> <li>- Temperature dependence due to magnet temperature limitation.</li> <li>- Exact position information requires ensuring synchronisation of magnetic field.</li> </ul>

### 2.3.1 Switched Reluctance Linear Synchronous Motor

In recent years, the switched reluctance linear synchronous motor (SRLSM) has been alternative to LIM or even to permanent magnet linear synchronous motor (PMLSM). This is due to a factor of their simple and robust structure due to concentric windings only either on stator or mover part, which results in easy maintenance and low manufacturing and operational cost <sup>(2.41) - (2.44)</sup>. The low manufacturing and operational cost feature of the SRLSM are not only due to the simple structure, but also caused by the absence of permanent magnet inside the structure. Addition, recently, it is reported that the permanent magnet materials especially rare earth material has facing supply chain problem and led to an increment of the material cost. Therefore, the SRLSM can improve the cost performance of the LSM <sup>(2.29)</sup>. With absence of the

---

permanent magnet in the SRLSM structure, eliminate cogging force and temperature dependency of the LSM <sup>(2.29), (2.41) - (2.44)</sup>.

Despite of its advantages, the SRLSM is producing higher ripple thrust compare to other types of the linear motor. The thrust ripples contribute to vibration and acoustic noise during operation. Furthermore, the SRLSM could not be driven by the main AC or DC supply. It requires proper current pulse signal for proper thrust production. However, continual development of power electronics and control strategies increases the reliability and effectiveness of switched reluctance type machine <sup>(2.45)</sup>. On top of that, the structure of the SRLSM made it could be driven only by unidirectional square pulse of current made the design of the motor driver simpler <sup>(2.46)</sup>.

### **2.3.2 Permanent Magnet Linear Synchronous Motor**

The permanent magnet linear synchronous motor (PMLSM) producing thrust by interaction of the magnetic field induced by a coil and the magnetic field produced by a permanent magnet. When the coil and the permanent magnet have similar magnetic pole, repulsive force will generate. When the coil and the permanent magnet have different magnetic pole, attractive force will generate. Compared to the SRLSM, the PMLSM use both repulsive and attractive force to produce the total thrust. Therefore, a bipolar excitation current is useful for the PMLSM in order to generate thrust.

The PMLSM has proven its superior performance. By comparing to the SRLSM, the PMLSM normally design with higher air gap length. It will reduce the manufacturing tolerance,  $\Delta x$  sensitivity <sup>(2.47)</sup>. The use of a permanent magnet as one of magnetic flux source made the PMLSM has a high thrust density <sup>(2.47), (2.48)</sup>. Furthermore, by using a permanent magnet operates at high efficiency, high power factor and reduce the driver rating <sup>(2.49) - (2.51)</sup>. Despite of its superior performance, the PMLSM suffers from thrust fluctuation especially during low speed operation. The thrust fluctuation is mainly due to existence of cogging force <sup>(2.49), (2.51)</sup>. However, several researchers have suggest various techniques to reduce the cogging force such as skewing the permanent magnet <sup>(2.52)</sup>, shifting the permanent magnet pole pair <sup>(2.53)</sup>,

changing the ratio of the permanent magnet width to the pole pitch <sup>(2.54)</sup> and averaging the permanent magnet position without skewing <sup>(2.55)</sup>.

## 2.4 Design Target and Restriction of the E-Cutter's Actuator

In order to ensure reliability of the E-Cutter, specific design target has been set for it in actuator design. There are two design targets have been set which are cutting force,  $F_{\text{cutting}}$  and total weight,  $W_{\text{tot}}$ . Since the E-Cutter use a sickle as a cutting tool, based on <sup>(2.56)</sup>, the average cutting force per unit area required to cut the oil palm frond is about  $94 \text{ N/cm}^2$ . Meanwhile, the biggest size of frond is about  $80 \text{ cm}^2$  cross sectional area <sup>(2.57)</sup>. Based on the facts mentioned above, there are about  $7.5 \text{ kN}$  to accomplish the cutting process once. Therefore, implementation of vibrating mechanism or also recognizes as rapid copping method could reduce the cutting force required. The rapid copping method accomplishes the cutting procedure gradually depending on the sickle displacement. Thus, the actual total force required in cutting process is lower than mentioned above.

Consider the cross sectional view of oil palm frond as shown in Figure 2.5. It has an area of  $80 \text{ cm}^2$ ,  $17 \text{ cm}$  in width and  $10 \text{ cm}$  in height. Assume that sickle displacement during cutting activity is  $0.2 \text{ cm}$ , thus the cutting force,  $F_{\text{cutting}}$ , required to cut that particular oil palm frond is as calculated in Eq. (2.1). Therefore, the cutting force,  $F_{\text{cutting}}$ , for E-Cutter' actuator should higher that  $188 \text{ N}$ . However, in order to ease the design process, the cutting force is target higher than  $200 \text{ N}$ .

$$\begin{aligned} F_{\text{cutting}} &= 94 \times (0.2 \times 10) \\ &= 188 \text{ N.} \end{aligned} \tag{2.1}$$

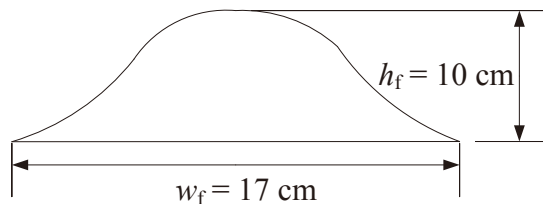


Figure 2.5 Cross sectional view of oil palm frond.

---

Nevertheless, the main constrain for the E-Cutter's actuator design was the total weight,  $W_{\text{tot}}$  of it. The total weight,  $W_{\text{tot}}$  of the E-Cutter's actuator is aimed below 2.0 kg. This design condition has been set based on the existing system of *Cantas*<sup>TM</sup>. The total weight,  $W_{\text{tot}}$  of this system is targeted to be below 7.5 kg similar to the total weight of the *Cantas*<sup>TM</sup>. The total weight,  $W_{\text{tot}}$  of this system includes the 2 stroke petrol engine, dynamo, pole and linear motor. The maximum weight of the E-Cutter's actuator allowed maintaining the total weight,  $W_{\text{tot}}$  of the overall system is 2.0 kg <sup>(2.15)</sup> about similar to the weight of gear in *Cantas*<sup>TM</sup>.

## 2.5 Performance Index of the E-Cutter's Actuator

Generally, the linear motor's performance is evaluated using thrust. However, thrust is directly proportional to other factors such as current,  $I$ , input power,  $P_{\text{in}}$  and overall size of the linear motor. Therefore, several performance indexes are adopted in order to make comparison between linear motors valid. The performance indexes are thrust constant,  $k_f$ , motor constant,  $k_m$  and motor constant square density,  $G$ . These performance indexes are calculated using,

$$k_f = \frac{F_{\text{ave}}}{I}, \quad (\text{N/A}) \quad (2.2)$$

$$k_m = \frac{F_{\text{ave}}}{\sqrt{P_{\text{in}}}}, \quad (\text{N}/\sqrt{\text{W}}) \quad (2.3)$$

$$G = \frac{F_{\text{ave}}^2}{P_{\text{in}} V_{\text{mot}}} \quad (\text{N}^2/(\text{Wm}^3)) \quad (2.4)$$

where,  $k_f$  is the thrust constant in (N/A),  $F_{\text{ave}}$  is the average thrust in (N),  $I$  is the current in each coil in (A),  $k_m$  is the motor constant in (N/ $\sqrt{\text{W}}$ ),  $P_{\text{in}}$  is the input power in (W),  $G$  is the motor constant square density in ( $\text{N}^2/(\text{Wm}^3)$ ) and  $V_{\text{mot}}$  is the motor volume in ( $\text{m}^3$ ).

The thrust constant,  $k_f$  is represent thrust produced at 1 A of current,  $I$ . Even though the thrust constant,  $k_f$  is just motor characteristics, however this characteristic

---

represent thrust sensitivity against current. The higher this characteristic, represent the higher thrust produced at similar current. Therefore, the thrust constant,  $k_f$  was used as the performance index to evaluate performance of the E-Cutter's actuator models. The motor constant,  $k_m$  is represent thrust produced at 1 W of input power,  $P_{in}$ . The higher the motor constant,  $k_m$  represent higher thrust could be produce at similar input power,  $P_{in}$ . On the other hand, the factor of linear motor volume,  $V_{mot}$  is considered through motor constant square density,  $G$ . The higher motor constant square density,  $G$  represent higher thrust produced at lower input power,  $P_{in}$  and smaller volume of the linear motor,  $V_{mot}$ .

Instead of above mentioned performance indexes, response of the linear motor can be evaluate using electrical time constant,  $\tau_e$ . The electrical time constant,  $\tau_e$  represent the current,  $I$  response of the linear motor. The lower the electrical time constant,  $\tau_e$  represent faster response of current,  $I$  hence higher frequency,  $f$  of power supply can be used. The electrical time constant,  $\tau_e$  can be calculated using Eq. (2.5). It also refer as ratio between the linear motor's coil inductance,  $L$  to it resistance,  $R$ .

$$\tau_e = \frac{L}{R} \quad (\text{s}) \quad (2.5)$$

where  $\tau_e$  is the electrical time constant in (s),  $L$  is the coil inductance in (H) and  $R$  is the coil resistance in ( $\Omega$ ).

In this research, the performance of the SRLSM and the PMLSM will be compared to commercialized permanent magnet linear motor (PMLM). There are 3 types of commercialized PMLM has been choose which are slot type PMLM, slotless type PMLM and shaft motor. It involves about 200 models from several motor manufacturers such as Yaskawa Electric Corporation, Rockwell Automation, Sanyo Denki Co. LTD, GMC Hillstone Co., LTD and etc. Figure 2.6 shows performance comparison of 5 samples of the commercialized PMLM for each type of linear motor. The sample of the commercialized PMLM has been chose base on the best performance on each performance index. Each axis on the Figure 2.6 also has been set so that the further the plot from its origin represent the better performance. Based on the Figure 2.6, the slot type of the PMLM has capability to fulfil the thrust required by

---

the E-Cutter's actuator. It also capable to produce high thrust at lower current,  $I$ , lower input power,  $P_{in}$  and smaller size compared to the slot less type of PMLM. Nevertheless, the slot type of PMLM has higher electrical time constant,  $\tau_e$  compared to the slotless type of PMLM. On the other hand, the shaft motor has a similar performance of thrust as the slot type PMLM and a current response as the slotless type of PMLM. However, in most cases, the coil of the shaft motor will be work as the mover that tends to slower the mover response due to weight of coils. On top of that, the stator part of the shaft motor is constructed by solely brittle permanent magnet, therefore, it seem to be unreasonable to be implement as the E-Cutter's actuator. Instead of comparing with each other, the performance comparison between commercialized PMLM with the designed linear motor will be discussed in further chapter.

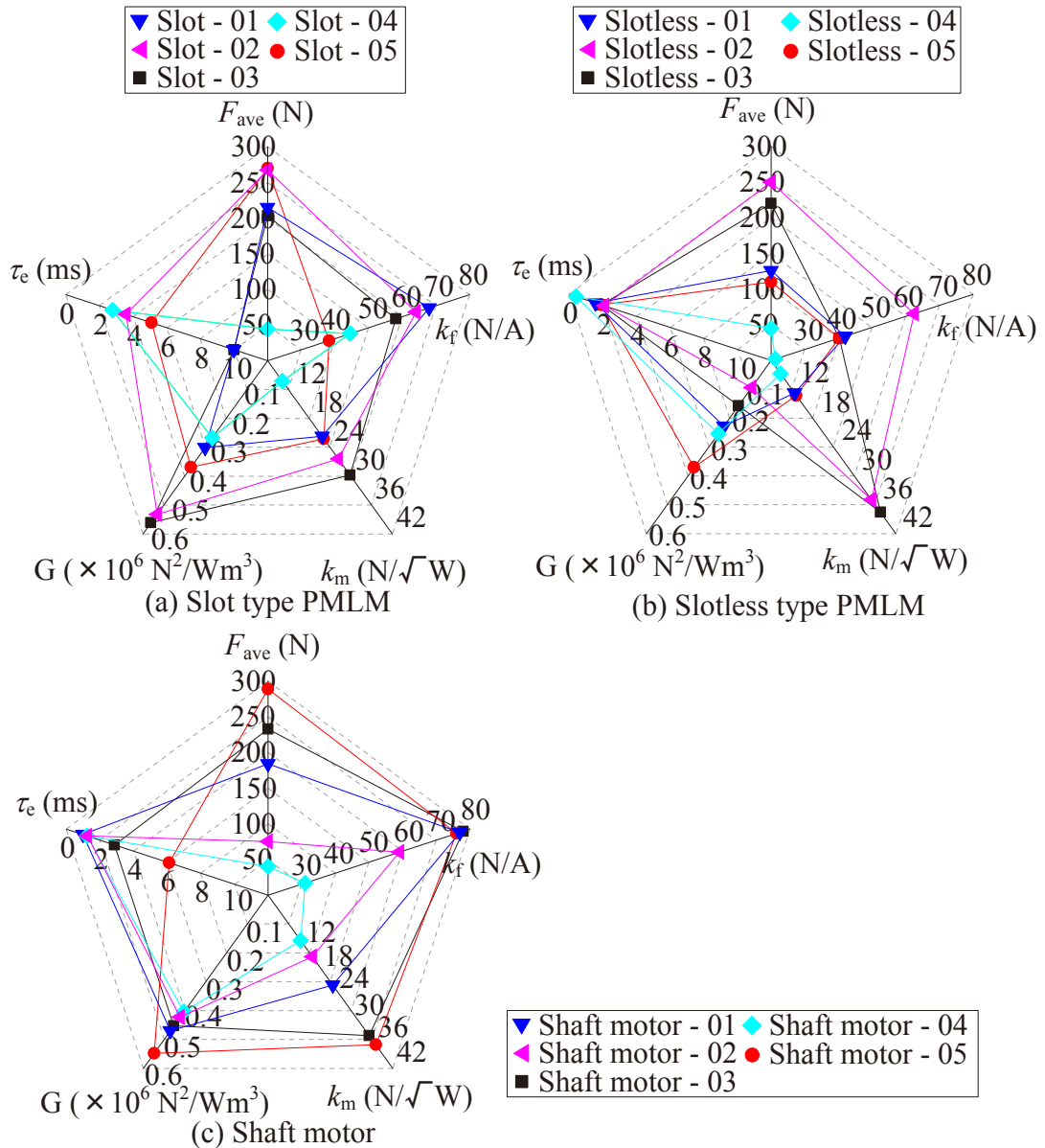


Figure 2.6 Comparison of performance index between difference types of commercialized PMLM.

## 2.6 Introduction to Finite Element Method

Generally, the electrical machine designs employ either permeance analysis method (PAM) or finite element method (FEM). Both of these techniques capable to analysed the electrical machine performance with high degree of accuracy<sup>(2.58)</sup>. The PAM is uses a magnetic equivalent circuit that is analogous to electrical circuit which is based on machine's geometry and estimated of magnetic flux path to solve the electrical machine analysis. It saves information of geometry and magnetic flux path within permeances. The connection scheme of permeances can either be in parallel or

---

in series and it is possible to represent a certain part of machine's geometry by one common permeance. However, the accuracy of PAM result depends on closeness of estimation of the magnetic flux path to the actual condition. Closer to the actual magnetic flux path, made higher level complexity of the mathematical modelling. Even though the mathematical modelling complexity could be reduced however, an acceptable accuracy of analysis output needs to be decided <sup>(2.59)</sup>.

The FEM is another method used to design an electrical machine. The FEM is a numerical method of solving linear and non-linear partial differential equations <sup>(2.60)</sup>. It offers an accurate and powerful design tool, allowing material properties, nonlinearities and structural details to be taken into account. FEM uses a complex system of points called nodes which make a grid called a mesh. This mesh is programmed to contain the material and structural properties which define how the structure will react to certain loading conditions. Nodes are assigned at a certain density throughout the material depending on the anticipated stress levels of a particular area. The mesh acts like a spider web in that from each node, there extends a mesh element to each of the adjacent nodes. This web of vectors is what carries the material properties to the object, creating many elements. The FEM calculation is based on the energy conversation. The law of conversation of energy in electric motor could derived from Maxwell's equation and can be expressed as <sup>(2.61)</sup>,

$$-\int_v \bar{E} \cdot \bar{J} dV = \int_v \bar{H} \cdot \frac{\partial \bar{B}}{\partial t} dV \quad (J) \quad (2.6)$$

where  $\bar{B}$  is magnetic flux density (T),  $\bar{H}$  is magnetic field intensity (kA/m),  $\bar{J}$  is current density (A/m<sup>3</sup>),  $\bar{E}$  is electric field (V) and  $V$  is volume enclosing the device analyzed (m<sup>3</sup>).

The recent high growth of the computer systems and development of the software to solve complicated problems made it possible to use precise methods of calculations in electric machinery to obtain the magnetic field analysis. The widespread FEM still demands too much computing power and memory space consuming to obtain the results in a short time <sup>(2.62), (2.63)</sup>. By using the FEM technique, it is possible to obtain the magnetic forces and other characteristics of electromagnetic equipment with a high degree of accuracy because it gives an approximation of the

---

magnetic flux distribution on a microscopic scale. On top of that, the FEM provide an accurate mean to determine the field distribution that takes into account the saturation (2.58), (2.64). Based on this fact, the FEM technique has been choose to be used in E-Cutter's actuator design.

The E-Cutter's actuator has been designed using JMAG Designer (x64) version 13.0.02I. Designing the E-Cutter's actuator using JMAG Designer (x64) version 13.0.02I involves sequential step as shown in Figure 2.7. Since the E-Cutter's actuator was design in cylindrical shape, 2D axisymmetric modelling was used. Figure 2.8 shows sample of the E-Cutter's actuators have been used during design stage. Once the model of the E-Cutter's actuator has been created, material setting of each part has been set. One of the determination factors of result's accuracy is mesh setting. Finer meshes relatively produce higher degree of result accuracy. However, the simulation time will be longer and memory size consumption will be higher. Therefore, the mesh size setting need to be set appropriately by considering simulation time, memory size consumption and accuracy level of results. The thrust of the E-Cutter's actuator is developing at air gap region between mover and stator. Therefore, the air gap region between mover and stator and it near region need to set finer compared to other region. Figure 2.9 shows the mesh of the E-Cutter's actuators. Once the mesh was created, the FEM will start to run element calculation. The result of the magnetic analysis will be form of magnetic flux density and magnetic flux line. Figure 2.10 and Figure 2.11 shows sample of magnetic analysis result of the E-Cutter's actuator. Instead of magnetic flux density and magnetic flux line, other output such thrust, current and voltage waveform, losses and etc. could be observed.

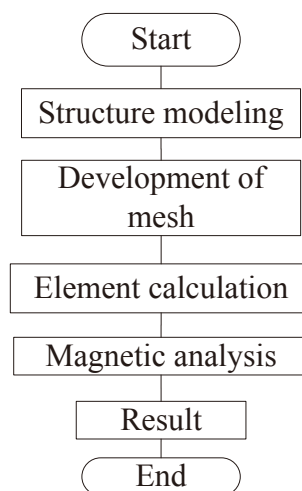


Figure 2.7 Design step of E-Cutter's actuator using FEM.

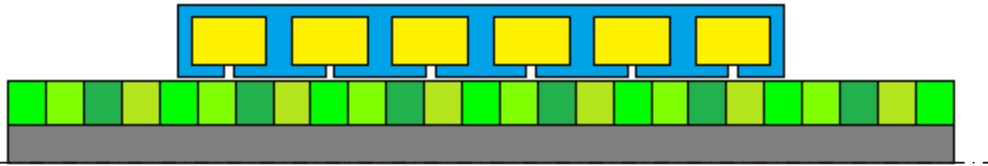
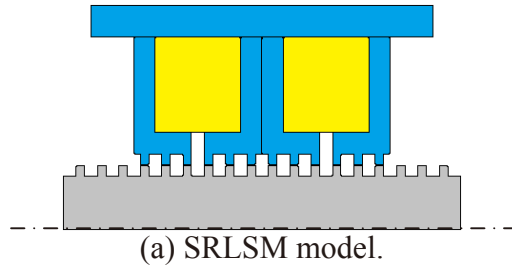


Figure 2.8 E-Cutter's actuator model.

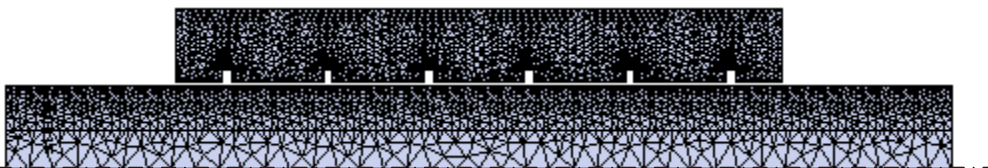
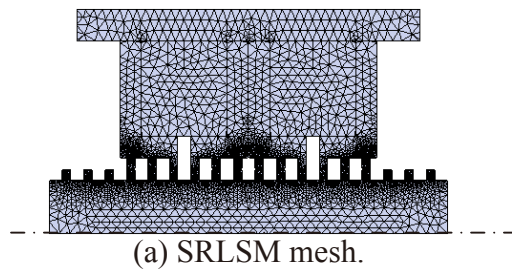


Figure 2.9 E-Cutter's actuator mesh.

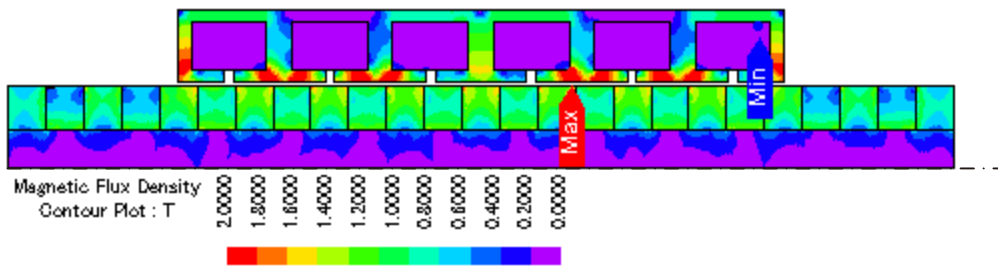
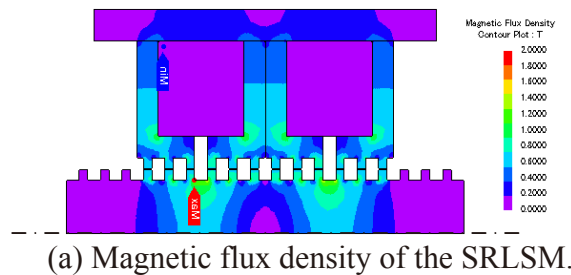


Figure 2.10 Magnetic flux density of the E-Cutter's actuator.

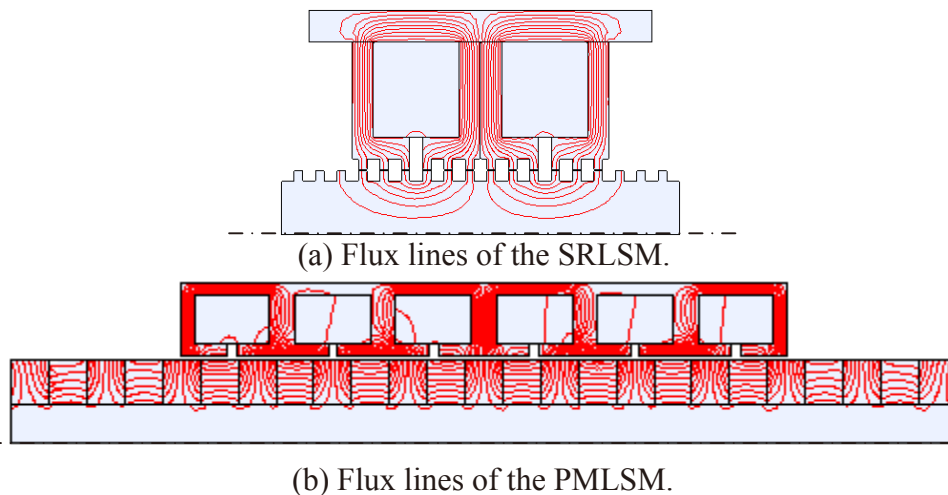


Figure 2.11 Flux lines of the E-Cutter's actuator.

## 2.7 References of Chapter 2

- (2.1) DA. Adetan, LO. Adekoya and KA. Oladejo, An Improved Pole-and-Knife Method of Harvesting Oil Palms. *Agricultural Engineering International: CIGR E-Journal*, Manuscript PM 06 027. Vol. IX., ISSN 1682-1130, 2007.
- (2.2) J. Abdul Razak, H. Ahmad, J. Johari, M. Noor, Y. Gono and O. Ariffin, *Cantas<sup>TM</sup>* - A tool for the efficient harvesting of oil palm fresh fruit bunches, *Journal of Oil Palm Research*, Vol. 20, pp. 548 – 558, 2008.
- (2.3) J. Abdul Razak, AR. Ahmad, D. Hitam, A. Yahya and J. Jamak, Reaction force and energy requirement for cutting oil palm fronds by spring powered sickle cutter, *Journal of Oil Palm Research*. Vol.11 (2). pp. 114 – 122, 1999.
- (2.4) JWL. Bevan and BS. Gray, *The organization and control of field practice for large-scale oil palm plantings in Malaysia*. Incorporated Society of Planters, Malaysia, 1969.
- (2.5) OB. Chirs, An impact analysis of the development of the rural road system on the production of oil palm in Imo State, Nigeria. *Agricultural Systems* 19(2), pp. 141 – 152, 1986.
- (2.6) AM. Ramsay, Mechanical Harvesting of Raspberries - A Review with Particular Reference to Engineering Development in Scotland, *Journal of Agricultural Engineering Research* 28, pp. 183-206, 1983.
- (2.7) G. Giametta, G. Zimbalatti, Mechanical Pruning in New Olive-Groves, *Journal of Agricultural Engineering Research* 68, pp. 15-20, 1997.
- (2.8) D. Erdogan, M. Guner, E. Dursun and I. Gezer, Mechanical Harvesting of Apricots, *Biosystems Engineering* 85 (1), pp. 19- 28, 2003.
- (2.9) A. Torregrosa, E. Orti, B. Martin, J. Gil, C. Ortiz, Mechanical harvesting of oranges and mandarins in Spain, *Biosystems Eng.* 104, pp. 18-24, 2009.
- (2.10) SH. Futch, JD. Whitney, JK. Burns and FM. Roka, *Harvesting: From Manual*

- 
- to Mechanical, HS-1017, one of a series of the Horticultural Sciences Department, Florida Cooperative Extension Service, Institute of Food and Agricultural Sciences, University of Florida. 2006.
- (2.11) J. Abdul Razak, S. Abdul Rahim, H. Ahmad, J. Johari and M. Mohd Noor, Hand-Held Cutter, MPOB Information Series, MPOB TT No. 180, ISSN 1511-7871, 2003.
- (2.12) J. Abdul Razak, S. Abdul Rahim, H. Ahmad, J. Johari and M. Mohd Noor, High Reach Oil Palm Motorized Cutter, MPOB Information Series, MPOB TT No. 349, ISSN 1511-7871, 2007.
- (2.13) F. Azhar, Design of a linear oscillatory actuator for oil palm mechanical cutter. MSc. Thesis, University Putra Malaysia, 2009.
- (2.14) F. Azhar, M. Norhisam, H. Wakiwaka, K. Tashiro, M. Nirei, Current Achievement and Future Plan for Improvement for E Cutter Development, The 24<sup>th</sup> Symposium on Electromagnetics and Dynamics, SEAD 24, Toyama, Japan, , pp. 459-464, 2012.
- (2.15) F. Azhar, M. Norhisam, H. Wakiwaka, K. Tashiro, M. Nirei, Initial Progress and Possible Improvement of E-Cutter Linear Actuator Development, IEEE International Conference on Power and Energy (PECon 2012), Sabah, Malaysia, pp. 933-938, 2012.
- (2.16) M. Norhisam, M. Norafiza, F. Azhar, NF. Mailah, H. Wakiwaka, M. Nirei, Optimization of Pole Numbers and Rotor Size for a Single Phase Slot-less Permanent Magnet Generator, International Review of Electrical Engineering (I.R.E.E.), Vol. 6, No. 5, pp. 2253 – 2260, 2011.
- (2.17) M. Norafiza, Design and Analysis of a Single and Double Stator of Single Phase Slotless Permanent Magnet Generator, MSc. Thesis, University Putra Malaysia, 2009.
- (2.18) R. Suhairi, Design and Analysis of Double Stator Permanent Magnet Generator for Palm Oil Mechanical Cutter Application, MSc. Thesis, University Putra Malaysia, 2010.
- (2.19) M. Norhisam, R. Suhairi , M. Norafiza, MAM. Radzi, I. Aris, M. Nirei and H. Wakiwaka, Comparison on Performance of a Single Phase and Three Phase Double Stator Type Permanent Magnet, Asia Pacific Symposium of Applied Electromagnetics and Mechanics (APSAEM2010) Kuala Lumpur, Malaysia, pp. 231 – 234, 2010.
- (2.20) M. Norhisam, K. Alias, RN. Firdaus, S. Mahmud and N. Mariun, Comparison on Thrust Characteristic of Linear of Actuators, IEEE International Conf. on Power and Energy Conference, 2006. PECon '06. pp. 470 – 475, 2006.
- (2.21) M. Norhisam, RN. Firdaus, F. Azhar, N. Mariun, I. Aris, J. Abdul Razak and H. Wakiwaka, Analysis of Thrust Constant, Electrical and Mechanical Time Constant for Slot-Less Moving Magnet Linear Oscillatory Actuator, Journal of the Japan Society of Applied Electromagnetics and Mechanics (JSAEM), Vol.17, Supplement, pp. S41 – S44, 2009.
- (2.22) M. Norhisam , RN. Firdaus, F. Azhar, N. Mariun, I. Aris, J. Abdul Razak, The

- 
- Analysis on Effect of Thrust Constant, Spring Constant, Electrical Time Constant, Mechanical Time Constant, to Oscillation Displacement of Slot-Less Linear Oscillatory Actuators, 2<sup>nd</sup> IEEE International Conf. on Power and Energy (PECon 2008), Johor Bahru, Malaysia, pp. 1076 - 1081, 2008.
- (2.23) M. Norhisam, F. Azhar, R.N. Firdaus, H. Hashim, M. Nirei, H. Wakiwaka and J. Abdul Razak, Effect of Spring Constant and Thrust Constant to Displacement Characteristics of LOA, Journal of the Japan Society of Applied Electromagnetics and Mechanics (JSAEM), Vol.17 No.3, pp. 437 – 440, 2009.
- (2.24) M. Norhisam, K. Alias , F. Azhar, RN. Firdaus, SM. Bashi, N. Mariun and J. Abdul Razak, Design of Linear Oscillatory Actuator for High Thrust Characteristics by Adjusting the Taper Parameters, Journal of Industrial Technology, Vol. 18 No. 2, pp. 13-23, 2009.
- (2.25) F. Azhar, M. Norhisam, NF. Mailah, MR. Zare, H. Wakiwaka and M. Nirei, Thrust Optimization of Linear Oscillatory Actuator Using Permeance Analysis Method, International Review of Electrical Engineering (I.R.E.E.), Vol. 6, No. 7, pp. 2929 – 2938, 2011.
- (2.26) Y. Bong Bang and K. Min Lee, Large thrust linear motors for low-duty-cycle operation, Mechatronics 14, pp. 891-906, 2004.
- (2.27) TH. Lee, KK. Tan, SN. Huang and HF. Dou, Intelligent control of precision linear actuators, Engineering Applications of Artificial Intelligence 13, pp. 671- 684, 2000.
- (2.28) M. Backman, A Comparison of Linear Motor and Rotary Servo Motor Systems, Small Motors and Motion Association (SMMA) Fall Technical Conference, 2005.
- (2.29) DG. Dorrell, Are wound-rotor synchronous motors suitable for use in high efficiency torque-dense automotive drive?, 38<sup>th</sup> Annual conference on IEEE Industrial Electronics Society, pp. 4880-4885, 2012.
- (2.30) M. Norhisam, H. Ezril, F. Azhar, RN. Firdaus, H. Wakiwaka and M. Nirei, Positioning System for Sensor Less Linear DC Motor, Journal of the Japan Society of Applied Electromagnetics and Mechanics (JSAEM), Vol.19, Supplement, pp. S91 – S94, 2011.
- (2.31) I. Boldea and SA. Nasar, Linear electric actuators and generators, Cambridge University Press, 1997.
- (2.32) AH. Toliyat and GB. Kliman, Handbook of Electric Motors, CRC Press, 2004, ISBN 0824741056.
- (2.33) I. Husain and M. Ehsani, Torque ripple minimization in switched reluctance motor drives by PWM current control, IEEE Transactions on Power Electronics, Vol. 11(1), pp. 83 – 88, 1996.
- (2.34) KJ. Tseng and S. Cao, A SRM variable speed drive with torque ripple minimization control, 16<sup>th</sup> Annual IEEE Applied Power Electronics Conference and Exposition, APEC 2001, Vol. 2, pp. 1083 – 1089, 2001.
- (2.35) Y. Yamamoto and H. Yamada, Analysis of magnetic circuit and starting characteristics of flat-type linear pulse motor with permanent magnets, T. IEE

- 
- Japan, Vol. 104-B, No. 5, pp. 265 – 272, 1984.
- (2.36) ER. Laithwaite, Linear electric machines - A personal view, Proceedings of the IEEE Vol. 63(2), pp. 250 – 290, 1975.
- (2.37) DJ. de Groot and CJ. Heuvelman, Tubular linear induction motor for use as a servo actuator, Electric Power Applications, IEE Proceedings B, Vol. 137(4), pp. 273 – 280, 1990.
- (2.38) M. Sanada, Y. Takeda and T. Hiras, Cylindrical Linear Pulse Motor with Laminated Ring Teeth, Proceedings of the Second International Conference on Electronic Materials (ICEM '90), Vol. 2, pp. 693-698, 1990.
- (2.39) JF. Eastham, R. Akmese and H C. Lai, Optimum design of brushless tubular linear machines, IEEE Transactions on Magnetics, Vol. 26 (5), pp. 2547 - 2549, 1990.
- (2.40) J. Wang, GW. Jewell, D. Howe, Design optimisation and comparison of tubular permanent machine topologies, IEE Proceeding Electrical Power Applications, Vol. 148 (5), pp. 456 - 464, 2001.
- (2.41) HK. Bae, BS. Lee, P. Vijayranganhan, and R. Krishnan, A Linear Switched Reluctance Motor: converter and control, IEEE Transactions on Industry Application, Vol.36, pp. 1351 – 1359, 2000.
- (2.42) WC. Gan, NC. Cheung, and L. Qiu, Position control of linear switched reluctance motors for high-precision applications, IEEE Transactions on Industry Application, Vol.39, pp. 1350 – 1362, 2003.
- (2.43) BS. Lee, HK. Bae, P. Vijayranganhan, and R. Krishnan, Design of a linear switched reluctance machine, IEEE Transactions on Industry Application, Vol.36, pp.1571 – 1580, 2000.
- (2.44) CT. Liu and TS. Chiang, On the magnetic saturation analyses of a micro linear switched-reluctance motor, IEEE Transactions on Magnetics, Vol. 40 (4), Part 2, pp. 2861 – 2863, 2004.
- (2.45) F. Daldaban and N. Ustkoyuncu, A novel linear switched reluctance motor for railway transportation systems, Energy Conversion and Management 51, pp. 465–469, 2010.
- (2.46) YJ. Wang, YY. Sun, CC. Huang and MC. Tsai, Rotor position detection of switched reluctance motors using FM technique, IEEE International Conference on Control Applications, Vol . 2, pp. 939 – 944, 1999.
- (2.47) S. Oshima, S. Tahara and K. Ogawa, Thrust and thrust ripple of linear reluctance motor compared permanent linear synchronous motor, 15<sup>th</sup> Inter. Conf. on Electrical Machine and Systems (ICEMS), pp. 1-4, 2012.
- (2.48) T. Mizuno and H. Yamada, Magnetic circuit analysis of a linear synchronous motor with permanent magnets, IEEE Transactions Magnetics, Vol.28 No. 5, pp. 3027-3029, 1992.
- (2.49) NR. Tarana and V. Dinavani, Design of slotted permanent magnet linear

- 
- synchronous motor for improved thrust density, IEEE International Conference on Electric Machines and Drives, pp. 1225-1228, 2013.
- (2.50) S. Vaez-Zadeh and MS. Hosseini, Design optimization of linear synchronous motors for overall improvement of thrust, efficiency, power factor and material consumption, Journal of Power Electronics, Vol. 11 No, 1, pp. 105-111, 2011.
- (2.51) Z. Jinghong, Z. Xiaofeng and Z. Junhong, Analysis and study thrust ripple of PMSLM, International Conference on Electrical Machines and Systems, 2008 (ICEMS 2008), pp. 3439-3442, 2008.
- (2.52) GH. Jang, JW. Yoon, KC. Ro, NY. Park and SM. Jang, Performance of a brushless DC motor due to the axial geometry of the permanent magnet, IEEE Transactions on Magnetics, Vol. 33, No. 5, pp. 4101-4103, 1997.
- (2.53) IS. Jung, SB. Yoon, JH. Shim, and DS. Hyun, Analysis of forces in a short primary type and a short secondary type permanent magnet linear synchronous motor, IEEE Transactions on Energy Conversion, Vol. 14, No. 4, pp. 1265-1270, 1999.
- (2.54) K. Touzhu Li and G. Slemon, Reduction of cogging torque in permanent magnet motors, IEEE Transactions on Magnetics, Vol. 24, No. 6, pp. 2901-2903, 1988.
- (2.55) T. Yoshimura, HJ. Kim, M. Watada, S. Torii, and D. Ebihara, Analysis of the reduction of detent force in a permanent magnet linear synchronous motor, IEEE Transactions on Magnetics, Vol. 31, no. 6, pp. 3728-3730, 1995.
- (2.56) J. Abdul Razak, A. Desa, H. Ahmad, Y. Azmi and J. Johari, Force and Energy Requirements for Cutting Oil Palm Frond, Journal of Oil Palm Research Vol. 10 No. 2, pp. 10-24, 1998.
- (2.57) J. Abdul Razak, A. Desa, H. Ahmad, Y. Azmi and J. Johari, Reaction Force and Energy Requirements for Cutting Oil Palm Fronds by Spring Powered Sickle Cutter, Journal of Oil Palm Research Vol. 11 No. 2, pp. 114-122, 1999.
- (2.58) K. Hirata, Y. Kagami, M. Yanosaka, Y. Ishihari and T. Todaka, Thrust Calculation Of Linear Pulse Motors Using A Combined Technique Employing The Finite Element Method And The Permeance Analysis Method, IEEE Transactions On Magnetics, Vol. 28, No. 2, pp 1394-1397, 1992.
- (2.59) J. Farooq, S. Srairi, A. Djerdir and A. Miraoui, Use of Permeance Network Method in the Demagnetization Phenomenon Modeling in a Permanent Magnet Motor, IEEE Transactions on Magnetics, Vol. 42, No. 4, pp. 1295 – 1298, 2006.
- (2.60) J. Rizk and M. Nagrial, Design of permanent-magnet generators for wind turbines, Australasian Universities Power Engineering Conference (AUPEC), University of Northern Territory, pp. 208-212, 1999.
- (2.61) AT. Hamid and BK. Gerald Handbook of Electric Motor, 2<sup>nd</sup> Edition, Marcel Dekker Inc., USA, 2004.
- (2.62) J. Chang, D. H. Kang, I.-A. Viorel, and S. Larisa, Transverse Flux Reluctance

- 
- Linear Motor's Analytical Model Based on Finite-Element Method Analysis Results, IEEE Trans. on Magnetics, Vol. 43, No. 4, pp. 1201-1204, 2007.
- (2.63) D. Petrichenko, M. Hecquet, P. Brochet, V. Kuznetsov and D. Laloy, Design and Simulation of Turbo-Alternators Using a Coupled Permeance Network Model, IEEE Trans. On Magnetics, Vol. 42, No. 4, pp. 1259 – 1262, 2006.
- (2.64) C. Delforge and B. Lemaire-Semail, Induction Machine Modeling Using Finite Element and Permeance Network Methods, IEEE Transactions On Magnetics, Vol. 31, No. 3, pp. 2092-2095, 1995.

---

## Chapter 3: Design and Development of the Switched Reluctance Cylindrical Linear Synchronous Motor (SRCLSM)

### 3.1 Initial Structure Parameter of the SRCLSM

Previously, SRLSM was never tried to be implemented as the E-Cutter's actuator. It is due to the SRLSM is known having lower performance characteristics compared to the PMLSM. However, because of absence of permanent magnet, the SRLSM performance does not affect by temperature rise. Therefore, thrust can be increase by injecting higher current to the SRLSM's coil. Furthermore, recently the Switched Reluctance Motor has been achieved similar performance compared to the Permanent Magnet Motor<sup>(3.1)</sup>. This factor has been importance motivation to design a SRCLSM for the E-Cutter's actuator.

The design of the SRCLSM starts from its basic design to observe feasibility of the SRCLSM as the E-Cutter's actuator. As discussed in the previous chapter, the major drawback of the SRLSM is high thrust ripple<sup>(3.2)</sup>. One of techniques can be used to reduce the thrust ripple is through mechanical design and geometrical optimization<sup>(3.3)-(3.5)</sup>. However, as the first stage of the SRCLSM design, a multiphase structure topology was used to be implemented in order to reduce thrust ripple<sup>(3.6)</sup>. Despite of possibility of reducing the thrust ripple, the multiphase structure topology also come with several advantages such as reducing rotor harmonic current<sup>(3.7), (3.8)</sup> and phase current without increasing phase voltage<sup>(3.7), (3.9)</sup>, lowering the DC link current harmonic<sup>(3.7)</sup>, higher reliability and fault tolerance<sup>(3.7)-(3.9)</sup>.

In this research, a 6 phase topology has been adopted to be implemented in SRCLSM structure. The outer dimension of the SRCLSM's stator was limited to  $\phi 40$  mm (diameter)  $\times$  150 mm (length). Therefore, each phase stator length are limited to 25 mm. Based on this consideration, the 6 phase SRCLSM outline structure can be depicted as Figure 3.1. There are two styles of six phase structure topology. First style is the traditional six phase structure topology where each stators phase is shifted  $60^\circ$  as shown in Figure 3.2 (a). By implementing this structure topology, a low

thrust ripple,  $\Delta F$  is feasible to produce. Second style is a combination of two sections of 3 phase structure topology. In order to create a six phase structure, the second section of 3 phase structure is shifted half of teeth pitch,  $\tau_p$  compared to the first section as shown in Figure 3.2 (b). Besides improving the thrust ripple,  $\Delta F$ , implementation of this structure also capable to increase the thrust of SRCLSM.

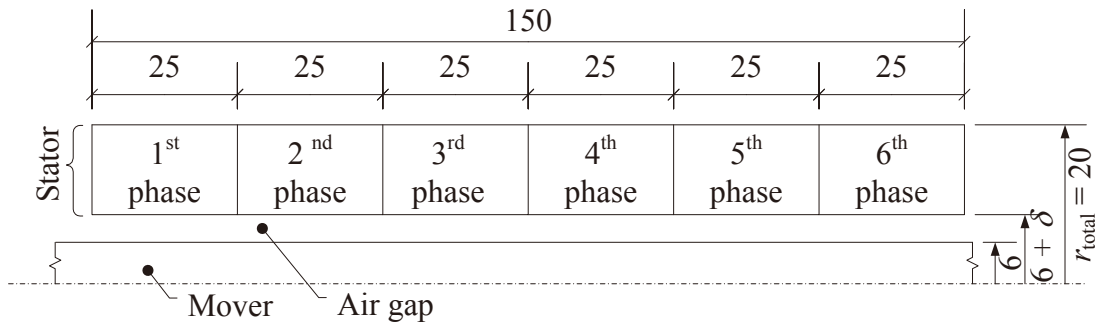


Figure 3.1 Outline structure of the six phase SRCLSM (unit : mm).

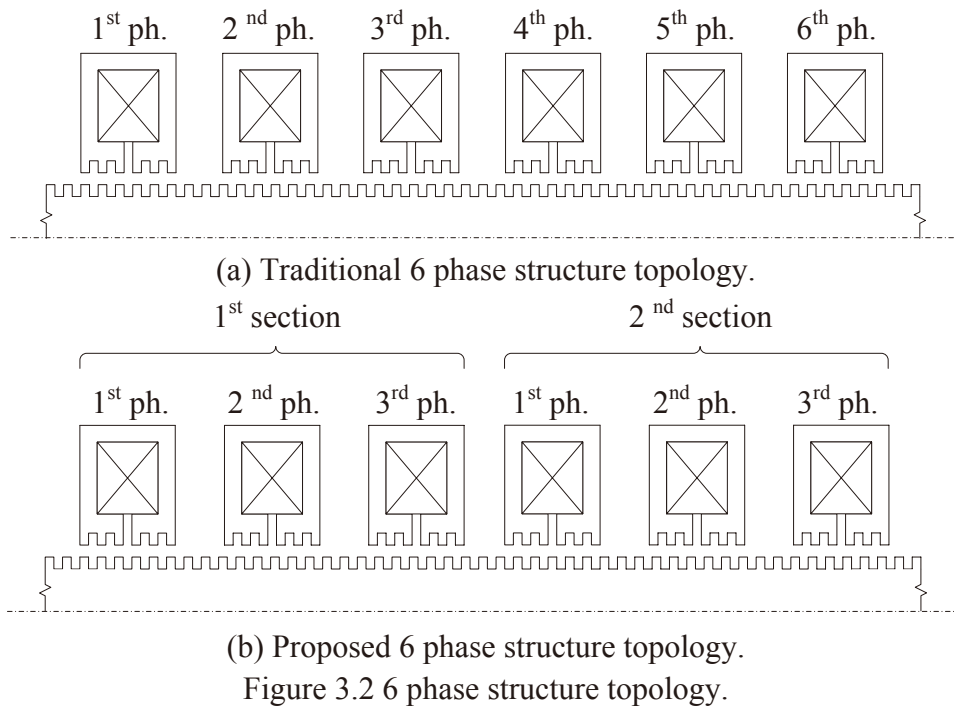


Figure 3.2 6 phase structure topology.

The sample of thrust characteristics of those two structure topologies are as shown in Figure 3.3. It is shown that, the proposed 6 phase structure topology improved thrust ripple compared to the traditional 6 phase structure topology from 17.9 % to 16.0 %. On top of that, the average thrust of proposed structure also

increased from 11.4 N to 19.8 N. It is shown capability of proposed 6 phase structure topology to improved thrust characteristics of the SRCLSM.

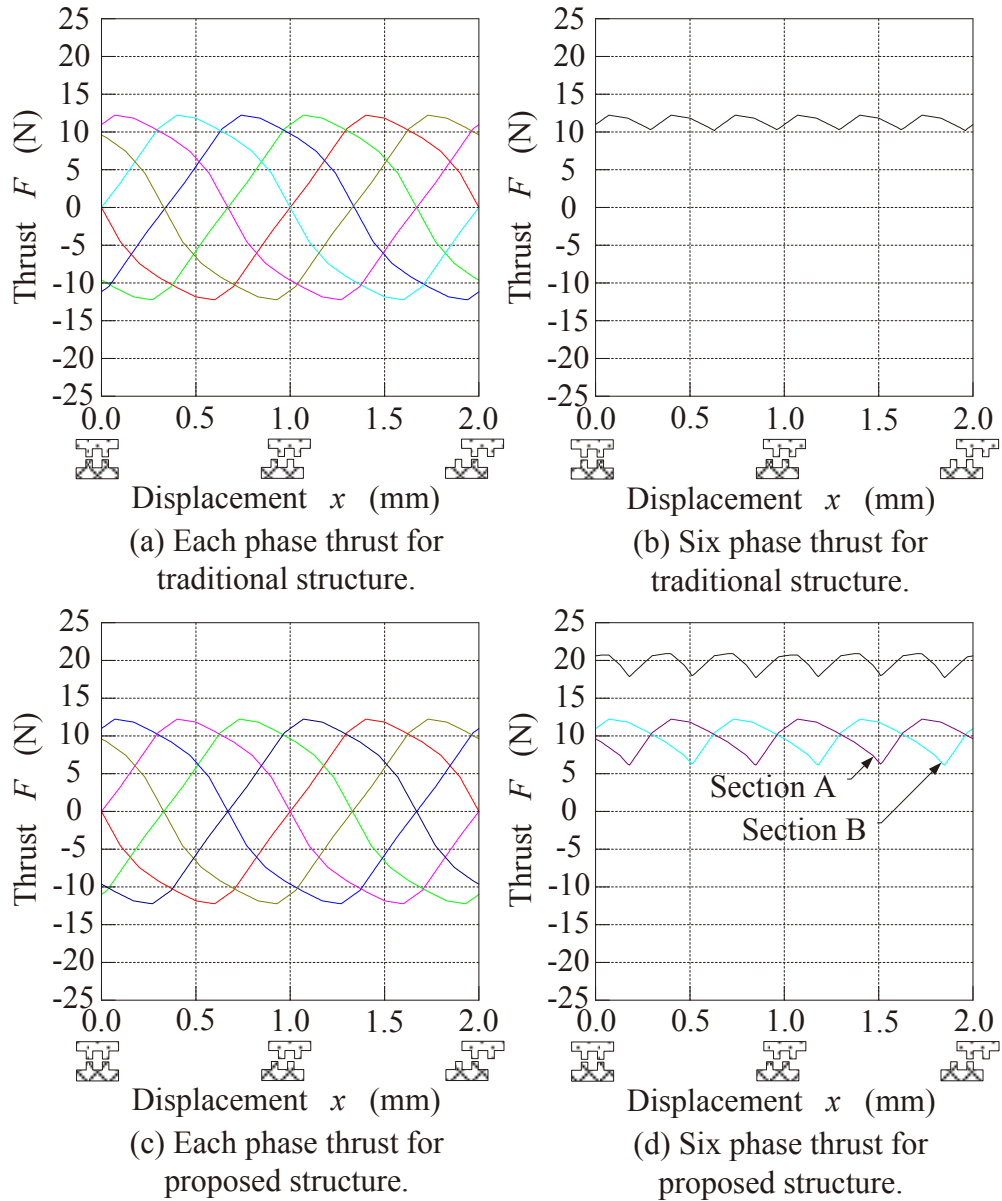


Figure 3.3 6 phase thrust characteristic.

Each phase stator can be designed either with single coil or multiple coils. In this research, only either single or double coil structure is considered. Initially, the air gap length,  $\delta$  of the SRCLSM was fixed to 0.1 mm. In order to make a valid comparison between the single and double coil structure, the total turns of each phase has been fixed to 672 turns. Figure 3.4 shows the comparison between single and double coil structure and the simulation setting is as shown in Table 3.1. Figure 3.5 shows comparison of thrust characteristics between single and double coil structure. It is shown that, the double coil structure of SRCLSM produced higher thrust at similar

current. Furthermore, the double coil structure has higher saturated thrust compared to single coil structure.

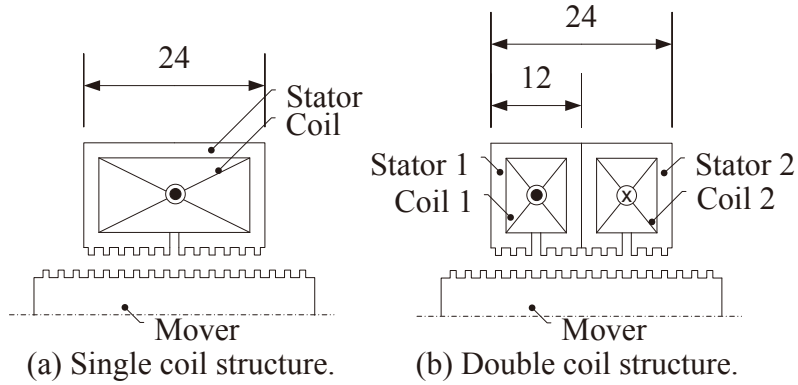


Figure 3.4 Comparison of single and double coil structure (unit : mm).

Table 3.1 : Simulation setting for SRCLSM.

No.	Parameter	Value	
		Single coil	Double coil
1	Coil turns (each coil)	672	336
2	Resistance, $R$ (each coil) ( $\Omega$ )	8.7	6.5
3	Copper wire dia., $\phi_C$ (mm)	0.37	0.32
4	Current, $I$ (A)	0.1 – 1.5	
5	Air gap length, $\delta$ (mm)	0.1	

Figure 3.6 shows the teeth parameter of the SRCLSM. Generally, the ratio between teeth width,  $t_w$  and teeth pitch,  $\tau_p$  is set to 0.5<sup>(3.10) – (3.12)</sup>. However, as discussed in<sup>(3.13)</sup>, the optimized ratio of teeth width,  $t_w$  and teeth pitch,  $\tau_p$  is in range of 0.38 to 0.45. Furthermore, several researchers used the ratio between teeth width,  $t_w$  and teeth pitch,  $\tau_p$  equal to 0.40<sup>(3.14), (3.15)</sup> and 0.45<sup>(3.16), (3.17)</sup>. Therefore, in order to determine the teeth width,  $t_w$  and teeth pitch,  $\tau_p$  of the SRCLM, a simple simulation was carried out. The teeth pitch,  $\tau_p$  was selected as 2 mm and three different teeth width,  $t_w$  which are 0.76 mm (0.38), 0.80 mm (0.40) and 0.90 mm (0.45) were set. Maximum thrust,  $F_{\max}$  and total harmonic distortion of thrust,  $THD_F$  then were observed.

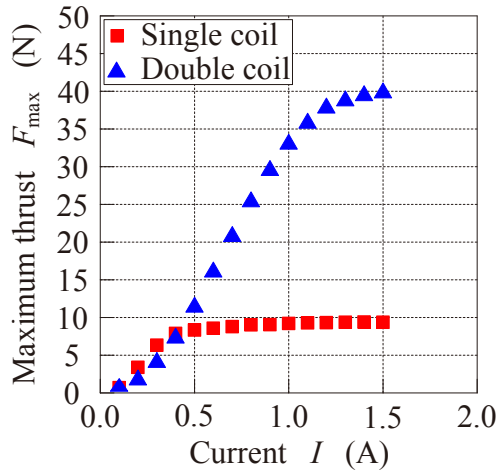
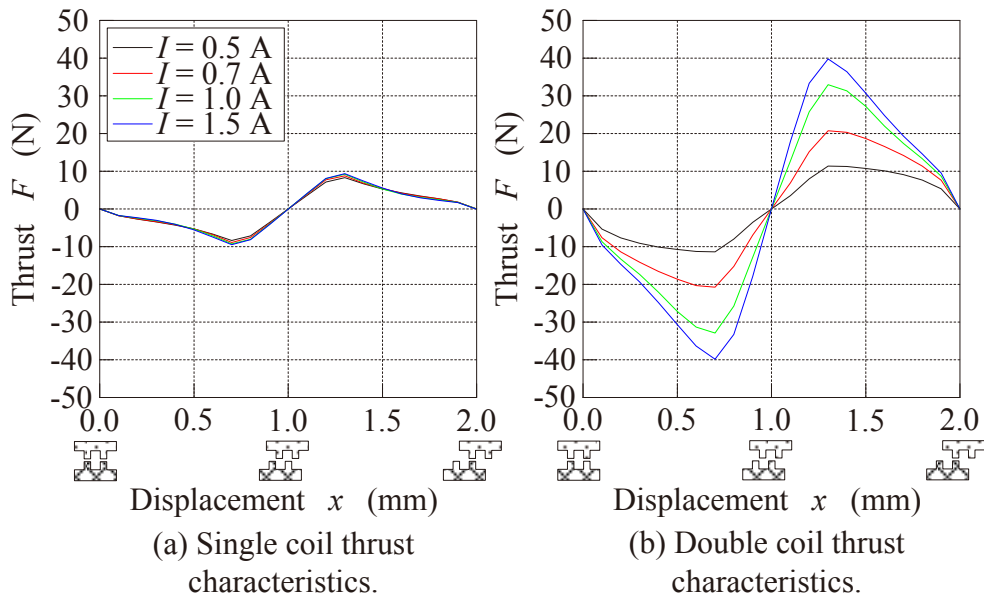


Figure 3.5 Comparison of thrust characteristics between single and double coil structure.

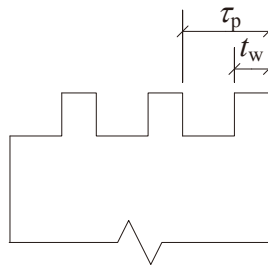


Figure 3.6 Teeth parameter of the SRCLSM.

Figure 3.7 shows the thrust characteristics, maximum thrust,  $F_{\max}$  and total harmonic distortion of thrust,  $THD_F$  of the SRCLM with difference teeth width,  $t_w$ . Based on Figure 3.7, it is shows that, the teeth width,  $t_w$  of 0.80 mm (0.40) gives

highest maximum thrust,  $F_{\max}$  compare to other models. Furthermore, with teeth width,  $t_w$  of 0.80 mm (0.40) as well have lowest total harmonic distortion of thrust,  $THD_F$ . It is shows that, the SRCLM with teeth width,  $t_w$  of 0.80 mm (0.40) not only have a capability to produce highest thrust, however, it also could result relatively low ripple thrust due to the lowest total harmonic distortion of thrust,  $THD_F$  compare to other models.

Base on the above discussion in Figure 3.8 shows the initial structure parameter of the six phase SRCLSM. In order to ease the manufacturing process, the symmetrical model of stator is used. The length of each phase stator and coil pitch was set to 24 and 12 mm respectively. Therefore, the total stator length by considering as well the distance between each phase stator has become 148.32 mm.

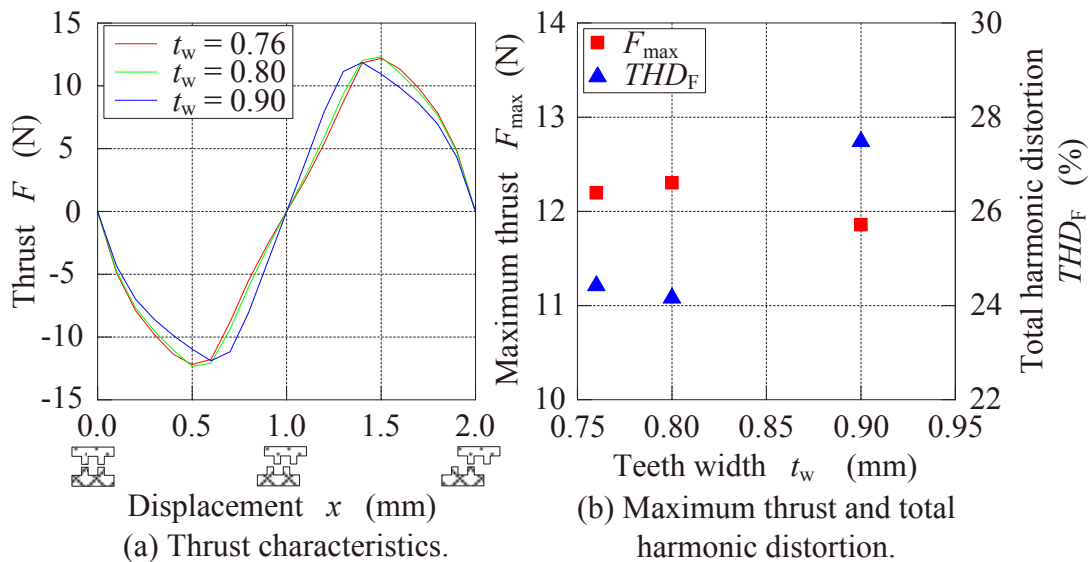


Figure 3.7 Performance comparison of the SRCLSM with different teeth width,  $t_w$ .

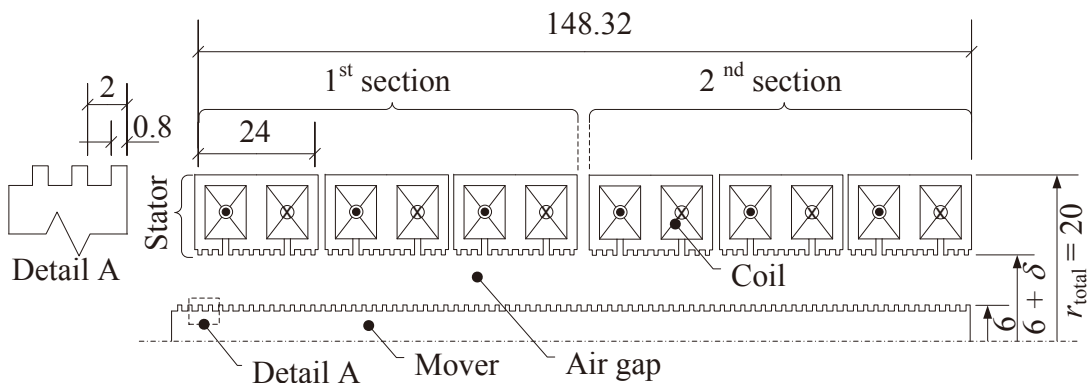


Figure 3.8 Initial structure parameter of the six phase SRCLSM (unit : mm).

### 3.2 Effect of air gap's length and teeth pitch to the SRCLSM thrust

The initial structure parameter of the SRCLSM has been proposed as shown in Figure 3.8. However, the optimized teeth pitch,  $\tau_p$  is depends on the air gap length,  $\delta$ . Therefore, the effect of the air gap length,  $\delta$  and the teeth pitch,  $\tau_p$  to the SRCLSM's thrust need to be established. The air gap's length,  $\delta$  and teeth pitch,  $\tau_p$  of the SRCLSM was varied from 0.1 mm to 0.5 mm and 1 mm to 4 mm respectively. At teeth pitch,  $\tau_p$  of 5 mm, the shape of stator will be unsymmetrical. The ratio of teeth width,  $t_w$  and teeth pitch,  $\tau_p$  was fixed to 0.40 as this ratio is the optimized ratio as discussed previously. The total radius of the SRCLSM was fixed to 20 mm. In this stage, only single phase structure of the SRCLSM was used. Figure 3.9 shows the SRCLSM structure with different teeth pitch,  $\tau_p$ . The thrust characteristics of the SRCLSM was simulated with current,  $I$  from 0.1 A to 2.0 A. In order to make valid comparison, the coil parameter of each model has been fixed. Table 3.2 shows the coil setting that has been used.

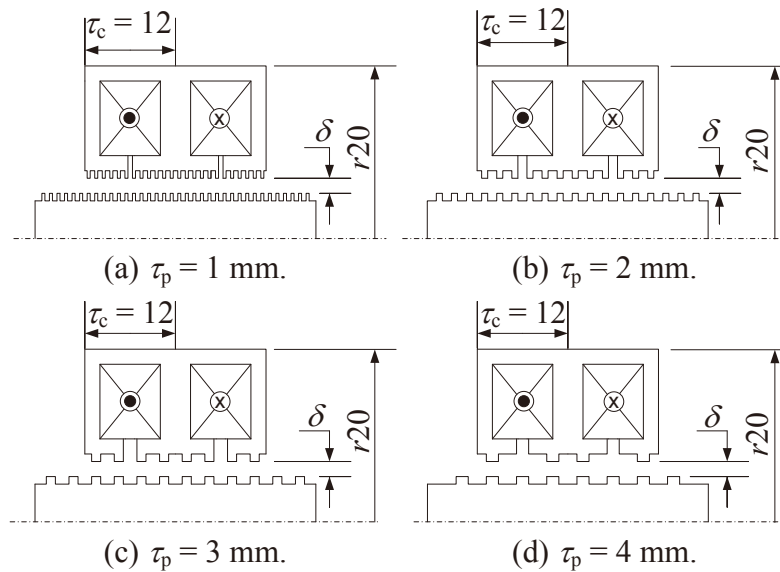


Figure 3.9 Single phase SRCLSM with different teeth pitch,  $\tau_p$  (unit : mm).

Table 3.2 : Coil settings for the SRCLSM.

No	Parameter	Value
1	Coil turns	336
2	Coil resistance ( $\Omega$ )	6.5
3	Copper wire diameter (mm)	0.32
4	Excitation current (A)	0.1–2.0

The stator material of the SRCLSM was set to SS400. The SS400 is one type of ferromagnetic material. It has high magnetic field saturation,  $B_r$ . Therefore, it is suitable to be used as the stator's material of the SRCLSM. The mover will be constructed in long cylindrical shape. Therefore, a strong material is needed due to withstand force produced by the SRCLSM especially in radial axis. A S45C material was suggested to be used as the mover. Even though the magnetic property is slightly low compared to SS400 material, however, it has stronger in terms of its mechanical property. It is shown in Table 3.3 where the S45C material has better characteristics of tensile and yield strength compared to the SS400 material. Figure 3.10 shows comparison between SS400 and S45C  $BH$  curve.

Table 3.3 : Mechanical properties comparison between SS400 and S45C material.

No	Mechanical property	SS400	S45C
1	Density, $\rho$ (kg/m <sup>3</sup> )	7860	7700-8030
2	Young Modulus, $E$ (GPa)	190-210	190-210
3	Tensile Strength, $\sigma_t$ (MPa)	400-510	569 (Standard) 686 (Quenched, tempered)
4	Yield Strength, $\sigma_y$ (MPa)	205-245	343 (Standard) 490 (Quenched, tempered)
5	Poisson ratio, $\nu$	0.26	0.27-0.30

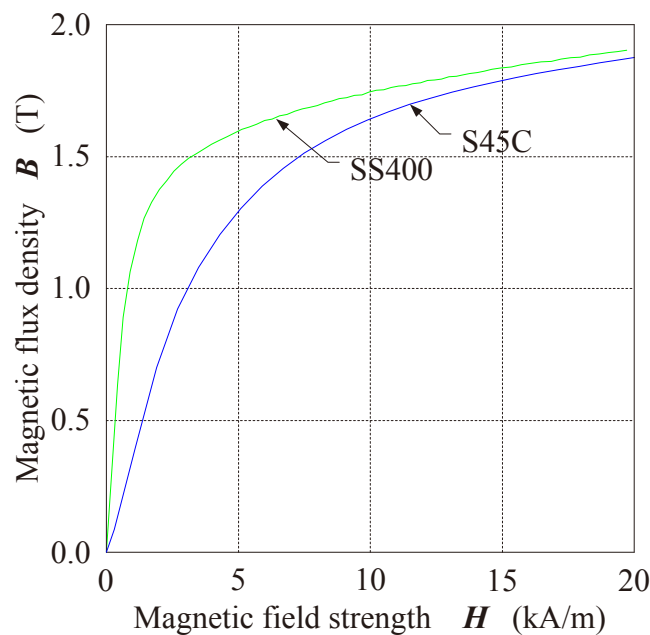


Figure 3.10 Comparison between material's  $BH$  curve.

Figure 3.11 shows sample of the SRCLSM thrust characteristics. Based on the thrust characteristics of the SRCLSM, the maximum thrust was identified. By referring to Figure 3.11, it is shown that, within same of teeth pitch,  $\tau_p$ , higher air gap length,  $\delta$  produce lower thrust. Figure. 3.11 (b) shows the thrust comparison of the SRCLSM with difference teeth pitch,  $\tau_p$  at air gap length,  $\delta$  of 0.1 mm. It is shows that, the maximum thrust of the SRCLSM with teeth pitch,  $\tau_p$  of 1 and 2 mm are similar. For higher teeth pitch,  $\tau_p$ , the maximum thrust is reducing.

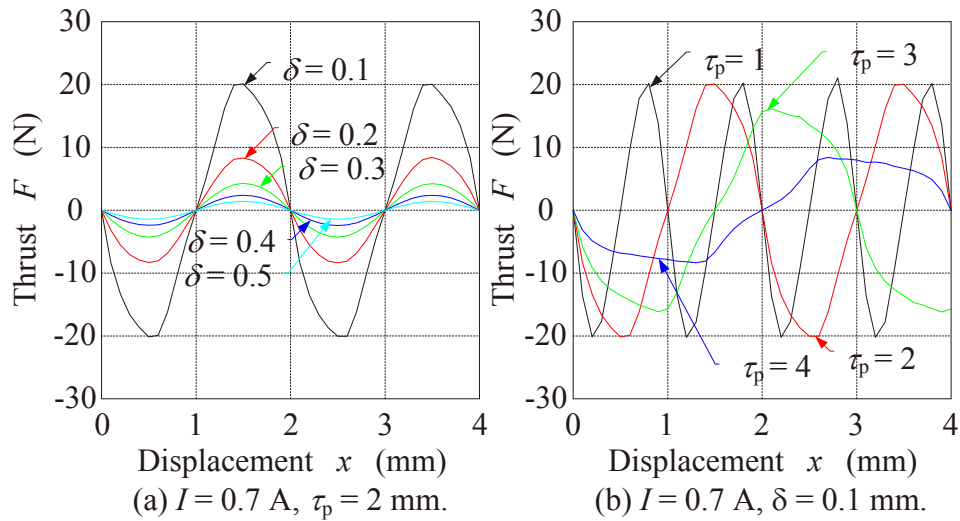


Figure 3.11 Sample of single phase thrust characteristics of the SRCLSM.

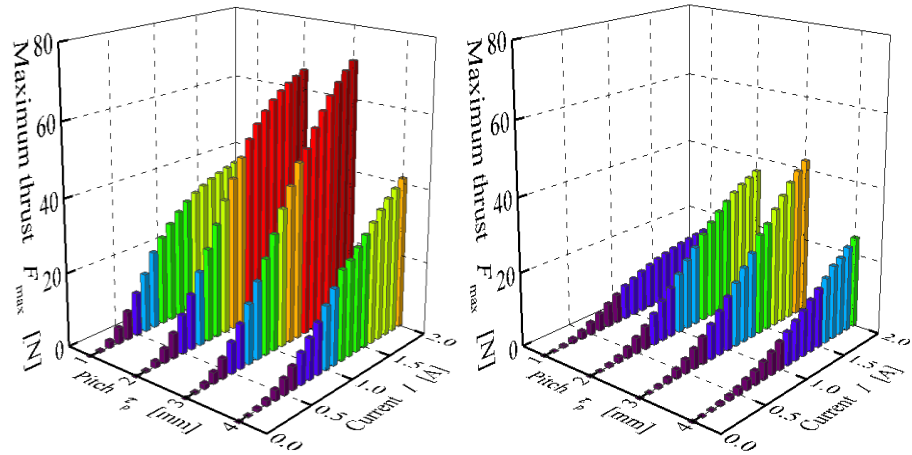
The maximum thrust of the SRCLSM of all models is as shown in Figure 3.12. As shown in in Figure 3.12, the maximum thrust of the SRCLSM will increase as the current is increased. The maximum thrust of the SRCLSM is seemed to be saturate only for the SRCLSM models with teeth pitch,  $\tau_p$  of 1mm. For other structure parameters, the SRCLSM, the thrust is not saturated. On the other hand, the maximum thrust of teeth pitch,  $\tau_p$  of 3 mm is found higher especially at current,  $I$  of 2 A regardless the air gap length,  $\delta$ . On the other hand, the higher air gap length,  $\delta$  made lower thrust will be produced.

Figure 3.13 shows the maximum thrust,  $F_{max}$  of all the SRCLSM models at current,  $I$  of 0.7 A. As shown in Figure. 3.13, the effect of air gap lengths,  $\delta$  at similar teeth pitches,  $\tau_p$  to the maximum thrust is clearly shows. However, the effect teeth

pitches,  $\tau_p$  on similar of air gap lengths,  $\delta$  to the maximum thrust is varies on air gap length,  $\delta$ . For example, on air gap length,  $\delta$  of 0.1 mm, teeth pitch,  $\tau_p$  of 1 mm gives highest maximum thrust,  $F_{\max}$  at 0.7 A compared to on air gap length,  $\delta$  of 0.2 mm, teeth pitch,  $\tau_p$  of 2 mm gives highest maximum thrust,  $F_{\max}$  at similar current. Table 3.4 shows the teeth pitch,  $\tau_p$  on specific air gap length,  $\delta$  that produce the first and second order of maximum thrust,  $F_{\max}$  at current,  $I$  of 0.7 A.

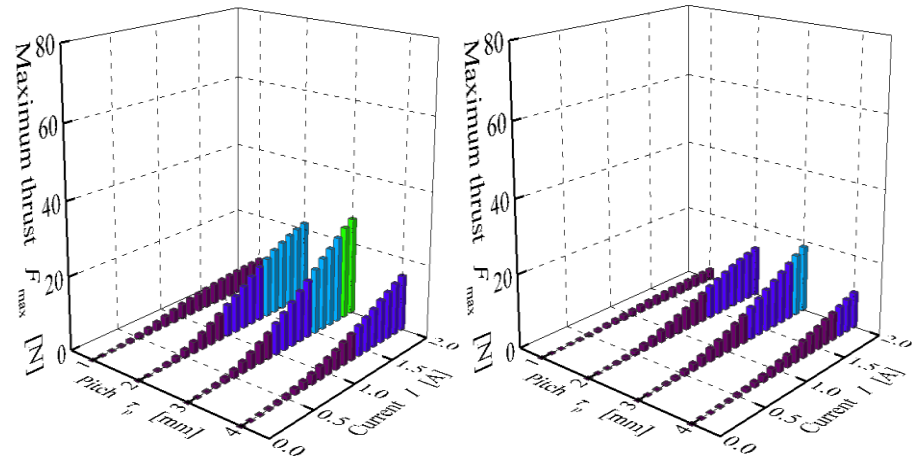
Table 3.4 : First and second order of maximum thrust,  $F_{\max}$  for each air gap length,  $\delta$  and corresponding teeth pitch,  $\tau_p$ .

No	Air gap length, $\delta$ (mm)	Teeth pitch, $\tau_p$ (mm)	Maximum thrust, $F_{\max}$ (N)
1	0.1	1	21.0
		2	20.1
2	0.2	2	8.4
		3	7.2
3	0.3	2	4.3
		3	4.1
4	0.4	2	2.4
		3	2.6
5	0.5	2	1.4
		3	1.7



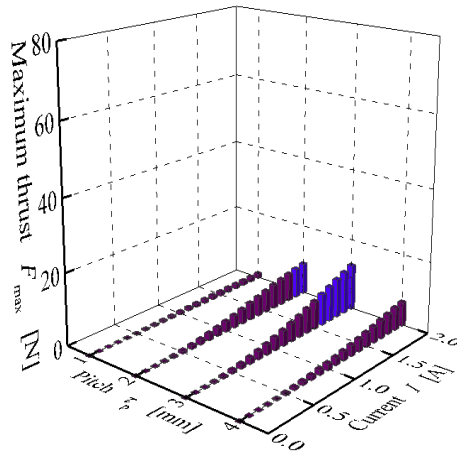
(a)  $\delta = 0.10$  mm.

(b)  $\delta = 0.20$  mm.



(c)  $\delta = 0.30$  mm.

(d)  $\delta = 0.40$  mm.



(e)  $\delta = 0.50$  mm.

Figure 3.12 Maximum thrust,  $F_{\max}$  of the SRCLSM.

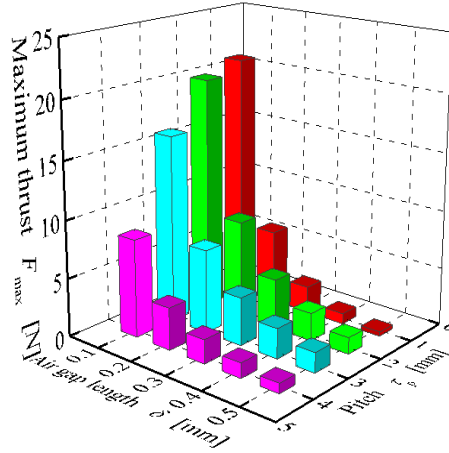


Figure 3.13 Maximum thrust of all the SRCLSM models at  $I = 0.7$  A.

### 3.3 Estimation and comparison of the SRCLSM six phase performance

Based on the single phase thrust, the six phase thrust of the SRCLSM could be estimated. From this stage, only the best model of the SRCLM at each air gap length,  $\delta$  is considered. However, for the air gap length,  $\delta$  of 0.1 mm, the height maximum thrust,  $F_{max}$  was obtained on teeth pitch,  $\tau_p$  of 1 mm. Based on Figure 3.12 (a), the SRCLSM with teeth pitch,  $\tau_p$  of 1 mm has a lower saturated maximum thrust,  $F_{max}$  compared to the SRCLSM model with teeth pitch,  $\tau_p$  of 2 mm. Therefore, for the SRCLSM with air gap,  $\delta$  of 0.1 mm, teeth pitch,  $\tau_p$  of 2 mm will be used to estimate the six phase performance of the SRCLSM. On the other hand, for other air gap length,  $\delta$  models, the teeth pitch,  $\tau_p$  that produced highest maximum thrust,  $F_{max}$  will be used.

Each phase of the SRCLSM has 2 coils. In order to increase the current response, a parallel connection will be used. Figure 3.14 shows the schematic diagram of each phase of the SRCLSM's coils. If each coils need to be excite by 0.7 A to produce similar thrust as previous result and considering the resistance of each coils is  $6.5 \Omega$ , each phase need a 4.55 V input voltage.

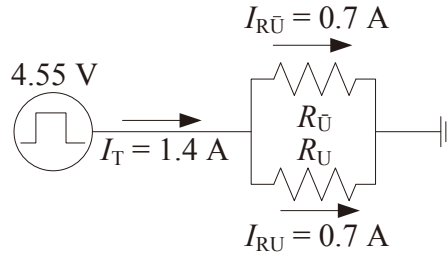


Figure 3.14 Connection of the SRCLSM coils.

By assuming each phase of the SRCLSM is excited using step voltage and current, with an appropriate excitation sequence as shown in Figure 3.15, the six phase thrust characteristics can be estimated as shown in Figure 3.16. Figure 3.16 shows the sample 6 phase thrust characteristics of SRCLSM at air gap length,  $\delta$  of 0.1 mm and teeth pitch,  $\tau_p$  of 2 mm. Based on the six phase thrust characteristics as shown in Figure 3.16, the average thrust,  $F_{ave}$  of the SRCLSM is 32.6 N. Since Each coils phase of the SRCLSM was connected parallel and considering the pulse excitation sequence, the total power consumption,  $P_T$  of the SRCLSM can be calculated using,

$$\begin{aligned}
 P_T &= 6 \times I_{\text{phase,rms}} \times V_{\text{phase,rms}} \\
 &= 6 \times \left( \sqrt{\frac{1}{x_T} \int_0^{x_T} i^2(t) dt} \right) \times \left( \sqrt{\frac{1}{x_T} \int_0^{x_T} v^2(t) dt} \right) \quad (3.1) \\
 &= 6 \times 0.81 \times 2.63 \\
 &= 12.78 \text{ W}.
 \end{aligned}$$

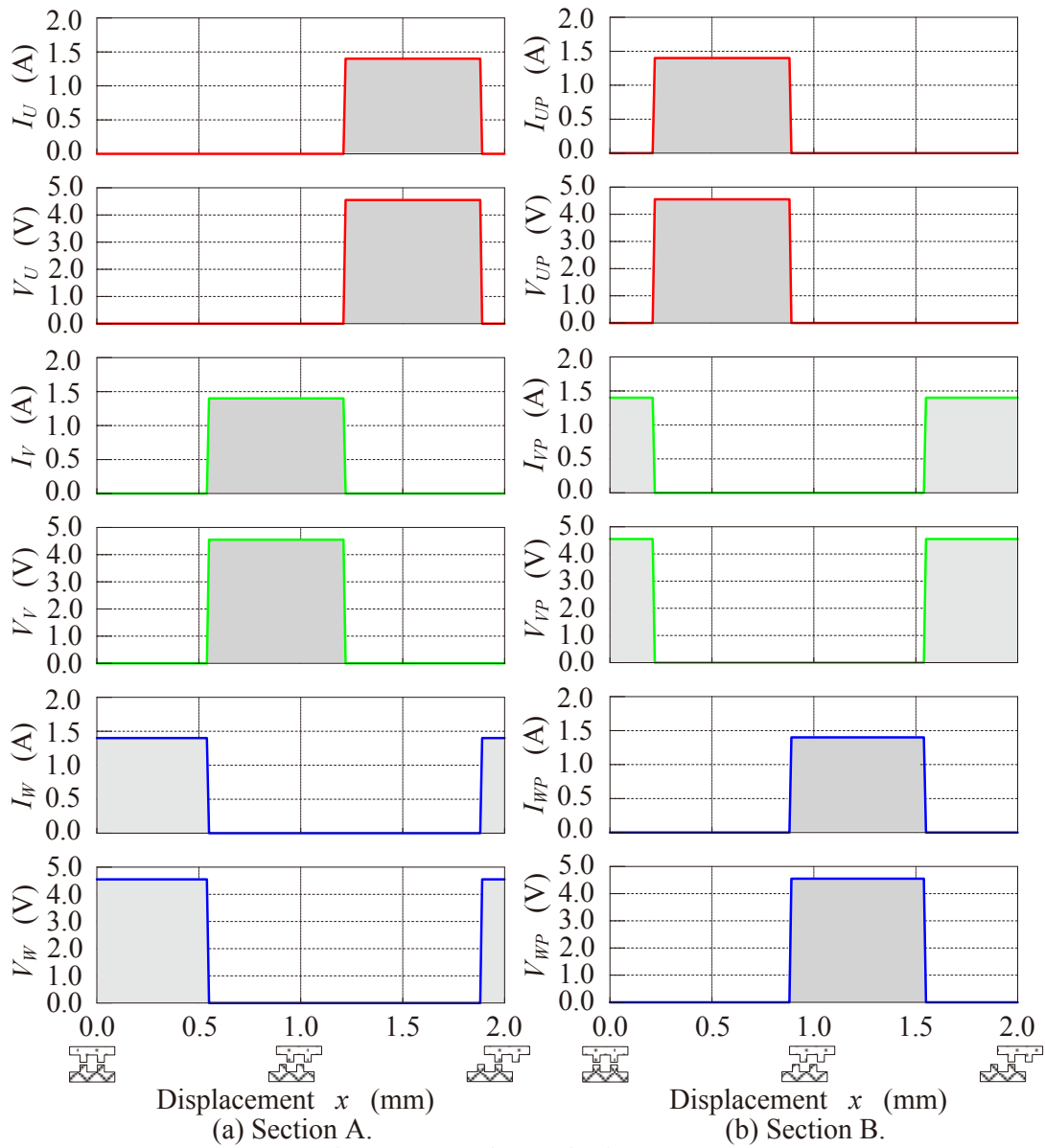


Figure 3.15 Pulse excitation sequence.

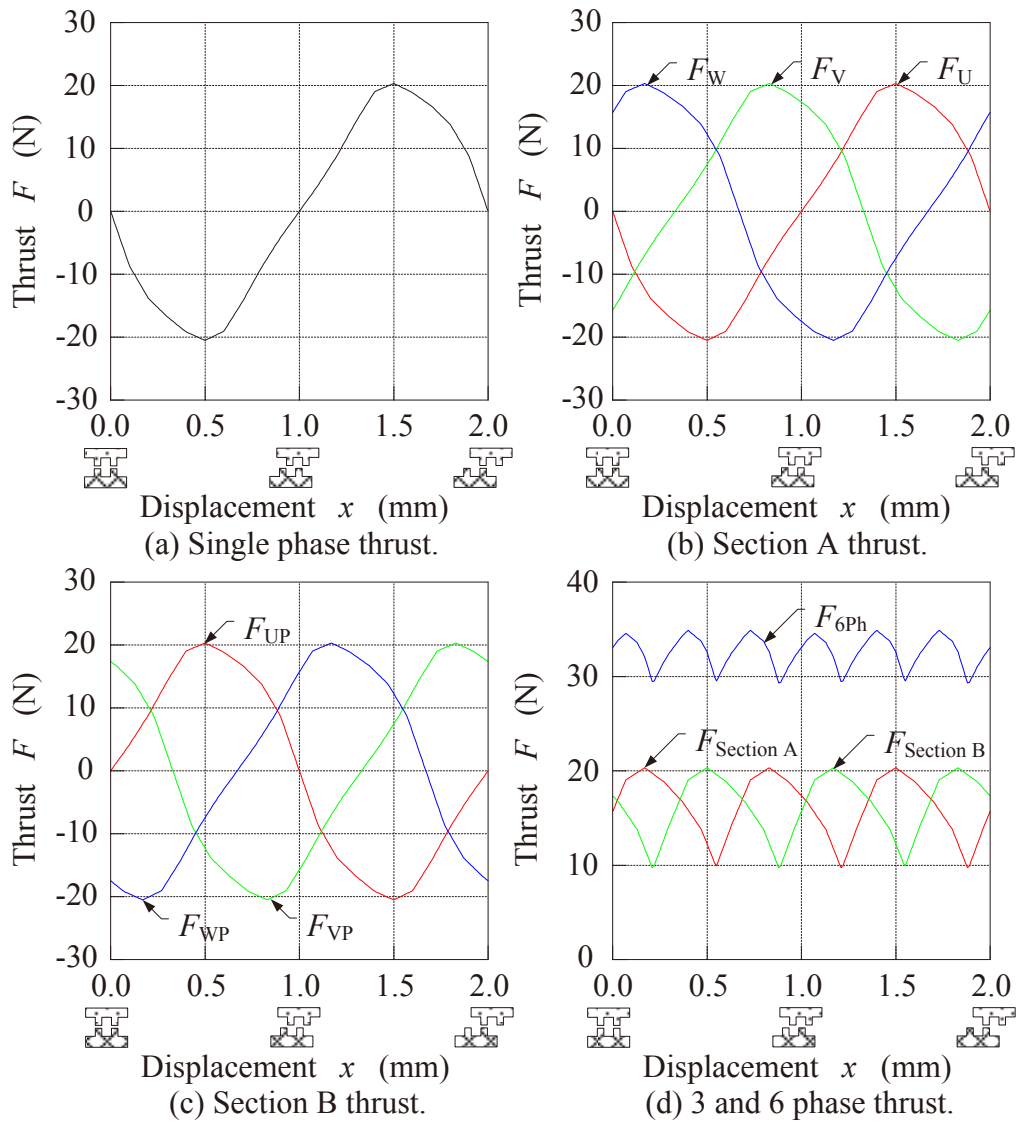


Figure 3.16 Single, three and six phase thrust characteristics of the SRCLSM.

Performance of the SRCLSM was evaluated using its thrust and performance index as discussed in Chapter 2. The comparison of performance index among the SRCLSM models is as shown in Figure 3.17. Since the increment of the air gap length,  $\delta$  made a decrement of the average thrust,  $F_{ave}$ , the other performance parameter is decreased as well. Based on Figure 3.17, it is shown that, the SRCLSM with air gap length,  $\delta$  of 0.1 mm gives the highest performance. Since the air gap length,  $\delta$  is the smallest compared to other models, it made the total magnetic resistance become low and allowed higher magnetic flux to be induced, thus producing higher thrust.

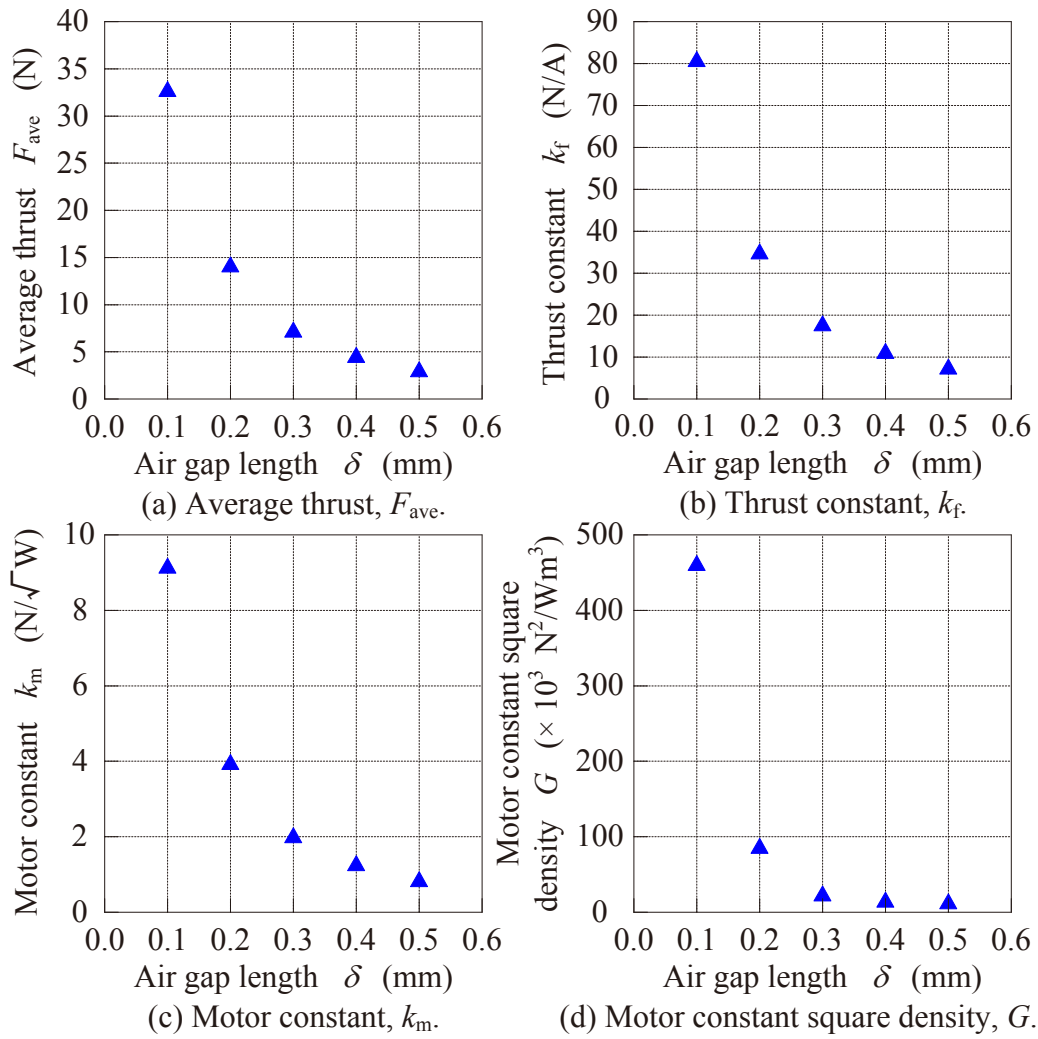


Figure 3.17 Performance comparison of the SRCLSM with optimized teeth pitch,  $\tau_p$  and difference air gap length,  $\delta$ .

The performance of the SRCLSM with air gap length,  $\delta$  of 0.1 mm was then compared to several type of commercialized PMLM performance using similar performance index. The performance comparison is as shown in Figure 3.18. All the performance characteristics were plotted against their volume,  $V_{mot}$ . Based on the Figure 3.18, it is shown that, the SRCLSM is having a capability to produce higher performance at similar volume,  $V$  compared to PMLM. The SRCLSM is also seen having capability to produce higher thrust,  $F$  at smaller size and lower input power,  $P_{in}$  compared to the commercialized PMLM as shown in Figure 3.18 (d).

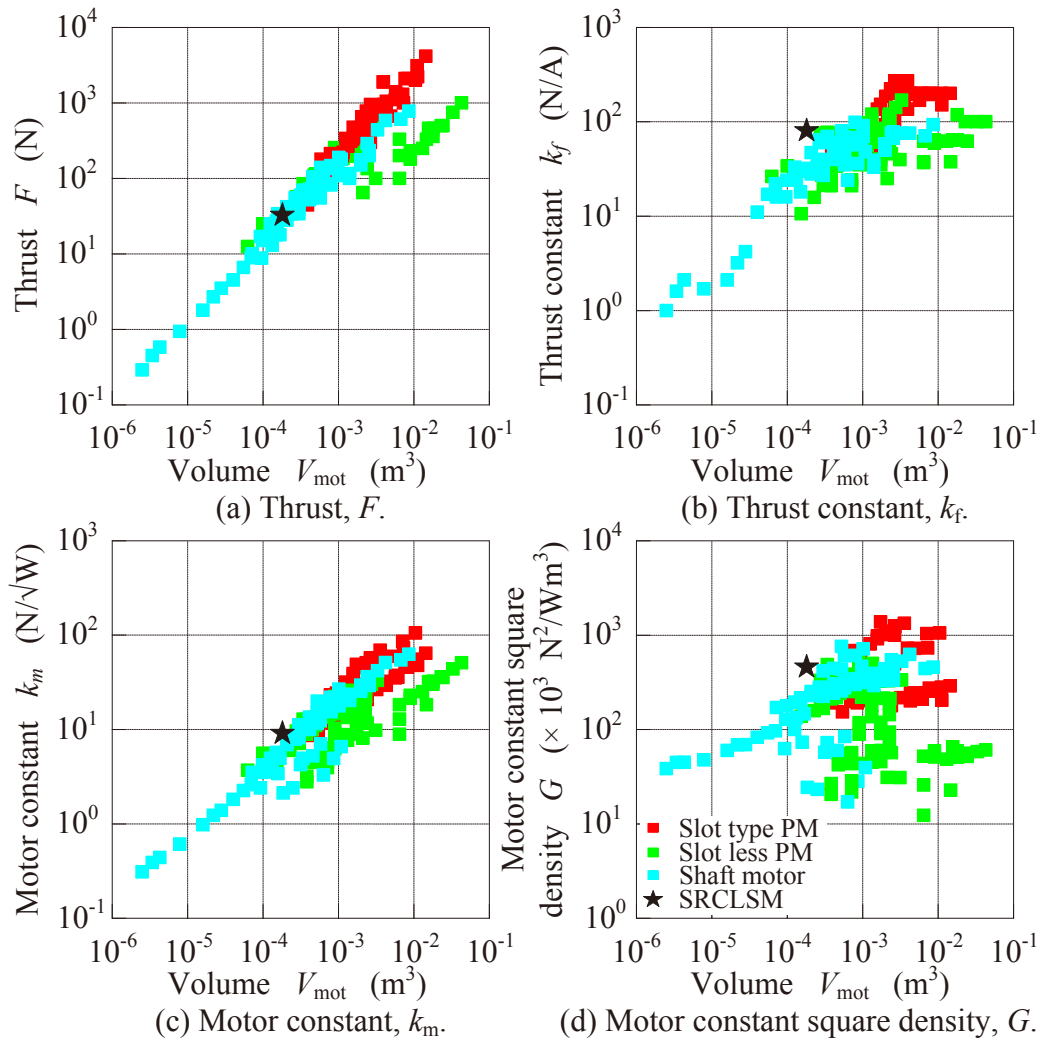


Figure 3.18 Performance comparison of the SRCLSM and commercialize PMLM.

### 3.4 Manufactured of the SRCLSM

For result validation, the SRCLSM was manufactured. It has air gap length,  $\delta$  of 0.1 mm, teeth pitch,  $\tau_p$  of 2 mm and teeth width,  $t_w$  of 0.8 mm. The SRCLSM was manufactured in single phase. It is estimate that, if the measurement results and the simulation output have a good agreement in single phase structure, it will result the same for the six phase structure. Figure 3.19 shows the manufactured SRCLSM. The single phase SRCLSM was manufactured vertically. It was manufactured in such way to ease alignment process especially during static characteristics measurement. At the bottom side of the SRCLSM's mover, a linear stage was located. The linear stage use to vary the mover displacement during static characteristics measurement. On top side

---

of the mover, a 1 kg counter weight has been placed. It uses to fix the mover displacement during static characteristics measurement. The single phase SRCLSM was manufactured with 2 coils. The coil parameter is similar as listed in Table 3.2 in previous sub chapter.

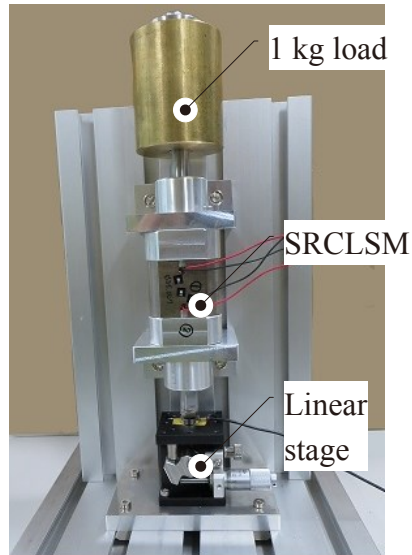


Figure 3.19 Manufactured single phase SRCLSM.

### 3.5 Static Characteristics Measurement of the SRCLSM

In order to validate the simulation output, static characteristics measurements were conducted. The static characteristics performances are including static thrust characteristics,  $RL$  characteristic and electrical time constant,  $\tau_e$  characteristic.

#### 3.5.1 Static Thrust Characteristic

The thrust characteristic of the SRCLSM was measured with the same condition as in simulation. As a comparison, the mover of the SRCLSM has been manufactured with unannealing and annealing S45C material. The experiment setup and schematic diagram for the thrust characteristics measurement are as shown in Figure 3.20 and Figure 3.21 respectively. The thrust was measured using load cell (LMA-A-50N) located between bottom side of the SRCLSM mover and the linear

stage. The load cell (LMA-A-50N) was connected to a digital indicator (TD-510). The digital indicator (TD-510) will give an equivalent thrust in voltage, (mV). Instead of act as counter weight, the 1 kg load is also used as calibration to the indicator in order to obtain conversion constant of the digital indicator (TD-510). The 2 channel DC power supply (IPS 303DD) was used to varied to excitation current from 0.2 A to 1.0 A. The linear stage's scale was used to estimate the mover displacement. The thrust characteristic for the SRCLSM then was captured and analysed.

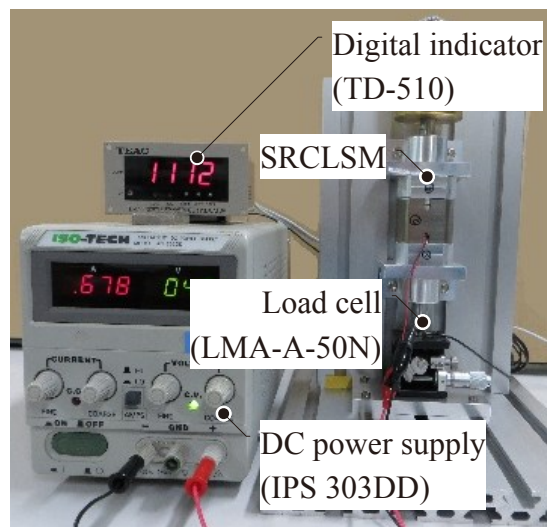


Figure 3.20 Experiment setup for the thrust characteristic measurement of the single phase SRCLSM.

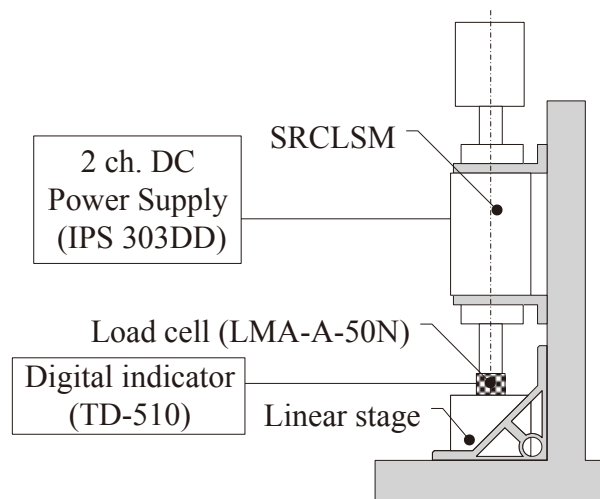


Figure 3.21 Schematic diagram for the thrust characteristic measurement of the single phase SRCLSM.

The thrust characteristic was measured in two different of mover direction. It is defined as forward direction and reverse direction. Despite of measuring the thrust, this measurement style also defines the friction force. Ideally the mover would be centred in the stator. However, there are variations due to physical limitations despite of bearings is practically consist of certain level of clearance. In addition, the shaft diameters must have a tolerance. Furthermore, there is a tolerance in the assembly of the SRCLSM. This condition create irregular magnetics field and cause friction force be produced <sup>(3.18)-(3.19)</sup>. The friction force usually obtains using measurement <sup>(3.20)-(3.22)</sup>. Existence of friction force may cause stick slip oscillation, steady state error, poor tracking performance <sup>(3.20)</sup>, increase thrust ripple <sup>(3.22)</sup>, limit achievable closed-loop bandwidth <sup>(3.23)</sup>, system instability and machine wearing <sup>(3.24)-(3.25)</sup>.

Figure 3.22 shows the thrust characteristic of the SRCLSM at current,  $I$  of 0.7 A in both direction of mover motion. Due to friction force, both direction of mover motion force had a different value. The thrust,  $F$  was determined by averaging instantaneous thrust at every mover displacement. Difference of instantaneous thrust at every mover displacement is the friction force,  $F_C$ . Figure 3.23 shows the sample of the SRCLSM's friction force,  $F_C$ . The friction force,  $F_C$  was measured at current,  $I$  of 0.7 A.

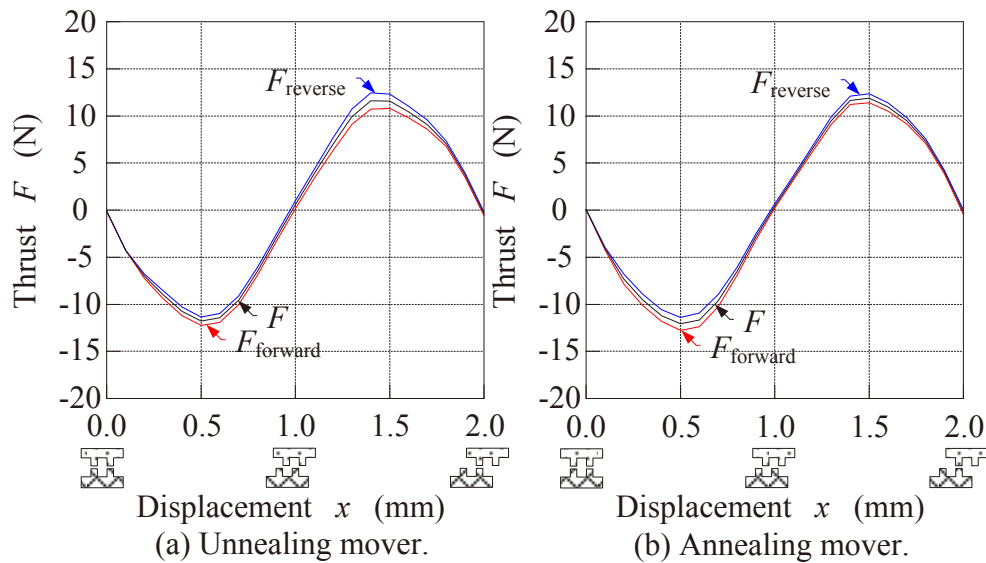


Figure 3.22 Thrust characteristics of the SRCLSM at current,  $I = 0.7$  A.

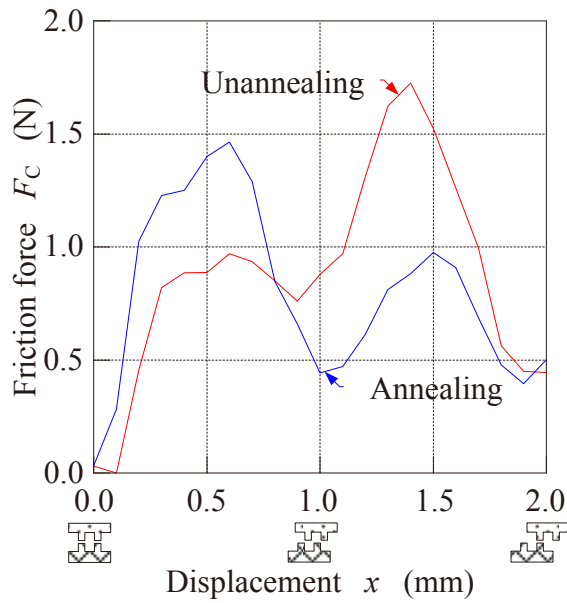


Figure 3.23 Friction force,  $F_C$  of the SRCLSM at current,  $I = 0.7$  A.

Figure 3.24 shows the thrust characteristic of the SRCLSM with difference treatment types on mover at several current,  $I$ . The thrust characteristic also was compared between measured result and simulation output. Based on the thrust characteristic, maximum thrust,  $F_{\max}$  of the SRCLSM with both treatment types on each current,  $I$  then was identified. The effect of current,  $I$  to maximum thrust,  $F_{\max}$  of the SRCLSM is as shown in Figure 3.25. It is shown that, the maximum thrust,  $F_{\max}$  of the SRCLSM with annealing mover is slightly higher compared to the SRCLSM with unannealing mover. However, the thrust improvement is seemed to be insignificant. On the other hand, the thrust error,  $\varepsilon_F$  of gives a significant value regardless the treatment types has been applied.

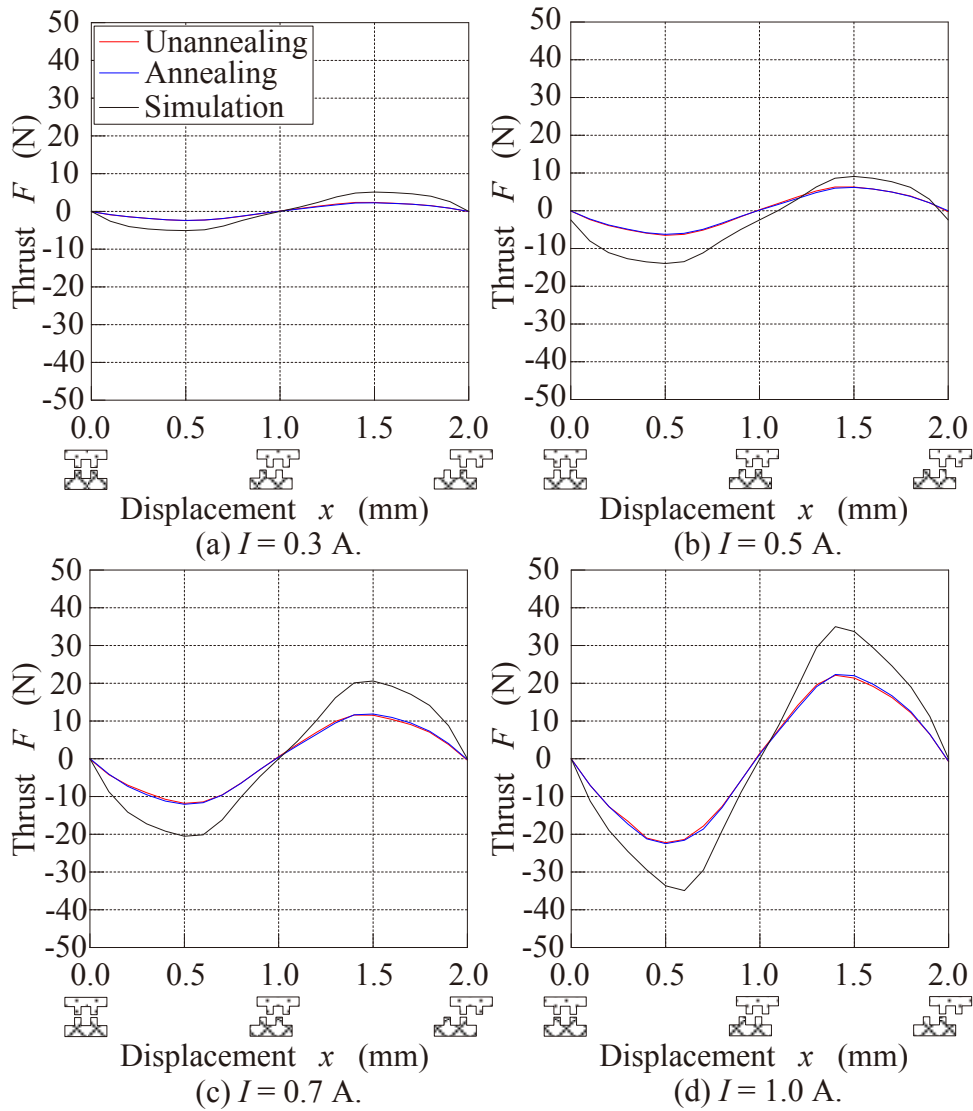


Figure 3.24 Comparison of thrust characteristics between simulation, measurement and mover treatment type.

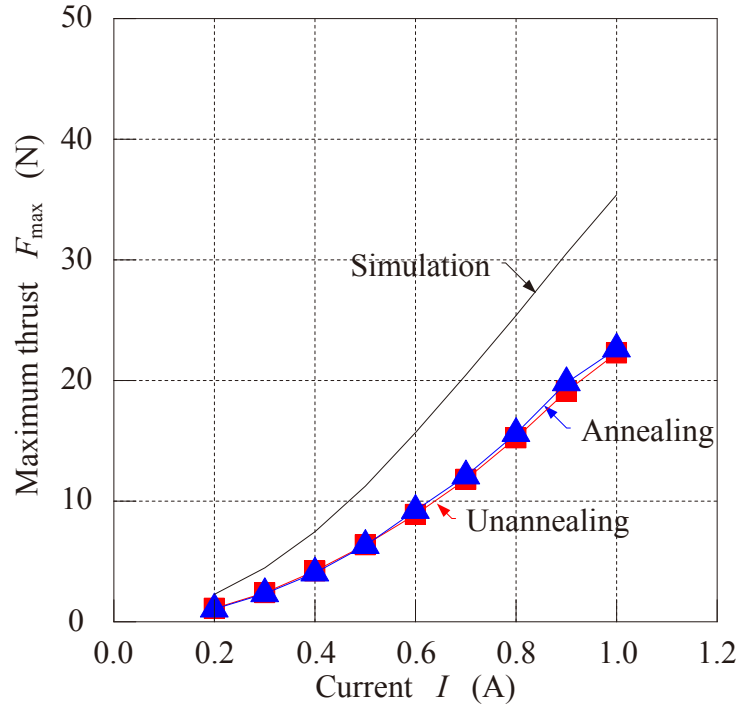


Figure 3.25 Effect of current,  $I$  to maximum thrust,  $F_{max}$ .

As shown in Figure 3.24 and Figure 3.25, there is a slightly difference between thrust produced by the SRCLSM with unannealing and annealing mover materials. Therefore, the differences of thrust between the treatment type mover materials need to be established in order to evaluate the performance of the SRCLSM. The thrust difference,  $F_D$  was calculated using Eq. (3.2) and it is shown as Figure 3.26. Based on Figure 3.26, the increment of thrust of the SRCLSM with annealing mover is insignificant compared to the SRCLSM with unannealing mover. Furthermore, at certain current,  $I$ , thrust produced by the SRCLSM with annealing mover was less compared to the SRCLSM with unannealing mover.

$$F_D = \frac{F_{\text{annealing}} - F_{\text{unannealing}}}{F_{\text{unannealing}}} \times 100. \% \quad (3.2)$$

where,  $\%F_D$  is the thrust difference in (%) and  $F_{\text{annealing}}$  and  $F_{\text{unannealing}}$  are thrust of the SRCLSM with annealing and unannealing mover respectively in (N).

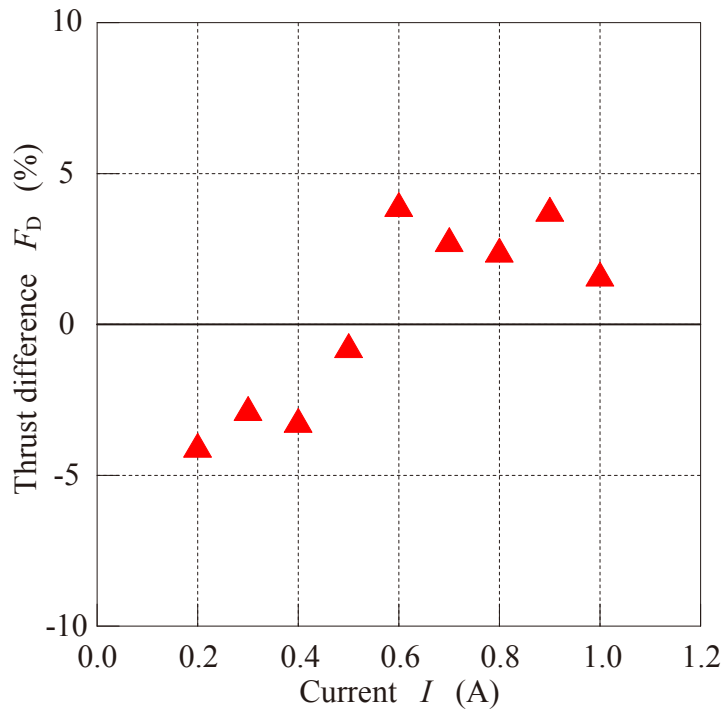


Figure 3.26 Thrust difference,  $F_D$  of the SCRLSM.

The friction force,  $F_C$  of the SRCLM with difference treatment type at several current,  $I$  is as shown in Figure 3.27. Based on Figure 3.27, the SRCLSM with either annealing or unannealing material produce similar friction force,  $F_C$ . However, higher current,  $I$  produce higher friction force,  $F_C$ . It is due to the friction force,  $F_C$  is proportional to the thrust,  $F$ . The higher current,  $I$ , the higher thrust,  $F$  thus the higher friction force,  $F_C$  produced. However, since the thrust of the SRCLSM is similar between unannealing and annealing materials, the friction force,  $F_C$  also will be similar.

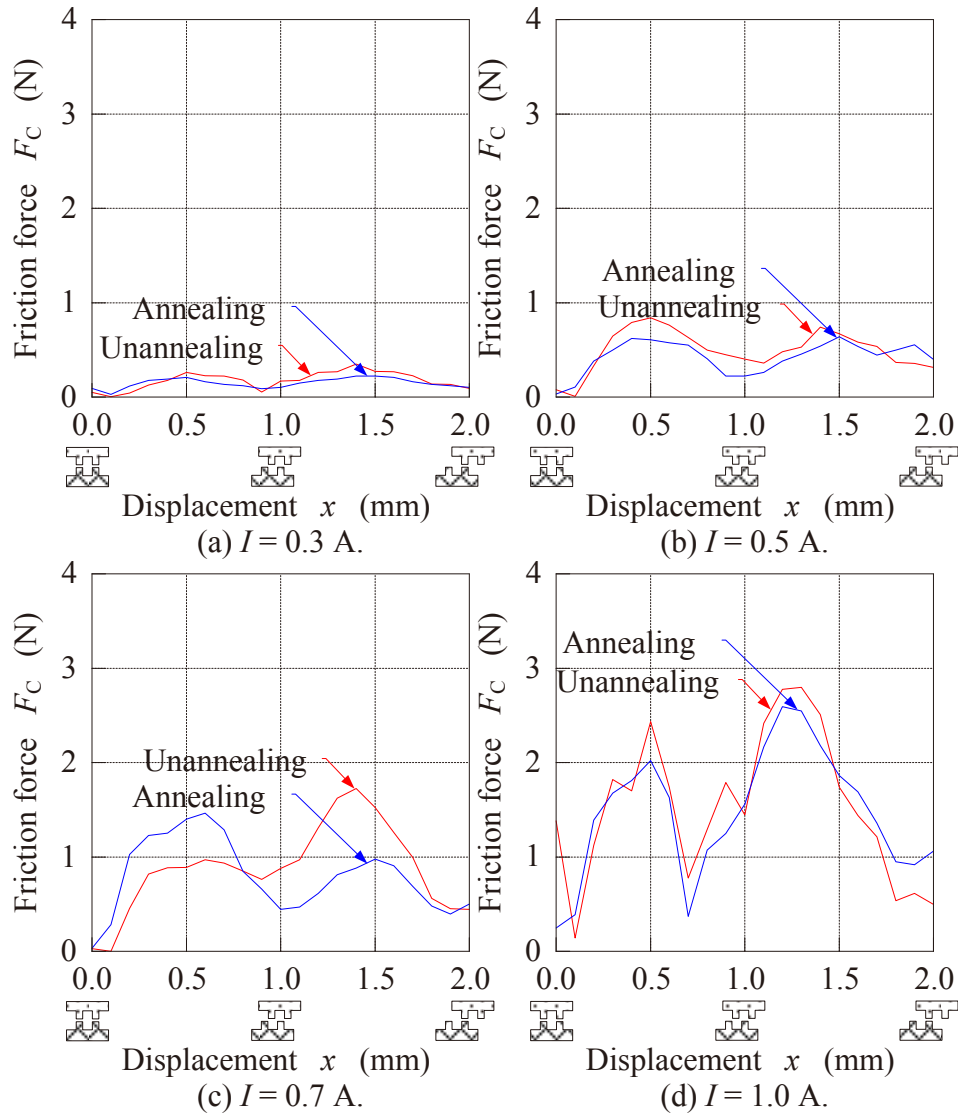


Figure 3.27 Friction force,  $F_C$  of the SRCLSM at several current,  $I$ .

### 3.5.2 $RL$ Characteristic

The experiment setup and schematic diagram for  $RL$  characteristics measurement is as shown in Figure 3.28 and Figure 3.29 respectively. Instead of observing effect of frequency,  $f$  to the resistance,  $R$  and inductance,  $L$ , in this experiment, the  $RL$  profile also being measured. The  $RL$  characteristic was measured with both mover treatment types by using FFT analyzer (CF-930). The frequency,  $f$  has been varied from 3 Hz to 1 kHz during the experiment in order to observe the effect of frequency,  $f$  to resistance,  $R$  and inductance,  $L$ . The mover displacement was varied by using the scale of the linear stage. In this experiment, the peak current,  $I_p$  was fixed to 0.5 A. Power supply from the FFT analyzer (CF-930) was amplified by

the power amplifier in order to obtain 0.5 A peak current and confirm by observed the waveform of the 2ch. oscilloscope. The FFT analyser (CF-930) will provide the gain,  $A_{DB}$  and phase different,  $\phi$  of the SRCLSM. Based on these parameters, the  $RL$  characteristic was calculated. The  $RL$  characteristic of the SRCLSM was calculated using Eq. (3.3) to Eq. (3.5). The measurement settings of  $RL$  characteristic of the SRCLSM is as listed in Table 3.5.

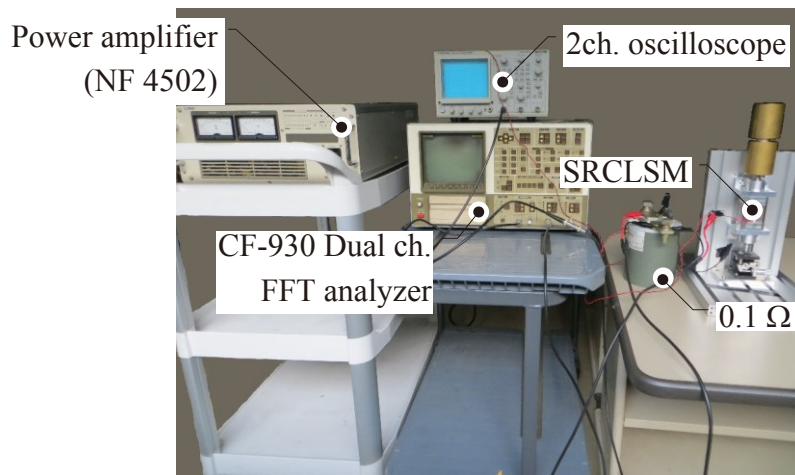


Fig. 3.28 Experimental setup for  $RL$  characteristic measurement.

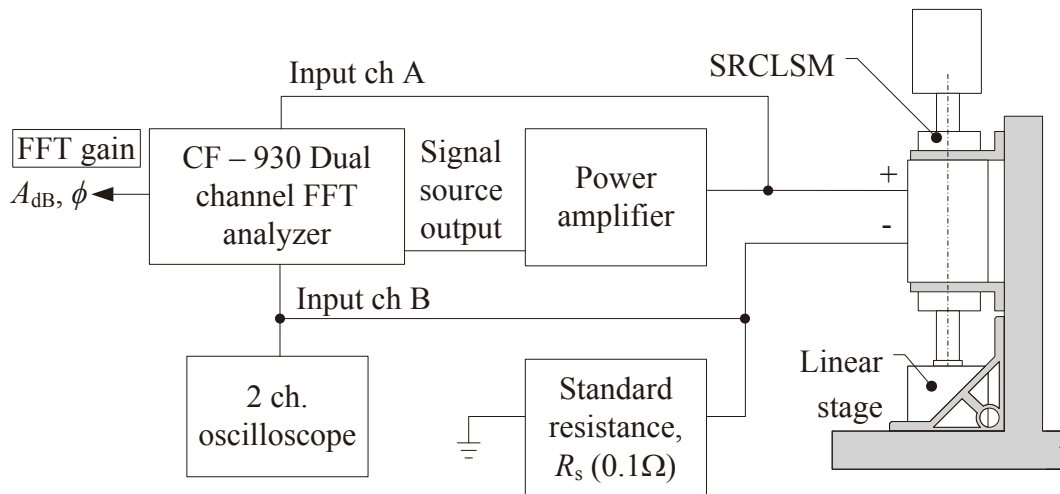


Fig. 3.29 Schematic diagram for  $RL$  characteristic measurement.

$$\begin{aligned}
 A &= \frac{R_S}{R + R_S + j\omega L} \quad , \\
 &= A_{dB}(\cos \phi + j \sin \phi)
 \end{aligned}
 \tag{3.3}$$

$$L = -\frac{R_S}{A} \frac{\sin \phi}{\omega 10^{/20}} \quad (\text{H}) \quad (3.4)$$

$$R = -\frac{R_S}{A} \frac{\cos \phi}{10^{/20}} \quad (\Omega) \quad (3.5)$$

where  $A_{\text{dB}}$  and  $\phi$  are the gain and phase shift based on the FFT analyzer output in (dB) and ( $^\circ$ ) respectively,  $R_S$  and  $R$  are the standard resistance and coil resistance respectively in ( $\Omega$ ),  $\omega$  is the frequency in (rad/s) and  $L$  is the coil inductance in (H).

Table 3.5 : Measurement settings for  $RL$  characteristic.

No	Parameter	Value
1	Peak excitation current, $I_p$ (A)	0.5
2	Frequency, $f$ (Hz)	3, 5, 7, 10, 30, 50, 70, 100, 300, 500, 1000
3	Mover displacement, $x$ (mm)	0.0 – 2.0
4	Coil connection	Parallel
5	Total coil resistance, $R$ ( $\Omega$ )	3.3
6	Standard resistance, $R_S$ ( $\Omega$ )	0.1

The measurement result also being compared to the simulation output. Magnetic, frequency analysis was used with similar excitation frequency with the measurement setup. The amplitude of current source has been set to 0.5 A. Due to high excitation frequency,  $f$  and eddy current losses could not be neglected. Therefore, “Allow Eddy Current” option in the material control setting need to be enabled. The eddy current calculation inside the stator yoke and mover was depends on the material resistivity. The resistivity of the SS400 and S45C were set to  $1.7 \times 10^{-7} \Omega\text{m}$  and  $2.1 \times 10^{-7} \Omega\text{m}$  respectively. Based on the simulation, the voltage and current of the SRCLSM in term of real and imaginary part as Eq. (3.6) and Eq. (3.7) were obtained. Based on the expression of voltage,  $v(t)$  and current,  $i(t)$  the resistance,  $R$  and the inductance,  $L$  were calculated using Eq. (3.8) and Eq. (3.9).

---


$$v(t) = \text{Re}\{V\} + \text{Im}\{V\}, \quad (\text{V}) \quad (3.6)$$

$$i(t) = \text{Re}\{I\} + \text{Im}\{I\}, \quad (\text{A}) \quad (3.7)$$

$$R = \frac{\text{Re}\{V\} \cdot \text{Re}\{I\} + \text{Im}\{V\} \cdot \text{Im}\{I\}}{\text{Re}\{I\}^2 + \text{Im}\{I\}^2}, \quad (\Omega) \quad (3.8)$$

$$L = \left( \frac{\text{Im}\{V\} \cdot \text{Re}\{I\} - \text{Re}\{V\} \cdot \text{Im}\{I\}}{\text{Re}\{I\}^2 + \text{Im}\{I\}^2} \right) \times \left( \frac{1}{2\pi f} \right) \quad (\text{H}) \quad (3.9)$$

where  $v(t)$  and  $i(t)$  are the function of voltage and current in time domain respectively in (V) and (A),  $\text{Re}\{V\}$  and  $\text{Im}\{V\}$  are the real and imaginary parts of voltage expression in (V),  $\text{Re}\{I\}$  and  $\text{Im}\{I\}$  are the real and imaginary parts of current expression in (A),  $R$  and  $L$  are the resistance and inductance in ( $\Omega$ ) and (H) respectively.

The  $RL$  characteristic of the SRCLSM is as shown in Figure 3.30 at fully aligned ( $x = 0.0$  mm) and fully unaligned ( $x = 1.0$  mm) mover displacement. At fully aligned ( $x = 0.0$  mm) mover displacement, maximum inductance,  $L_{\max}$  has been produced. On the other hand, at fully unaligned ( $x = 1.0$  mm) mover displacement, minimum inductance,  $L_{\min}$  has been produced. It is shown that, higher frequency,  $f$  cause the resistance,  $R$  of the SRCLSM is increased due to influence of skin effect phenomena. At higher frequency,  $f$ , the current,  $I$  will flow near to the skin of the copper wire and made the effective cross section of the coil is decreased. It tends to increase the resistance of the SRCLSM's coil especially during high frequency. On the other hand, the skin effect made inductance,  $L$  of the SRCLSM is reduced. Since the current,  $I$  only flow at the surface of the coil wire, it will cause the magnetic field inside the wire is reduced. Therefore, it will reduce the inductance,  $L$  as the frequency,  $f$  is increased. Furthermore, based on the Figure 3.30, the annealing to the mover material cause the resistance,  $R$  and inductance,  $L$  of the SRCLSM is increased compared to unannealing mover material.

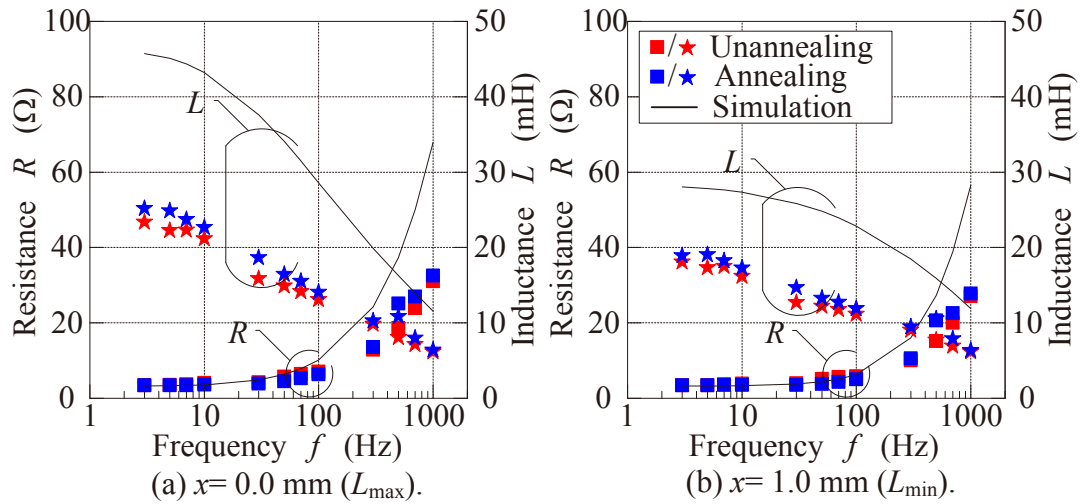


Figure 3.30  $RL$  characteristics of the SRCLSM.

Based on the  $RL$  characteristics, the resistance,  $R$  and inductance,  $L$  profile of the SRCLSM was estimated as shown in Figure 3.31. It is shown that, higher frequency,  $f$  made higher difference between minimum and maximum resistance,  $R$  has been recorded. However, the increment of frequency,  $f$  made difference between minimum and maximum inductance,  $L$  is lower. Despite of the measured  $RL$  characteristics and profile, Figure 3.30 and Figure 3.31 also shows comparison of measured and simulated output. It is shown that, the difference between measured and simulated of  $RL$  characteristic of the SRCLSM has a significant difference. On top of that, the graph profile simulated  $RL$  characteristic has a steep slope compared to measured  $RL$  characteristic.

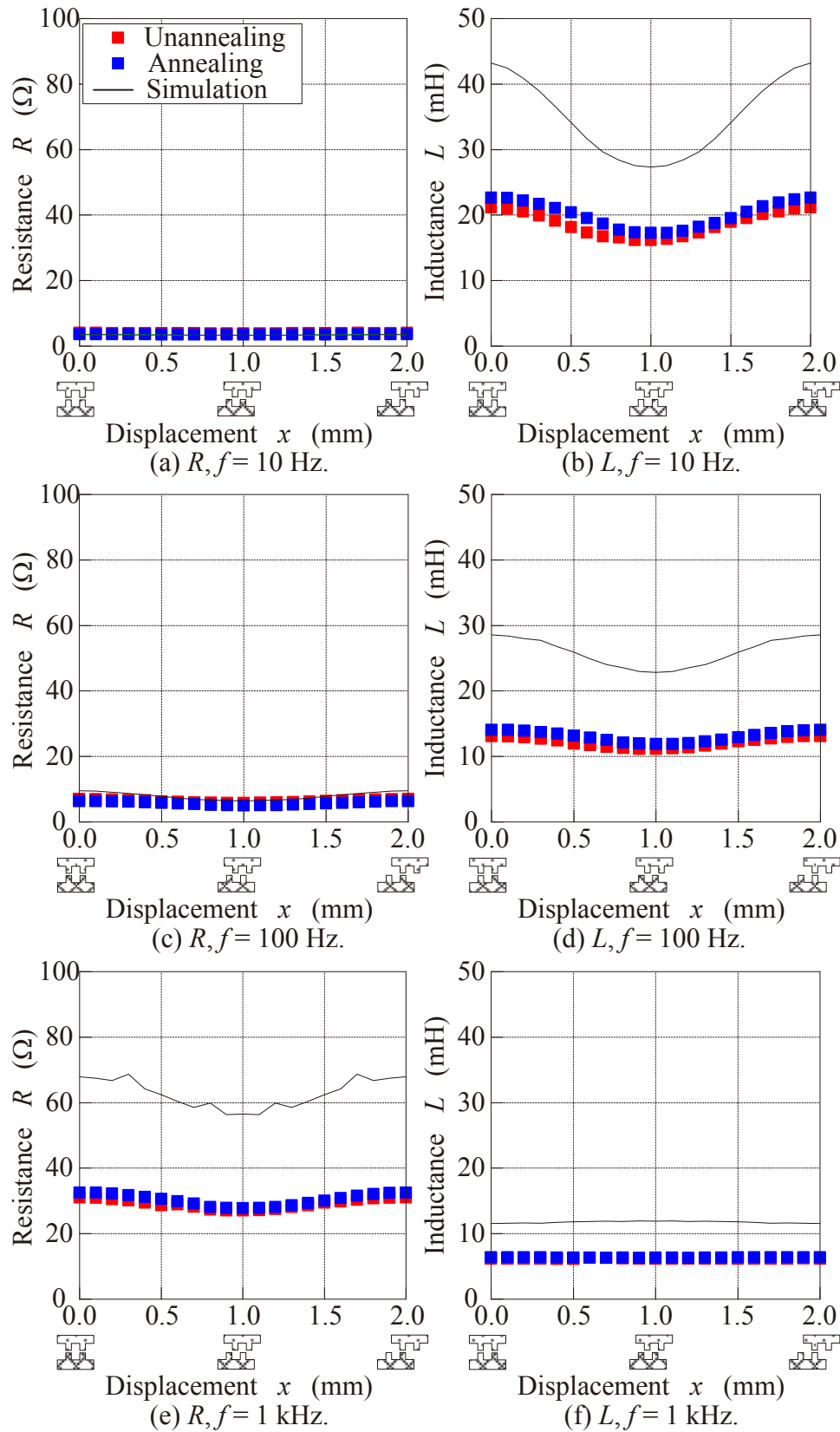


Figure 3.31  $RL$  profile of the SRCLSM at several frequency,  $f$ .

---

### 3.5.3 Electrical Time Constant Characteristic

Generally, the current response is estimate by using electrical time constant,  $\tau_e$ . The lower electrical time constant,  $\tau_e$  represent faster current response. Based on the  $RL$  characteristics of the SRCLSM, the electrical time constant,  $\tau_e$  could be estimated. The electrical time constant,  $\tau_e$  could be calculated using Eq. (3.10). By using this method, the electrical time constant,  $\tau_e$  of the SRCLM under sinusoidal excitation could be estimated. Therefore, the electrical time constant,  $\tau_e$  of the SRCLSM at several excitation frequencies could be estimated.

$$\tau_e = \frac{L}{R}. \quad (s) \quad (3.10)$$

where  $\tau_e$  is the electrical time constant in (s),  $L$  is the coil inductance in (H) and  $R$  is the coil resistance in ( $\Omega$ ).

Since the  $RL$  characteristic has been measured on peak current,  $I_p$  of 0.5 A, the electrical time constant,  $\tau_e$  also will be considered the same amount of peak current,  $I_p$ . Figure 3.32 shows the electrical time constant,  $\tau_e$  characteristics of the SRCLSM at fully aligned teeth position ( $x=0.0$  mm) and fully unaligned teeth position ( $x=1.0$ mm). As shown in Figure 3.32, the electrical time constant,  $\tau_e$  of the SRCLSM is decreased as the frequency,  $f$  is increase.

It is due to increment rate of resistance,  $R$  is higher compared to rate of decrement inductance,  $L$  against frequency,  $f$ . As shown in Figure 3.30, the resistance,  $R$  has rate of increment about 10 times at frequency,  $f$  of 1 kHz compared to the resistance,  $R$  at frequency,  $f$  of 3 Hz. On the other hand, decrement rate of the inductance,  $L$  is about 5 times at frequency,  $f$  of 1 kHz compared to the inductance,  $L$  at frequency,  $f$  of 3 Hz. Based on this fact, it cause the electrical time constant,  $\tau_e$  is decreased as the frequency,  $f$  is increase. Based on the Figure 3.34 also, it is shown that, the electrical time constant,  $\tau_e$  of the annealing mover is higher compared to the unannealing mover. It is due to, the  $RL$  characteristic of the annealing mover is higher compared to the unannealing mover as discussed in previous sub chapter. Therefore,

it result the higher electrical time constant,  $\tau_e$  of annealing mover compared to its counterpart.

Figure 3.33 shows the electrical time constant,  $\tau_e$  profile of the SRCLSM. At lower frequency,  $f$ , the profile of electrical constant,  $\tau_e$  is similar as inductance,  $L$  profile. However, at higher frequency,  $f$  such as at 100 Hz, the electrical time constant,  $\tau_e$  characteristics has been inversely compared to the inductance,  $L$  profile. Whereas at fully aligned teeth position, the electrical time constant,  $\tau_e$  produce minimum value and at fully unaligned teeth position, the electrical time constant,  $\tau_e$  produce maximum value.

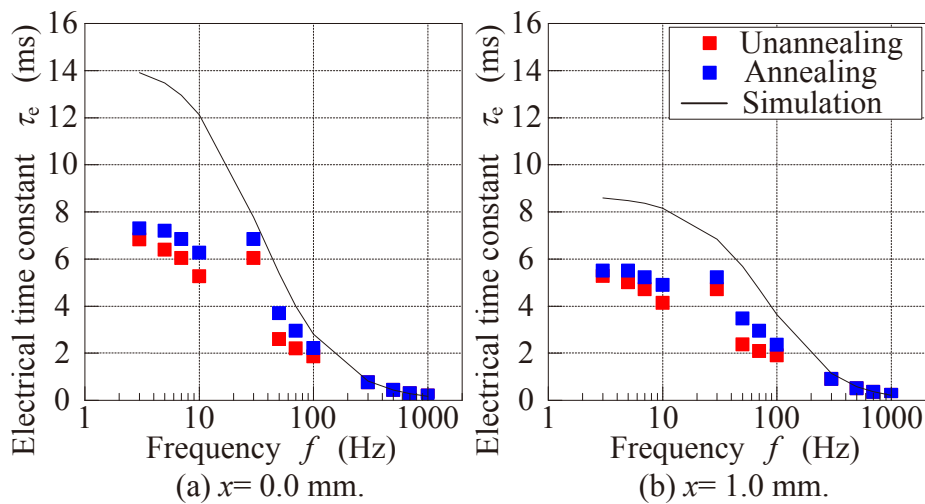


Figure 3.32 Electrical time constant,  $\tau_e$  characteristics of the SRCLSM.

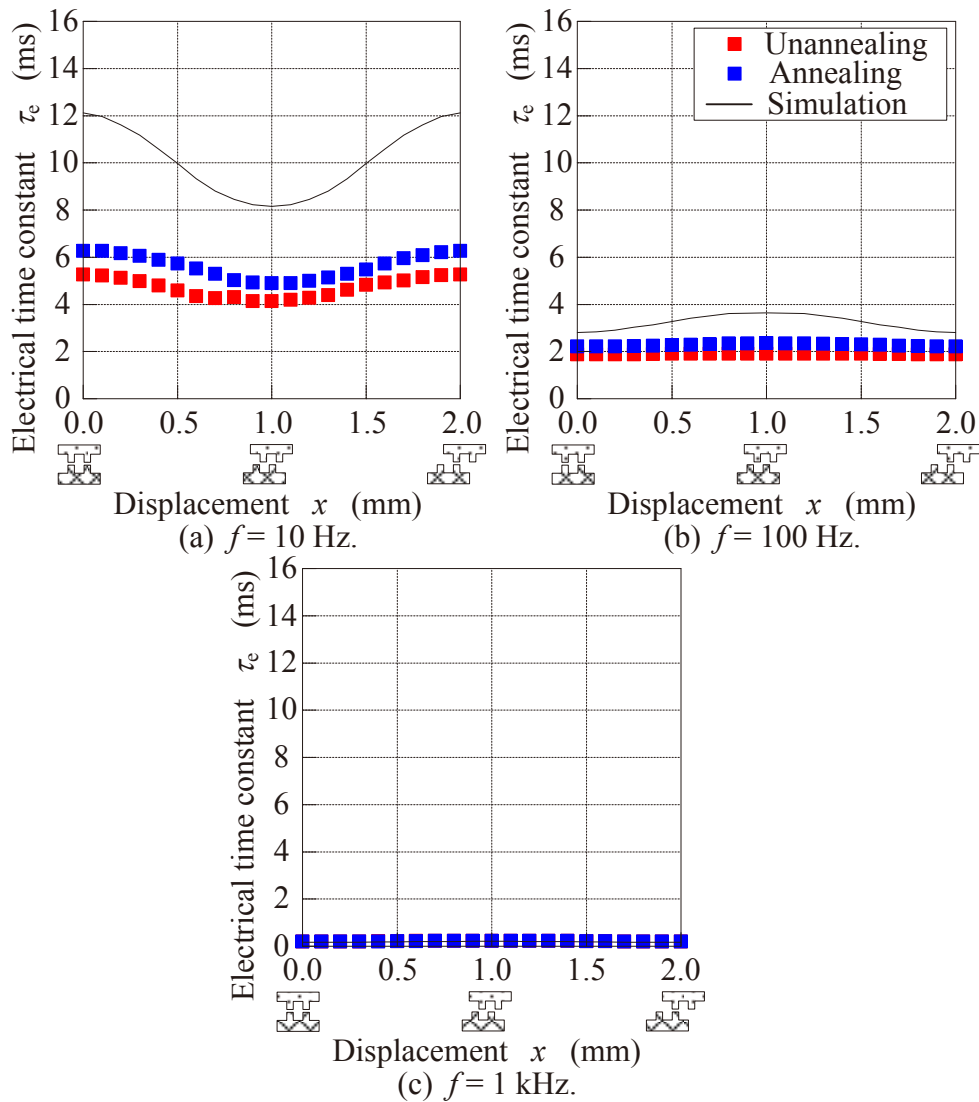


Figure 3.33 Electrical time constant,  $\tau_e$  profile of the SRCLSM at several frequency,  $f$ .

### 3.5.4 Effect of Manufacturing Tolerance to Static Thrust Characteristic

There are several factors that influence difference between simulation output and measurement result of the SRCLSM static characteristics. One of the factors is manufacturing tolerance,  $\Delta x$ . The manufacturing tolerance,  $\Delta x$  is a key factor to determine the manufacturing cost. Even though the higher manufacturing tolerance,  $\Delta x$  help reduce cost, however it will affect the performance of an electrical machine. The manufacturing tolerance,  $\Delta x$  is exist due to limitation on the manufacturing process and measuring precision on every part <sup>(3.26)-(3.27)</sup>. Several researchers have suggested doing an analysis to determine maximum manufacturing tolerance,  $\Delta x$

---

before the electrical machines undergo manufacturing process. Several design technique could be apply to achieve that aimed such as Monte Carlo technique as discussed in <sup>(3.28)</sup>-<sup>(3.29)</sup> and Stochastic Response Surface Method as discussed in <sup>(3.30)</sup>.

In this research, the effect of manufacturing tolerance,  $\Delta x$  to static thrust will be discussed. The SRCLSM was modelled by considering certain range of manufacturing tolerance,  $\Delta x$  and each model will be simulate and compared with measurement result. On the same time, the mover of the SRCLSM has been measured by a vision measuring system. Based on measured mover dimension, the SRCLSM has been modelled and simulated. Based on the simulation result, the manufacturing tolerance,  $\Delta x$  on stator part was estimated.

The manufacturing tolerance,  $\Delta x$  should be considered in all part of the SRCLSM including, stator yoke and coil part on the stator part and mover part. Furthermore, manufacturing tolerance,  $\Delta x$  became more significant to stacked part such as in stator part of the SRCLSM that consist of 4 sets of stator yoke and 2 sets of coil. However, in order to reduce simulation scope, the manufacturing tolerance,  $\Delta x$  only was considered on the teeth of mover side. Meanwhile, the stator yoke and coil part is assumed to be manufactured without manufacturing tolerance,  $\Delta x$ . Figure 3.34 shows the SRCLSM structure by considering the manufacturing tolerance,  $\Delta x$ . The manufacturing tolerance,  $\Delta x$  was considered in range of  $-100 \mu\text{m}$  to  $100 \mu\text{m}$  with resolution of  $10 \mu\text{m}$ . The negative sign of manufacturing tolerance,  $\Delta x$  represent the SRCLSM mover parameter was built smaller than it design value, while the positive sign of the manufacturing tolerance,  $\Delta x$  represent otherwise. During simulation of the SRCLSM models, the current,  $I$  have been set in range of  $0.1 \text{ A}$  to  $1.0 \text{ A}$ . Figure 3.35 shows several SRCLSM's model on several manufacturing tolerance,  $\Delta x$ .

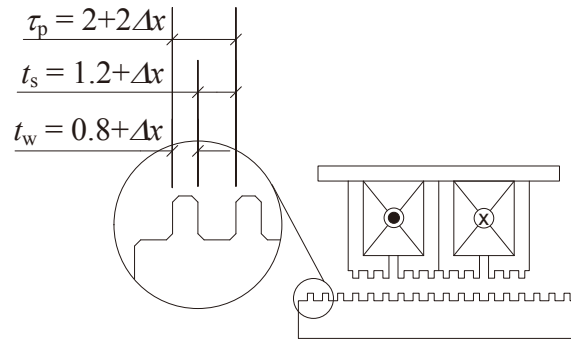


Figure 3.34 The SRCLSM structure with consideration of the manufacturing tolerance,  $\Delta x$ .

Figure 3.36 shows static thrust characteristics of the SRCLSM on several manufacturing tolerance,  $\Delta x$  and current,  $I$  of 0.5 A. It is shown that, higher absolute manufacturing tolerance,  $|\Delta x|$  give lower static thrust. On top of that, the static thrust is shifted compared to the static thrust with no manufacturing tolerance,  $\Delta x$  is considered. Based on each model's thrust characteristics, the maximum thrust,  $F_{\max}$  at each current,  $I$  have been identified. The effect of manufacturing tolerance,  $\Delta x$  to the maximum thrust,  $F_{\max}$  at various current,  $I$  is as shown in Figure 3.37. Based on Figure 3.37, it is shows that,  $\pm 10 \mu\text{m}$  of manufacturing tolerance,  $\Delta x$  does not much influence to the maximum thrust,  $F_{\max}$  compared to the ideal case. It can be seen as shown in Figure 3.38 that the structure of the SRCLSM with  $10 \mu\text{m}$  of the absolute manufacturing tolerance,  $|\Delta x|$  does not affect so much. As the absolute manufacturing tolerance,  $|\Delta x|$  is increase, the maximum thrust,  $F_{\max}$  at similar current,  $I$  will be reduced.

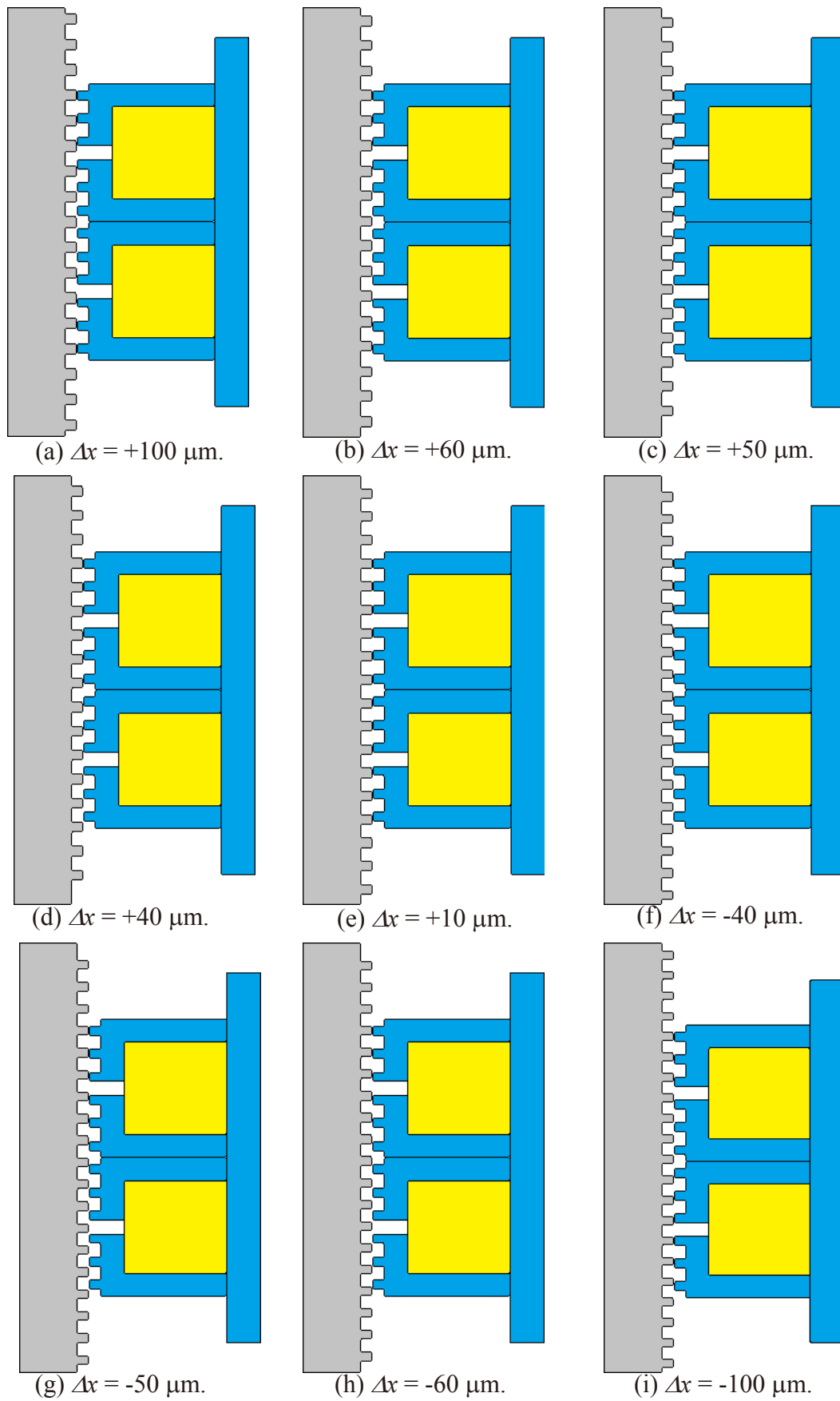


Figure 3.35 The SRCLSM's model on several manufacturing tolerance,  $\Delta x$ .

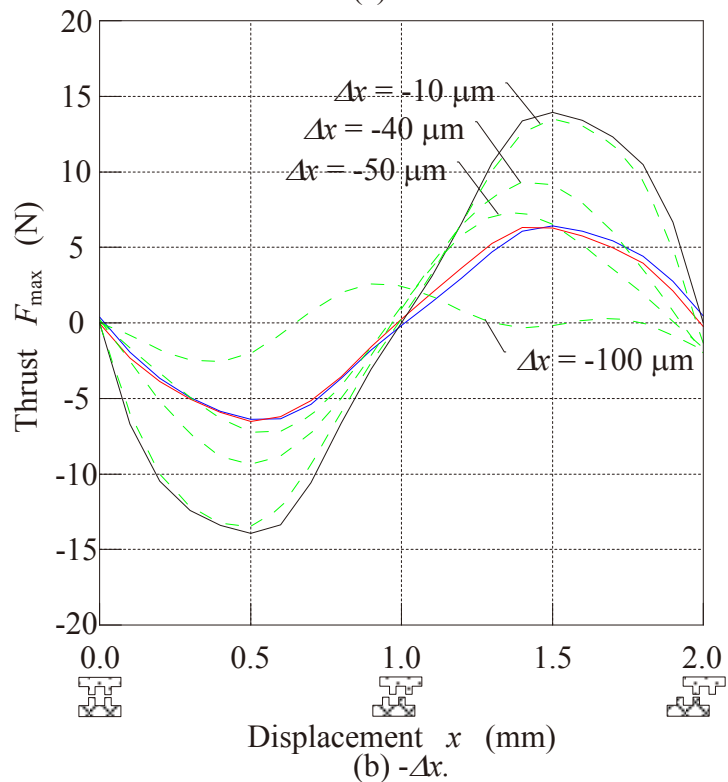
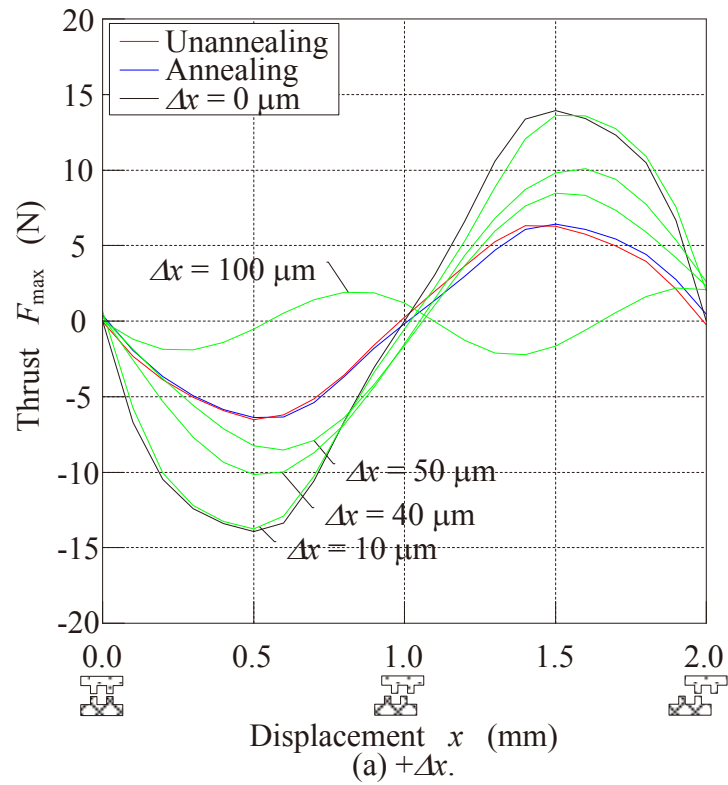


Figure 3.36 The SRCLSM's static thrust characteristics on several manufacturing tolerance,  $\Delta x$  and current,  $I = 0.5$  A.

Based on Figure 3.35 also, it can be seen that, the manufacturing tolerance,  $\Delta x$  will made the mover's teeth will be shifted compared to it stator's teeth on several

mechanical degree. The teeth shifted made the value and direction thrust of the SRCLSM on specific mover displacement might be change. The change of thrust especially in term of direction against it mover motion direction will cause a reduction to the total thrust. For example, on manufacturing tolerance,  $\Delta x$  of  $\pm 100 \mu\text{m}$ , some of the mover teeth have shifted more than  $180^\circ$  mechanical degree. Due to thrust of SRCLSM sole depend on attractive force between its teeth, it will create opposite thrust direction at certain mover displacement compared to its main thrust and cause reduction to the total thrust. This condition causes the thrust on manufacturing tolerance,  $\Delta x$  of  $\pm 100 \mu\text{m}$  give lowest value. Nevertheless, the maximum thrust,  $F_{\text{max}}$  of the SRCLSM model with manufacturing tolerance,  $\Delta x$  of  $-50 \mu\text{m}$  gives closest value compared to measurement result. Therefore, due to the definition of manufacturing tolerance,  $\Delta x$  as shown in Figure 3.34, the teeth width,  $t_w$  and slot width,  $t_s$  of the SRCLSM has been manufactured by  $-50 \mu\text{m}$  of the manufacturing tolerance,  $\Delta x$  At the same time, it made the manufacturing tolerance,  $\Delta x$  of the teeth pitch,  $\tau_p$  is  $-100 \mu\text{m}$ .

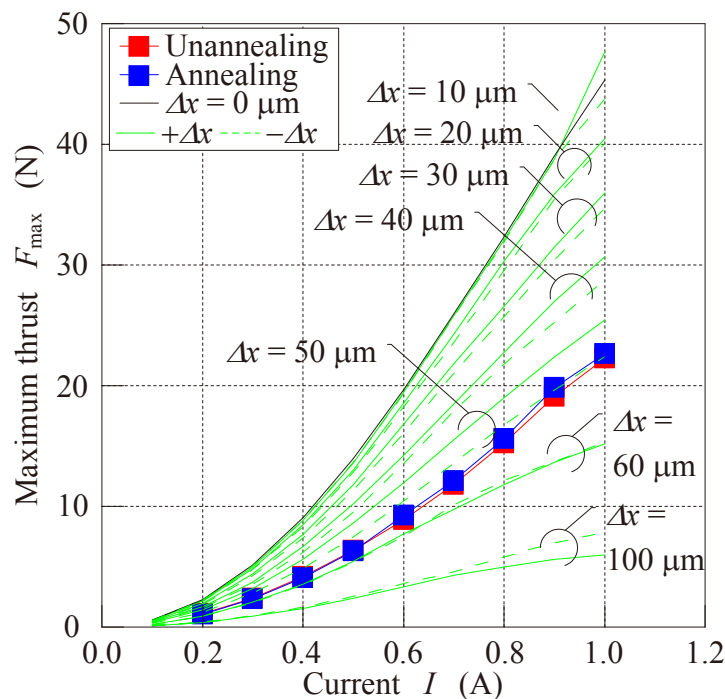


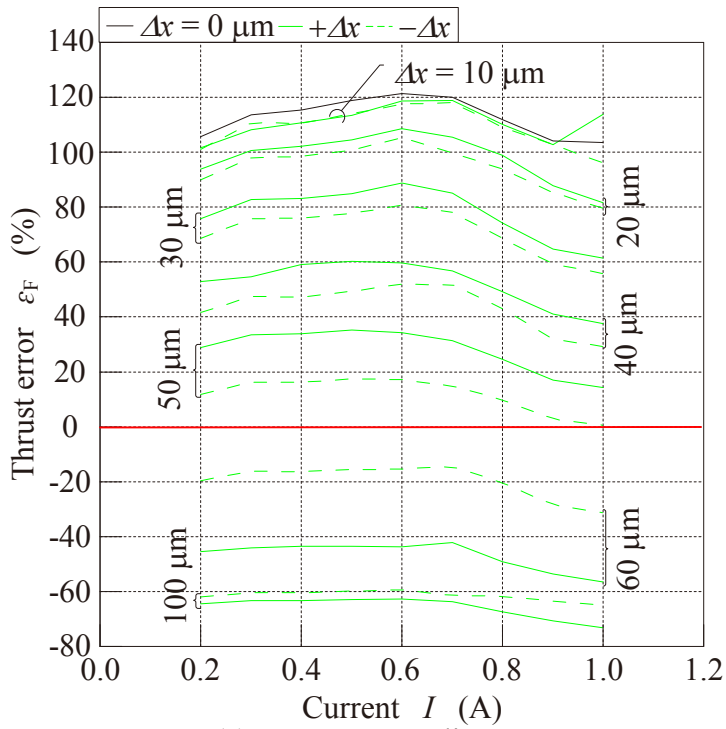
Figure 3.37 Effect of manufacturing tolerance,  $\Delta x$  to the maximum thrust,  $F_{\text{max}}$ .

---

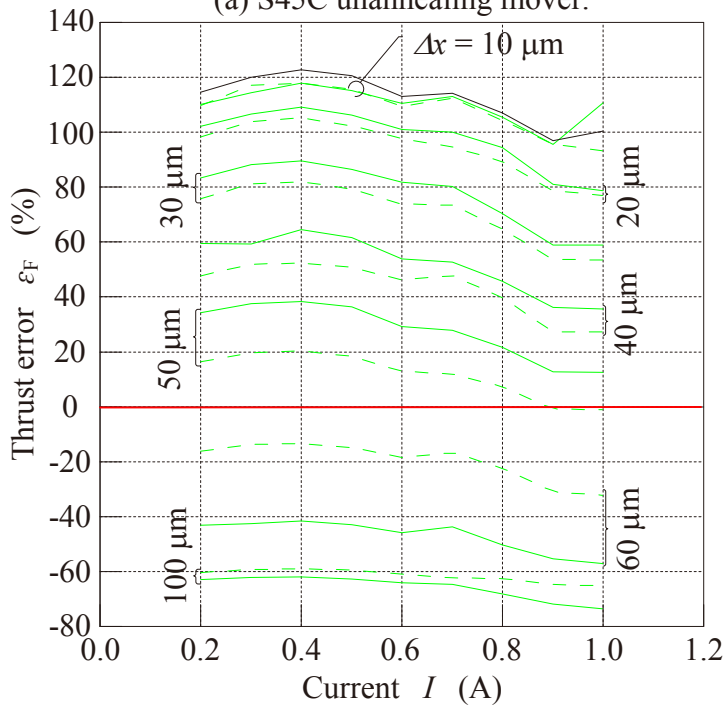
In order to make clear decision on the total manufacturing tolerance,  $\Delta x$  of the SRCLSM, the thrust error,  $\varepsilon_F$  for each SRCLSM model with difference manufacturing tolerance,  $\Delta x$  were calculated. The thrust error,  $\varepsilon_F$  was calculated using Eq. (3.11). Figure 3.38 shows the thrust error,  $\varepsilon_F$  of the SRCLSM with considering manufacturing tolerance,  $\Delta x$ . Based on Figure 3.38, on the absolute manufacturing tolerance,  $|\Delta x|$  lower than 50  $\mu\text{m}$  produced higher simulation static thrust characteristics compared to it measurement result. However, if higher absolute manufacturing tolerance,  $|\Delta x|$  is considered, the thrust comparison will be otherwise. Furthermore, on negative manufacturing tolerance,  $-\Delta x$  gives nearer simulated compared measured thrust since absolute manufacturing tolerance,  $|\Delta x|$  lower than 50  $\mu\text{m}$  is considered, the thrust error,  $\varepsilon_F$  on negative manufacturing tolerance,  $-\Delta x$  is lower compared to when positive manufacturing tolerance,  $+\Delta x$  is considered. For the absolute manufacturing tolerance,  $|\Delta x|$  higher that 50  $\mu\text{m}$ , inversely condition has been produced. Yet, the manufacturing tolerance,  $\Delta x$  of -50  $\mu\text{m}$  is seen gives lowest thrust error,  $\varepsilon_F$  on both mover material treatment types.

$$\varepsilon_F = \frac{F_{\text{simulated}} - F_{\text{measured}}}{F_{\text{measured}}} \times 100. \quad (\%) \quad (3.11)$$

where,  $\% \varepsilon_F$  is the thrust error in (%),  $F_{\text{measured}}$  and  $F_{\text{simulated}}$  are the measured and simulated thrust respectively in (N).



(a) S45C unannealing mover.



(b) S45C annealing mover.

Figure 3.38 Thrust error,  $\varepsilon_F$  by considering manufacturing error,  $\Delta x$ .

---

### 3.6 Feasibility of the SRCLSM Implement as E-Cutter's Actuator

The SRCLSM design and development has been discussed. In order to validate the simulation output, a single phase SRCLSM has been manufactured. The static characteristics has been measured and compared to simulation output. Despite of capability to produce high thrust density, however, difference between simulation output and measurement result is high. Therefore, if the full structure performance is concern, it will produce only half compared to that has been estimated in Figure 3.18. Based on Figure 3.25, it is shown that, the thrust constant,  $k_f$ , of the single phase SRCLSM based on measured static thrust at current,  $I$  of 0.7 A was about 17.1 N/A. Based on the facts discussed in sub chapter 3.1, the thrust constant,  $k_f$  of the SRCLSM with 6 phase structure is about 27.4 N/A. It need about 7.3 A of current,  $I$  to make the 6 phase SRCLSM fulfil the thrust requirement by the E-Cutter's actuator. The amount of current,  $I$  is seem high compared to size of copper wire used to construct the SRCLSM coil and yet the thrust at current,  $I$  of 1.0 A is far below that the targeted thrust. Even though coil parameter design is conduct, reduction of coil turn due to use bigger size of copper wire to allow higher rated current, will also cause reduction on thrust produced. On the other hand, the total weight,  $W_{tot}$  of the 6 phase SRCLSM was 1.41 kg. It is about 30 % lower than the E-Cutter's actuator restricted. Nevertheless, even if further structure design is conducted to the SRCLSM, due to the thrust produced is significantly lower compared to the targeted thrust, process to make the SRCLSM fulfil both design target is seem to be unfeasible. Furthermore, the SRCLSM structure parameter especially in term of teeth pitch,  $\tau_p$  is too sensitive to the manufacturing tolerance,  $\Delta x$ . Only about 5 % difference compared to its design value caused reduction about 50 % of it thrust. Therefore, the designed SRCLSM of this research is not fit to be implemented as the E-Cutter's actuator.

### 3.7 Summary

Previously, the SRLSM was never being implemented as the E-Cutter's actuator. Therefore, in this research a fundamental study of designing the switched reluctance cylindrical linear synchronous motor or called as the SRCLSM has been conducted. Based on several facts, the initial structure of the SRCLSM has been proposed. The performance of the 6 phase SRCLSM was compared to commercialized PMLM to prove the SRCLSM has been designed with high performance. Based on the comparison, it is found that, the SRCLSM has capability to produce high thrust density compared to the commercialized PMLM. Instead of producing similar performance as the commercialized PMLM, the designed SRCLSM was found not fit to be implement as the E-Cutter's actuator as discussed in sub chapter 3.6. Table 3.6 shows summary of the SRCLSM design and develop results.

Table 3.6 Summary of the SRCLSM design and develop results.

Characteristics	Design target	6 phase SRCLSM	
		Simulation ( $I = 0.7$ A)	Measurement ( $I = 0.7$ A)
Thrust, $F$ (N)	$> 200$	32	19
Weight, $W_{tot}$ (kg)	$< 2.0$	1.40	1.40
Volume, $V_{mot}$ ( $m^3$ )	-	$1.90 \times 10^{-4}$	$1.90 \times 10^{-4}$
Thrust constant, $k_f$ (N/A)	-	46	27
Motor constant, $k_m$ (N/ $\sqrt{W}$ )	-	9	5
Motor constant square density, $G$ ( $\times 10^3$ N $^2$ /Wm $^3$ )	-	425	153

### 3.8 References of Chapter 3

- (3.1) A. Chiba, Y. Takano, M. Takeno, T. Imakawa, N. Hoshi, M. Takemoto, and S. Ogasawara, Torque density and efficiency improvements of a switched reluctance motor without rare-earth material for hybrid vehicles, IEEE Transactions on Industry Applications, Vol. 47(3), pp. 1240-1246, 2011.
- (3.2) F. Daldaban and N. Ustkoyuncu, A novel linear switched reluctance motor for railway transportation systems, Energy Conversion and Management 51, pp. 465–469, 2010.
- (3.3) PO. Rasmussen, F. Blaabjerg, JK. Pedersen and F. Jensen, Switched

- 
- reluctance-shark machines-more torque and less acoustic noise, Industry Applications Conference, Vol. 1, pp. 93-98, 2000.
- (3.4) Y. Ozoglu, M. Garip and E. Mese, New pole tip shapes mitigating torque ripple in short pitched and fully pitched switched reluctance motors, 37<sup>th</sup> IAS Annual Meeting, Vol. 1, pp. 43–50, 2002.
- (3.5) HO. Ju and IK. Byung, New rotor shape design of SRM to reduce the torque ripple and improve the output power, 8<sup>th</sup> International Conference on Electrical Machines and Systems, ICEMS, Vol. 1, pp. 652 – 654, 2005.
- (3.6) CS. Edrington, DC. Kaluvagunta, J. Joddar and B. Fahimi, Investigation of electromagnetic force components in SRM under single and multiphase excitation, IEEE Trans. on Industry Appl., Vol. 41 (4), pp. 978-988, 2005.
- (3.7) HA. Toliyat and H. Xu, A novel direct torque control (DTC) method for five-phase induction machines, 15<sup>th</sup> annual IEEE Applied Power Electronics Conference and Exposition (APEC), pp. 162-168, 2000.
- (3.8) E. Levi, R. Bojoi, F. Profumo, HA. Toliyat and S. Williamson, Multiphase induction motor drives a technology status review, IET Electrical Power Application, Vol. 1 (4), pp. 489–516, 2007.
- (3.9) F. Locment, E. Semail and F. Piriou, Design and study of a multiphase axial-flux machine, IEEE Trans. on Magnetics, Vol. 42(4), pp. 1427 – 1430, 2006.
- (3.10) JH. Park, SM. Jang, JY. Choi, SY. Sung and IJ. Kim, Dynamic and experimental performance of linear-switched reluctance machine with inductance variation according to air gap length, IEEE Transactions on Magnetics, Vol. 46 (6), pp. 2334 – 2337, 2010.
- (3.11) SM. Jang, JH. Park, DJ. You, HW. Cho and HK. Sung, Design of high speed linear switched reluctance motor, International Conference on Electrical Machines and Systems 2007, pp. 1668 – 1671, 2007.
- (3.12) ASC. Kwok, WC. Gan and NC. Cheung, Improvements in the mechanical structure of the linear switched reluctance motor, 2<sup>nd</sup> Inter. Conf. on Power Electronics Systems and Applications, ICPESA '06, pp. 186 – 288, 2006.
- (3.13) H. Yamada, Fundamental of linear pulse motor, In Handbook of linear motor application, Kogyo Chosakai, pp. 242-243, 1986.
- (3.14) J. Corda and B. Ouhab, Electromagnetic design optimisation of a linear-cylindrical variable-reluctance motor, 9<sup>th</sup> International Conference on Electrical Machines and Drives, pp. 276 – 280, 1999.
- (3.15) H. Yamada, T. Yano, H. Wakiwaka, Y. Yamamoto, H. Nakagawa and Y. Maeda, Development of high power linear pulse motor for artificial heart, 5<sup>th</sup> International Conf. on Electrical Machines and Drives, pp. 110-114, 1991.
- (3.16) Y. Takeda, M. Sanada, S. Morimoto, T. Hirasa and K. Taniguchi, Cylindrical linear pulse motor with interior permanent magnet mover, IEEE Transactions on Industry Applications, Vol. 30, pp. 141 – 145, 1994.
- (3.17) Y. Takeda, M. Sanada, S. Morimoto and T. Hirasa, Linear pulse motors for accurate positioning, IEEE Industry Appl. Soc. Meeting, pp. 144-149, 1991.

- 
- (3.18) IS. Jung, J. Hur and DS. Hyun, 3D Analysis of permanent magnet linear synchronous motor with magnet arrangement using equivalent magnetic circuit network method, *IEEE Transactions on Magnetics*, Vol. 35(5), pp. 3736–3738, 1999.
- (3.19) RJ. Cruise and CF. Landy, Reduction of detent forces in linear synchronous motors, 2<sup>nd</sup> International Symposium on Linear Drives for Industry Applications, pp. 412–415, 1998.
- (3.20) Chin-Sheng Chen, The feedforward friction compensation of linear motor using genetic learning algorithm, 17<sup>th</sup> World Congress the International Federation of Automatic Control, pp. 15696 – 15701, 2008.
- (3.21) C. Röhrig and A. Jochheim, Motion control of linear permanent magnet motors with force ripple compensation, *The 3th International Symposium on Linear Drives for Industry Applications, LDIA*. 2001.
- (3.22) G. Stumberger, B. Stumberger and D. Dolinar, Position and current dependent flux linkages, thrust and friction force of linear synchronous reluctance motor, *Thirty-Sixth IAS Annual Meeting IEEE Industry Applications Conference*, 2001 Vol. 4, pp. 2310-2317, 2001.
- (3.23) H. Olsson and KJ. Astrom, Friction generated limit cycles, *IEEE Transactions Control System Technology*, Vol. 9 (4), pp. 629–636, 2001.
- (3.24) MS. Kim and CS. Chung, Friction identification of ball-screw driven servomechanisms through the limit cycle analysis, *Mechatronic* 16, pp. 131-140, 2006.
- (3.25) KK. Tan, TH. Lee, SN. Huang and X. Jiang, Friction modelling and adaptive compensation using a relay feedback approach, *IEEE Transactions of Industrial Electronics*, Vol. 48 (1), pp. 169-176, 2001.
- (3.26) YK. Kim, JP. Hong, and J. Hur, Robust optimization of electric machine using stochastic finite element method, *Journal of Electrical Engineering*, Vol. 1, No. 1, pp. 69–72, 2001.
- (3.27) CM. Creveling, *Tolerance Design a Handbook for Developing Optimal Specifications*. Reading, MA: Addison-Wesley, 1995.
- (3.28) RY. Rubinstein, *Simulation and the Monte Carlo Method*. New York: Wiley, 1981.
- (3.29) JS. Gao, KW. Chase, and SP. Magleby, Comparison of assembly tolerance analysis by the direct linearization and modified Monte Carlo simulation methods, *Proceedings ASME*, Vol. 82, No. 1, pp. 353–360, 1995.
- (3.30) YK. Kim, JP. Hong, and J. Hur, Torque Characteristic Analysis Considering Manufacturing Tolerance for Electric Machine by Stochastic Response Surface Method *IEEE Trans. on Ind. Appl.*, Vol. 39 (3), pp. 713 – 719, 2003.

---

## Chapter 4: Design and Development of the Permanent Magnet Cylindrical Linear Synchronous Motor

### 4.1 Basic Structure Parameter of the PMCLSM

Previously, there are four linear motors has been designed and developed for E-Cutter's actuator <sup>(4.1),(4.2)</sup>. All the linear motors had undergone several laboratory testing sessions to ensure its feasibility on cutting activity. Despite of all the linear motors, the linear motor in <sup>(4.3)-(4.5)</sup> or called as 1PhSTLOA is the best linear motor as E-Cutter actuator. The 1PhSTLOA has been designed in single phase structure topology. However, the new PMCLSM was designed using 3 phase structure topology. The 3 phase structure topology was chosen because it provides relatively low ripple thrust, ease of displacement and motion direction control by controlling the 3 phase sequence compare to single phase structure topology. A 6 slot 8 pole 3 phase structure type has been chosen as a first initiative to design a 3 phase PMCLSM for E-Cutter's actuator.

The PMCLSM structure is consists of stator and mover part. 6 coils and stator yoke will be used to construct the PMCLSM's stator. The stator part of the PMCLSM can be designed either in slot type or slotless type. Even though the slot type of stator could provide the PMCLSM with better static performance such as static thrust, however, the slotless stator has better dynamic performance such as lower inductance and electrical time constant <sup>(4.6)</sup>. Therefore, a comparison between these stator types is essential in order to decide which stator type is the best candidate to be applied in the PMCLSM.

The mover part of the PMCLSM is made by ring shape permanent magnets attached with a shaft. Currently, there are various permanent magnet magnetization arrangement has been invented to improve performance of linear motor. The main consideration factor is to direct the magnetic flux to flow at specific direction. It includes simple N-S magnetization arrangement either in the axial <sup>(4.4), (4.7), (4.8)</sup> or radial direction <sup>(4.9) - (4.11)</sup> and more complicated magnetization arrangement such halbach

array <sup>(4.11) - (4.13)</sup> to achieve optimum performance of the linear motor. Instead of choosing the stator types, on the mover part, the optimum magnetization arrangement will be search.

Figure 4.1 shows skeleton of the 6 slot 8 pole slot type and slotless type of 3 phase PMCLSM. In order to made a valid comparison between slot type and slotless of the PMCLSM, several stator's structure parameters need to be fixed. The stator's structure parameters involved coil pitch,  $\tau_c$ , input power,  $P_{in}$  and coil turns,  $N$ . On mover part, several permanent magnet's magnetization direction arrangement were applied. Nine difference permanent magnet's magnetization direction arrangements have been chosen. It is as shown in Figure 4.2. For the mover part, magnetic pole pitch,  $\tau_{pm}$  and radius of permanent magnet,  $r_{pm}$  was fixed in order to create a valid comparison. The structure parameters of the PMCLSM used is as listed in Table 4.1.

The performance of all the PMCLSMs was evaluated using dynamic thrust. For the dynamic thrust, correlation between frequency,  $f$  of input power and mover speed,  $v$  is essential to simulate the dynamic thrust. The input power for each phase of the PMCLSM was set to 150 W at frequency,  $f$  of 70 Hz. At frequency,  $f$  of 70 Hz, and consideration of the magnetic pole pitch,  $\tau_{pm}$  of 12 mm as stated in Table 4.1, the PMCLSM mover speed,  $v$  was set to 1.68 m/s as calculated using Eq. (4.1).

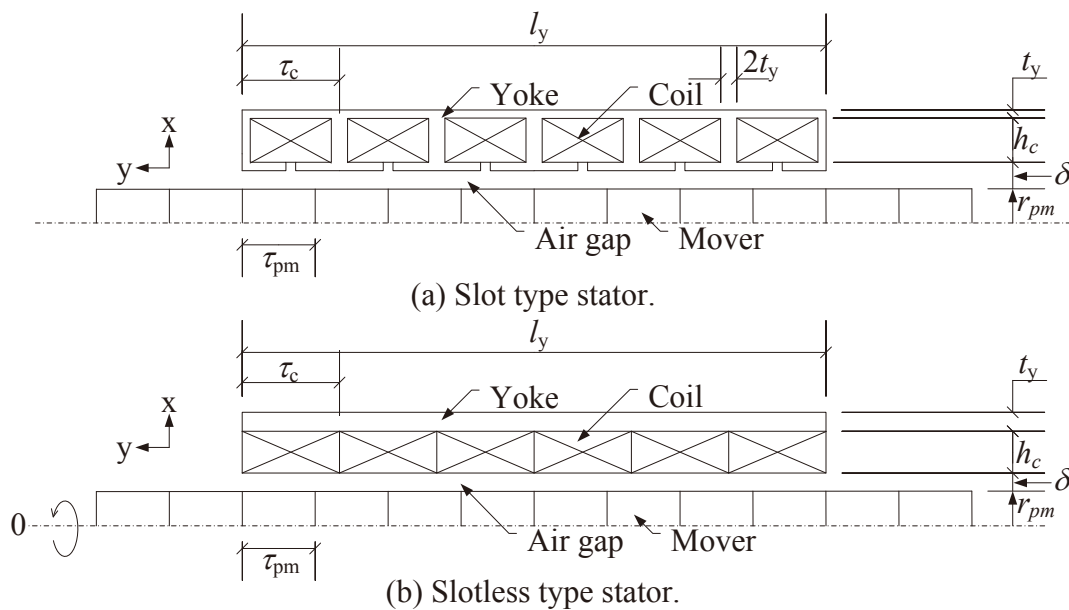


Figure 4.1 Skeleton of 6 slot 8 pole PMCLSM.

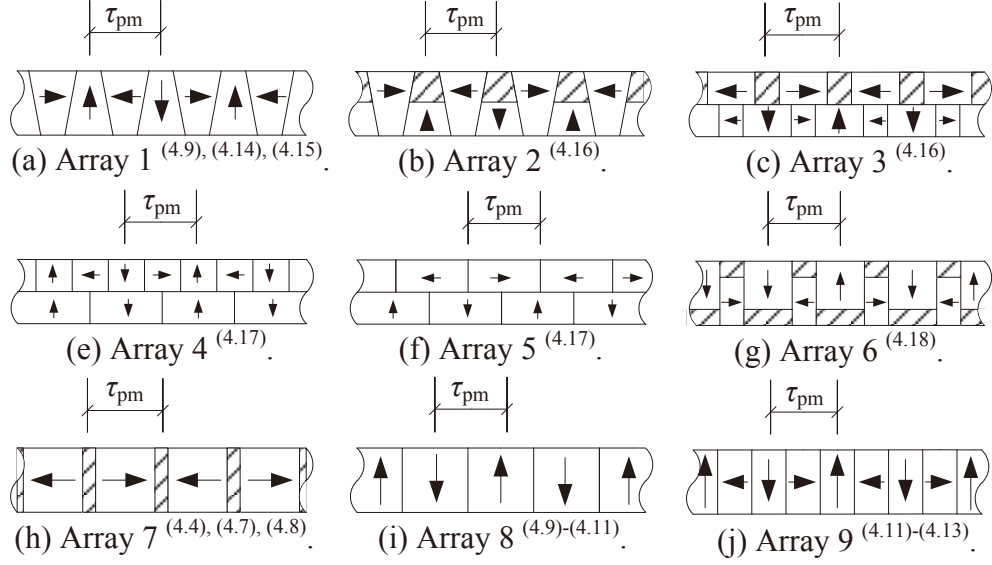


Figure 4.2 Permanent magnet magnetization arrangement and pitch of magnetization,  $\tau_{pm}$ .

$$\begin{aligned}
 v_m &= 2f\tau_{pm} \\
 &= 2(70)(12 \times 10^{-3}) \\
 &= 1.68 \text{ m/s.}
 \end{aligned} \tag{4.1}$$

where  $v_m$  is the mover speed in (m/s),  $f$  is the frequency of input power in (Hz) and  $\tau_{pm}$  is the magnetic pole pitch in (m).

Table 4.1 : The PMCLSM structure parameters.

Part	Parameter	unit	Value	
			Slot type	Slotless
Stator	Coil pitch, $\tau_c$	mm	16	16
	Coil turns, $N$		704	704
	Coil resistance, $R$	$\Omega$	18.26	14.89
	Height of coil, $h_c$	mm	6.5	5.5
	Yoke thickness, $t_y$	mm	2.5	2.5
	Length of stator, $l_y$	mm	96	96
Mover	Magnetic pole pitch, $\tau_{pm}$	mm	12	12
	Permanent magnet radius, $r_{pm}$	mm	10	10
Gap	Air gap length, $\delta$	mm	0.5	0.5

Generally, the performance of linear motors is evaluating using thrust characteristic <sup>(4.6), (4.11), (4.19), (4.20)</sup>. Nevertheless, several researcher has suggest to add some other performance characteristics such as thrust constant,  $k_f$ , motor constant,  $k_m$ , motor constant square density,  $G$ , electrical time constant,  $\tau_e$  and mechanical time

constant,  $\tau_m$  <sup>(4.4), (4.21) - (4.24)</sup>. As addition to the performance of the PMCLSM, thrust ripple,  $\Delta F$  and total weight,  $W_{tot}$  of all models will be used. While the thrust constant,  $k_f$ , the motor constant,  $k_m$  and the motor constant square density,  $G$  could be calculated using Eq. (2.2) to Eq. (2.4) as discussed in Chapter 2, the other performance characteristics used in the evaluation of PMCLSM performance are as listed in Table 4.2. Figure 4.3 shows sample of thrust characteristics of the slot type and slotless PMCLSM. Based on the thrust characteristics, most of the performance characteristics were derived. Except for time constants,  $\tau_e$  and  $\tau_m$  and total weight,  $W_{total}$  where depends on the structural parameters such as size of each parts and number of coil turns.

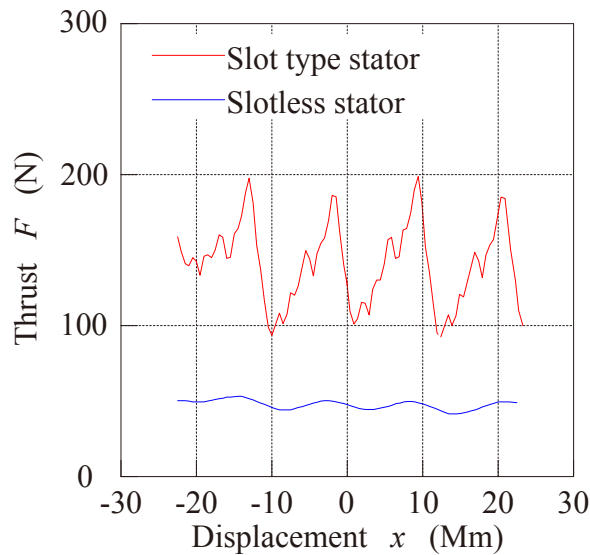


Figure 4.3 Sample of dynamic thrust characteristics of the PMCLSM.

Comparison of performance characteristics of all PMCLSM models is as shown in Figure 4.4. For the average thrust,  $F_{ave}$ , thrust constant,  $k_f$ , motor constants,  $k_m$  and motor constant square density,  $G$ , the higher value of its represent the better performance. On the other hand, for the rest of the performance characteristics, the lower value was aimed to represent better performance of the PMCLSM. Therefore, the graph in Figure 4.4 was set, so that the outer the plots of each performance characteristics on each axis represent better performance. Based on the Figure 4.4, it is shown that, within similar size of the PMCLSM, the slot type produced higher static performance characteristics such as average thrust,  $F_{ave}$ , thrust constant,  $k_f$ ,

motor constant,  $k_m$  and motor constant square density,  $G$ . Due to higher performance of static performance characteristics, the mover response is better for the slot type by evaluating its mechanical time constant,  $\tau_m$ . Both types of stator have a similar performance in terms of electrical time constant,  $\tau_e$ , however, the slotless type of the PMCLSM has significantly better performance in terms of ripple thrust,  $\Delta F$  and total weight,  $W_{tot}$  compared to slot type of the PMCLSM.

Table 4.2 : List of performance characteristics and its equation.

No.	Performance characteristics	Equation	Unit
1	Average thrust, $F_{ave}$ (N)	$F_{ave} = \frac{1}{x_T} \left( \int_0^{+x} F(x) dx + \int_{-x}^0 F(x) dx \right)$	(N) (4.2)
2	Electrical time constant, $\tau_e$ (ms)	$\tau_e = \frac{L}{R}$	(ms) (4.3)
3	Mechanical time constant, $\tau_m$ (ms)	$\tau_m = \frac{mR^2}{k_f}$	(ms) (4.4)
4	Thrust ripple, $\Delta F$ (%)	$\Delta F = \frac{F_{max} - F_{min}}{F_{ave}} \times 100\%$	(%) (4.5)
5	Total weight, $W_{tot}$ (kg)	$W_{tot} = W_{coil} + W_{pm} + W_{yoke}$	(kg) (4.6)

For Eq. (4.2) – Eq. (4.6),  $F_{ave}$  is the average thrust in (N),  $x_T$  is the total displacement of the PMCLSM in (m),  $+x$  and  $-x$  are the most positive and negative displacement respectively in (m),  $\tau_e$  and  $\tau_m$  are the electrical and mechanical time constant respectively in (ms),  $L$  is the PMCLSM inductance in (mH),  $R$  is the PMCLSM resistance in ( $\Omega$ ),  $m$  is the mass of PMCLSM's mover in (kg),  $\Delta F$  is the ripple thrust in (%),  $F_{max}$  is the maximum thrust in (N),  $W_{tot}$  is the total weight in (kg) and  $W_{coil}$ ,  $W_{pm}$  and  $W_{yoke}$  are the the PMCLSM particular parts (kg) respectively.

- Model array 1    ○ Model array 2    △ Model array 3    ◇ Model array 4    ◊ Model array 5  
 ▷ Model array 6    ◊ Model array 7    ☆ Model array 8    ⬠ Model array 9

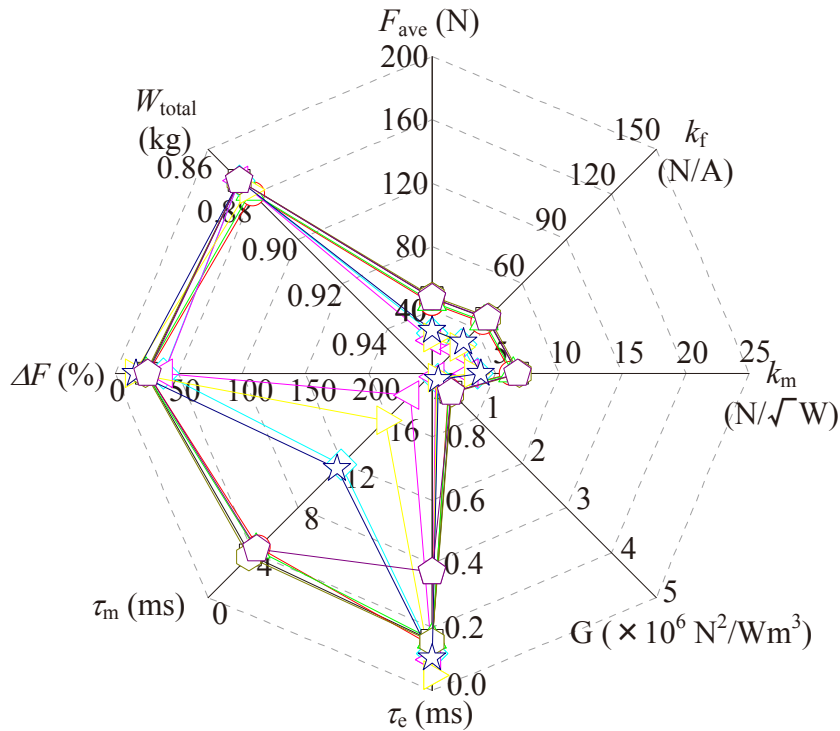
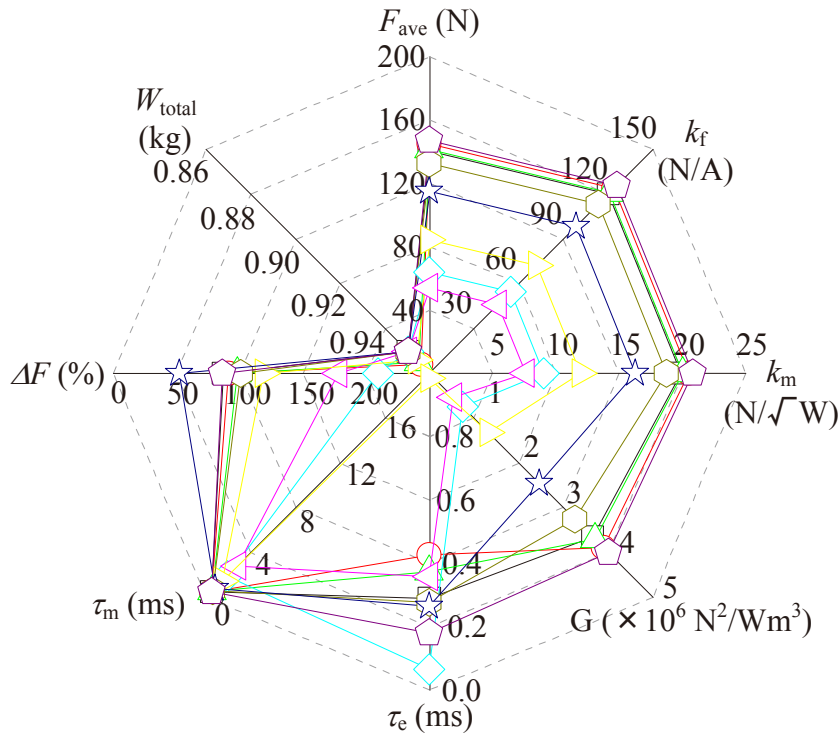


Figure 4.4 Performance comparison of the PMCLSM between difference stator types and magnetization direction arrangements.

---

The comparison of the slot type stator of the PMCLSM performance is as shown in Figure 4.4 (a). Based on the comparison, the slot type of the PMCLSM has a similar value of total weight,  $W_{\text{tot}}$  and mechanical time constant  $\tau_m$ . Nevertheless, the slot type of the PMCLSM magnetization direction arrangement 4, 5 and 6 have the lowest performance in almost all performance characteristics except for the electrical time constant  $\tau_e$ , where the PMCLSM with magnetization direction arrangement 4 has the best performance compared to other models. Even though the model with magnetization direction arrangement 8 gives the lowest value of thrust ripple  $\Delta F$ , it gives the lowest value in other performance characteristics, especially on average thrust  $F_{\text{ave}}$ , motor constants  $k_m$  and motor constants square density  $G$ , with the exception of models with the magnetization direction arrangement 4, 5 and 6. Apart from other models which were observed with similar performance characteristics, the slot type linear actuator with permanent magnet magnetization arrangement 2 and 9 have the best performance in all characteristics except the thrust ripple  $\Delta F$  and the electrical time constant,  $\tau_e$ .

The comparison slotless type of the PMCLSM performance characteristics is shown in Figure 4.4 (b). Based on the plot, all models of the slotless type of the PMCLSM have a similar value of all performance characteristics except for the electrical time constant,  $\tau_e$  and mechanical time constant,  $\tau_m$ . However, the slotless type of the PMCLSM with magnetization direction arrangement 5 and 6 have the lowest performance in almost all characteristics except for the electrical time constant  $\tau_e$  compared to other models of slotless type of the PMCLSM. Due to elimination of the slotless type of the PMCLSM models with magnetization direction arrangement 5 and 6, the model with magnetization direction arrangement 4 and 8 were observed with the lowest thrust ripple,  $\Delta F$  and electrical time constant,  $\tau_e$ . However, it gave a low performance on other characteristics, especially average thrust,  $F_{\text{ave}}$  and the mechanical time constant,  $\tau_m$ . On the other hand, the slotless type of the PMCLSM with magnetization direction arrangement of 1 and 7 are seen as the best two models for the slotless type of the PMCLSM since they have the best performance in all performance characteristics except for the ripple thrust,  $\Delta F$  for both models and electrical time constant,  $\tau_e$  for the slot-less PMCLSM with magnet direction

magnetization arrangement 7. Table 4.3 shows the summary of comparison between the best two models of slot and slotless type of the PMCLSM.

Table 4.3 : Comparison of best two model of slot-less and slot type PMCLSM.

Performance characteristics	Unit	Magnetization direction arrangement			
		Slot type		Slotless type	
		Model array 2	Model array 9	Model array 1	Model array 7
Average thrust, $F_{ave}$	N	145.06	147.06	47.65	48.70
Thrust constant, $k_f$ .	N/A	123.93	125.65	36.82	37.63
Motor constant, $k_m$ .	N/ $\sqrt{W}$	20.51	20.80	6.74	6.89
Motor constant square density, $G$ .	$\times 10^6$ N <sup>2</sup> /Wm <sup>3</sup>	3.90	4.00	0.42	0.44
Electrical time constant, $\tau_e$ .	ms	0.43	0.18	0.16	0.15
Mechanical time constant, $\tau_m$ .	ms	0.50	0.48	3.77	3.62
Ripple thrust, $\Delta F$	%	90.63	86.04	24.69	23.79
Total weight, $W_{tot}$ .	kg	0.96	0.95	0.87	0.87

Based on Table 4.3, the model array 9 is the best model for the slot type of the PMCLSM. On the other hand, the model 7 is the best model for the slotless type of the PMCLSM. Even though, neither of slot type nor slotless type of the PMCLSM has fulfilled the thrust,  $F$  requirement by the E-Cutter, however, the total weight,  $W_{tot}$  are far below than its restricted value. Therefore, a design step via structure parameter variation is necessary to make sure the PMCLSM achieves its thrust requirement. Despite of that, the slot type of the PMCLSM with model array 9 has a great possibility to function as E-Cutter's actuator. It is due to the ratio of thrust over weight is higher compared to other models and it shows feasibility of it to reach aimed thrust at restricted weight.

#### 4.2 Design of the Structure Parameter of the PMCLSM

The slot type PMCLSM with model array 9 (or Halbach array) requires a further design stage to make it fulfill E-Cutter's actuator requirement. During design stage, several structure parameters of the PMCLSM will be varied. Dynamic thrust and total

---

weight of it will be calculated and compared to decide the finalized structure parameter. The design of the PMCLSM was done in two stages. First stage, effect of coil height,  $h_c$  and radius of permanent magnet,  $r_{pm}$  to PMCLSM performance were observed. Aim during the first stage was to made the PMCLSM fulfil its design target.

Based on result from first stage, second stage of the design stage was carried out. During the second stage of design, the shaft radius,  $r_s$  and height of permanent magnet,  $h_{pm}$  were varied within fixed radius of permanent magnet,  $r_{pm}$ . The aim of second stage of the design is to strengthen the mover part of the PMCLSM. During the second stage of design, thrust reduction is expected due to reduction of the size of permanent magnet. The of combination shaft radius,  $r_s$  and height of permanent magnet,  $h_{pm}$  that give insignificant thrust reduction will be used as the final structure parameter of the PMCLSM.

#### **4.2.1 Effect of coil height and permanent magnet radius to the PMCLSM performance**

In the first stage of design, the effect of height of coil,  $h_c$  and radius of permanent magnet,  $r_{pm}$  to the PMCLSM performance were examined. Figure 4.5 shows the basic structure and structure parameter of the 6 slot 8 pole slot type of PMCLSM. Several structure parameters has been fixed such as coil pitch,  $\tau_c$ , magnetization pitch,  $\tau_{pm}$ , yoke thickness,  $t_y$  and air gap,  $\delta$ . The total radius,  $r_{total}$  has been set at 20 mm, 25 mm and 30 mm and the shaft radius,  $r_s$  was set to 1mm. At the same time, the height of coil,  $h_c$  and radius of permanent magnet,  $r_{pm}$  have been varied at all possible dimensions at fixed total radius,  $r_{total}$ . The average thrust,  $F_{ave}$  and total weight,  $W_{tot}$  of the PMCLSM were calculated for all models. The design procedure of the first stage of design is as shown in Figure. 4.6.

Due to variation of height of coil,  $h_c$ , the coil turns,  $N$  of each model of PMCLSM will be varied too. It also will affect the resistance,  $R$  and current,  $I$  for each coil. By considering the input power,  $P_{in}$  for each model has been fixed to 150 W for each phase, coil turns,  $N$ , coil resistance,  $R$  and current,  $I$  were calculated using Eq. (4.7), Eq. (4.8) and Eq. (4.9). The total weight,  $W_{tot}$  of each PMCLSM models can be calculated using Eq. (4.10).

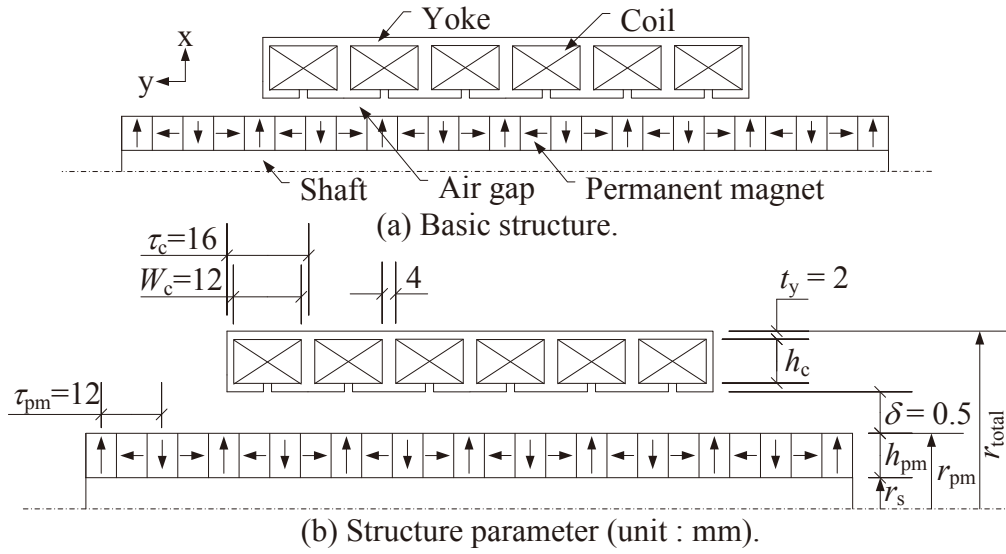


Figure 4.5 Basic structure and structure parameter of the 6 slot 8 pole slot type PMCLSM.

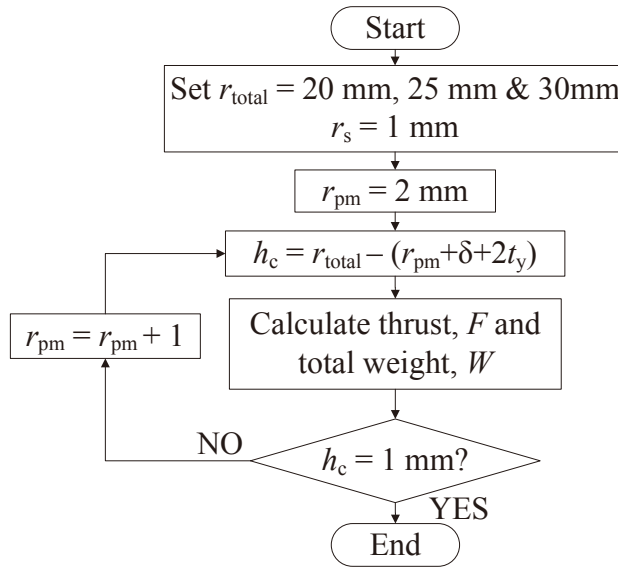


Figure 4.6 Design procedure of first stage of design.

$$N = \frac{1}{\xi} \left( \frac{W_c}{\phi_C} \times \frac{h_c}{\phi_C} \right), \quad (4.7)$$

$$R = N^2 \frac{\rho l}{a} = \frac{1}{\xi^2} \left( \frac{W_c}{\phi_C} \times \frac{h_c}{\phi_C} \right)^2 \frac{8\pi\rho \left( r_{pm} + \delta + t_y + \frac{h_c}{2} \right)}{\pi\phi_C^2}, \quad (\Omega) \quad (4.8)$$

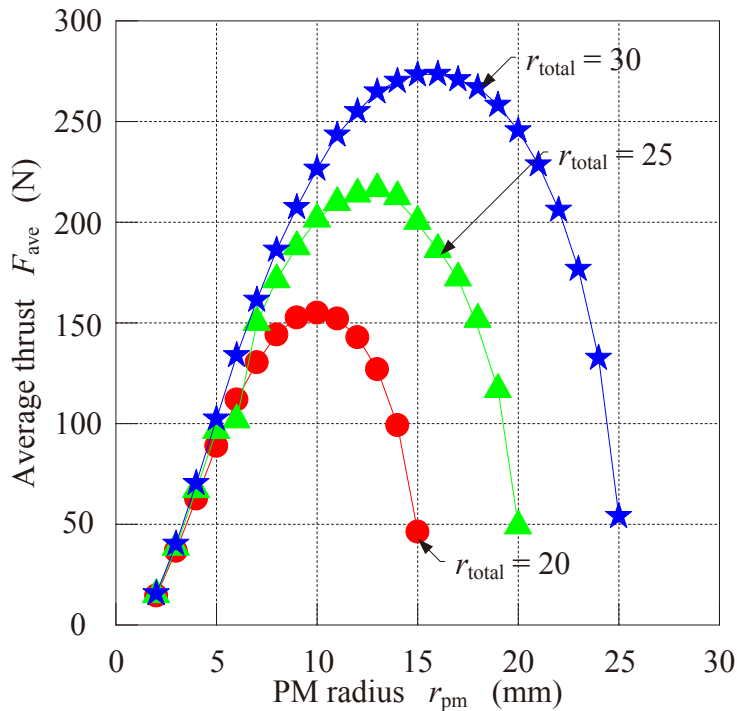
$$\begin{aligned}
I_\phi &= \sqrt{\frac{P_{in}}{2R}} \\
&= \sqrt{\frac{150}{2R}},
\end{aligned}
\tag{A} \quad (4.9)$$

$$W_{tot} = \rho_{copper} v_{coil} + \rho_{NdFeB} v_{pm} + \rho_{SS400} v_{yoke} + \rho_{SUS304} v_{shaft}. \quad (\text{kg}) \quad (4.10)$$

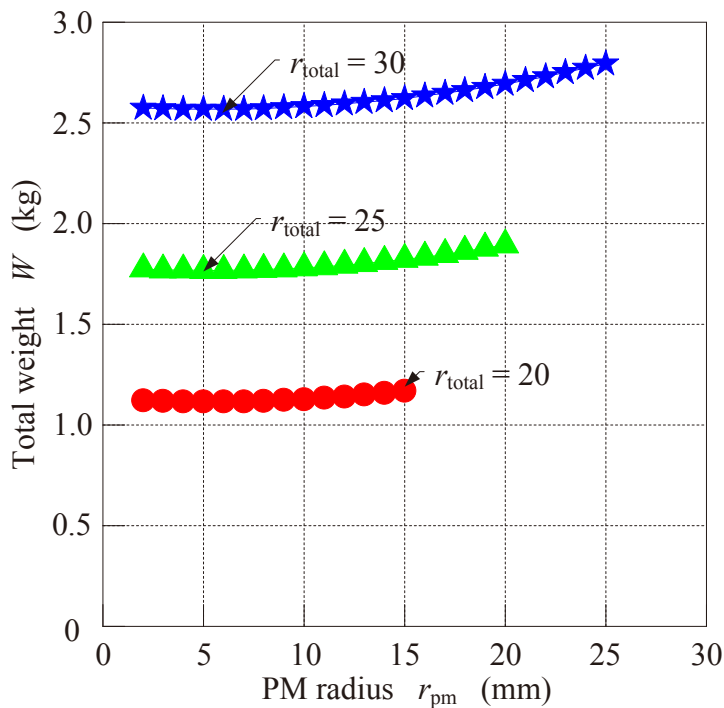
where  $W_c$  is the coil width in (m),  $\xi$  is the space factor equal to 0.6,  $\phi_c$  is the copper wire diameter in (m),  $\rho$  is the copper resistivity equal to  $1.67 \times 10^{-6} \Omega \cdot \text{m}$ ,  $l$  is the copper wire length in (m),  $a$  is the copper wire cross sectional area in ( $\text{m}^2$ ),  $\delta$  is the air gap length in (m),  $I_\phi$  is the phase current in (A),  $P_{in}$  is the input power in (W),  $\rho_{material}$  is the material density in ( $\text{kg}/\text{m}^3$ ) and  $v_{part}$  is the volume of PMCLSM part in ( $\text{m}^3$ ).

Figure 4.7 shows the effect of permanent magnet (PM) radius,  $r_{pm}$  to average thrust,  $F_{ave}$  and total weight,  $W_{tot}$  of the PMCLSM. By increasing permanent magnet radius,  $r_{pm}$ , average thrust,  $F_{ave}$  will also increase until it reaches maximum value. This is due to higher magnetic energy providing by permanent magnet to produce higher thrust. However, beyond the maximum point, increment of permanent magnet size does not contribute to produce higher thrust. Instead, the thrust is reducing despite the larger size of permanent magnet. It is because of smaller size of coil produce lower magnetomotive force by the PMCLSM.

The effect of permanent magnet radius,  $r_{pm}$  to total weight,  $W_{tot}$  of the PMCLSM is as shown in Figure 4.7 (b). Increment of permanent magnet radius,  $r_{pm}$  does not give significant changes to total weight,  $W_{tot}$ . On the other hand, the total weight,  $W_{tot}$  of the PMCLSM is only influence by the total radius,  $r_{total}$ . The higher total radius,  $r_{total}$  produce the higher total weight,  $W_{tot}$ . It is due to higher volume of each PMCLSM's parts on higher total radius,  $r_{total}$ .



(a) Effect of PM radius to average thrust.



(b) Effect of PM radius to total weight.

Figure 4.7 Average thrust  $F_{ave}$  and total weight,  $W$  of the PMCLSM.

The model of the PMCLSM gives highest thrust on each difference total radius,  $r_{total}$  is as listed in Table 4.4. Based on Table 4.4, the PMCLSM with total radius,  $r_{total}$  of 25 mm and 30 mm are exceeding the thrust requirement with producing



optimizing is to select the combination of these structure parameters that give insignificant thrust reduction.

In this stage, the structure parameter of the PMCLSM will follow similar as shown in Figure 4.8. The shaft radius,  $r_s$  will be increased by 1 mm and made the height of permanent magnet,  $h_{pm}$  will be reduce by 1 mm due to fixed of radius of permanent magnet,  $r_{pm}$ . For each models, the average thrust,  $F_{ave}$  will be calculated and compared. The current,  $I$  of the PMCLSM was varied from 1.0 A to 3.0 A. The design procedure of the second stage of design is as shown in Figure 4.9.

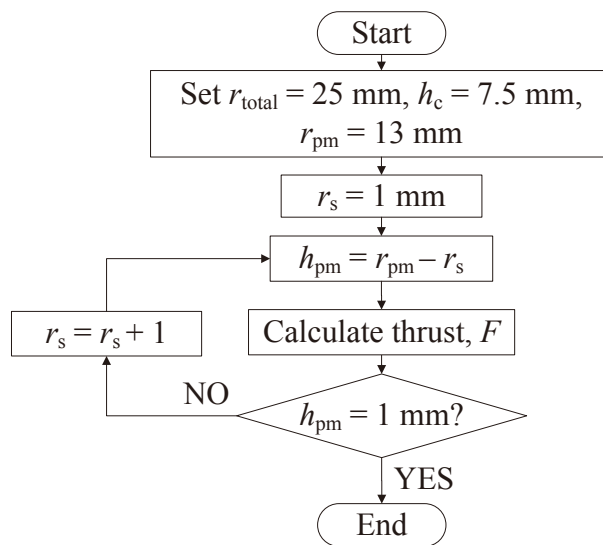


Figure 4.9 Design procedure of second stage of design.

The effect of shaft radius,  $r_s$  to average thrust,  $F_{ave}$  of the PMCLSM is as shown in Figure 4.10. As shown in Figure 4.10, thrust reduction is not significant for a shaft radius,  $r_s$  below than 6 mm. On the other hand, thrust reduction become significant for shaft radius,  $r_s$  higher than 6 mm. Therefore, the shaft radius,  $r_s$  of 6 mm is considered as optimal.

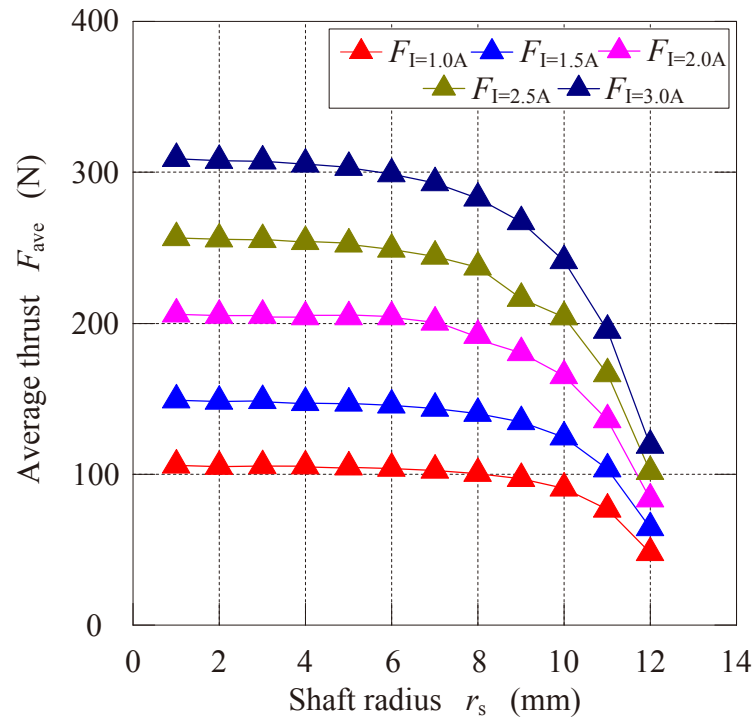


Figure 4.10 Effect of shaft radius,  $r_s$  to average thrust,  $F_{ave}$  of the PMCLSM.

The final structure of the PMCLSM is as shown in Figure 4.11. Each coil of the PMCLSM has 462 coil turns and  $14.2 \Omega$  of each coil resistance. Figure 4.12 shows effect of current,  $I$  to thrust,  $F$  of the PMCLSM. Based on Figure 4.12, it shows that, at current,  $I$  of 2.0 A, average thrust,  $F_{ave}$  is 208.50 N. It is already exceed the thrust required to function as E-Cutter's actuator. At current,  $I$  of 2.0 A, input power,  $P_{in}$  of the PMCLSM is 113.6 W.

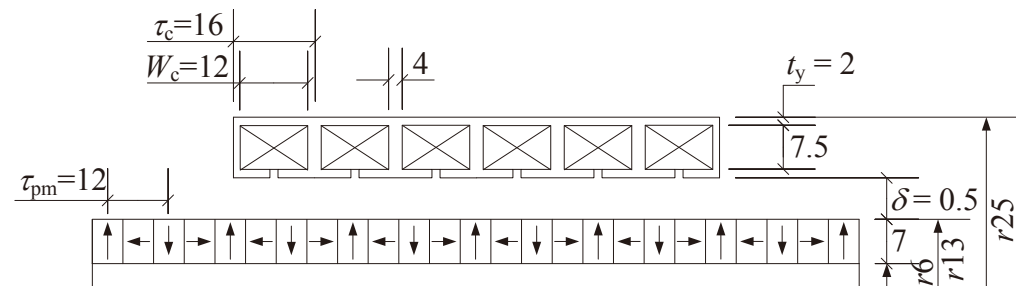
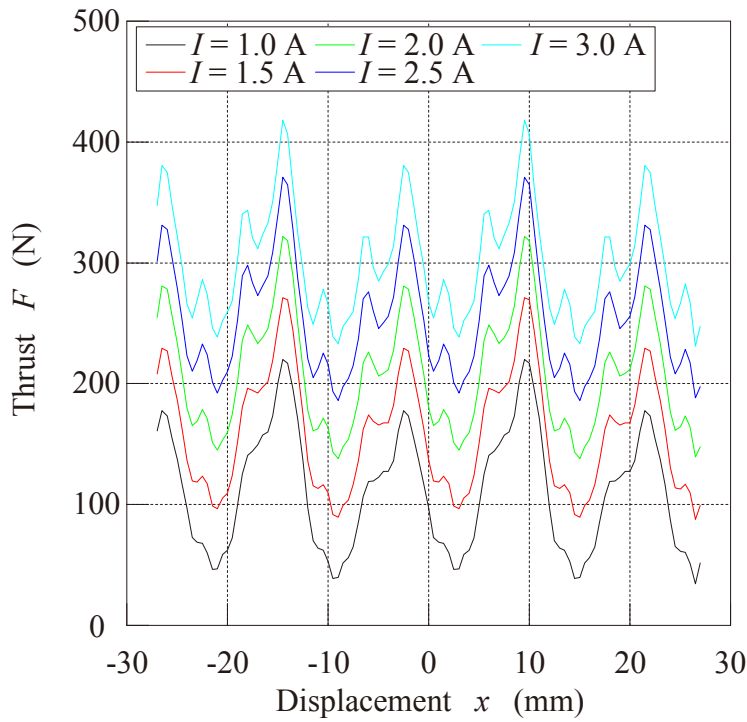
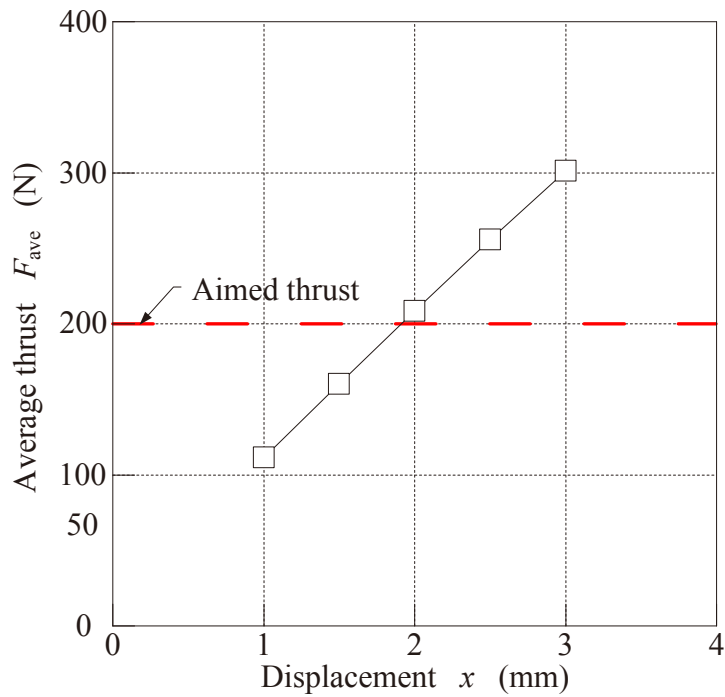


Figure 4.11 Final structure parameter of the PMCLSM (unit : mm)



(a) Dynamic thrust,  $F$  of the PMCLSM at difference current,  $I$ .



(b) Effect of current,  $I$  to average thrust,  $F_{ave}$ .

Figure 4.12 Effect of current to thrust of the PMCLSM.

---

### 4.2.3 Comparison of the PMCLSM performance with commercialize linear motor

The performance of the PMCLSM is then compared to commercialized permanent magnet linear motor (PMLM). The performance comparison was done by utilizing performance index as discussed in Chapter 2. All the performance index of the commercialized PMLM were obtained from manufacturer product technical information. Some of the performance characteristics might be could not be obtain directly, however, it was calculated by using Eq. (2.2) to Eq. (2.4) as discussed in Chapter 2.

Performance comparison between the PMCLSM with commercialized PMLM is as shown in Figure 4.13. The comparison was done with volume,  $V_{\text{mot}}$  of each linear motor model is made as reference. Based on Figure 4.13, it shown that, the PMCLSM capable to produce higher performance compared to similar volume,  $V_{\text{mot}}$  of the commercialized PMLM. Generally, the linear motor performance depends on the input power,  $P_{\text{in}}$ . Therefore, by using motor constant square density,  $G$ , the input power,  $P_{\text{in}}$  of each model of PMLM including PMCLSM has been equalized as shown in Figure 4.13(d). Based on Figure 4.13 (d) shows capability of the PMCLSM to produce higher thrust,  $F$  at similar input power,  $P_{\text{in}}$  compared to similar volume of the commercialized PMLM.

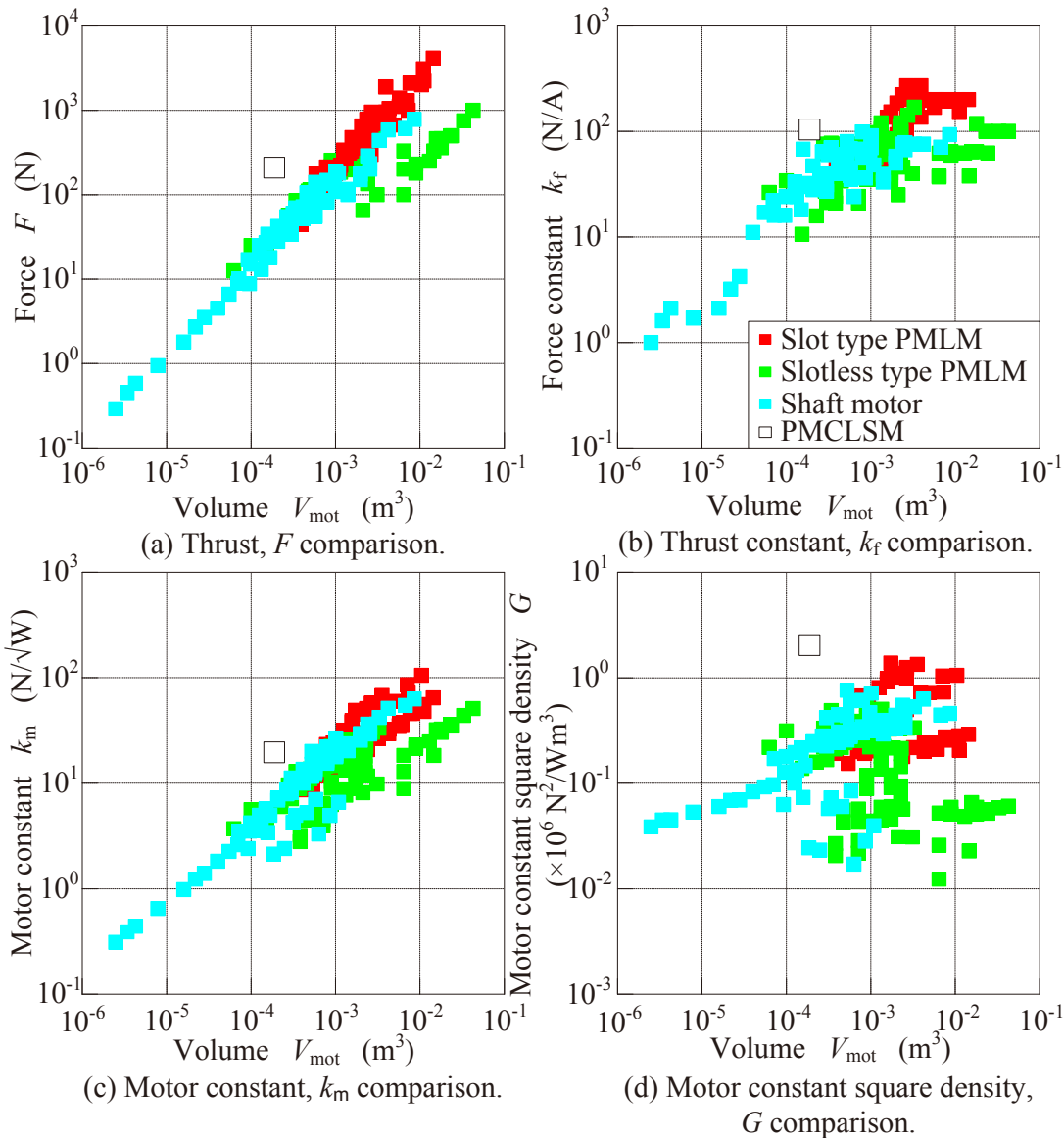


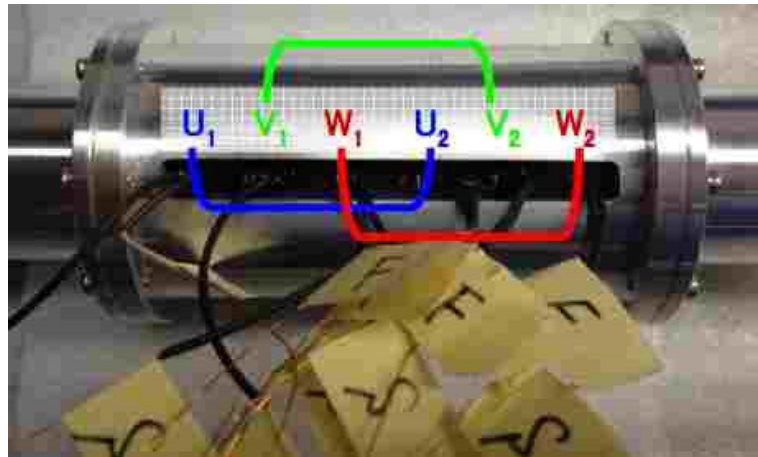
Figure 4.13 Comparison between the PMCLSM and commercialized permanent magnet linear motor (PMLM) performance characteristics.

### 4.3 Manufactured of the PMCLSM

Based on result of design, the PMCLSM has been manufactured. Figure 4.14 shows the manufactured PMCLSM. Figure 4.14 (a) shows the stator part and casing of the PMCLSM. The stator part is consisting of 6 coil arranged for 3 phase topology. Each phase consist of 2 coils that connected in series. The mover part of the PMCLSM is as shown in Figure 4.14 (b). It consists of halbach magnetization direction arrangement as was designed. Table 4.5 shows the specification of the PMCLSM.

Table 4.5 : Specifications of the PMCLSM.

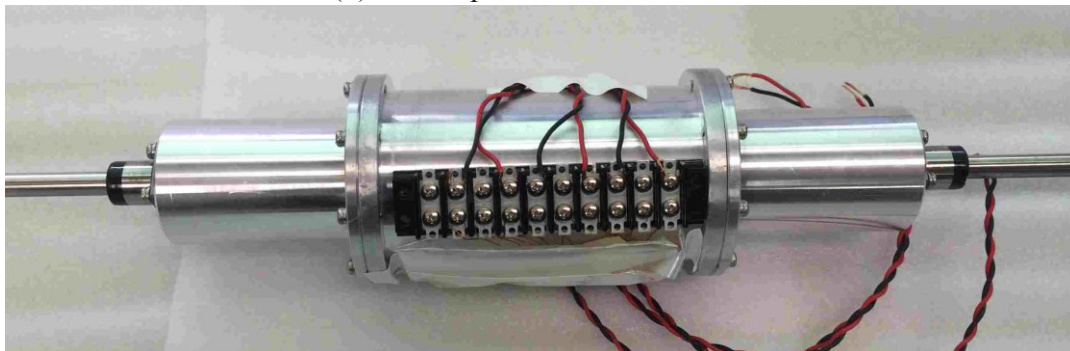
Part	Item		Value
Size motor	Stator length		96 mm
	Total radius		25 mm
	Slot/pole number		6/8
Stator part	Yoke thickness, $t_y$		2 mm
	Length between coils, $2t_y$		4 mm
	Yoke material		SS400
	Coil	Diameter wire, $\phi_c$	0.3 mm
		Insulation Class	H (180 <sup>0</sup> )
		Turns, N	462 turns
		Resistance, $\Omega$	13.6 $\Omega$
Number of coil each/connection		2/Series	
Mover part	Permanent Magnet	Material	NdFeB
		Type	N42SH
		Maximum Operating Temperature, $T_w$	340 <sup>0</sup> C
		Remanent magnetic flux density, $B_r$	1.27-1.32 T
		Coercive force, $H_c$	$\geq 955$ kA/m
		Shape	Ring type
		Size ( $r_{outer}/r_{inner}/length$ )	13 mm/6 mm/6 mm



(a) Stator part of the PMCLSM.



(b) Mover part of the PMCLSM.



(c) Assembled PMCLSM.

Figure 4.14 Manufactured PMCLSM.

#### 4.4 Static Characteristics Performance of the PMCLSM.

In order to evaluate performance of the PMCLSM, static characteristics measurements were conducted. The static characteristics performances are including static thrust characteristic,  $RL$  characteristic and electrical time constant,  $\tau_e$  characteristic.

---

#### 4.4.1 Static Thrust Characteristic

Figure 4.15 and Figure 4.16 shows experiment setup and schematic diagram for thrust characteristic measurement respectively. The static thrust of the PMCLSM was measured using load cell (TCLP-50KA). The current of the PMCLSM was varied from 0.0 A to 2.5 A using DC power supply (IPS 303DD) and power amplifier (NF 4502). The multimeter was used to observe the terminal voltage of the PMCLSM's coil equivalent to specific current.

The static thrust characteristic of the PMCLSM were measured on full scale of it mover displacement. The PMCLSM was rest on movable table and the mover was locked at header. The PMCLSM displacement was varied by using handle. The PMCLSM was moved in forward and reverse direction. Despite of measuring thrust, through this measurement style, friction force of the PMCLSM also can be captured. The thrust characteristic of the PMCLSM was measured on each individual phase and the measurement result and simulation output was compared for result validation.

Figure 4.17 shows sample of thrust characteristic of the PMCLSM. In this case, current was set to 0 A. Due to existence of friction force,  $F_C$ , the thrust in forward and reverse direction has different value. Based on the forward and reverse direction thrust, the thrust,  $F$  and friction force,  $F_C$  were calculated. The thrust,  $F$  and friction force,  $F_C$  were calculated using equation below,

$$F = \frac{F_{\text{fwd}} + F_{\text{rev}}}{2}, \quad \text{N} \quad (4.11)$$

$$F_C = |F_{\text{fwd}} - F_{\text{rev}}| \quad \text{N} \quad (4.12)$$

where  $F$  is the thrust in (N),  $F_{\text{fwd}}$  and  $F_{\text{rev}}$  are the forward and reverse direction force respectively in (N) and  $F_C$  is the friction force in (N).

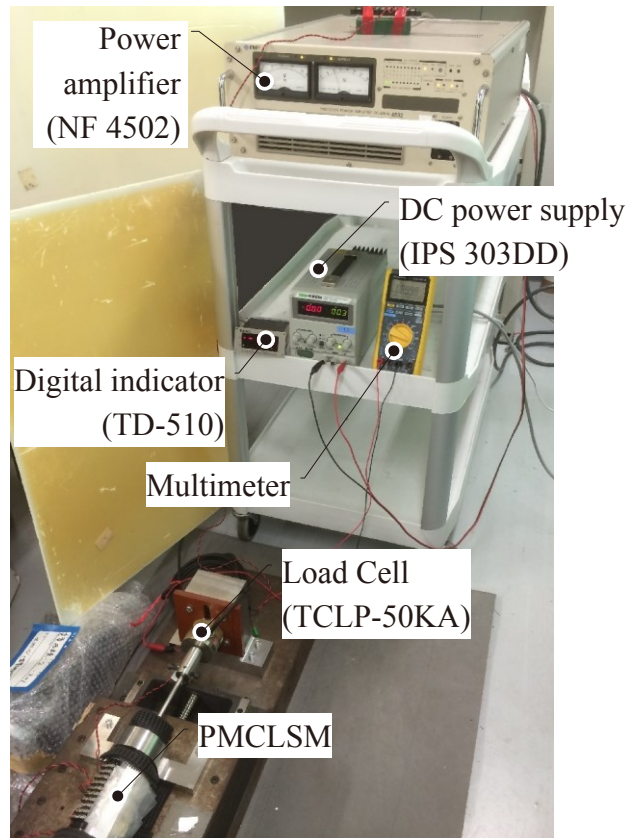


Figure 4.15 Experiment setup for static thrust characteristic measurement.

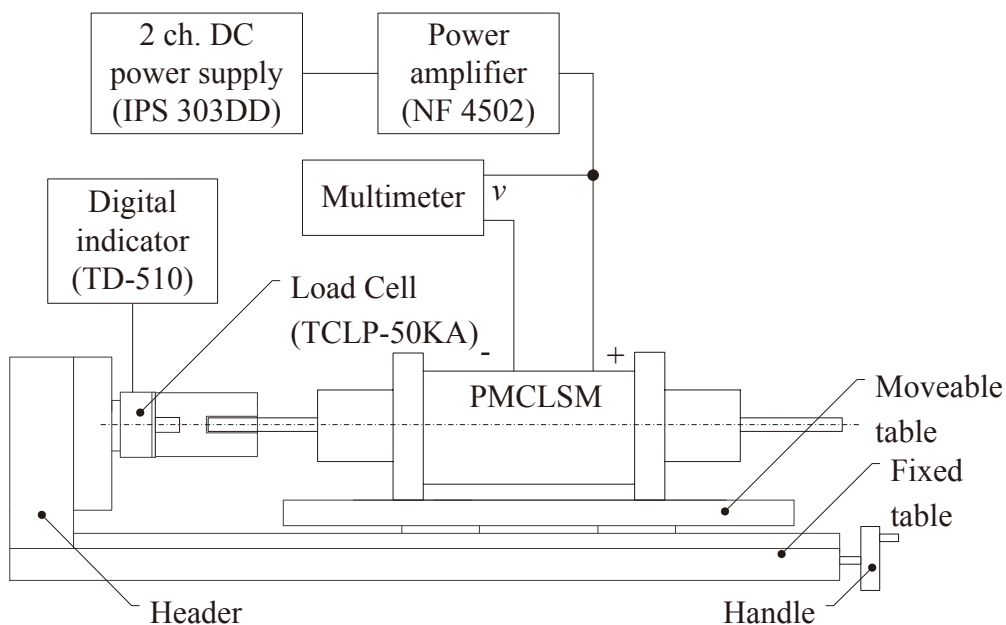
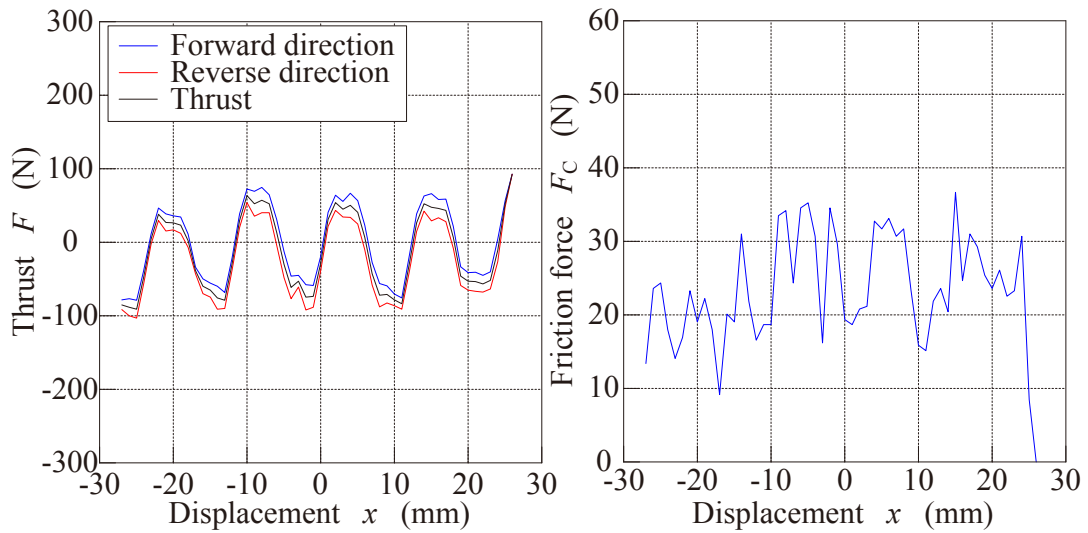


Figure 4.16 Schematic diagram for static thrust characteristic measurement.



(a) Thrust. (b) Friction force.  
 Figure 4.17 Sample of thrust and friction force of the PMCLSM.

Figure 4.18 shows comparison between measured and simulated cogging force characteristics. It shows that, the profile of measured and simulated cogging force characteristics is in good agreement. However, it shows a difference in maximum value of cogging force. The maximum cogging force via measurement was 63.26 N while via simulation was 89.25 N. On the other hand, the friction force,  $F_C$  during 0 A excitation was in range between 10 N to 38 N.

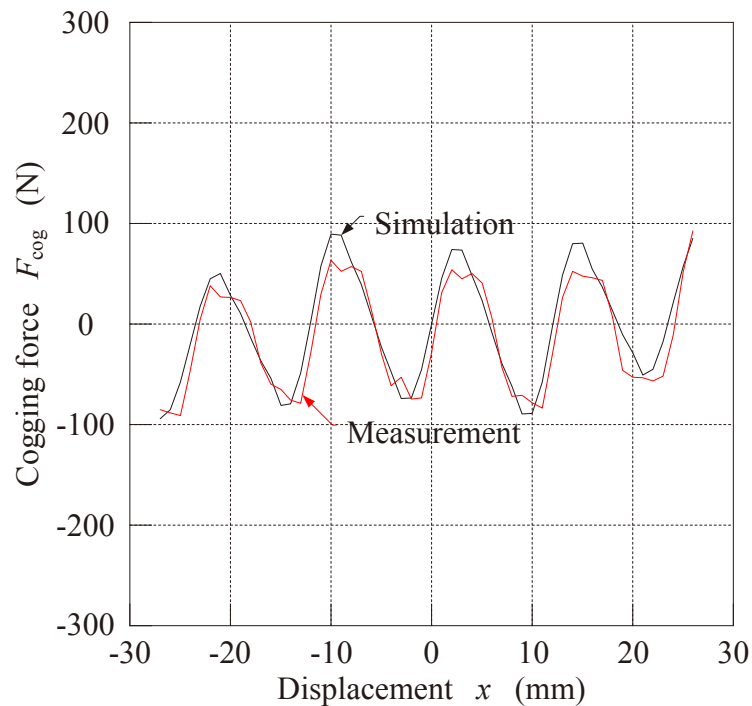


Figure 4.18 Cogging force characteristic of the PMCLSM.

---

As shown in Figure 4.18, cogging force of the PMCLSM is relatively high. There are various methods can be applied to reduce cogging force. One of the most common methods is via skewing of permanent magnet <sup>(4.25)-(4.27)</sup>. However, this method will make design and manufacturing process of the E-Cutter's actuator more complicated. On the other hand, the simplest technique to reduce cogging force is via optimization on slot and pole combination <sup>(4.28)</sup>. Generally, by increasing number of combination of slot and pole will reduce cogging force naturally. But it will also reduce thrust of the PMCLSM. J. Lim and HK. Jung was suggested phase set shift method to minimize cogging force <sup>(4.29)</sup>. Yet, additional set of stator to the existing PMCLSM structure will increase total weight,  $W_{tot}$  and exceed the aimed weight of the E-Cutter's actuator. AS. Mahdi *et al.* 2007, on the other hand suggest magnet dividing method to reduce cogging force <sup>(4.30)</sup>. Similar to skewing permanent magnet method, it will complicate the design and manufacturing process of the PMCLSM and also will reduce thrust due to reduction of permanent magnet volume.

Several methods on cogging force reduction have been discussed from simple methods like optimizing on slot and pole combination and phase set shift to complicated methods like permanent magnet skewing and dividing. Based on finding of several researcher <sup>(4.25)-(4.30)</sup>, these methods successfully reducing the cogging force. Nevertheless, these methods produce side effect to the PMCLSM's performance such as thrust reduction and complicated design and manufacturing process. The main consideration during E-Cutter's actuator is cutting force,  $F_{cutting}$ . As long as, the PMCLSM could provide adequate cutting force,  $F_{cutting}$ , cogging force is not a crucial consideration. Therefore, in order to maintain thrust and simple structure of the E-Cutter's actuator, cogging force reduction is not an important step for the PMCLSM design.

The thrust characteristics at different current,  $I$  of U, V and W phase are as shows in series of Figure 4.19 to Figure 4.21. Similar to cogging thrust characteristics, the profile of measured and simulated thrust has a good agreement. However, difference of maximum value was obtained between measurement and simulation result. It also shows that, the higher current produce higher difference of maximum thrust. The difference of the maximum and minimum thrust,  $F_{max}$  and  $F_{min}$  between measured and simulated result and measurement error,  $\varepsilon$  was summarized as

---

in Figure 4.22. Based on Figure 4.22, magnetic density saturation was seemed not occurred in simulation result. However, magnetic density saturation was occurred at current,  $I$  higher than 1.5 A. At current,  $I$  higher than 1.5 A, the measured thrust is not increased. It made the measurement error become higher at current,  $I$  higher than 1.5 A.

The profile of thrust characteristics of U and W phase has a similar profile. However, it is inverse compared to each other. It is due to similar location of coil for both phases but the current direction compared to both phases in inverse. It explained the similarity of its profile but inverse in direction. On the other hand, the profile of the V phase thrust characteristics was difference compared to U and W phase. It is due to location of V phase coil is in between U and W phase.

On the Figure 4.19 to Figure 4.21 also, the friction force,  $F_C$  on each phase and different current,  $I$  was shown. Based on the series of figures, the friction force,  $F_C$  is directly proportional with the thrust,  $F$  produced. At similar current,  $I$ , the PMCLSM produced about similar of friction force,  $F_C$ . For example, at current,  $I$  of 0.5 A, the friction force,  $F_C$  produced is in range or 8 N to 40 N for U, V and W phase.

Based on the static thrust characteristic result, it is shown that, 200 N of thrust was not able to be achieved. The magnetic density saturation seem to be happened at current,  $I$  of 1.5 A and the maximum thrust,  $F_{\max}$  is about 133 N for U phase, 157 N for V phase and 180 N for W phase. In order to resolve the magnetic density saturation occurrence, the appropriate size of yoke thickness needs to be determine. In the same time, the magnetomotive force value need also to be considered to make sure the PMCLSM fulfil the cutting thrust,  $F_{\text{cutting}}$  requirement.

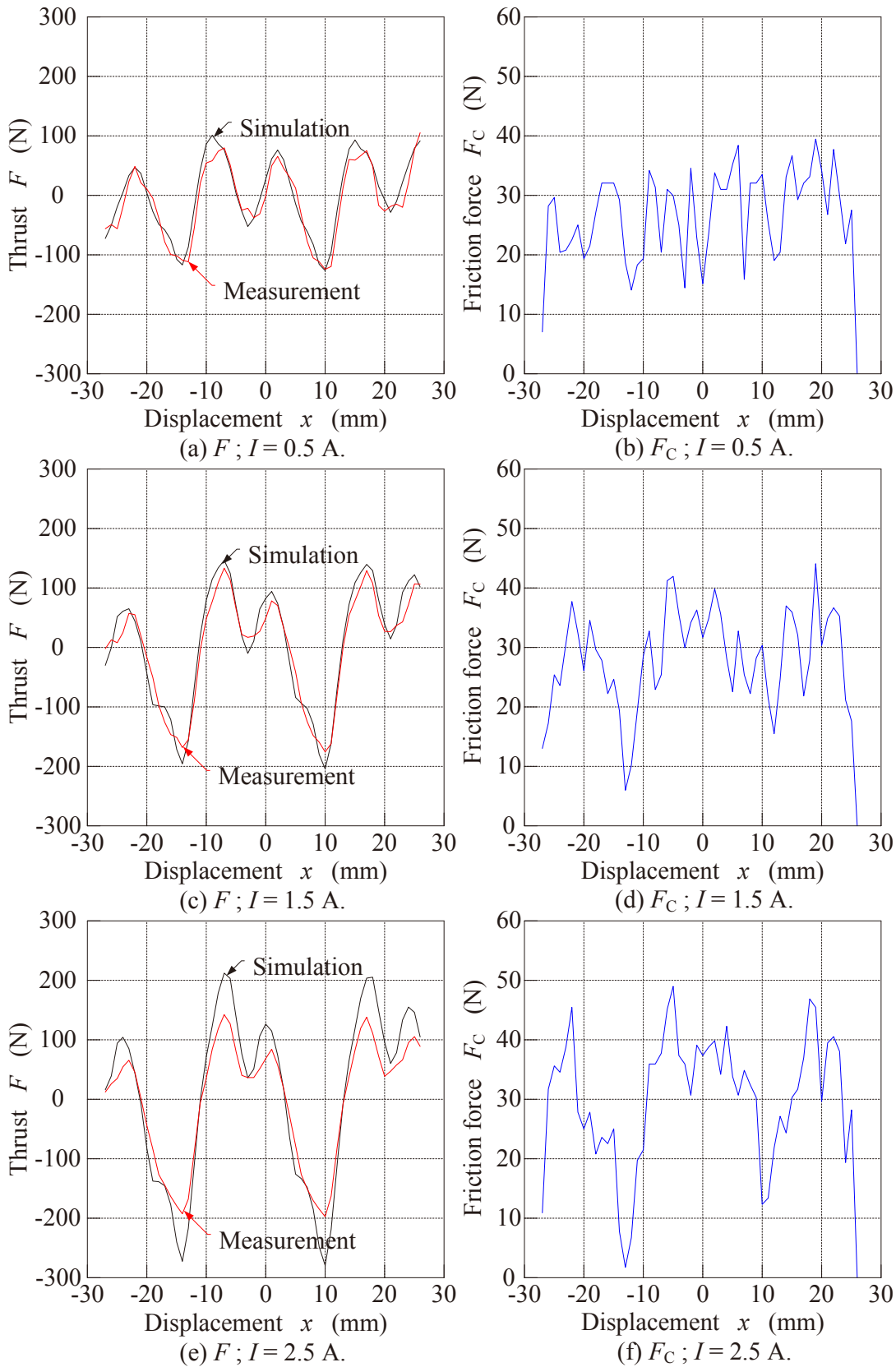


Figure 4.19 Thrust characteristic of the U phase.

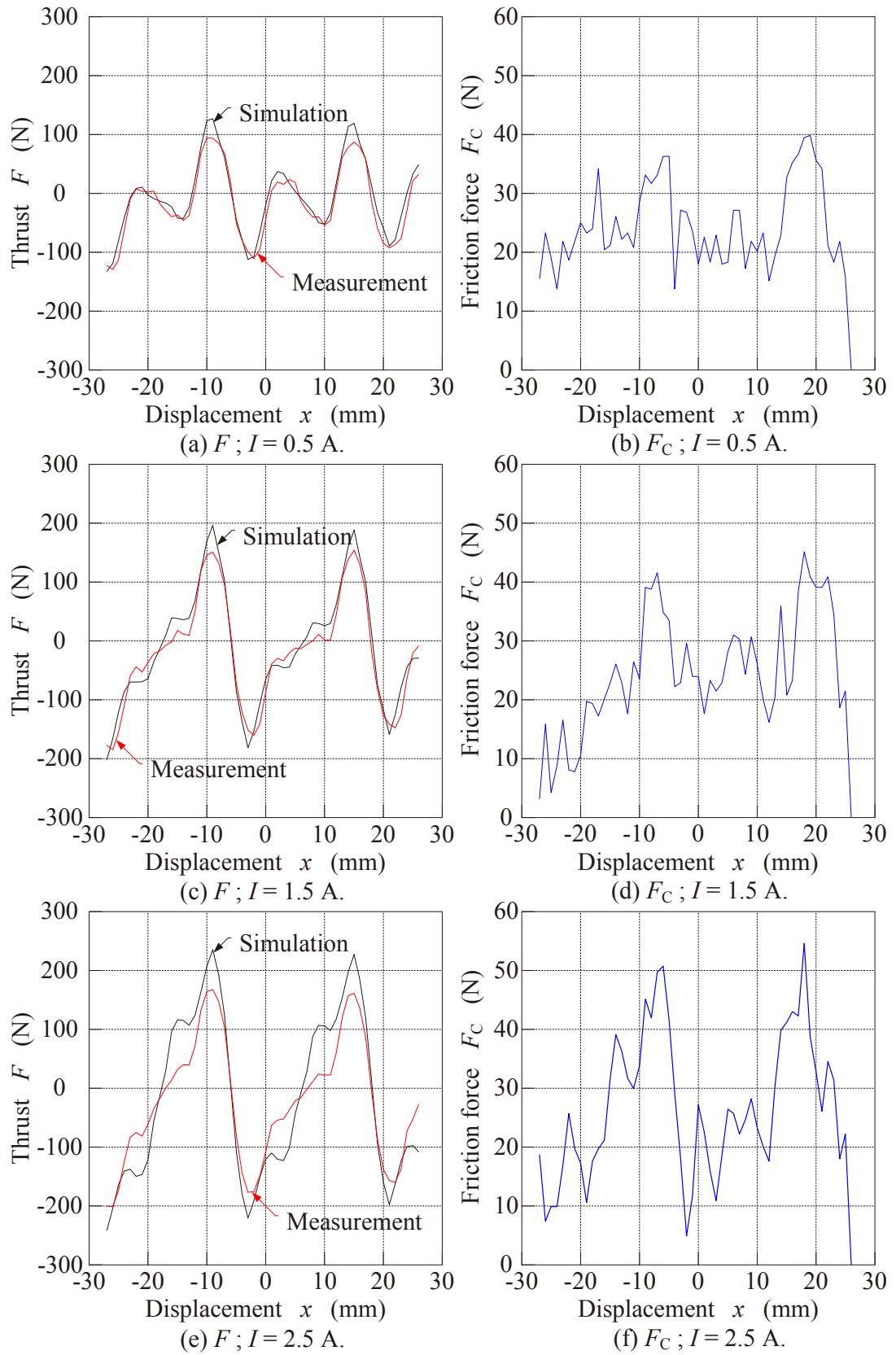


Figure 4.20 Thrust characteristic of the V phase.

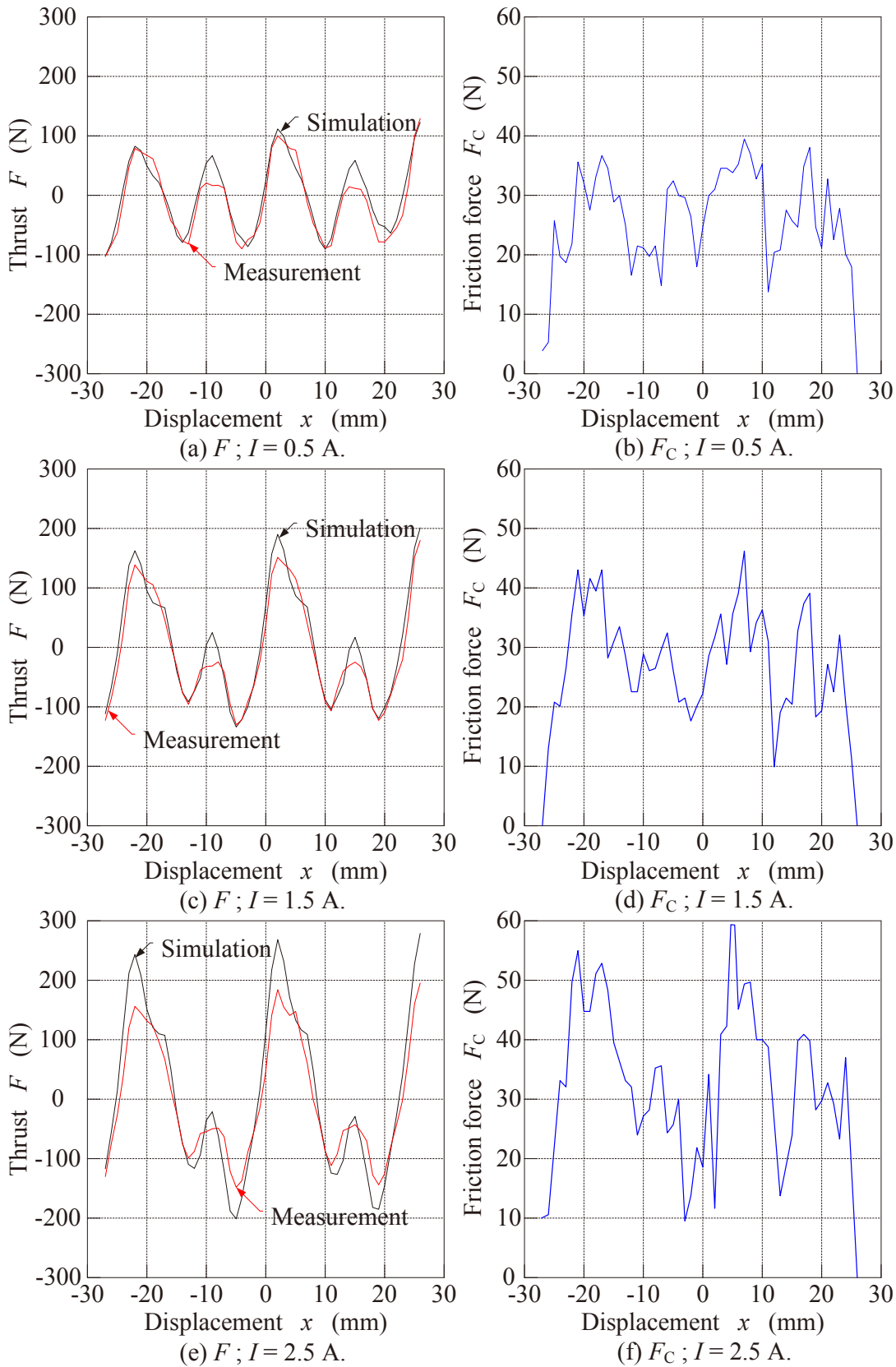


Figure 4.21 Thrust characteristic of the W phase.

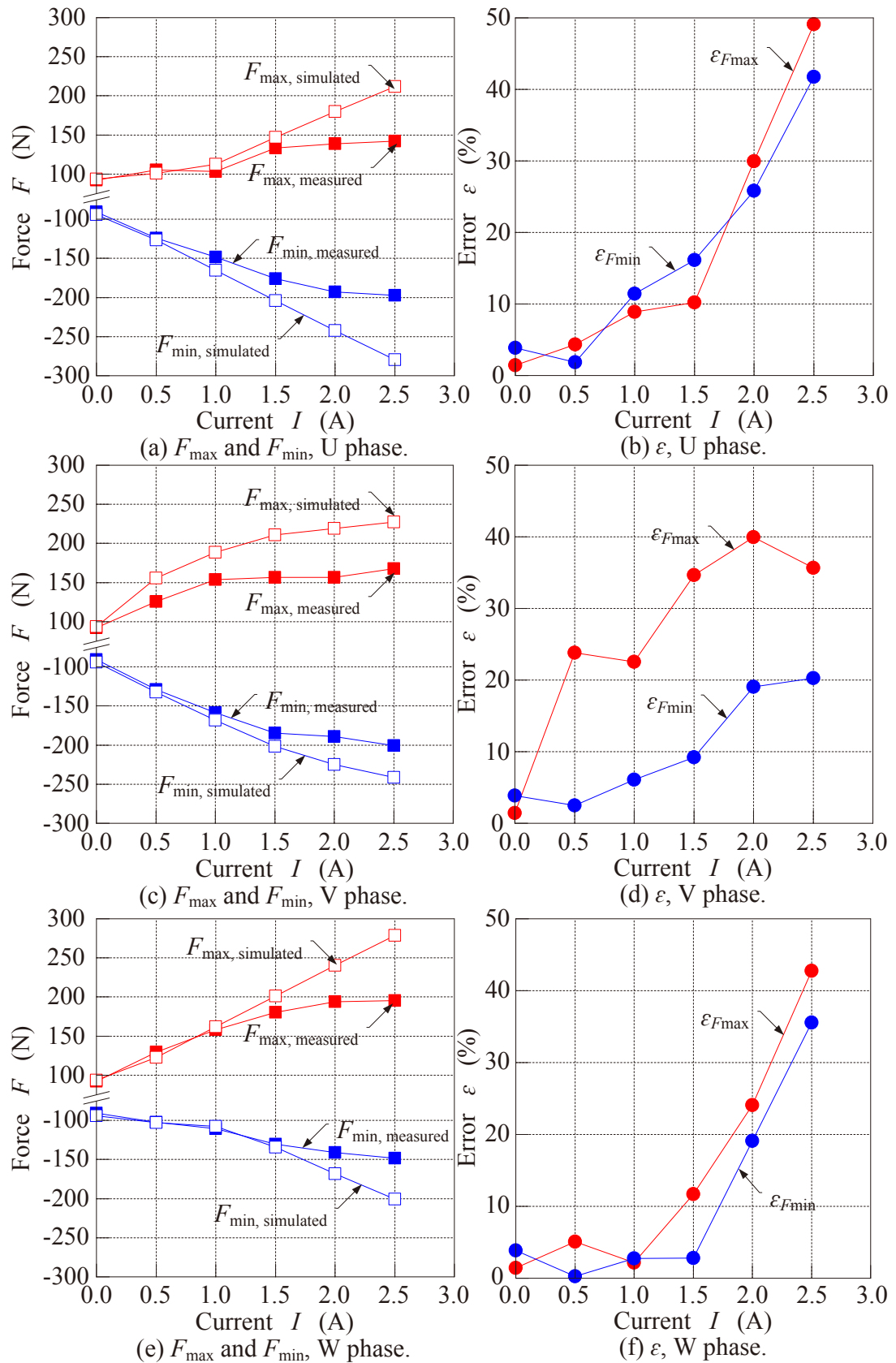


Figure 4.22 Comparison of maximum and minimum thrust,  $F_{\max}$  and  $F_{\min}$  between measured and simulated result and measurement error,  $\varepsilon$ .

---

#### 4.4.2 *RL* Characteristic

Figure 4.23 and Figure 4.24 shows experiment setup and schematic diagram for *RL* characteristic measurement respectively. Instead of observing effect of frequency,  $f$  to the resistance,  $R$  and inductance,  $L$ , in this experiment, the *RL* profile also being measured. This information's are useful in estimating power consumption of the PMCLSM at several frequencies. On top of that, the current response at various frequencies also could be estimated based on frequency characteristics.

The *RL* characteristic was observed at range of frequency between 10 Hz to 100 Hz. This range of frequency is representing the operational frequency of the PMCLSM. The peak current,  $I_p$  was fixed at 0.5 A and was confirm by observing the oscilloscope by measuring the potential across 0.1  $\Omega$  resistance. While measuring the frequency characteristics, the PMCLSM's mover was moved at it full range of displacement so that the *RL* profile and *RL* characteristics of the PMCLSM at full range of mover displacement can be captured. Furthermore, the frequency profile characteristics were measured for each individual phase of the PMCLSM.

Figure 4.25 shows the *RL* profile of each phase of the PMCLSM. Based on Figure 4.25, it is shows that, the resistance,  $R$  of the PMCLSM on each phase is increase as the frequency,  $f$  is increase. Inversely condition was happened to the inductance,  $L$ . The inductance,  $L$  is decrease as the frequency,  $f$  is increase. It is due to when the frequency is increase, the current will tend to flow near to the surface of conductor. It will limit the current flowing and the resistance of the conductor seems to be increase. Limitation of current, made the magnetic flux induced reduced. This condition made the inductance in decrease.

The range and pattern of the *RL* profile of U and W phase is similar however in inverse respective to mover displacement direction. This is due position of the U and W phase is in similar position as shown in Figure 4.11. However, the magnetic flux path direction is inverse cause by inversely PM pole facing on the U and W phase. On the other hand, the value and pattern of the V phase *RL* profile is not similar compared to the other phase due to the position of the V phase is in between U and W phase.

The  $RL$  characteristics of the PMCLSM are as shown in Figure 4.26. In the Figure 4.26, the effect of frequency to maximum and minimum both of resistance ( $R_{\max}$  and  $R_{\min}$ ) and inductance ( $L_{\max}$  and  $L_{\min}$ ) are clearly can be observed. Furthermore, for the resistance,  $R$ , difference between maximum resistance,  $R_{\max}$  and minimum resistance,  $R_{\min}$  become higher at higher frequency,  $f$ . On the other hand, difference between maximum inductance,  $L_{\max}$  and minimum inductance,  $L_{\min}$  become lower at higher frequency,  $f$ . The range of maximum and minimum value for resistance,  $R$  and inductance,  $L$  for U and W phase is about similar due to similarity of its position compared to the condition for V phase. Based on the frequency characteristics result, the resistance,  $R$  and inductance,  $L$  for each phase at simulation frequency ( $f = 70$  Hz) is as summarized in Table 4.6.

Table 4.6 : Resistance,  $R$  and inductance,  $L$  at  $f = 70$  Hz.

Element	Type	U phase	V phase	W phase
Resistance	Maximum, $R_{\max}$ ( $\Omega$ )	38.22	36.03	38.33
	Minimum, $R_{\min}$ ( $\Omega$ )	36.13	34.81	35.81
Inductance	Maximum, $L_{\max}$ (mH)	79.49	75.42	75.95
	Minimum, $L_{\min}$ (mH)	67.11	70.52	63.91

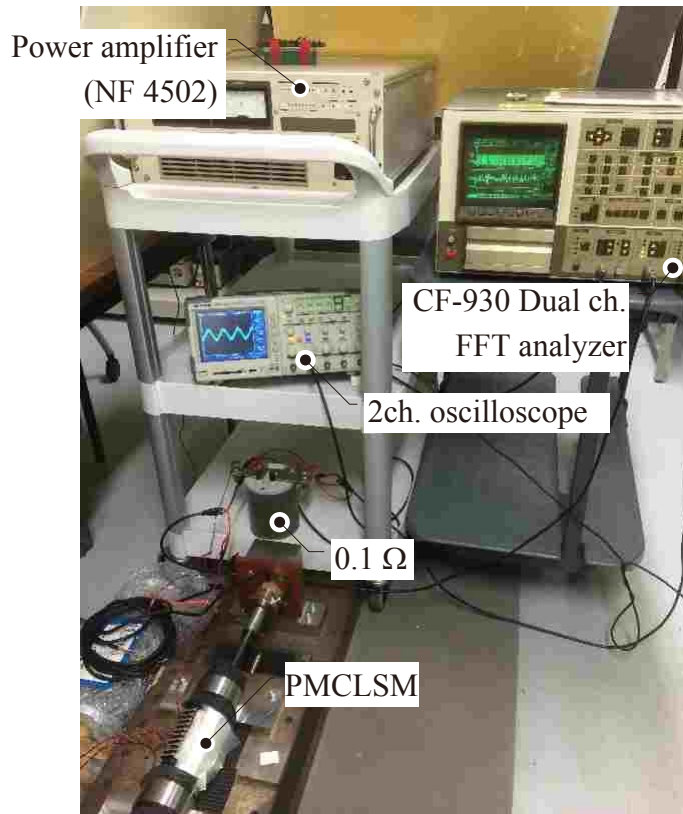


Figure 4.23 Experiment setup for the  $RL$  characteristic measurement.

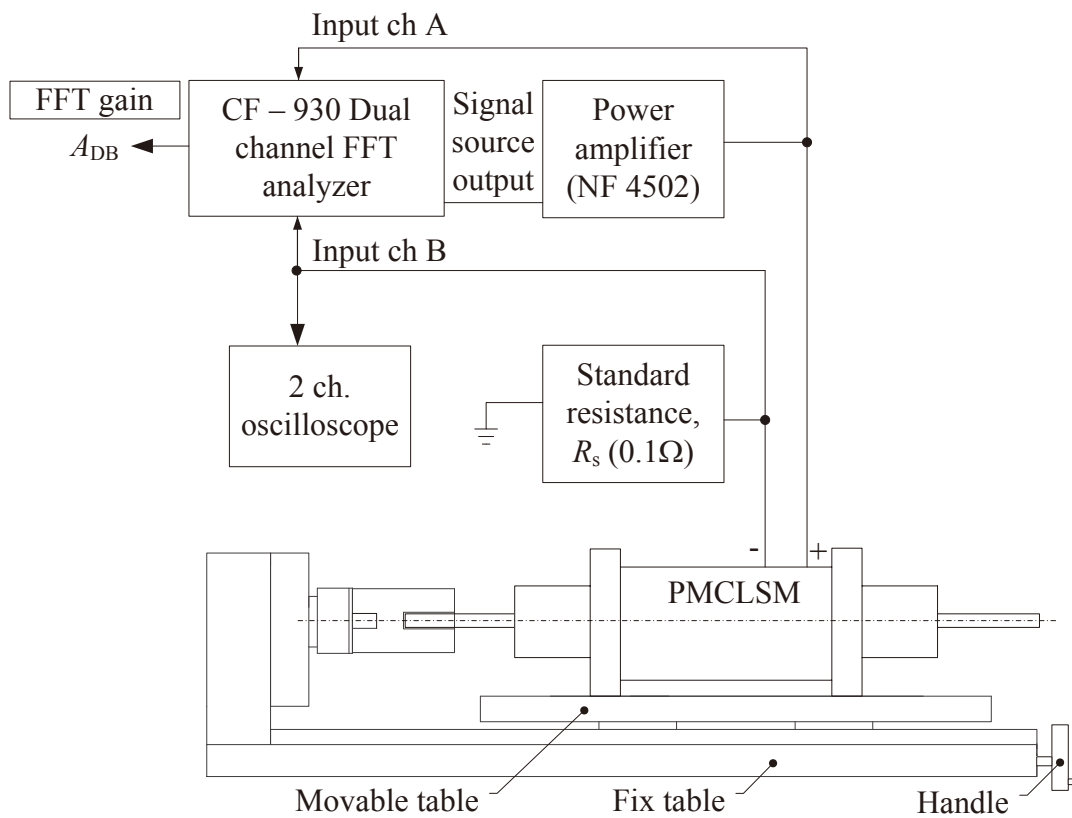


Figure 4.24 Schematic diagram for the  $RL$  characteristic measurement.

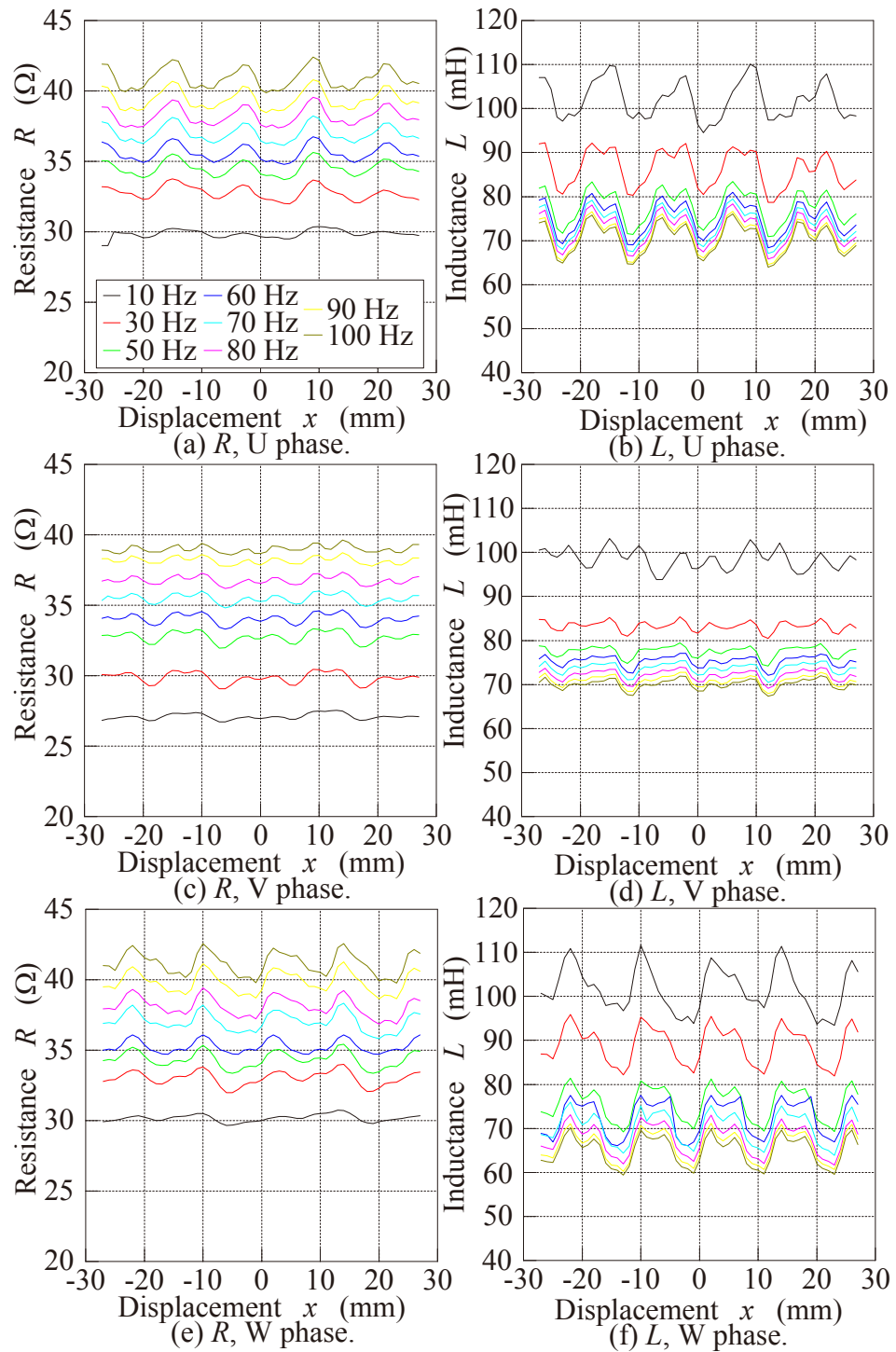
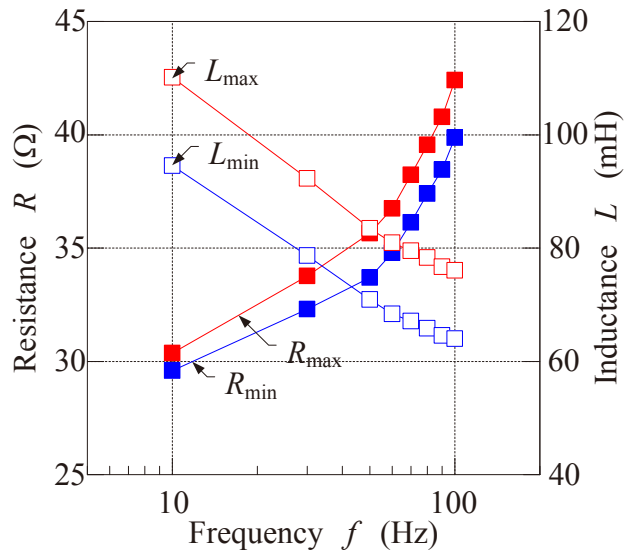
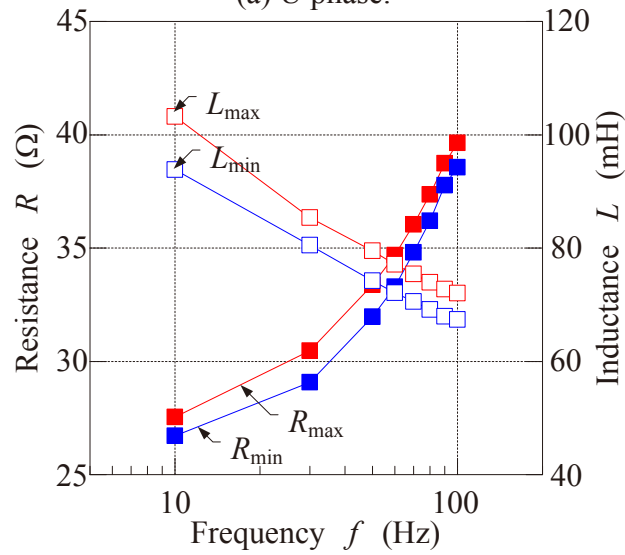


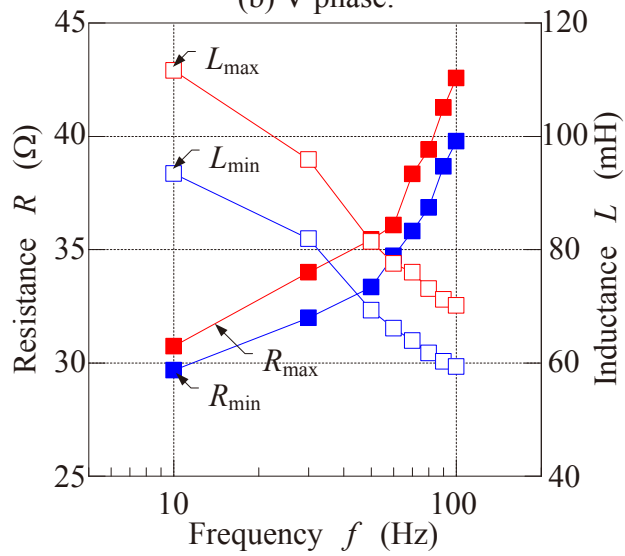
Figure 4.25  $RL$  profile of PMCLSM for each phase at several frequencies.



(a) U phase.



(b) V phase.



(c) W phase.

Figure 4.26  $RL$  characteristic of PMCLSM on each phase.

---

### 4.4.3 Electrical Time Constant Characteristic

Generally, the PMCLSM will be energized by a rectangular shape voltage waveform either in simple square wave or PWM shape of waveform. When the coil of the PMCLSM is energized by a step voltage, the current will rise eventually due to existence of the coil inductance,  $L$ . The time taken to current rise is depend on the ratio between coil inductance,  $L$  and resistance,  $R$ . This time constant is known as electrical time constant,  $\tau_e$ . The electrical time constant,  $\tau_e$  is a parameter that represents current response. The lower the electrical time constant,  $\tau_e$  faster the current time reach it steady state.

Based on the result of frequency characteristics, the electrical time constant,  $\tau_e$  characteristics can be calculated. Both electrical time constant,  $\tau_e$  profile against the PMCLSM mover displacement,  $x$  and frequency,  $f$  will be observed. From the result, the electrical time constant,  $\tau_e$  at simulation frequency can be estimated. The electrical time constant,  $\tau_e$  was calculated using,

$$\tau_e = \frac{L}{R} \quad (\text{ms}) \quad (4.13)$$

where  $\tau_e$  is the electrical time constant in (ms),  $L$  is the coil inductance in (mH) and  $R$  is the coil resistance in ( $\Omega$ ).

The electrical time constant,  $\tau_e$  characteristics of the PMCLSM is as shown in Figure 4.27. Due to the coil resistance,  $R$  is increase and the coil inductance,  $L$  is decrease as the frequency is increase, based on Eq. (4.15), this condition made the electrical time constant,  $\tau_e$  will be decreasing as the frequency is increase. This phenomenon is as shown in Figure 4.27. Furthermore, the higher frequency,  $f$  made the difference between maximum and minimum electrical time constant,  $\tau_e$  become lower.

The range and pattern of the electrical time constant,  $\tau_e$  profile of U and W phase is similar however in inverse respective to mover displacement direction. This is due position of the U and W phase is in similar position as shown in Figure 4.11. However, the magnetic flux path direction is inverse cause by inversely PM pole

---

facing on the U and W phase. On the other hand, the value and pattern of the V phase electrical time constant,  $\tau_e$  profile is not similar compared to the other phase due to the position of the V phase is in between U and W phase.

Even though the lower electrical time constant,  $\tau_e$  is better for the current response, however, higher frequency,  $f$  made lower steady state current at fixed voltage. It also may reduce the thrust produced by the PMCLSM. Therefore, the balance point between electrical time constant,  $\tau_e$  and adequate current,  $I$  is essential to ensure reliability of the PMCLSM. Based on the result, the resistance, the electrical time constant,  $\tau_e$  for each phase at simulation frequency ( $f = 70$  Hz) is as summarized in Table 4.7.

Table 4.7 : The electrical time constant,  $\tau_e$  at  $f = 70$  Hz.

Electrical time constant, $\tau_e$	U phase	V phase	W phase
Maximum, $\tau_{e,max}$ (mH)	2.17	2.15	2.04
Minimum, $\tau_{e,min}$ (mH)	1.83	1.98	1.76

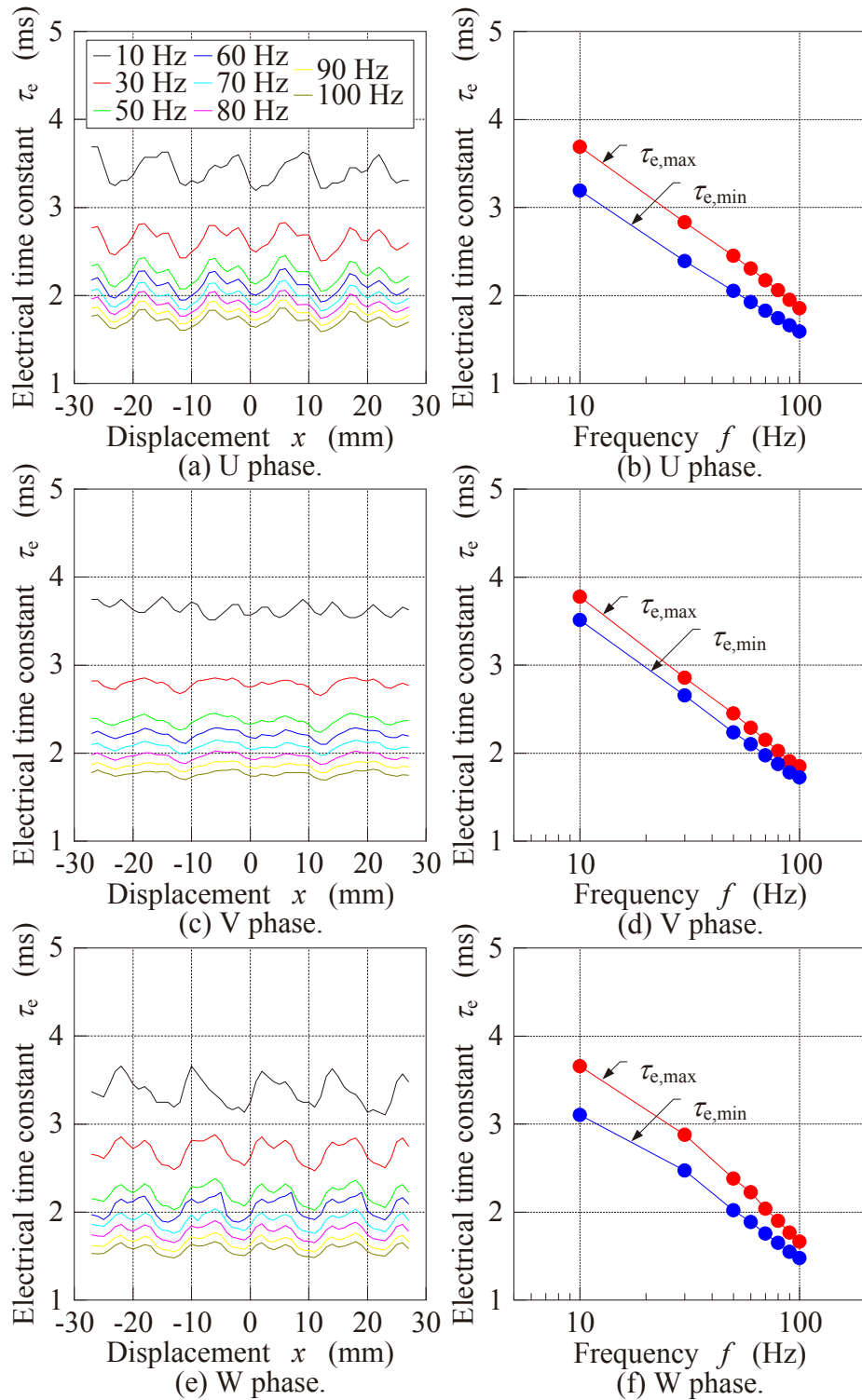


Figure 4.27 Electrical time constant,  $\tau_e$  characteristic of PMCLSM on each phase.

---

#### 4.5 Feasibility of the PMCLSM Implement as E-Cutter's Actuator

The PMCLSM design and development has been discussed. Based on result of design, the PMCLSM could be fulfil thrust required by current,  $I$  of 2.0 A. However, based on measurement result, magnetic flux density saturation start to be occur at current,  $I$  of 1.5 A. By referring to the design output, the average thrust,  $F_{ave}$  at current,  $I$  of 1.5 A is about 142 N. By considering the measurement error,  $\varepsilon$  especially at current,  $I$  lower than 1.5 A, the measurement dynamic thrust of the PMCLSM is estimated will be almost similar to simulation result with similar measurement error,  $\varepsilon$ . However, the PMCLSM has a potential to be implement as E-Cutter's actuator due to capability to produce high thrust at lower than it restricted weight. However, the magnetic flux density saturation occurrence make the PMCLSM's thrust was limited. Design step of the PMCLSM need to continue by optimizing the coil and stator yoke size. On top of that, the coil parameter such as copper wire diameter,  $\phi_c$  and coil turn,  $N$  also need to be decided.

#### 4.6 Summary

The PMLSM is a common type used to be implemented as the E-Cutter's actuator. However, lack in term dynamic performance made a new PMLSM is needed. In this research, a three phase permanent magnet cylindrical linear synchronous motor (PMCLSM) was design and develop in order to observed the feasibility to implement as E-Cutter's actuator. The PMCLSM has been design to makes sure it fulfil design target. The design stage includes searching the appropriate magnetization direction arrangement on mover side and optimizing the coil's height,  $h_c$ , permanent magnet radius,  $r_{pm}$  and shaft radius,  $r_s$ . The PMCLSM has been manufactured based on structural parameter from design result. The static characteristics of the SRCLSM has been measured and compared with simulation output for result validation. Based on static thrust characteristic of the PMCLSM between simulation output and measurement result, it is found that, it shows that, the simulation output and measurement result has a good agreement especially in term of static thrust profile. However, difference between these result become significant at current,  $I$  higher than 1.5 A. It shows that, higher than 1.5 A, static thrust of the

PMCLSM start to saturate based on the measurement result. Table 4.8 shows summary of the PMCLSM design and develop results.

Table 4.8 Summary of the PMCLSM design and develop results.

Characteristics	Design target	PMCLSM	
		Simulation (U phase, $I = 1.5$ A)	Measurement (U phase, $I = 1.5$ A)
Thrust, $F$ (N)	> 200	148	134
Weight, $W_{tot}$ (kg)	< 2.0	1.8	1.8
Volume, $V_{mot}$ (m <sup>3</sup> )	-	$1.9 \times 10^{-4}$	$1.9 \times 10^{-4}$
Thrust constant, $k_f$ (N/A)	-	99	90
Motor constant, $k_m$ (N/ $\sqrt{W}$ )	-	19	17
Motor constant square density, $G$ ( $\times 10^3$ N <sup>2</sup> /Wm <sup>3</sup> )	-	1,900	1,600

#### 4.7 References of Chapter 4

- (4.1) F. Azhar, M. Norhisam, H. Wakiwaka, K. Tashiro, M. Nirei, Current Achievement and Future Plan for Improvement for E Cutter Development, The 24<sup>th</sup> Symposium on Electromagnetics and Dynamics, SEAD 24, Toyama, Japan, , pp. 459-464, 2012.
- (4.2) F. Azhar, M. Norhisam, H. Wakiwaka, K. Tashiro, M. Nirei, Initial Progress and Possible Improvement of E-Cutter Linear Actuator Development, IEEE International Conference on Power and Energy (PECon 2012), Sabah, Malaysia, pp. 933-938, 2012.
- (4.3) F. Azhar, Design of a linear oscillatory actuator for oil palm mechanical cutter. MSc. Thesis, University Putra Malaysia, 2009.
- (4.4) M. Norhisam, F. Azhar, R.N. Firdaus, H. Hashim, M. Nirei, H. Wakiwaka and J. Abdul Razak, Effect of Spring Constant and Thrust Constant to Displacement Characteristics of LOA, Journal of the Japan Society of Applied Electromagnetics and Mechanics (JSAEM), Vol.17 No.3, pp. 437 – 440, 2009.
- (4.5) F. Azhar, M. Norhisam, NF. Mailah, MR. Zare, H. Wakiwaka and M. Nirei, Thrust Optimization of Linear Oscillatory Actuator Using Permeance Analysis Method, International Review of Electrical Engineering (I.R.E.E.), Vol. 6, No. 7, pp. 2929 – 2938, 2011.
- (4.6) M. Norhisam, K. Alias, RN. Firdaus, S. Mahmood and N. Mariun, Comparison on Thrust Characteristic of Linear of Actuators, IEEE International Conference on Power and Energy Conference, 2006. PECon '06. pp. 470 – 475, 2006.
- (4.7) ZQ. Zhu, PJ. Hor, D. Howe, and J. Rees-Jones, Calculation of Cogging Force

- 
- in a Novel Slotted Linear Tubular Brushless Permanent Magnet Motor, IEEE Transactions on Magnetics, Vol. 33, No. 5, pp. 4098 – 4100, 1997.
- (4.8) WJ. Kim and BC. Murphy, Development of a Novel Direct-Drive Tubular Linear Brushless Permanent-Magnet Motor, International Journal of Control, Automation and Systems, Vol. 2, No. 3, pp. 279-288, 2004.
- (4.9) SM. Jang, JY. Choi, SH. Lee, SK. Cho, WB. Jang, Analysis of the tubular motor with Halbach and radial magnet array, 6<sup>th</sup> Inter. Conf. on Electrical Machines and Systems, 2003. ICEMS 2003, China, pp. 250 – 252, 2003.
- (4.10) C. Lucas, F. Tootoonchian and Z. Nasiri-Gheidari, Multi-Objective Design Optimization of a Linear Brushless Permanent Magnet Motor Using Particle Swarm Optimization (PSO), Iranian Journal of Electrical and Electronic Engineering, Vol. 6, No. 3, pp. 183-189, 2010.
- (4.11) K. Nakaiwa, H. Wakiwaka and K. Tashiro, Thrust Characteristics Comparison of Interior Magnet Type Pencil Size Cylinder Linear Motor, Journal of the Japan Society of Applied Electromagnetics and Mechanics, Vol 19, No. 3, pp. 509 -512, 2011.
- (4.12) SM. Jang, SH. Lee, and IK. Yoon, Design Criteria for Detent Force Reduction of Permanent-Magnet Linear Synchronous Motors With Halbach Array, IEEE Trans. on Magnetics, Vol. 38, No. 5, pp. 3261 – 3263, 2002.
- (4.13) J. Wang and D. Howe, Tubular Modular Permanent-Magnet Machines Equipped With Quasi-Halbach Magnetized Magnets—Part I: Magnetic Field Distribution, EMF, and Thrust Force, IEEE Transactions on Magnetics, Vol. 41, No. 9, pp. 2470 – 2478, 2005.
- (4.14) KJ. Meessen, L. Bart, J. Gysen, JH. Johannes and AL. Elena, Halbach Permanent Magnet Shape Selection for Slotless Tubular Actuators, IEEE Transactions on Magnetics, Vol. 44, No. 11, pp. 4305 - 4308, 2008.
- (4.15) KJ. Meessen, L. Bart, J. Gysen, JH. Johannes and AL. Elena, Halbach Permanent Magnet Shape Selection for Slotless Tubular Actuators, IEEE Transactions on Magnetics, Vol. 44, No. 11, pp. 4305 - 4308, 2008.
- (4.16) A. Toyota, T. Shikayama and M. Kakihara, Using the Same Periodic Magnetic Field Generation Device, and linear motor and rotary motor, U.S Patent, US 2011/0012440A1, Jan. 20, 2011.
- (4.17) S. Tahara, Y. Ishida and K. Ogawa, Application of Flux Concentrated Permanent Magnet Arrangement with Halbach Array for 2-pole PMLSM, The 7<sup>th</sup> International Symposium on Linear Drives for Industry Applications, LDIA 2009, Korea, pp. 39 – 49, 2009.
- (4.18) M. Soga, H. Furukawa, K. Suzuki, J. Kajinami, K. Otaku and S. Ueda, Linear Motor, Japan Patent 2010-632201A, March. 18, 2010 (In Japanese).
- (4.19) J. Wang, D. Howe and Z. Lin, Comparative study of winding configurations of short-stroke single phase tubular permanent magnet motor for refrigeration applications, The 42<sup>nd</sup> IAS Annual Meeting Industry Applications, pp. 311 - 318, 2007.
- (4.20) Y. Bong Bang and K. Min Lee, Large thrust linear motors for low-duty-cycle

- 
- operation, *Mechatronics* 14, pp. 891-906, 2004. [44]
- (4.21) H. Yajima, H. Wakiwaka, K. Minegishi, N. Fujiwara, K. Tamura, Design of linear DC motor for high-speed positioning, *Sensors and Actuators* 81, pp. 281–284, 2000.
- (4.22) M. Norhisam, H. Ezril, F. Azhar, RN. Firdaus, H. Wakiwaka and M. Nirei, Positioning System for Sensor Less Linear DC Motor, *Journal of the Japan Society of Applied Electromagnetics and Mechanics (JSAEM)*, Vol.19, Supplement, pp. S91 – S94, 2011.
- (4.23) Y. Miyamoto, T. Hoshi, The Performance Goodness Factor for the Applications of Linear Motor, *The 7<sup>th</sup> International Symposium on Linear Drives for Industry Applications, LDIA 2009, Korea*, pp. 260 – 263, 2009.
- (4.24) T. Mizuno, M. Kawai, F. Tsuchiya, M. Kosugi and H. Yamada, An Examination for Increasing the Motor Constant of a Cylindrical Moving Magnet-Type Linear Actuator, *IEEE Transactions on Magnetics*, Vol. 41, No. 10, pp. 3976 – 3978, 2005.
- (4.25) F. Caricchi, F. Capponi, F. Crescimbin, and L. Solero, Experimental study on reducing cogging torque and no-load power loss in axial-flux permanent magnet machines with slotted winding, *IEEE Transactions Industry Applications*, Vol. 40(4), pp. 1066–1074, 2004.
- (4.26) JLG. Janssen, JJH. Paulides, EA. Lomonova and AJA. Vandenput, Cogging force reduction in tubular permanent magnet actuators, *IEEE International Electric Machines & Drives Conference 2007, (IEMDC '07)* pp. 266-271, 2007.
- (4.27) J. Wang, M. Inoue, Y. Amara and D. Howe, Cogging-force-reduction techniques for linear permanent-magnet machines, *IEE Proceedings Electric Power Applications*, Vol. 152(3), Pp. 731 - 738, 2005.
- (4.28) W. Huang, S. Yang, G. Song and L. Wang, Analysis of the optimal slots and poles combination for reducing cogging force in permanent magnet linear motor, *Sixth International Conference on Electromagnetic Field Problems and Applications (ICEF)*, pp. 1 -4, 2012.
- (4.29) J. Lim, HK. Jung, Cogging Force Reduction in Permanent Magnet Linear Motor using Phase Set Shift, *International Conference on Electrical Machines 2008 (ICEM 2008)*, pp. 1-4, 2008.
- (4.30) AS. Mahdi, M. Jafar, T. Samad, Cogging force mitigation of tubular permanent magnet machines with magnet dividing, *Proceeding of International Conference on Electrical Machines and Systems 2007, Seoul, Korea*, pp. 810-814, 2007.



---

## Chapter 5: Conclusions and Recommendation for Future Work

### 5.1 Conclusions

In this research, design of linear motor for E-Cutter' actuator has been discussed. It starts with explanation of basic concept of *Cantas*<sup>TM</sup> and E-Cutter structure and operation, previous achievement of the E-Cutter's actuator and requirement of new linear motor. For the new linear motor for E-Cutter's actuator, 2 type of linear motor has been designed which are switched reluctance cylindrical linear synchronous motor (SRCLSM) and permanent magnet cylindrical linear synchronous motor (PMCLSM). Despite of designing the E-Cutter's actuator, this research also aimed to observed suitable linear motor type to be used as the E-Cutter's actuator. In the end, based on the measured performance characteristics, it is found that, the PMCLSM has potential to be used as E-Cutter's actuator. In other hand, due to performance limitation, the SRCLSM is seen unsuitable candidate as the E-Cutter's actuator.

The design of E-Cutter's actuator starts with determination of design target. 2 design targets have been aimed. The E-Cutter's actuator is aimed to having average thrust,  $F_{ave}$  at least 200 N at total weight,  $W_{tot}$  below than 2 kg. Instead of achieving the design target, several other performance indexes have been used. There are thrust constant,  $k_f$ , motor constant,  $k_m$ , motor constant square density,  $G$  and electrical time constant,  $\tau_e$ . Furthermore, the performances of the SRCLSM and PMCLSM also have been compared to commercialized PMLM. As much as about 200 linear motors from 3 types of linear motor and several linear motor manufacturers have been selected. 3 types of linear motor are slot type PMLM, slotless type PMLM and shaft motor.

Design and development of the SRCLSM for E-Cutter's actuator has been discussed in chapter 3. Because of the switched reluctance type of linear motor never has been used previously, therefore, a basic study on SRCLSM performance characteristics was focused. Based on several considerations, initial structure of the SRCLSM has been decided. It includes teeth pitch,  $\tau_p$ , air gap length,  $\delta$ , phase number and structure topology. In order to validate the simulation output, single phase

---

SRCLSM has been manufactured. The static characteristics of the SRCLSM has been measured and compared to simulation output. Based on the results, it is shows that, the measurement result of static characteristics of the SRCLSM is about 2 times lower compared to the simulation result. Manufacturing tolerance,  $\Delta x$  has been estimated as caused of the discrepancy. Based on this facts, thrust of the SRCLSM is about 5 times below than E-Cutter's actuator while the total weight,  $W_{\text{tot}}$  of the SRCLSM is only about 30 % below than E-Cutter's actuator restricted weight. Therefore, the SRCLSM is seen as incompatible to be used as the E-Cutter's actuator.

In chapter 4, design and development of the PMCLSM as E-Cutter's actuator has been discussed. This time, a 3 phase structure topology has been selected to be used. Several permanent magnet magnetization direction arrangements have been tested on both slot type and slotless type has been evaluated in order to select an appropriate structure topology. The structure of the PMCLSM was underwent several design stages in order to made it fulfil E-Cutter's actuator design target. Based on the simulation result, the PMCLSM has been design with structure parameter that fulfils its design target. The PMCLSM has been manufactured to validate the simulation output. The static characteristics of the PMCLSM has been measured and compared to the simulation output. Based on the comparison, it is shown that the static characteristics especially static thrust has a good agreement between measured and simulated result. However, the difference of measured and simulated thrust has a significant difference at current,  $I$  higher than 1.5 A. At current,  $I$  higher 1.5 A, the static thrust of the PMCLSM is started to saturated. It is due to magnetic flux density,  $B$  was saturated and temperature rise limit the magnetic flux produced by the permanent magnet. At current,  $I$  of 1.5 A and the maximum thrust,  $F_{\text{max}}$  is about 133 N for U phase, 157 N for V phase and 180 N for W phase. However, the PMCLSM has a potential to be implement as E-Cutter's actuator due to capability to produce high thrust at lower than it restricted weight. However, the magnetic flux density saturation occurrence make the PMCLSM's thrust was limited. Design step of the PMCLSM need to continue by optimizing the coil and stator yoke size. On top of that, the appropriate coil parameter such as copper wire diameter,  $\phi_c$  and coil turn,  $N$  also need to be determined.

---

## 5.2 Recommendation for Future Work

The PMCLSM shows a capability to work as E-Cutter's actuator. However, the main drawback of the PMCLSM so far was magnetic flux density saturation seem to be occurred at current,  $I$  of 1.5 A. The next step of the research, the stator yoke thickness,  $t_y$  and coil size need to be determined. On top of that, the copper wire diameter,  $\phi_c$  at appropriate size allowing maximizing the magnetomotive force of the PMCLSM.

The PMCLSM need a motor driver to excite it with optimum operation. Generally, the PMCLSM will be energized by a sine wave voltage shape. However, instead of pure sine wave excitation, a PWM voltage signal will be used. Therefore, an experiment to determine the electrical time constant,  $\tau_e$  of the PMCLSM coil under step voltage excitation need to be execute. Based on this experiment result, an appropriate carrier frequency of the PWM voltage signal can be estimate, hence the motor driver of the PMCLSM could be develop.

The motor driver for the PMCLSM needs instantaneous mover displacement information. The mover displacement can be estimated by using Hall elements. The Hall elements need to be arranged in specific arrangement to produce a signal that proportional to the mover displacement. By using appropriate signal conditioning method, the instantaneous mover displacement can be estimated and required driving signal to the motor drive can be generate.

Once the motor driver system of the PMCLSM has been developed, dynamic characteristics of the PMCLSM should be measured. The result from this experiment will be compared to simulation output for result validation. From this experiment as well, the actual performance of the PMCLSM can be observed.



---

## Appendices

### Appendix A List of publications

#### Reviewed Journal.

1. F. Azhar, H. Wakiwaka, K. Tashiro, H. Yajima, T. Kanazawa and N. Fujiwara, Performance Evaluation and Comparison of Switched Reluctance Cylindrical Linear Motor, Journal of the Japan Society of Applied Electromagnetics and Mechanics, Vol. 22 No. 2, pp. 158 - 163, 2014.

#### Reviewed proceeding.

1. F. Azhar, M. Norhisam, H. Wakiwaka, K. Tashiro, M. Nirei, Evaluation of Various Permanent Magnet Arrangements on Linear Actuator, Asia-Pacific Symposium on Applied Electromagnetics and Mechanics 2012, APSAEM 2012, Ho Chi Minh City, Vietnam, (25 – 27 July 2012), pp. 50 - 55, 2012.
2. F. Azhar, M. Norhisam, H. Wakiwaka, K. Tashiro, M. Nirei, Initial Progress and Possible Improvement of E-Cutter Linear Actuator Development, 2012 IEEE International Conference on Power and Energy (PECon 2012), Kota Kinabalu, Sabah, Malaysia, (2 – 5 December 2012), pp. 940-945, 2012.
3. F. Azhar, M. Norhisam, H. Wakiwaka, K. Tashiro, M. Nirei, Structure Optimization of a 6 Slot 8 Pole Permanent Magnet Linear Motor, The 7th IET international conference on Power Electronics, Machines and Drives, PEMD 2014, Manchester, UK , (8 - 10 April 2014), pp. 0039 2014. ISBN: 978-1-84919-815-8.

#### Other research theme proceeding.

Nil.

---

**Non-reviewed proceeding.**

1. F. Azhar, M. Norhisam, H. Wakiwaka, Kunihisa Tashiro, M. Nirei, Current Achievement and Future Plan for Improvement for E Cutter Development, The 24<sup>th</sup> Symposium on Electromagnetics and Dynamics, SEAD 24, Toyama, Japan, (16 – 18 May 2012), pp. 459-464, 2012.
2. F. Azhar, M. Norhisam, H. Wakiwaka, K. Tashiro, M. Nirei, Design and Consideration of Driving Method of Cylindrical VR Type Linear Pulse Motor, Technical Meeting on Linear Drives of IEE Japan, Tokyo, Japan, (22 Feb. 2013), LD – 13 – 14, pp. 23-28, 2013.
3. F. Azhar, H. Wakiwaka, K. Tashiro, H. Yajima, T. Kanazawa and N. Fujiwara, Performance Evaluation and Comparison of Switched Reluctance Cylindrical Linear Motor, The 22th MAGDA Conference, Miyazaki, Japan, (2-3 December 2013), pp. 369 – 374, 2013.
4. F. Azhar, M. Norhisam, H. Wakiwaka, K. Tashiro, M. Nirei, Design of a Permanent Magnet Linear Motor for Oil Palm Cutter, Technical Meeting on Linear Drives of IEE Japan, Shizuoka, Japan, (6 Aug. 2014), RM-14-68, LD – 14 – 52, HCA-14-39, pp. 57 - 62, 2014.

---

**Appendix B**  
**Reprint of publications**





## Performance Evaluation and Comparison of Switched Reluctance Cylindrical Linear Motor

F. Azhar\*<sup>1</sup>, H. Wakiwaka\*<sup>1</sup>, K. Tashiro\*<sup>1</sup>, H. Yajima\*<sup>2</sup>, T. Kanazawa\*<sup>2</sup> and N. Fujiwara\*<sup>2</sup>

Nowadays, most of the researchers have put a lot of effort in designing the permanent magnet type of linear motor. However, due to resource problem occur recently to the permanent magnet material has led to increment of the material cost. This situation made the linear motor productivity is reduced. Because of this reason, most of linear motor manufacturers are prefer to development non-permanent magnet type to ensure product competitiveness and increase cost performance. Therefore, in this research, a switched reluctance linear motor was designed. The teeth shape has been varied in order to observed the effect to it's performance. As a result, the best model of switched reluctance linear motor with optimum teeth shape has been proposed. The performance of the model also has been compared to other similar type of linear motor and the permanent magnet type of linear motor.

*Keywords:* Cylindrical shape, linear motor, non-permanent magnet, switched reluctance type.

### 1. Introduction

Linear motor is an actuator that provide a linear motion with absence of motion translator such as belt, ball screw and gears [1,2]. This system is called as direct linear motion system. The direct linear motion system offers high flexibility of operation eliminates system limitation and reduce to total number of components used hence increase the system reliability [1-4]. The linear motor can be classified as permanent magnet type and switched reluctance type [5]. Due to superior performance of permanent magnet type especially in term of thrust density and better dynamic response made numerous of researchers put a lot of effort to develop it.

Recently, it is reported that the permanent magnet material especially sintered neodymium magnet material has facing supply chain problem. It has made the increment of it price and as well the linear motor development cost. Most of the manufacturers are currently prefer to use readily source material in order to ensure stability and competitive price [6]. Therefore, non-permanent magnet type of linear motor such as switched reluctance type is seen as an alternative. Several of researchers have discussed advantages of switched reluctance type machine. Apart of it such as robust construction, low cost in mass production, fault tolerance, high efficiency, rugged behavior, and large thrust output over very wide speed [7-10]. Furthermore, the windings are concentrated rather than distributed, making them ideal for low cost of maintenance [10]. With the continual development of power electronics and control strategies increase the reliability and effectiveness of switched reluctance type machine [11].

**Correspondence:** H. Wakiwaka, Faculty of Engineering, Shinshu University, 4-17-1 Wakasato, Nagano, 380-8553, Japan. email: wakiwak@shinshu-u.ac.jp

\*<sup>1</sup> Shinshu University, \*<sup>2</sup> SMC Corporation

In this paper, a switched reluctance linear motor was designed. The switched reluctance linear motor can be designed either in rectangular or cylindrical shape [5]. The cylindrical shape is seen has a capability to minimize the attractive force between the mover and the stator when coils are energized. This feature is due to existence of counterpart of coil compared to rectangular shape. On top of that, it also can reduce the requirement of support mechanism thus increase the thrust to size ratio [12].

The main focus of this research is to improve the performance characteristics of switch reluctance cylindrical linear motor (SRCLM). As suggested in [13] and [14], there three characteristics were used to evaluate the performance of SRCLM. There are thrust to weight ratio,  $F/W$ , thrust to volume ratio,  $F/V$  and thrust to power ratio,  $F/P$ . As report in [15], the researcher as well used ratio force to volume ratio,  $F/V$  in order to compare their findings with [13]. As a result, a switched reluctance cylindrical linear motor (SRCLM) has been designed with 123 N of average thrust,  $F_{ave}$ . It also has 45.15 N/kg of thrust to weight ratio,  $0.38 \times 10^6$  N/m<sup>3</sup> of thrust to volume ratio and 2.45 N/W thrust to power ratio.

### 2. Basic Principle of SRCLM

#### 2.1 Basic Structure of SRCLM

The partial structure of SRCLM is as shown in Fig. 1. The mover consists of a cylindrical shape of iron shaft with 3 mm pitch of teeth,  $\tau_p$ . The stator consists of a stator yoke and coils. The stator and mover are separated by a 0.05 mm air gap. Each phase of SRCLM stator consists of 4 coils. A non-magnetic separator was used to insulate the SRCLM stator one phase to another. On top of that, the non-magnetic separators also use to maintain similar phase distance of each stator SRCLM phase. Table 1 shows the per phase coil characteristics of SRCLM.

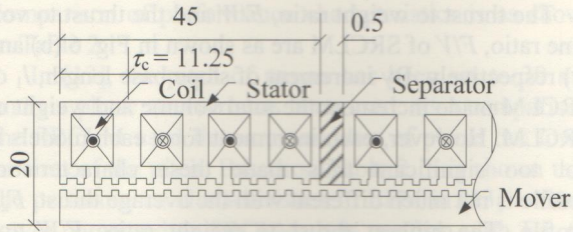


Fig. 1 Partial of SRCLM structure (unit in mm)

Table 1 Per phase coil characteristics.

No.	Parameter	Value
1	Coil turns	327
2	Coil resistance ( $\Omega$ )	7.06
3	Phase resistance ( $\Omega$ )	28.2
4	Phase Input power (W)	50
5	Number of coils	4

2.2 Basic Thrust Equation of SRCLM

When the coil of SRCLM is energized by certain current,  $I$ , a magnetic flux,  $\phi$  is induced and flow from the stator to mover. The thrust of SRCLM is developed when unaligned teeth are attracted to each other until align position is achieved. The magnetic flux,  $\phi$  can be expressed as Fourier Series as in Eq. (1) [5].

$$\phi = \phi_{DC} + \sum_{n=1}^{\infty} \phi_n \cos \frac{2\pi}{\tau_p} nx \quad (1)$$

Where  $\phi_{DC}$  is the DC component of magnetic flux in (Wb),  $n$  is the Fourier order,  $\phi_n$  is  $n$ th Fourier component of magnetic flux in (Wb),  $\tau_p$  is teeth pitch in (m) and  $x$  is the mover displacement in (m).

The magnetic energy of SRCLM,  $W$  can be calculated using Eq. (2).

$$W = N \int_0^I \phi dI \quad (2)$$

Where  $W$  is magnetic energy in (J),  $N$  is coil turns,  $\phi$  is the magnetic flux expression in (Wb) and  $I$  is the input current in (A).

Base on Eq. (1), the expression of magnetic energy,  $W$  can be rewritten as Eq. (3).

$$W = \sum_{n=0}^{\infty} \omega_{An} \cos \frac{2\pi}{\tau_p} nx \quad (3)$$

Where  $\omega_{An}$  is the Fourier coefficient.

The thrust,  $F$  can be calculated by differentiating Eq. (3) with respect to mover displacement,  $x$ . It is shown in Eq. (4). By considering the expression of magnetic flux,  $\phi$  as Eq. (1) and the higher order Fourier coefficients are

neglected, the general thrust expression for the SRCLM can be express as Eq. (5) [5].

$$F = \frac{dW}{dx} = -\frac{2\pi}{\tau_p} \sum_{n=1}^{\infty} n \omega_{An} \sin \frac{2\pi}{\tau_p} nx \quad (4)$$

$$F = -\frac{4\pi NI}{\tau_p} \left\{ \phi \sin \left( \frac{2\pi}{\tau} nx \right) \right\} \quad (5)$$

Base on Eq. (5), despite of coil parameter such as coil turns,  $N$  and current,  $I$ , the thrust of SRCLM also depends on the teeth pitch,  $\tau_p$ .

2.3 Teeth Shape Variation of SRCLM

By referring to Eq. (5), smaller teeth pitch,  $\tau_p$  is used, higher thrust,  $F$  will be produced. In this paper, 3 mm has been selected for the SRCLM mover and stator teeth pitch,  $\tau_p$ . The teeth width,  $w_d$  was fixed to 1.2 mm.

Instead of rectangular shape, a trapezoidal shape has been used of SRCLM teeth shape. In order to evaluate the effect of teeth shape to the SRCLM performance characteristics, the slope base length,  $l_1$  was varied in a range of 0.0 – 0.9 mm. Fig. 2 shows the detail figure of teeth shape of SRCLM.

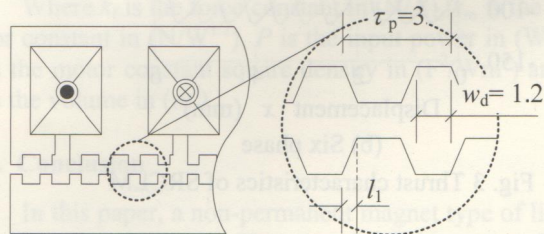
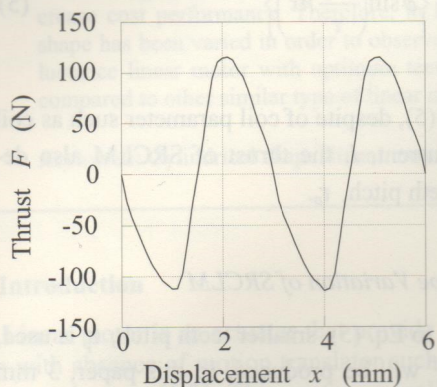


Fig. 2 Teeth shape detail of SRCLM

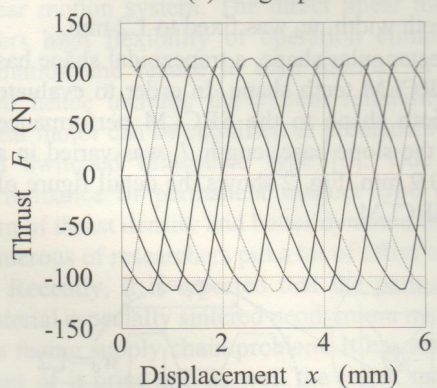
3. Thrust Characteristics of SRCLM

Each model of SRCLM was simulated using FEM software. Based on the FEM output, thrust characteristics of each SRCLM models was plotted. Based on the thrust characteristics, the performance characteristics of SRCLM were evaluated and the best model was identified. The thrust of SRCLM was simulated at input power,  $P$  of each phase of 50 W. The 50 W of input power,  $P$  is equivalent to 1.33 A of excitation current. Based on the observation, the value of excitation current, the magnetic saturation was not occurred. Fig. 3 shows the example of thrust characteristics of SRCLM. Base on single phase thrust characteristics as shown in Fig. 3 (a), the thrust characteristics of other stator phase of SRCLM can be derived as Fig. 3 (b).

The SRCLM is exciting by 1 phase excitation. Each phase of coil is exciting one by one. The sequence of excitation base on the phase number is 6-5-4-3-2-1. Fig. 4 shows the excitation sequence of SRCLM. Based on this excitation sequence, the six phase thrust characteristics is as shown in Fig. 5. The six phase thrust characteristics of all SRCLM models were plotted. Each model of SRCLM has been evaluated using average thrust,  $F_{ave}$ , thrust to weight ratio,  $F/W$ , thrust to volume ratio,  $F/V$  and thrust to power ratio,  $F/P$ .



(a) Single phase



(b) Six phase

Fig. 3 Thrust characteristics of SRCLM

#### 4. Performance Comparison of SRCLM

##### 4.1 Comparison between Similar Type of Linear Motor

The SRCLM models were evaluated using average force,  $F_{ave}$ , thrust to weight,  $F/W$ , thrust to volume,  $F/V$  and thrust to power ratio,  $F/P$  in order to search the optimum teeth shape. The teeth shape was differentiated using the slope base length,  $l_1$ .

Fig. 6 (a) shows the comparison of SRCLM average thrust,  $F_{ave}$ . It shows that, the average thrust,  $F_{ave}$  of SRCLM is increase as the slope base length,  $l_1$  is increase until it reach the maximum value at slope base length,  $l_1$  equal to 0.2 mm. At the slope base length,  $l_1$  is higher than 0.2 mm, the average thrust,  $F_{ave}$  is reducing significantly. Therefore, the best teeth shape of SRCLM is at slope base length,  $l_1$  of 0.2 mm with average thrust,  $F_{ave}$  of 117 N.

The thrust to weight ratio,  $F/W$  and the thrust to volume ratio,  $F/V$  of SRCLM are as shown in Fig. 6 (b) and (c) respectively. By increment of slope base length,  $l_1$  of SRCLM made increment the total volume and weight of SRCLM. However, each increment form each models is not too significant thus made these characteristics profile is not much different with the average thrust,  $F_{ave}$  profile. The highest thrust to weight ratio,  $F/W$  and thrust to volume ratio,  $F/V$  of SRCLM are 45.15 N/kg and  $0.38 \times 10^6$  N/m<sup>3</sup> respectively.

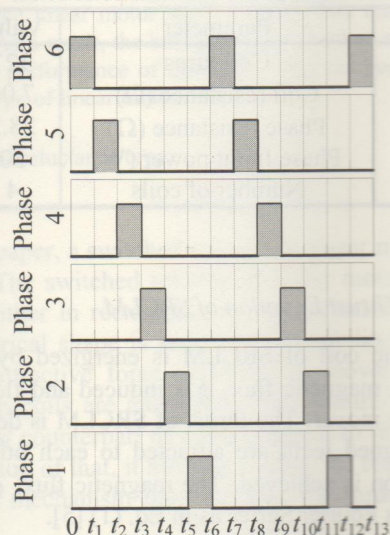


Fig. 4 Excitation sequence of SRCLM coil

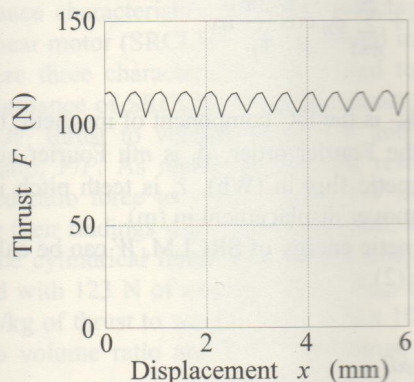


Fig. 5 Six phase characteristics of SRCLM

The input power of SRCLM was fixed to 50 W. Therefore, the profile of the thrust to power ratio,  $F/P$  is exactly the same as profile of average thrust,  $F_{ave}$  as shown in Fig. 6(d). The highest thrust to power ratio,  $F/P$  is obtained at slope base length,  $l_1$  of 0.2 mm with value of 2.45 N/W.

All these performance characteristics of best model SRCLM is then compared to the other similar type of linear motor. In this case, the linear motor in [13], [14] and [15] were referred. Even though in [13] and [14], a linear pulse motor (LPM) were designed, however, due to similar structure to switched reluctance type of linear motor were used, these model was taken as comparison model. Furthermore, the performance of SRCLM is compared to common reluctance type performance. The

comparison of performance characteristics is as shown in Table 2.

In [13], the pitch of mover has been set to 30 mm and six phase structure has been used. As a comparison, the SRCLM used the same number of phase but lower in term of the pitch. Based on Table 2, it is shown that, the performance characteristics of LPM in [13] is much lower compared to SRCLM. It is confirm with Eq. (5) that the thrust of switched reluctance motor is inversely to the pitch,  $\tau_p$ .

The LPM in [14], is has better performance compared to the SRCLM in term of thrust to volume ratio,  $F/V$  and thrust to power ratio,  $F/P$ . This is due to use of permanent magnet in the LPM structure. By using the permanent magnet in the motor structure, higher thrust can be obtain over the same size hence increase the thrust to size ratio. However, the LPM in [14] is having lower in term of thrust to weight ratio,  $F/W$  compared to the SRCLM. Even though the lower pitch has been set in this LPM which 2.2 mm compared to the SRCLM, due to different of structure topology such as number of phase used, the thrust to weight ratio  $F/W$  of LPM [14] is lower than SRCLM.

In the switched reluctance linear motor (SRLM) in [15], the higher pitch has been used. The SRLM has been designed with 10 mm pitch and produced  $0.25 \times 10^6 \text{ N/m}^3$  compared to  $0.38 \times 10^6 \text{ N/m}^3$  produced by the SRCLM. However, the other performance characteristics are not reported in [15].

As shown in Table 2, the SRCLM not only having the best performance in term of thrust to weight ratio,  $F/W$  compared to other model, it also has been improved the common range of reluctance type performance. Even though the thrust to volume ratio,  $F/V$  and thrust to power ratio,  $F/P$  of the SRCLM are locates inside the common reluctance type performance range, however the value of both performances are locates near to the upper boundary of common reluctance type performance range.

#### 4.2 Comparison of the SRCLM and Permanent Magnet Type of Linear Motor Performance.

The SRCLM performance also has been compared to permanent magnet type of linear motor (PMLM). There are three type of PMLM has been choose for comparison which are double magnet core type linear motor (DMC), permanent magnet coreless type linear motor (PMCL) and shaft motor. All of these PMLMs were selected from the commercialize PMLM from several linear motor manufacturer companies. Almost 200 PMLMs has been selected and their performance has been recorded.

The performance of PMLM normally measured by three performance indexes such as force constant,  $k_f$ , motor constant,  $k_m$  and motor constant square density,  $G$  [16]. These performance indexes were calculated using Eq. (6) - (8).

Fig. 7 shows the performance comparison between the SRCLM and the PMLMs. Apart of the three performance indexes that has been mention previously, the average thrust,  $F_{ave}$  also has been used in this comparison. All the performance indexes were plotted against their volume,  $V$ . Based on the Fig. 7, it is shown that, the SRCLM is have a capability to produce higher performance at similar volume,  $V$  compared to PMLM. The SRCLM is also seen having capability to produce higher thrust,  $F$  at smaller size and lower input power,  $P$ .

Table 2 Comparison of SRCLM with Similar Type of Motor Characteristics.

Performance	Best model SRCLM	LPM [13]	LPM [14]	SR [15]	Common Reluctance type
$F/W$ (N/kg)	45.15	15.00	43.20	-	20 - 30
$F/V$ ( $\times 10^6 \text{ N/m}^3$ )	0.38	0.075	0.43	0.25	0.06 - 0.40
$F/P$ (N/W)	2.45	1.38	5.10	-	0.5 - 3.0

$$k_f = \frac{F}{I} \tag{6}$$

$$k_m = \frac{F}{\sqrt{P}} \tag{7}$$

$$G = \frac{F^2}{PV} \tag{8}$$

Where  $k_f$  is the force constant in (N/A),  $k_m$  is the motor constant in (N/W<sup>1/2</sup>),  $P$  is the input power in (W),  $G$  is the motor constant square density in (F<sup>2</sup>/Wm<sup>3</sup>) and  $V$  is the volume in (m<sup>3</sup>).

### 5. Conclusion

In this paper, a non-permanent magnet type of linear motor was designed. The aimed of this paper is to improve the performance of switched reluctance cylindrical linear motor (SRCLM). From the analysis results, the following conclusions are obtained.

1. The teeth pitch,  $\tau_p$  is playing a significant role in increase the thrust,  $F$ . as can be seen from the thrust comparison of the SRCLM with the LPM in [13].
2. The SRCLM has improved the performance of common reluctance type in term of thrust to weight ratio,  $F/W$ .
3. Even though the other two performance characteristics of SRCLM which are thrust to volume ratio,  $F/V$  and thrust to power ratio  $F/P$  are located in common reluctance type range performance, however its located near to the boundary of the range.
4. The SRCLM is capable to produce high thrust,  $F$  base on the comparison it performance indexes to the PMLM.

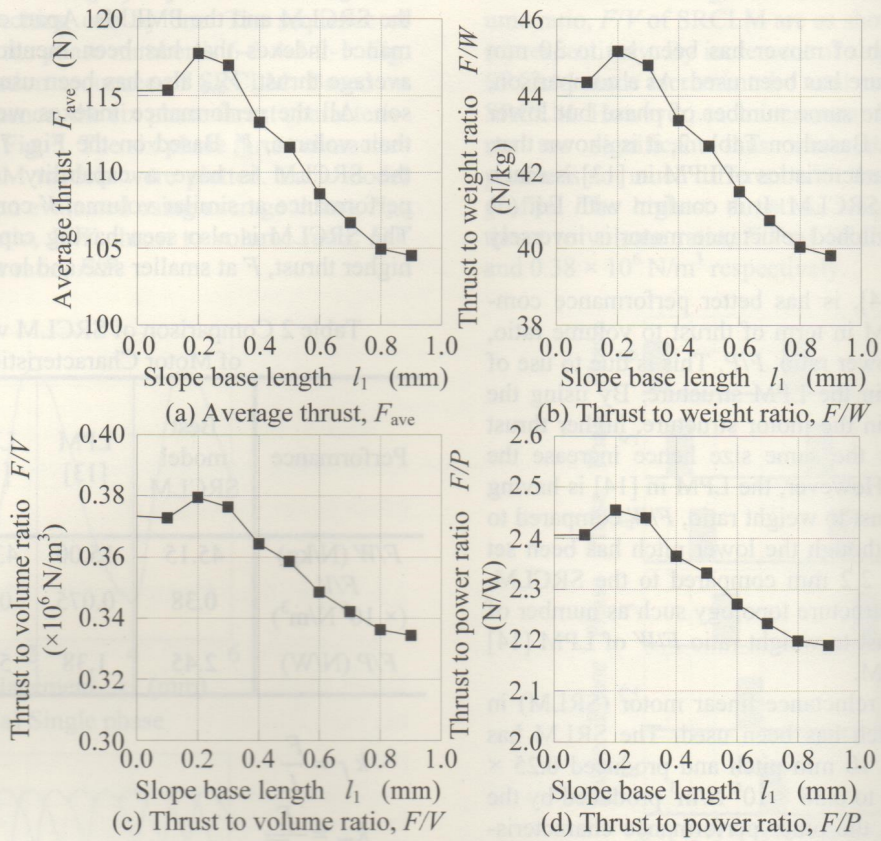


Fig. 6 Performance comparison of SRCLM

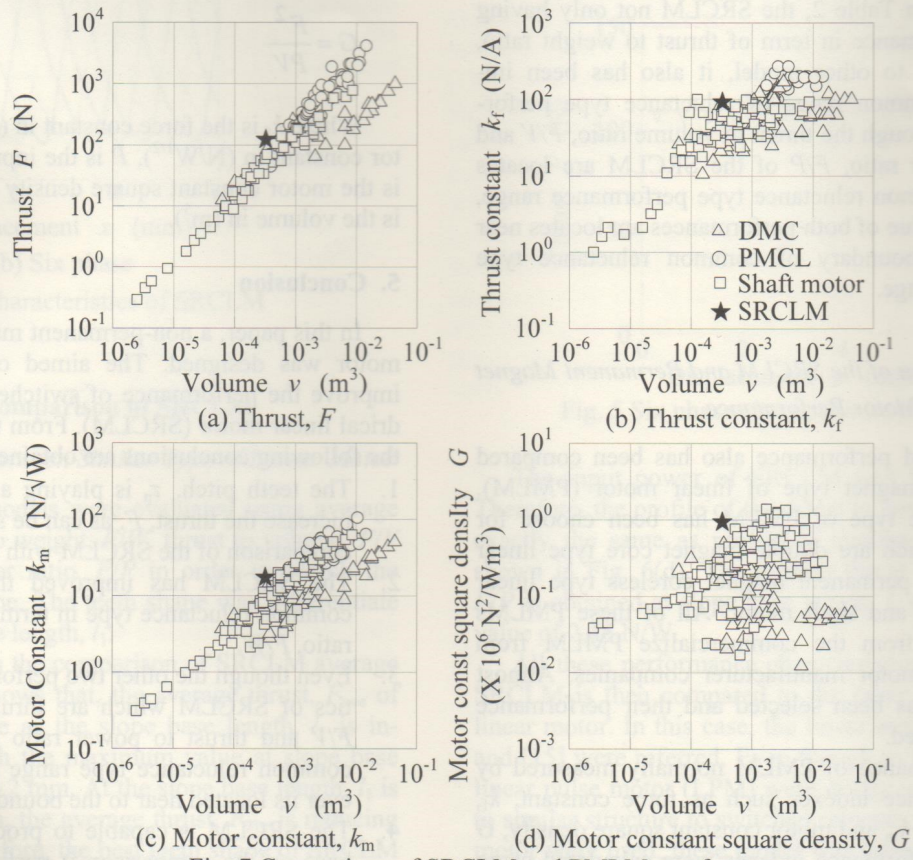


Fig. 7 Comparison of SRCLM and PMLMs performance

## Acknowledgment

F. Azhar wishes to acknowledge the Universiti Teknikal Malaysia Melaka (UTeM), and Ministry of Higher Education of Malaysia, for giving him the opportunity to pursue his PhD study and for their financial support in Shinshu University.

(Received: 6 February 2014)

## References

- [1] M. Norhisam, H. Ezril, R. N. Firdaus, F. Azhar, H. Wakiwaka, M. Nirei, "Positioning System for Sensor Less Linear DC Motor," *Asia Pacific Symposium of Applied Electromagnetics and Mechanics (APSAEM2010)*, Kuala Lumpur, (Malaysia), July 2010, pp. 215 – 218.
- [2] Ji-Young Lee, Jung-Pyo Hong, Do-Hyun Kang, "Analysis of Permanent Magnet Type Transverse Flux Linear Motor by Coupling 2D Finite Element Method on 3D Equivalent Magnetic Circuit Network Method," *IEEE conference of 39<sup>th</sup> IAS Annual Meeting Industry Applications*, Seattle, WA (USA) Oct. 2004, pp. 2092 – 2098.
- [3] Jiabin Wang, Howe D., Zhengyu Lin, "Comparative study of winding configurations of short-stroke single phase tubular permanent magnet motor for refrigeration applications," *IEEE conference of 42<sup>nd</sup> IAS Annual Meeting Industry Applications*, Louisiana, (USA), Sept, 2007, pp. 311 - 318.
- [4] R. C. Okonkwo, "Design and Performance of Permanent-Magnet DC Linear Motors," *IEEE Transactions on Magnetics*, Vol. 42, No. 9, pp. 2179 – 2183, 2006.
- [5] Y. Yamamoto and H. Yamada, "Analysis of magnetic circuit and starting characteristics of flat-type linear pulse motor with permanent magnets", *T. IEE Japan*, Vol. 104-B, No. 5, pp. 265 – 272, 1984.
- [6] David G. Dorrell, "Are wound-rotor synchronous motors suitable for use in high efficiency torque-dense automotive drive?", *38<sup>th</sup> Annual conference on IEEE Industrial Electronics Society*, Montreal (Canada), Oct. 2012, pp. 4880-4885.
- [7] Deshpande U., "Two-dimensional finite element analysis of a high force-density linear switched reluctance machine including three dimensional-effects", *IEEE Transactions Industry Application*, Vol. 36, No. 3, pp. 1047–1052, 2000.
- [8] Gan WC, Cheung NC, Qiu L., "Position control of linear switched reluctance motors for high precision applications", *IEEE Transactions Industry Application*, Vol. 39, No. 5, pp. 1350 –1362, 2003.
- [9] Stumberger G, Stumberger B, Dolinar D., "Identification of linear synchronous reluctance motor parameters", *IEEE Transactions Industry Application*, Vol. 40, No. 5, pp. 1317 –1324, 2004.
- [10] Ferhat Daldaban, Nurettin Ustkoyuncu, "A new double sided linear switched reluctance motor with low cost", *Energy Conversion and Management* 47, pp. 2983–2990, 2006.
- [11] Ferhat Daldaban, Nurettin Ustkoyuncu, "A novel linear switched reluctance motor for railway transportation systems", *Energy Conversion and Management* 51, pp. 465–469, 2010.
- [12] M. Sanada, Y. Takeda and T. Hiras, "Cylindrical Linear Pulse Motor with Laminated Ring Teeth," *Proceedings of the Second International Conference on Electronic Materials (ICEM '90)*, Vol. 2, New Jersey (U.S.A), Sept. 1990, pp. 693-698.
- [13] H. Yamada, T. Hamajima, S. Xiang and N. Nishizawa, "Six-Phase Cylindrical Linear Pulse Motor as Linear Oscillatory Actuator", *IEEE Transactions on Magnetic*, Vol. Mag-23, No. 5, pp. 2841 – 2843, 1987.
- [14] Yoji Takeda, Masayuki Sanada, Shigeo Morimoto, Takao Hirasa and Katsunori Taniguchi, "Cylindrical Linear Pulse Motor with Interior Permanent Magnet Mover", *IEEE Transactions on Industry Applications*, Vol. 30, No. 1, pp. 141 – 145, 1994.
- [15] Corda J. and Skopljak E., "Linear switched reluctance actuator", *Sixth International Conference on Electrical Machines and Drives*, Oxford, (England), Sept. 1993, pp. 535 – 539.
- [16] T. Mizuno, M. Kawai, F. Tsuchiya, M. Kosugi and H. Yamada, "An Examination for Increasing the Motor Constant of a Cylindrical Moving Magnet-Type Linear Actuator", *IEEE Transactions on Magnetics*, Vol. 41, No. 10, pp. 3976–3979, 2005.

## Evaluation of Various Permanent Magnet Arrangements on Linear Actuator

F. Azhar<sup>\*1</sup>, M. Norhisam<sup>\*2</sup>, H. Wakiwaka<sup>\*1</sup>, K. Tashiro<sup>\*1</sup>, M. Nirei<sup>.\*3</sup>

Linear actuators are used to provide linear motion in the absence of a motion translator. By using the linear actuator, the linear motion can be produced with a high degree of efficiency. Linear actuators can be designed with and without slots; moreover, there are various types of magnetization arrangements that can be applied to the mover. In this paper, ten different magnetization arrangements were used to evaluate slot and slot-less linear actuators. Nine different performance characteristics were used to find the best structure of linear actuator. Results show that, the slot-less types of linear actuators generally have a better dynamic performance, while the slot types of linear actuators have a better static performance. Four different structures with different magnetization arrangements were selected as the best models of linear actuators.

*Keywords:* Linear actuator, magnetization arrangement, permanent magnet.

### 1. Introduction

Conventionally, linear motion is achieved by conversion of rotational motion via a motion translator such as a crank shaft, gear, ball screw, belt or motor coupling system [1-4]. However, the conventional linear motion system often functions with low efficiency due to mechanical friction and wear [1,2]. Moreover, the system operates with low acceleration and low impact power, in addition to an increase in the mechanical complexity [5].

Currently, most linear motion systems employ linear actuators, in a system called direct linear motion. The direct linear motion produces a linear motion without the need of a motion translator [4,6]. This system offers high efficiency and flexibility of operation, eliminates the requirement of lubrication and reduces the total number of components used in the system [1,4,6,7]. However, by applying this system, the overall cost will increase as the length of displacement is increased.

Due to numerous advantages offered by direct linear motion systems, this system has been applied to various applications. Beginning with its use in transportation systems, linear actuators are currently being implemented in various applications such as automated manufacturing [8], embedded power generation [9,10], healthcare [11,12] and household appliances [5,13].

Several researchers have been put significant effort in the development of different types of linear actuators with several types of shapes, structural arrangements, and most of the time, permanent magnet types of linear

actuators are considered [1-7,10-13]. Furthermore, due to advantages such as high power density, strength of field, low weight, and high efficiency, the moving magnet structure of the linear actuator is chosen for study. The moving magnet linear actuator is mostly designed in a tubular shape. In order to strengthen the mover, the ring shape of the permanent magnet attached to the shaft is used. The coil is wound at the stator side of the linear actuator and a gap between the stator and the mover allows the mover to freely oscillate along the axial air gap [14].

Apart from being designed as tubular shape with a moving magnet structure, the linear actuator can be classified as either a slot type or a slot-less type. The classification depends on the type of stator used. Even though the slot type of linear actuator has shown its advantage in static performance such as static thrust [15], the slot-less type has better dynamic performance such as with inductance and when under time constants. Therefore, a proper comparison between these structures is essential in order to decide which type of structure will be used, depending on the appropriate design target.

On the mover side, the arrangement of the permanent magnet magnetization arrangement is a significant factor in determining the performance of the linear actuator. Presently, various permanent magnet magnetization arrangements have been invented in order to improve the linear actuator performance by directing the magnetic flux to flow in a certain path.

A revolution of permanent magnet magnetization direction has occurred since its first implementation in a linear actuator. Several researchers have tried different magnetization directions, from simple N-S arrangement either in the axial [16-18] or radial [19-21] direction, to the halbach array [21-23] in order to evaluate linear actuator performance.

In this study several permanent magnet magnetization arrangements of tubular shape linear actuators were evaluated. Even though no specific design target has been set up, the evaluation was performed in order to observe the effect of permanent magnet mag-

---

**Correspondence:** F. Azhar, Dept. of Electrical & Electronic, Fac. of Engineering, Shinshu University, 4-17-1 Wakasato, Nagano. 380-8553, Japan

email: [fairul.azhar@utem.edu.my](mailto:fairul.azhar@utem.edu.my)

<sup>\*1</sup> Shinshu University <sup>\*2</sup> Universiti Putra Malaysia

<sup>\*3</sup> Nagano National College of Technology

netization arrangement on the performance of a linear actuator.

**2. Structure of the permanent magnet linear actuator**

In this study, two types of stator were simulated: a slot type and a slot-less type. In order to make a valid comparison between these types of linear actuators, several parameters of the stator part need to be fixed, specifically the coil pitch  $\tau_c$ , input power  $P_{in}$ , and number of coil turns  $N$ . Therefore, the size of both stators type was slightly different in order to fix the parameters. Six coils and three phase power supply with 50W input power,  $P_{in}$  and 70 Hz frequency were set. Fig. 1 shows the structure of the slot and slot-less types of linear actuators.

Ten magnetization arrangements of permanent magnets were used in this study. The magnetization arrangements were taken from several sources of reference of previous studies. To make a valid comparison between these models, magnetic pole pitch,  $\tau_{PM}$  and radius of permanent magnet,  $r_{PM}$  were fixed. The stroke direction of the mover in the Y axis is shown in Fig. 1. Each model of linear actuator is set so that it makes a

3-slot 4-pole structure. Fig.2 shows the magnetization arrangement of the permanent magnet that was used. Table 1 shows the structural parameters of the both slot and slot-less types of linear actuators.

Table 1 : Linear actuator structure parameter

Part	Parameter	unit	Value	
			Slot-less	Slot type
Stator	Coil pitch, $\tau_c$	mm	15	15
	Turns		704	704
	Coil resistance, $R$	$\Omega$	14.89	18.26
	Height of coil, $h_c$	mm	5.5	6.5
	Yoke thickness, $t_y$	mm	2.5	1.25
	Length of stator, $l_y$	mm	90	90
Mover	Magnetic pole pitch, $\tau_{PM}$	mm	11.25	11.25
	PM radius, $r_{PM}$	mm	10	10
Gap	Gap length, $\delta$	mm	0.5	0.5

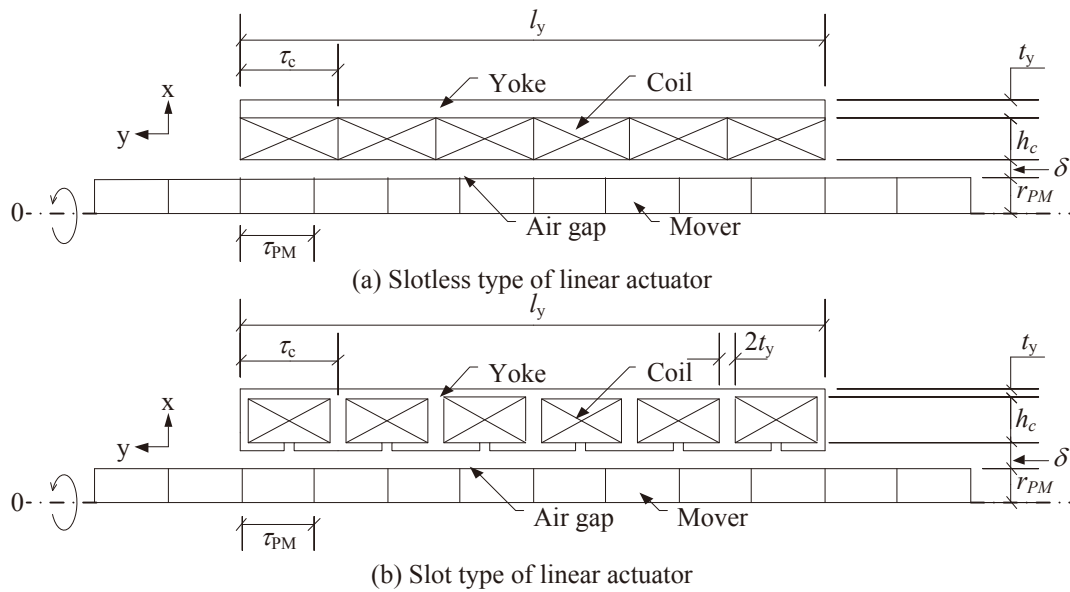


Fig. 1 : Linear actuator structure

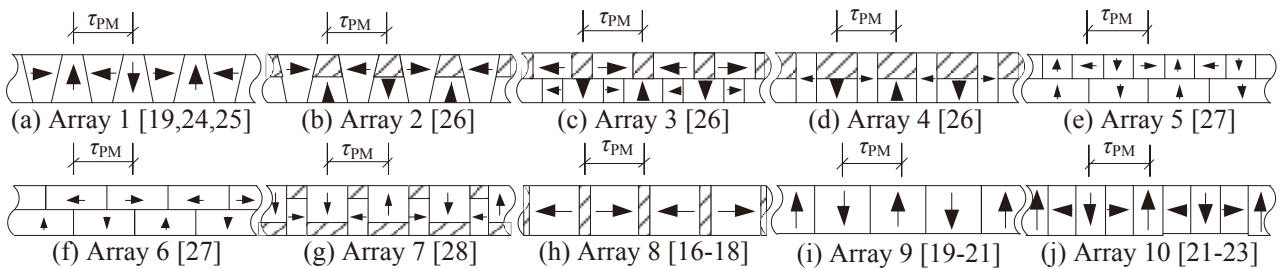


Fig. 2 : Permanent magnet magnetization arrangement and pitch of magnetization,  $\tau_{pm}$

### 3. Performance characteristics of the linear actuator

The performance of a linear actuator is evaluated using several criteria. Most researchers use thrust,  $F$  as the main factor to design a high performance linear actuator [1,2,15,21]. At the same time, characteristics such as the thrust constant  $k_f$ , the motor constant  $k_m$ , the total displacement  $x$ , the volume  $v$ , the electrical time constant  $\tau_e$  and the mechanical time constant  $\tau_m$  also need to be considered in order to design the linear actuator [3,4,16,29,30].

In order to evaluate the performance of linear actuators with different permanent magnet magnetization arrangements, nine criteria were used:

- i. Average thrust,  $F_{ave}$ .
- ii. Ripple thrust,  $\Delta F$ .
- iii. Thrust constant,  $k_f$ .
- iv. Motor constant,  $k_m$ .
- v. Motor constant square density,  $G$ .
- vi. Tangential thrust,  $\sigma$ .
- vii. Total weight,  $W$ .
- viii. Electrical time constant,  $\tau_e$ .
- ix. Mechanical time constant,  $\tau_m$ .

Fig. 3 shows an example of the thrust characteristics of slot and slot-less linear actuators at full displacement. The first six criteria (i - vi) will use some of the information as shown in the thrust characteristics of linear actuator. The criteria of linear actuators are indicated in (1) - (6).

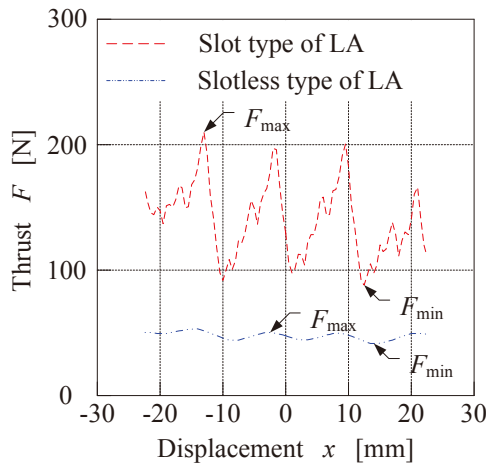


Fig. 3 : Thrust characteristics of linear actuator

The total weight of the linear actuator  $W$  was calculated based on the structure size. The volume of each element of the linear actuator was calculated and multiplied with its corresponding material density. The total weight of the linear actuator is indicated in (7).

$$F_{ave} = \frac{1}{x_T} \left( \int_0^{+x} F(x) dx + \int_{-x}^0 F(x) dx \right) = \frac{1}{45} \left( \int_0^{+22.5} F(x) dx + \int_{-22.5}^0 F(x) dx \right) \quad (1)$$

$$\Delta F = \frac{F_{max} - F_{min}}{F_{ave}} \times 100\% \quad (2)$$

$$k_f = \frac{F_{ave}}{I_{rms}} \quad (3)$$

$$k_m = \frac{F_{ave}}{\sqrt{P_{in}}} \quad (4)$$

$$G = \frac{F_{ave}^2}{P_{in} \times V} \quad (5)$$

$$\sigma = \frac{F_{ave}}{S} \quad (6)$$

$$W = \rho_{iron} V_{yoke} + \rho_{copper} V_{coil} + \rho_{magnet} V_{magnet} \quad (7)$$

$F_{ave}$  is the average thrust in N,  $x_T$  is the total displacement of the linear actuator in millimeters,  $+x$  is the most positive displacement of the linear actuator in mm,  $-x$  is the most positive displacement of the linear actuator in mm,  $\Delta F$  is the ripple thrust in %,  $F_{max}$  is the maximum thrust in N,  $F_{ave}$  is the average thrust in N,  $k_f$  is the thrust constant in N/A,  $I_{rms}$  is the root mean square of input current in A,  $k_m$  is the motor constant in N/√W,  $P_{in}$  is the input power in W,  $G$  is the motor constant square density in N<sup>2</sup>/Wm<sup>3</sup>,  $V$  is the linear actuator volume in m<sup>3</sup>,  $\sigma$  is the tangential thrust in N/m<sup>2</sup>,  $S$  is the area of permanent magnet surface corresponding to the area of thrust developed in m<sup>2</sup>,  $W$  is the total weight in kg,  $\rho_{iron,copper,magnet}$  is the particular material density in kg/m<sup>3</sup> and  $V_{iron,copper,magnet}$  volume of each element linear actuator structure in m<sup>3</sup>.

The electrical time constant  $\tau_e$  is used to measure the current response of the linear actuator. The mechanical time constant  $\tau_m$  is used to measure the response of the linear actuator's mover. Lower time constants correlate to a good response for the linear actuator's current and mover. These characteristics are calculated in steps (8) and (9).

$$\tau_e = \frac{L}{R} \quad (8)$$

$$\tau_m = \frac{mR^2}{k_f} \quad (9)$$

where  $\tau_e$  is the electrical time constant in ms,  $L$  is the linear actuator inductance in mH,  $R$  is the linear actuator resistance in  $\Omega$ ,  $\tau_m$  is the mechanical time constant in ms, and  $m$  is the mass of linear actuator's mover in kg.

**4. Comparison of linear actuator performance characteristics.**

Fig. 4 shows the comparison of characteristics between the slot and slot-less linear actuators at different permanent magnet magnetization arrangements. Based on the comparison, it is shown that the slot type of linear actuator has better performance characteristics such as average thrust  $F_{ave}$ , thrust constant  $k_f$ , motor constant  $k_m$ , motor constant square density  $G$  and tangential thrust  $\sigma$ . Conversely, when the slot-less stator was used, the linear actuator had less thrust ripple  $\Delta F$ , was lighter in total weight  $W$ , and faster current and mover response.

The comparison slot-less linear actuator performance characteristics is shown in fig. 4 (a). Based on the plot, all models of the slot-less type of linear actuators have a similar value of all performance characteristics except for the electrical time constant  $\tau_e$  and mechanical time constant  $\tau_m$ . However, the slot-less linear actuator with permanent magnet magnetization arrangement 6 and 7 have the lowest performance in almost all characteristics except for the electrical time constant  $\tau_e$  compared to other models of slot-less linear actuators. Due to elimination of the slot-less linear actuator models with permanent magnet magnetization arrangement 6 and 7, the model with permanent magnet magnetization arrangement 5 and 9 was observed with the lowest thrust ripple  $\Delta F$  and electrical time constant  $\tau_e$ . However, it gave a low performance on other

characteristics, especially average thrust  $F_{ave}$  and the mechanical time constant  $\tau_m$ . On the other hand, the slot-less linear actuators with permanent magnet magnetization in arrangement 8 and 10 are seen as the best two models for the slot-less linear actuator since they have the best performance in all performance characteristics except for the ripple thrust  $\Delta F$  for both models and electrical time constant  $\tau_e$  for the slot-less linear actuator with permanent magnet magnetization arrangement 8.

The comparison of the slot type linear actuator performance characteristics is shown in fig. 4 (b). Based on the plot, the slot type of linear actuator has a similar value of total weight  $W_{total}$  and mechanical time constant  $\tau_m$ . Nevertheless, the slot type linear actuator with the permanent magnet magnetization arrangement 5, 6 and 7 have the lowest performance in almost all performance characteristics except for electrical time constant  $\tau_e$ , where the model with permanent magnet magnetization arrangement 5 has the best performance compared to other models. Even though the model with permanent magnet magnetization arrangement 9 gives the lowest value of thrust ripple  $\Delta F$ , it gives the lowest value in other performance characteristics, especially on average thrust  $F_{ave}$ , motor constants  $k_m$  and motor constants square density  $G$ , with the exception of models with the permanent magnet magnetization arrangement 5, 6 and 7. Apart from other models which were observed with similar performance characteristics, the slot type linear actuator with permanent magnet magnetization arrangement 4 and 10 have the best performance in all characteristics except the thrust ripple  $\Delta F$  and the electrical time constant,  $\tau_e$ . Table 2 shows the summary of comparison between the best two models of slot type and slot-less type of linear actuators.

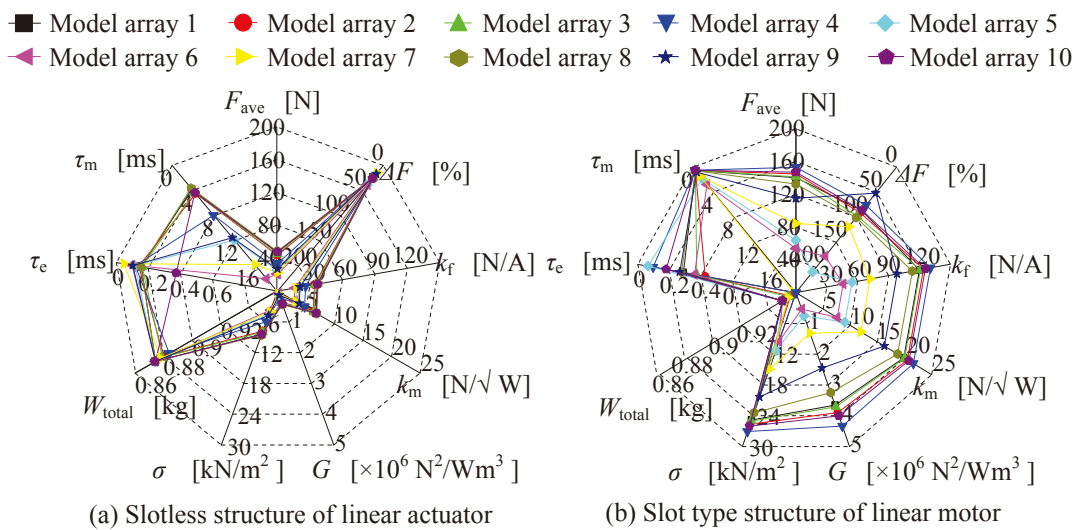


Fig. 4 : Performance comparison of linear actuator models

Table 2 : Comparison of best two model of slot-less and slot type linear actuator

Parameter	Unit	Number of permanent magnet magnetization arrangement			
		Slot less type linear actuator		Slot type linear actuator	
		model array 8	model array 10	model array 4	model array 10
Average thrust, $F_{ave}$	N	48.70	47.77	153.03	147.06
Ripple thrust, $\Delta F$	%	23.79	25.76	75.96	86.04
Thrust constant, $k_f$	N/A	37.63	36.91	130.74	125.65
Motor constant, $k_m$	N/ $\sqrt{W}$	6.89	6.76	21.64	20.80
Motor constant square density, $G$	$\times 10^6 \text{ N}^2/\text{Wm}^3$	0.44	0.42	4.34	4.00
Tangential thrust, $\sigma$	kN/m <sup>2</sup>	8.61	8.45	27.06	26.00
Total weight, $W$	kg	0.87	0.87	0.96	0.95
Electrical time constant, $\tau_e$	ms	0.15	0.37	0.11	0.18
Mechanical time constant, $\tau_m$	ms	3.62	4.34	0.48	0.48

As shown in table 2, the linear actuator models with permanent magnet magnetization arrangement 10 and 8 are listed as the best two models for the slot-less type of linear actuator. The best models for the slot type of linear actuator were observed to be arrangement 10 and 4. Arrangement 10 uses a halbach magnetization arrangement of permanent magnet. The model with permanent magnet magnetization arrangement 8 uses the axial magnetization direction and each permanent magnet faces the same pole of each other. Meanwhile, the model with permanent magnet magnetization arrangement 4 uses a similar halbach arrangement but has a magnetic spacer on the outer side and inner side of the permanent magnet.

#### 4. Conclusion

Previously, linear motion is produced by converting the rotational motion to linear motion by using a motion translator. However, this linear motion system comes with an operational limitation. In order to eliminate this drawback, a direct linear motion system that consists of a linear actuator can be used. The structure of the linear actuator can be designed with either a slot or slot-less type of stator structure. On the mover side, various permanent magnet magnetization arrangements can be implemented in order to obtain high performance of the linear actuator. In this study, 10 different magnetization arrangements were used to evaluate the performance of a linear actuator. The performances of the linear actuators were measured using several criteria, and nine characteristics were used to obtain the best model, specifically force, size and response related characteristics. The force related characteristics used were average thrust  $F_{ave}$ , ripple thrust  $\Delta F$ , thrust constant  $k_f$ , motor constant  $k_m$ , motor constant square density  $G$  and tangential thrust  $\sigma$ . The size related characteristics used were total weight  $W$ , and the response related characteristics were the electrical time constant  $\tau_e$  and the mechanical time constant  $\tau_m$ . Based on the results, the slot type of linear actuator

has higher force related characteristics compared to the slot-less type of linear actuator. On the other hand, the slot-less type of linear actuator has smaller size and faster response related characteristics compared to the slot type of linear actuator. Furthermore, for the slot-less type of linear actuator, the permanent magnet with magnetization arrangement 8 and 10 are the best two models, while for the slot type of linear actuator, the permanent magnet with magnetization arrangement 4 and 10 are the best two models.

#### Acknowledgment

F. Azhar wishes to acknowledge the Universiti Teknikal Malaysia Melaka (UTeM), and Ministry of Higher Education of Malaysia, for giving him the opportunity to pursue his PhD study and for their financial support in Shinshu University.

#### References

- [1] Jiabin Wang, Howe D., Zhengyu Lin, "Comparative study of winding configurations of short-stroke single phase tubular permanent magnet motor for refrigeration applications," *IEEE conference of 42<sup>nd</sup> IAS Annual Meeting Industry Applications*, pp. 311 - 318, 2007.
- [2] Young-Bong Bang, Kyung-Min Lee, "Large thrust linear motors for low-duty-cycle operation," *Mechatronics 14*, pp. 891 - 906, 2004
- [3] H. Yajima, H. Wakiwaka, K. Minegishi, N. Fujiwara, K. Tamura, "Design of linear DC motor for high-speed positioning," *Sensors and Actuators 81*, pp. 281-284, 2000
- [4] M. Norhisam, H. Ezril, R. N. Firdaus, F. Azhar, H. Wakiwaka, M. Nirei, "Positioning System for Sensor Less Linear DC Motor," *Asia Pacific Symposium of Applied Electromagnetics and Mechanics (APSAEM2010)*, Kuala Lumpur, pp. 215 - 218, Malaysia, July 2010.
- [5] K. Park, E. P. Hong and K. H. Lee, "Development of a linear motor for compressors of household refrigerators", *Proceeding of 2001 Linear Drives and Industry Applications (LDIA'2001)*, Nagano, Japan, pp. 283-286, 2001.
- [6] Ji-Young Lee, Jung-Pyo Hong, Do-Hyun Kang, "Analysis of Permanent Magnet Type Transverse Flux Linear Motor by Coupling 2D Finite Element Method on 3D

- Equivalent Magnetic Circuit Network Method,” *IEEE conference of 39<sup>th</sup> IAS Annual Meeting Industry Applications*, pp. 2092 – 2098, 2004.
- [7] R. C. Okonkwo, “Design and Performance of Permanent-Magnet DC Linear Motors,” *IEEE Transactions on Magnetics*, Vol. 42, No. 9, pp. 2179 – 2183, 2006.
- [8] Masada E., “Linear drives for industrial applications in Japan history, existing state and future prospect,” *Proceeding LDIA'95*, Nagasaki, Japan, pp. 9-12, 1995.
- [9] White, M.A, Colenbrander, K., Olan R.W and Penswick, L.B., “Generators that won't wear out,” *Mechanical Engineering*, pp. 92-96, 1996.
- [10] Cawthorne, W.R., Famouri, P., Chen, J., Clarke, N.N., McDaniel, T.I., Atkinson, R.J., Nandkumar, S., Atkinson, C.M., Petreanu, S., “Development of linear alternator engine for electric vehicle applications,” *IEEE Transactions on Vehicle Technology*, pp. 1797-1802, 1999.
- [11] Clark, R.E., Smith, D.S., Mellor, P.H., and Howe, D., “Design optimization of moving-magnet actuators for reciprocating electro-mechanical systems,” *IEEE Transaction on Magnetic*, pp. 3746-3748, 1995.
- [12] Watada, M., Yanashima, K., Oishi, Y., and Ebihara, D., Improvement on characteristics of linear oscillatory actuator for artificial hearts, *IEEE Transaction on Magnetic*, pp. 3361-3363, 1995.
- [13] Utsuno, M., Takai, M., Yaegashi, T., Mizuno, T., Yamamoto, H., Shibuya, K., and Yamada, H., “Efficiency characteristics of a linear oscillatory actuator under simulated compressor load,” *Proceeding LDIA'2001, Nagano, Japan*, pp. 264-267, 2001.
- [14] Gieras, J. and Wing, M., “Permanent Magnet Motor Technology,” *Marcel Dekker Inc.*, 2002, USA.
- [15] M. Norhisam, Alias K., R.N Firdaus, S. Mahmud, N. Mariun, “Comparison on Thrust Characteristic of Linear of Actuators,” *Power and Energy Conference, PECon '06. IEEE International*, pp. 470 – 475, 2006.
- [16] M. Norhisam, F. Azhar, R.N. Firdaus, H. Hashim, M. Nirei, H. Wakiwaka, Abdul Razak J., “Effect of Spring Constant and Thrust Constant to Displacement Characteristics of LOA,” *Journal of the Japan Society of Applied Electromagnetics and Mechanics (JSAEM)*, Vol.17 No.3, pp. 437 – 440, 2009.
- [17] Z. Q. Zhu, P. J. Hor, D. Howe, and J. Rees-Jones, “Calculation of Cogging Force in a Novel Slotted Linear Tubular Brushless Permanent Magnet Motor,” *IEEE Transactions on Magnetics*, Vol. 33, No. 5, pp. 4098 – 4100, 1997.
- [18] Won-jong Kim and Bryan C. Murphy, “Development of a Novel Direct-Drive Tubular Linear Brushless Permanent-Magnet Motor,” *International Journal of Control, Automation and Systems*, Vol. 2, No. 3, pp. 279-288, 2004.
- [19] Seok Myeong Jang, Jang Young Choi, Sung Ho Lee, Sung Kook Cho, Won Bum Jang, “Analysis of the tubular motor with Halbach and radial magnet array,” *Sixth International Conference on Electrical Machines and Systems, 2003. ICEMS 2003*, China, pp. 250 – 252, 2003.
- [20] C. Lucas, F. Tootoonchian and Z. Nasiri-Gheidari, “Multi-Objective Design Optimization of a Linear Brushless Permanent Magnet Motor Using Particle Swarm Optimization (PSO),” *Iranian Journal of Electrical and Electronic Engineering*, Vol. 6, No. 3, pp. 183-189, 2010.
- [21] Koichi Nakaiwa, Hiroyuki Wakiwaka, Kunihiisa Tashiro, “Thrust Characteristics Comparison of Interior Magnet Type Pencil Size Cylinder Linear Motor,” *Journal of the Japan Society of Applied Electromagnetics and Mechanics*, Vol 19, No. 3, pp. 509 -512, 2011.
- [22] Seok-Myeong Jang, Sung-Ho Lee, and In-Ki Yoon, “Design Criteria for Detent Force Reduction of Permanent-Magnet Linear Synchronous Motors With Halbach Array,” *IEEE Transactions on Magnetics*, Vol. 38, No. 5, pp. 3261 – 3263, 2002.
- [23] Jiabin Wang and David Howe, “Tubular Modular Permanent-Magnet Machines Equipped With Quasi-Halbach Magnetized Magnets—Part I: Magnetic Field Distribution, EMF, and Thrust Force,” *IEEE Transactions on Magnetics*, Vol. 41, No. 9, pp. 2470 – 2478, 2005.
- [24] Koen J. Meessen, Bart L. J. Gysen, Johannes J. H. Paulides, and Elena A. Lomonova, Halbach Permanent Magnet Shape Selection for Slotless Tubular Actuators, *IEEE Transactions on Magnetics*, Vol. 44, No. 11, pp. 4305 - 4308, 2008.
- [25] Moon G. Lee, Dae-Gab Gweon, Optimal design of a double-sided linear motor with a multi-segmented trapezoidal magnet array for a high precision positioning system, *Journal of Magnetism and Magnetic Materials 281*, pp. 336-346, 2004.
- [26] Akihito Toyota, Toru Shikayama, Masanobu Kakihara, “Using the Same Periodic Magnetic Field Generation Device, and linear motor and rotary motor,” *U.S Patent*, US 2011/0012440A1, Jan. 20, 2011.
- [27] Shunji Tahara, Yuta Ishida and Kokichi Ogawa, “Application of Flux Concentrated Permanent Magnet Arrangement with Halbach Array for 2-pole PMLSM,” *The 7<sup>th</sup> International Symposium on Linear Drives for Industry Applications, LDIA 2009*, Korea, pp. 39 – 49, 2009.
- [28] Soga Mitchiharu, Furukawa Hidetoshi, Suzuki Kenschichi, Kajinami Jun, Otaku Kazuhiro and Ueda Shunichi, “Linear Motor,” *Japan Patent 2010-632201A*, March. 18, 2010 (*In Japanese*).
- [29] Yasuhiro Miyamoto, Toshiyuki Hoshi, “The Performance Goodness Factor for the Applications of Linear Motor,” *The 7<sup>th</sup> International Symposium on Linear Drives for Industry Applications, LDIA 2009*, Korea, pp. 260 – 263, 2009.
- [30] Tsutomu Mizuno, Masanori Kawai, Fumiaki Tsuchiya, Masashi Kosugi and Hajime Yamada, “An Examination for Increasing the Motor Constant of a Cylindrical Moving Magnet-Type Linear Actuator,” *IEEE Transactions on Magnetics*, Vol. 41, No. 10, pp. 3976 – 3978, 2005.

# Initial Progress and Possible Improvement of E-Cutter Linear Actuator Development

F. Azhar<sup>1</sup>, M. Norhisam<sup>2</sup>, H. Wakiwaka<sup>1</sup>, K. Tashiro<sup>1</sup>, M. Nirei<sup>3</sup>

<sup>1</sup>Dept. of Electrical & Electronic, Fac. of Engineering, Shinshu University,  
4-17-1 Wakasato, Nagano. 380-8553, JAPAN

<sup>2</sup>Electrical and Electronic Dept., Engineering Fac., Universiti Putra Malaysia,  
43400 Selangor, MALAYSIA

<sup>3</sup>Department of Electronics and Computer Science, Nagano National College of Technology,  
716 Tokuma, Nagano City, 381-8550, JAPAN

Corresponding author email : fairul.azhar@utem.edu.my

**Abstract**— Currently, palm oil has become the most consumed vegetable oil type. This is due to an awareness of the effect Trans Fat has on human health. Therefore, increasing productiveness is a crucial factor to ensure its continued availability as a product in the marketplace. One of the processes that should be improved to increase productivity is harvesting. The Malaysian Palm Oil Board (MPOB) has put a lot of effort into developing a mechanized harvesting tool called the *Cantas*<sup>TM</sup>. This efficient tool has been shown to increase oil palm harvesting productivity by a factor of 3. However, *Cantas*<sup>TM</sup> is ineffective at harvesting oil palm fruit in trees taller than 8m. Therefore, a new tool called the E-Cutter was introduced. In this paper, the development progress of specifically the E-Cutter's linear actuator part was discussed. The previous type of linear actuator for the E-Cutter is also mentioned. Improvement in the planning and design target of the linear actuator is also addressed. The potential linear actuator structure and type is also identified.

**Keywords**-component; *Cantas*<sup>TM</sup>; E-Cutter; permanent magnet generator; slot type linear actuator.

## I. INTRODUCTION

Palm oil has been recognized as the healthiest vegetable oil due to high beta-carotene and saturated vegetable fat content [1]. Since 2009, palm oil has become the most consumed vegetable oil type [2]. Nowadays, Malaysia and Indonesia have become top producers of palm oil products [3, 4]. In order to support world demand for palm oil, production is projected to increase 3.47% every year [5]. One option to increase palm oil production is to improve the harvesting technique of the oil palm's fresh fruit bunch (FFB) [1].

In this paper, the evolution of the oil palm FFB harvesting mechanism is discussed. The traditional technique and tools have been mechanized in order to make the harvesting activity more effortless and productive [6]. The mechanization using *Cantas*<sup>TM</sup> has undergone several tests in order to prove its usefulness in increasing the productivity of oil palm harvesting [7].

Even though the test results were impressive, there are other aspects of the *Cantas*<sup>TM</sup> especially limitations in operation and maintenance, which need to be improved. Thus, a new mechanized FFB harvesting system called the E-Cutter has been introduced [8]. For now, the design and development of the actuator for the E-Cutter is still in progress. The previous

achievements and the possibility of improving the actuator will be reviewed.

## II. EVOLUTION OF THE OIL PALM HARVESTING MECHANISM

The oil palm harvesting process sequence involves cutting the fronds and fruit bunches, stacking the fronds, collecting the loose fruits and carrying the harvested fruit to the collection point. All these activities have been mechanized apart from cutting and stacking the fronds [6].

Historically, a cutlass or chisel was used to harvest the oil palm FFBs that are within arm's reach. However, for taller oil palm trees, a sickle attached to a bamboo or aluminum pole is the preferred mechanism. The length of the pole depends on the average height of the trees on the plantation plot to be harvested. The harvester stands on the ground while the pole and knife are raised to the tree crown in order to harvest the fruit bunches and fronds [1].

Even though this technique is seen as a favorable mechanism, a new harvesting technique is needed to ensure that palm oil productivity is aligned with targets. A mechanization mechanism is one of the options to be implemented. Like in other agricultural sectors such as apples [9], apricots [10] and oranges [11], the mechanization of harvesting tools could improve oil palm harvesting productivity.

### A. *Cantas*<sup>TM</sup>

In Malaysia, the mechanization of oil palm harvesting tools has been started by the Malaysian Palm Oil Board (MPOB). The MPOB invented a tool called the *Cantas*<sup>TM</sup>. The tool's construction can be seen in Fig. 1 [6, 7, 12].

The *Cantas*<sup>TM</sup> uses a two stroke engine located as the base of the tool as its power source. It retains the use of a sickle since these prove to be efficient in harvesting oil palm FFBs. The *Cantas*<sup>TM</sup> applies a rapid chopping method to harvest an oil palm FFB. Using this method, the frond cutting process will be performed gradually based on the displacement of the vibrating sickle [6, 7, 12].

Fig. 1 : *Cantas*<sup>TM</sup> for FFB harvesting tools

The engine provides the *Cantas*<sup>TM</sup> with mechanical energy in the form of rotational motion. The rotational motion is converted to linear motion needed to vibrate the sickle by using a bevel gear. Mechanical energy is transferred from the bottom to the bevel gear at the top of the tool via a transmission shaft inside the pole [6, 7, 12]. Table I shows the operation characteristics of a *Cantas*<sup>TM</sup>.

TABLE I. OPERATION CHARACTERISTICS OF *CANTAS*<sup>TM</sup>

Characteristics	Unit	Value
Vibration speed	cycle/min	3000
Total weight	kg	7.5
Max height	m	8

The *Cantas*<sup>TM</sup> has gone through several field tests. One of them was done in the Tereh Selatan Estate. This estate belongs to the Kulim Plantations Group and is located in Kluang, Johor, Malaysia. The estate started operations in 1974 and covers about 2726.89 ha [12]. This tool was shown to increase the ratio of worker to land area (ha) to about 1:38 as compared with 1:18 by using manual harvesting. Furthermore, the *Cantas*<sup>TM</sup> has also increased FFB productivity from 4.19 tonnes/day to 11.60 tonnes/day.

Even though the *Cantas*<sup>TM</sup> has proven its significant contribution in improving harvesting output productivity, its use is inefficient for trees taller than 8m. Due to the weight of the bevel gear and sickle, the pole will start to bend at lengths over 8m. This causes the transmission shaft inside the pole to bend and does not allow mechanical energy to be transferred [6, 7]. Therefore, another type of tool needs to be introduced. This new tool not only aims to have performance at least similar to the *Cantas*<sup>TM</sup>, but its operation should not be limited by the pole bending problem.

### B. E-Cutter

To counter the drawbacks of *Cantas*<sup>TM</sup>, the E-Cutter was proposed [8]. The E Cutter structure is as shown in Fig. 2. The 2 stroke engine used in the *Cantas*<sup>TM</sup> will still be used in E Cutter. However, the engine will be attached to a mobile electrical generator in order to convert mechanical energy into electrical energy. The bevel gear will be replaced by a linear actuator in order to provide direct linear vibration motion to the sickle in order to accomplish the harvesting activity. A copper

wire will replace the shaft inside the aluminum pole in order to transmit the electrical energy provided by the generator to the linear actuator [8]. Therefore, due to the flexibility of the copper wire, this tool will continue to operate efficiently even if the pole bends at increased heights.

### III. PROGRESS OF E-CUTTER DEVELOPMENT

E-Cutter overall development depends on the progress of development of the mobile electrical generator and the linear actuator. The development progress of the E-Cutter's electrical generator was discussed in [13-16]. There are three types of electrical generators that have been optimized for E-Cutter implementation. To meet the needs of a light weight and small electrical generator, a permanent magnet type generator (PMG) was used. The PMG's output was single and three phase depending on which type of PMG was appropriate for energizing the linear actuator. Table II shows the type of PMGs that have been developed and their characteristics.

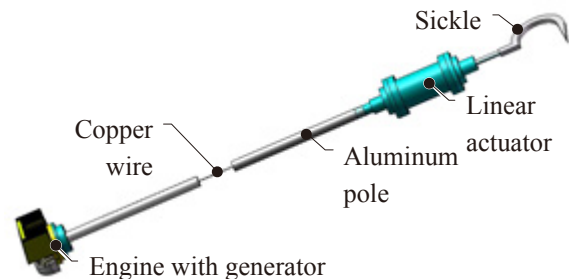


Fig. 2 : E Cutter for FFB harvesting tools

TABLE II. CHARACTERISTICS OF PMG FOR E-CUTTER

Type of PMG	Output phase	Output power, $P_{OP}$ (W)	Speed, $n$ (rpm)	Efficiency, $\eta$ (%)
Slotless [13,14]	Single phase	103	1500	88
Double stator [15,16]	Three phase	170	1500	93
Double stator [15,16]	Three phase	90	1500	90

Even though the PMG development seems to be established, improvement is still in progress. However, progress in the development of the E-Cutter's linear actuator is more crucial for its overall development. The development progress of the E-Cutter's linear actuator was discussed in [8, 17-19]. Each type of linear actuator that has been developed has gone through a design optimization process to make sure it operates at peak performance. Each linear actuator has also

F. Azhar wishes to acknowledge the Universiti Teknikal Malaysia Melaka (UTeM), and Ministry of Higher Education of Malaysia, for giving him the opportunity to pursue his PhD study and for their financial support in Shinshu University, Nagano, Japan.

undergone laboratory and field testing to ensure performance. The performance characteristics of each linear actuator are as shown in Table III.

TABLE III. CHARACTERISTICS OF LINEAR ACTUATOR FOR E-CUTTER

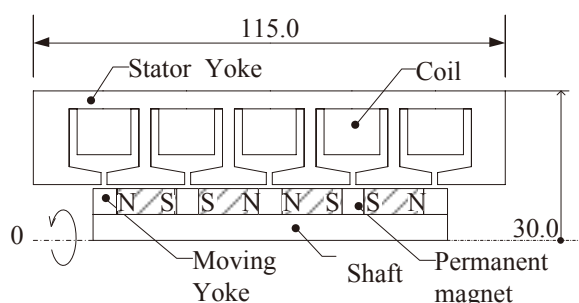
Type of linear actuator	Force (N)	Motor constant, $k_m$ (N/W <sup>1/2</sup> )	Motor constant square density, G (X 10 <sup>6</sup> N <sup>2</sup> /Wm <sup>3</sup> )
Slot less [17]	50	8.5	0.58
Slot type [18]	100	22.1	1.97
Slot type [8,19]	222	32.5	3.40

#### IV. LINEAR ACTUATOR IMPROVEMENT PROGRESS

##### A. Previous Achievement of Linear Actuator Development

The latest linear actuator which was discussed in [8,19] was the E-Cutter's best performing linear actuator. The structure and construction of this actuator, known as STLOA-a, is as shown in Fig. 3. The STLOA-a was designed based on the target of having a minimum thrust of 200 N and a total weight of less than 2.0 kg. The thrust characteristics of the STLOA-a are as shown in Fig. 4. The details of STLOA-a's performances are listed in Table IV.

Based on the results of several testing sessions that have been carried out, it was determined that frond and bunch cutting was feasible. Fig. 5 shows the laboratory testing session carried out [8]. Several fresh oil palm fronds were brought to the laboratory and cut testing was performed. Based on the testing session, the STLOA-a has proven it can accomplish the cutting for various sized oil palm fronds.



(a) The STLOA-a structure (unit in mm)



(b) Construction of STALOA-a

Fig. 3 : Structure and construction of STLOA-a

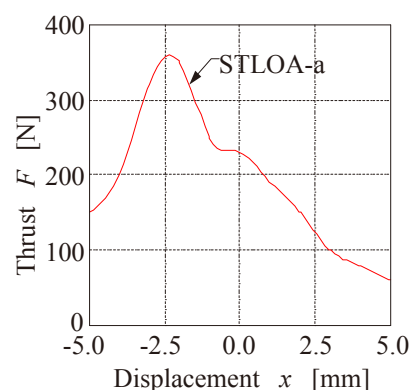
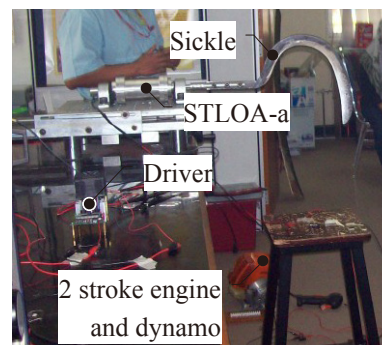


Fig. 4 : Thrust characteristics of STLOA-a



(a) Equipment setup for cutting evaluation



(b) During cutting evaluation



(c) Cutting process successfully done

Fig. 5 : Cutting evaluation of STLOA-a

##### B. Structure and Design Target for Linear Actuator Improvement.

In spite of its proven functionality, the STLOA-a has a slightly longer harvesting cycle time when compared to the *Cantas*<sup>TM</sup>. The main drawbacks of the STLOA-a as compared to *Cantas*<sup>TM</sup> are the total displacement and oscillation frequency. From observation, the *Cantas*<sup>TM</sup> has a constant sickle vibration displacement of 16 mm and a frequency oscillation range between 60 Hz to 80 Hz depending on the

position of the diesel engine throttle. In contrast, the STLOA-a has a total displacement of 9.39 mm and an oscillation frequency of 68 Hz. These characteristics will be a primary concern in E-Cutter linear actuator development without affecting the other performance characteristics. Table V shows the design target of the new linear actuator for the E-Cutter labeled STLOA-b.

TABLE IV. STLOA-A PERFORMANCE CHARACTERISTICS

Performance characteristics	Symbol	Unit	Value
Starting thrust	$F_{x=0}$	N	222
Maximum thrust	$F_{\max}$	N	360
Minimum thrust	$F_{\min}$	N	60
Dimension	$d$	mm	$115 \times \Phi 60$
Weight	$W$	kg	2.0
Thrust constant	$k_f$	N/A	58.15
Motor constant	$k_m$	N/ $\sqrt{W}$	32.5
Motor constant square density	G	$\times 10^6 \text{ N}^2/\text{Wm}^3$	3.40
Displacement	$x$	mm	9.39
Oscillation frequency	$f_{\text{osc}}$	Hz	68
Electrical time constant	$\tau_e$	ms	8.12
Mechanical time constant	$\tau_m$	ms	2.75

TABLE V. COMPARISON OF STLOA A-A AND STLOA-B SPECIFICATION

STLOA-a [8,19]		STLOA-b	
Starting thrust	222 N	Average thrust	222 N
Thrust constant	58.15 N/A	Thrust constant	58.15 N/A
Total weight	2.0 kg	Total weight	2.0 kg
Displacement	10 mm	Displacement	16 mm
Oscillation frequency	68 Hz	Oscillation frequency	80 Hz

For the STLOA-b, the 3 phase linear actuator will be designed compared to the previous single phase STLOA-

a. The 3 phase type was chosen because it provides relatively low ripple thrust, ease of displacement and motion direction control by reversing the 3 phase sequence.

In the STLOA-a, an anti-parallel permanent magnet arrangement was used. The purpose of using this arrangement was to double up the magnetic flux density inside the air gap. However, for the STLOA-b's design and development, a halbach array of permanent magnets will be used to control their magnetic flux path direction and increase efficiency. The structure of STLOA-b is as shown in Fig. 5. The stroke of STLOA-b is in the Y-axis direction. The permanent magnet and coil pitch are set to 11.25 mm and 15 mm respectively. A three phase current with an amplitude of 1.66 A and a frequency of 70 Hz were used to energize the STLOA-b. The coil turns were set to 704 with a coil resistance of 18.26  $\Omega$ .

### C. Initial Findings Comparison of Linear Actuator Improvement.

The STLOA-b model was simulated in order to evaluate the performance. The full displacement of thrust characteristics of STLOA-b is as shown in Fig. 6. It has a maximum thrust,  $F_{\max}$  of 208 N, a minimum thrust,  $F_{\min}$  of 92 N and an average thrust,  $F_{\text{ave}}$  of 142.4 N. The comparison details of STLOA-a and STLOA-b performance characteristics are as listed in Table VI.

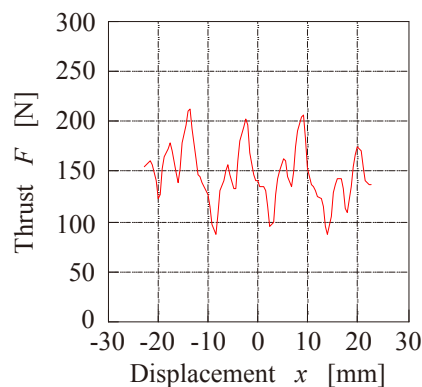


Fig. 6 : Thrust characteristics of STLOA-b

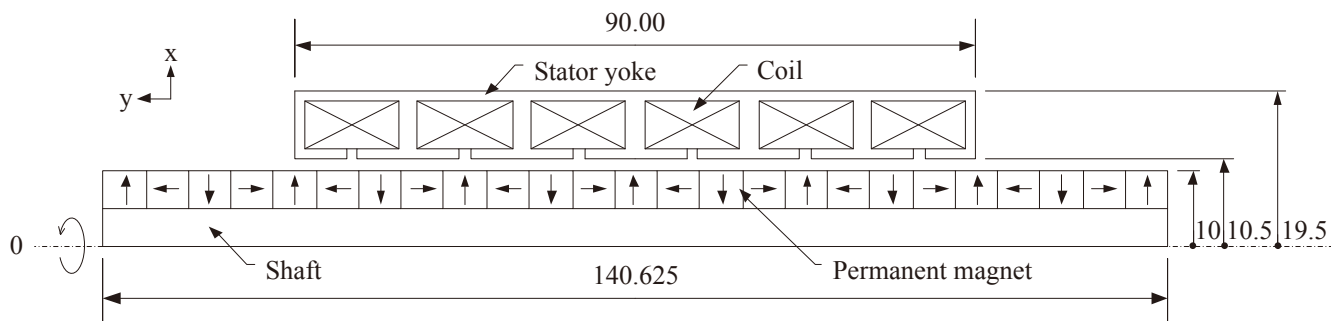


Fig. 5 : STLOA-b structure (unit : mm)

TABLE VI. COMPARISON OF STLOA-A AND STLOA-B PERFORMANCE CHARACTERISTICS

Performance characteristics	Symbol	Unit	STLOA-a	STLOA-b
Maximum thrust	$F_{\max}$	N	360	208
Minimum thrust	$F_{\min}$	N	60	92
Weight	$W$	kg	2.0	0.95
Thrust constant	$k_f$	N/A	58.15	125.65
Motor constant	$k_m$	N/ $\sqrt{W}$	32.5	20.80
Motor constant square density	$G$	$\times 10^6$ N <sup>2</sup> /Wm <sup>3</sup>	3.40	4.00
Electrical time constant	$\tau_e$	ms	8.12	0.18
Mechanical time constant	$\tau_m$	ms	2.75	0.48

Based on table VI, the maximum thrust,  $F_{\max}$  of STLOA-b has been reduced 42.2% when compared to the maximum thrust,  $F_{\max}$  of STLOA-a. However, the increment of minimum thrust,  $F_{\min}$  of STLOA-b is as much as 53.5% when compared to the minimum thrust,  $F_{\min}$  of STLOA-a. This proves that the 3 phase linear actuator could relatively reduce thrust ripple. Even though the average thrust,  $F_{\text{ave}}$  of STLOA-b does not yet meet the design target of about 35.8%, its structure size could possibly be increased since the weight of STLOA-b is far below the design target.

The thrust constant represents the ratio between the injected current and the average thrust developed. The higher value of thrust constant indicates that higher thrust could be produced with the same excitation current value. The thrust constant,  $k_f$  of STLOA-b was calculated using (1). As shown in table VI, the STLOA-b has a greater thrust constant value,  $k_f$  compare to STLOA-a by about 116.08%, from 58.15 N/A to 125.65 N/A.

$$k_f = \frac{F_{\text{ave}}}{I_{\text{rms}}}, \text{N/A} \quad (1)$$

Where  $k_f$  is the thrust constant in N/A,  $F_{\text{ave}}$  is the average thrust in N and  $I_{\text{rms}}$  is the RMS value of the excitation current in A.

The motor constant,  $k_m$ , is used to evaluate the ratio between thrust and input power. The higher the value of the motor constant,  $k_m$ , the higher the thrust of the linear actuator with the same input power. The motor constant,  $k_m$  of STLOA-b was calculated using (2). But in this case, the motor constant,  $k_m$  of STLOA-b was lower by 56.25% when compared to STLOA-a. Nevertheless, this parameter is expected to increase as structural and thrust optimization is done.

$$k_m = \frac{F_{\text{ave}}}{\sqrt{P_{\text{in}}}}, \text{N}/\sqrt{\text{W}} \quad (2)$$

Where  $k_m$  is the motor constant in N/ $\sqrt{W}$ ,  $F_{\text{ave}}$  is the average thrust in N and  $P_{\text{in}}$  is the input power of the linear actuator in W.

The motor constant square density,  $G$ , is used to estimate the ratio between thrust, input power and the size of the linear actuator. The higher the value of the motor constant square density,  $G$ , the higher the thrust of the linear actuator with the same input power and size. The motor constant square density,  $G$  of STLOA-b was calculated using (3). In this case, the motor constant square density,  $G$  of STLOA-b was higher by 17.65% when compared to STLOA-a. The motor constant square density,  $G$ , of STLOA-b and STLOA-a were  $4.00 \times 10^6$  N<sup>2</sup>/Wm<sup>3</sup> and  $3.40 \times 10^6$  N<sup>2</sup>/Wm<sup>3</sup> respectively.

$$G = \frac{k_m^2}{v} = \frac{F_{\text{ave}}^2}{P_{\text{in}} v}, \text{N}/\sqrt{\text{W}} \quad (3)$$

Where  $G$  is the motor constant square density in N<sup>2</sup>/Wm<sup>3</sup>,  $k_m$  is the motor constant in N/ $\sqrt{W}$ ,  $v$  is the volume of the linear actuator in m<sup>3</sup>,  $F_{\text{ave}}$  is the average thrust in N and  $P_{\text{in}}$  is the input power of the linear actuator in W.

The electrical time constant,  $\tau_e$  is used to evaluate the current response of a linear actuator. The lower the value of the electrical time constant,  $\tau_e$ , the faster the response of the current. The current will reach its final value when the inductance no longer affects the response of the current, corresponding to the frequency of the power supply in a short time. The electrical time constant,  $\tau_e$ , of STLOA-b was calculated using (4). The design target for the electrical time constant,  $\tau_e$ , depends on the frequency of the power supply,  $f$  and the mover's oscillation,  $f_{\text{osc}}$  of STLOA-b. In order to make the STLOA-b operates similar to a *Cantas*<sup>TM</sup>, the frequency of mover's oscillation,  $f_{\text{osc}}$  of STLOA-b was targeted to equal 80 Hz. Since the total displacement target is 16 mm, the velocity of the mover is estimated to be equal to 1.28 m/s. Based on several simulation trials, the appropriate frequency of the power supply for STLOA-b,  $f$  is 70 Hz. Therefore, the electrical time constant,  $\tau_e$ , of STLOA-b needs to be less than half of the complete cycle time of the power supply which is 7.14 ms.

$$\tau_e = \frac{L}{R}, \text{ms} \quad (4)$$

Where  $\tau_e$  is the electrical time constant in ms,  $L$  is the coil inductance in mH and  $R$  is the coil resistance in  $\Omega$ .

The mechanical time constant,  $\tau_m$ , is used to evaluate the mover response of the linear actuator. The lower value of the mechanical time constant,  $\tau_m$ , means a faster mover response. The mover as well will reach the desired final displacement in a short time. The mechanical time constant,  $\tau_m$ , of STLOA-b was calculated using (5). As discussed, the oscillation frequency,  $f_{\text{osc}}$  of STLOA-b was targeted to equal 80 Hz. The total displacement target is 16 mm and the mover velocity is

estimate to equal 1.28 m/s. Therefore, the mechanical time constant,  $\tau_m$ , of STLOA-b needs to be less than half of the complete cycle time of the oscillation which is 6.25 ms.

$$\tau_m = \frac{mR}{k_f^2}, \text{ ms} \quad (5)$$

Where  $\tau_m$  is the mechanical time constant in ms,  $m$  is the mover weight in mH,  $R$  is the coil resistance in  $\Omega$  and  $k_f$  is the thrust constant in N/A.

Based on these observations, there are some characteristics of STLOA-a that have been improved by the STLOA-b such as the thrust constant,  $k_f$ , the motor constant square density,  $G$ , the electrical time constant,  $\tau_e$  and the mechanical time constant,  $\tau_m$  while the other characteristics seem to be reduced especially for the average thrust. Yet, since the total of weight of STLOA-b is much lower as compared to its design target, design optimization is possible to increase the parameter between weight restrictions.

## V. CONCLUSION

World demand for palm oil products has been increased year over year. Therefore, increasing production is essential to ensure its availability in the market. To achieve this, one aspect could be to improve harvesting. In Malaysia, research to improve productivity of oil palm fresh fruit bunch (FFB) harvesting has begun by the Malaysia Palm Oil Board (MPOB). The MPOB has invented a new mechanized harvesting tool called the *Cantas*<sup>TM</sup>. *Cantas*<sup>TM</sup> has demonstrated impressive improvements in oil palm FFB harvesting output. Yet, improvements need to be done due to height limitations that affect the operation of *Cantas*<sup>TM</sup>. Thus the E-Cutter was introduced. The E-Cutter solves the operation limitation of *Cantas*<sup>TM</sup> due to a part elimination in the transmission shaft which causes the operation limitation of the *Cantas*<sup>TM</sup>. The progress of E-Cutter development is discussed in this paper. The main concern was progress with the linear actuator as it is a key success point for E-Cutter development. The STLOA-a linear actuator of the E-Cutter has been established previously. Several tests conducted prove that the STLOA-a could perform the required harvesting activity. Improvement to the STLOA-a is essential, especially to improve dynamic operation of the E-Cutter. Therefore, a new linear actuator for the E-Cutter is required. The initial findings and the possibility of improving E-Cutter operation was discussed in this paper.

## REFERENCES

- [1] D. Adetan, L. Adekoya and K. Oladejo. An Improved Pole-and-Knife Method of Harvesting the Oil Palm. *Agricultural Engineering International: the CIGR Ejournal*. Manuscript PM 06 027. Vol. IX. June, pp. 1 – 11, 2007.
- [2] YB Tan Sri Benard Giluk Dompok, Chapter 9, Palm Oil of Economic Transformation Programme : A Roadmap for Malaysia, pp. 280 – 314, 2009.
- [3] World Growth (2011). Palm Oil Green Development Campaign: The Economic Benefit of Palm Oil to Indonesia accessible at: [http://www.worldgrowth.org/assets/files/WG\\_Indonesian\\_Palm\\_Oil\\_Benefits\\_Report-2\\_11.pdf](http://www.worldgrowth.org/assets/files/WG_Indonesian_Palm_Oil_Benefits_Report-2_11.pdf).
- [4] FAOSTAT (2010), <http://faostat.fao.org/site/291/default.aspx>, accessed in October 2011.
- [5] Yusof Basiron and Mohd Arif Simeh, Vision 2020 – The Palm Oil Phenomenon, *Oil Palm Industry Economic Journal* Vol. 5(2), pp. 1 – 10, 2005.
- [6] Abdul Razak J, Abdul Rahim S., Ahmad H., Johari J. and M. Mohd Noor, 2007, High Reach Oil Palm Motorized Cutter, MPOB Information Series, MPOB TT No 349, ISSN 1511-7871.
- [7] Abdul Razak Jelani, Ahmad Hitam, Johari Jamak, Malik Noor, Yosri Gono and Omar Ariffin, *Cantas*<sup>TM</sup> - A tool for the efficient harvesting of oil palm fresh fruit bunches, *Journal of Oil Palm Research*, Vol. 20, pp. 548 - 558, 2008.
- [8] F. Azhar., 2008. Design of a Linear Oscillatory Actuator for Oil Palm Mechanical Cutter, Msc. Thesis, Universiti Putra Malaysia
- [9] Johan Baeten, Kevin Donn'e, Sven Boedrij, Wim Beckers, and Eric Claesen, *Autonomous Fruit Picking Machine: A Robotic Apple Harvester*, C. Laugier and R. Siegwart (Eds.): *Field and Service Robotics*, STAR 42, pp. 531–539, 2008.
- [10] D. Erdogan, M. Guner, E. Dursun, and I. Gezer, *Mechanical Harvesting of Apricots*, *Biosystems Engineering* 85 (1), pp. 19–28, 2003.
- [11] A. Torregrosa, E. Ort, B. Martin, J. Gil, C. Ortiz, *Mechanical harvesting of oranges and mandarins in Spain*, *Biosystems Engineering*, 104, pp. 18 – 24, 2009
- [12] Abdul Razak J, Ahmad H., Johari J., M. Mohd Noor, Yosri Gono and Omar Ariffin, *Cantas*<sup>TM</sup> - A tool for the efficient harvesting of oil palm fresh fruit bunches, *Journal of Oil Palm Research*, Vol. 20, pp. 548 - 558, 2008.
- [13] M. Norhisam, M. Norafiza, F. Azhar, N.F. Mailah, H. Wakiwaka, M. Nirei, *Optimization of Pole Numbers and Rotor Size for a Single Phase Slot-less Permanent Magnet Generator*, *International Review of Electrical Engineering (I.R.E.E.)*, Vol. 6, No. 5, pp. 2253 – 2260, 2011.
- [14] M. Norafiza, 2009, *Design and Analysis of a Single and Double Stator of Single Phase Slotless Permanent Magnet Generator*, MSc. Thesis, University Putra Malaysia.
- [15] R. Suhairi, 2010, *Design and Analysis of Double Stator Permanent Magnet Generator for Palm Oil Mechanical Cutter Application*, MSc. Thesis, University Putra Malaysia.
- [16] M. Norhisam, R. Suhairi, M. Norafiza, MAM Radzi, I. Aris, M. Nirei, H. Wakiwaka, 2010, *Comparison on Performance of a Single Phase and Three Phase Double Stator Type Permanent Magnet*, *Asia Pacific Symposium of Applied Electromagnetics and Mechanics (APSAEM2010) Kuala Lumpur, Malaysia*. 28-30th July 2010, pp. 231 – 234, 2010
- [17] Firdaus R.N., 2006. *Linear Actuator for Palm Mechanical Cutter*, B.Eng. Thesis, University Putra Malaysia.
- [18] Alias K., 2007. *Design of Slot Type Linear Oscillatory Actuator by Adjustment Thrust Characteristics*, MSc. Thesis, University Putra Malaysia.
- [19] F. Azhar, M. Norhisam, N.F. Mailah, M.R. Zare, H. Wakiwaka, M. Nirei, *Thrust Optimization of Linear Oscillatory Actuator Using Permeance Analysis Method*, *International Review of Electrical Engineering (I.R.E.E.)*, Vol. 6, N. 5, pp. 2929 – 2938, 2011.

[1] D. Adetan, L. Adekoya and K. Oladejo. An Improved Pole-and-Knife Method of Harvesting the Oil Palm. *Agricultural Engineering*

# Structure optimization of a 6 slot 8 pole permanent magnet linear motor.

**F. Azhar\***, **M. Norhisam<sup>x</sup>**, **H. Wakiwaka\***, **K. Tashiro\***, **M. Nirei<sup>†</sup>**

<sup>\*</sup>Faculty of Engineering, Shinshu University, 4-17-1 Wakasato, Nagano, 380-8553, Japan.

<sup>x</sup>Faculty Engineering, Universiti Putra Malaysia, 43400 Selangor, Malaysia

<sup>†</sup>Department of Electronics and Computer Science, Nagano National College of Technology, 716 Tokuma, Nagano City, 381-8550, Japan.

Corresponding author email : fairul.azhar@utem.edu.my (F. Azhar)

**Keywords:** Commercialize PMLM, E-Cutter, performance comparison, PM and coil size, PMLM.

## Abstract

Palm oil has become the most consumed vegetable oil. In order to ensure its sustainability, the productivity of oil palms is targeted to increase by about 3.5% each year. Mechanization is one method to improve the oil palm productivity. Most activities in the oil palm process have been mechanized, and the mechanization of the harvesting process still need to be established. Tools to this end have been introduced by the Malaysian Palm Oil Board (MPOB) in Malaysia with the introduction of the *Cantas*<sup>TM</sup>, however, due to their operational limitations, the E-cutter was later introduced. In this paper, the design of the E-cutter's actuator is discussed. The design targets of the actuator are also briefly explained. In the end, an E-cutter's actuator with 218 N of average thrust,  $F_{ave}$  and a total weight,  $W$ , of 1.8 kg has been designed. The performance of the E-cutter's actuator is also compared to a commercialized linear motor to prove its high performance.

## 1 Introduction

In Malaysia, the mechanization of oil palm harvesting began with the introduction of a tool named *Cantas*<sup>TM</sup>. The *Cantas*<sup>TM</sup> is a mechanical based tool developed by the Malaysian Palm Oil Board (MPOB). Fig. 1 shows the structure of the *Cantas*<sup>TM</sup>. It uses a petrol engine to provide mechanical energy to the system located at the bottom of the tool and a gear system located at the top of the tool to convert rotational motion to linear motion in order to vibrate the sickle during harvesting activities. Mechanical energy is transferred from the engine to the gears via a transmission shaft located inside the pole [1-2].



Fig. 1 : *Cantas*<sup>TM</sup> for oil palm harvesting tools

The *Cantas*<sup>TM</sup> has undergone several fields testing sessions in order to prove its capabilities. The results of the tests are presented in [2]. Based on the results, it was found that the *Cantas*<sup>TM</sup> is able to improve harvesting productivity threefold when compared to manual labour.

Despite of impressive performance shown by the *Cantas*<sup>TM</sup>, its operation was greatly reduced during harvesting of palm oil fresh fruit bunches (FFBs) located higher than 8 meters. At a height of more than 8 meters, the pole of the *Cantas*<sup>TM</sup> starts to bend and cause the transmission shaft to bend as well. This condition made the *Cantas*<sup>TM</sup> operate inefficiently [2-3].

In order to address this problem, an electrical based tool called the E-cutter was introduced. The structure of the E-cutter is as shown in Fig. 2. The E-cutter replaced the transmission shaft used as an energy transfer medium in the *Cantas*<sup>TM</sup> with copper wire. The mechanical energy produced by the petrol engine is converted to electrical energy by an electrical generator and the function of the gear is replaced by a linear actuator. By using this structure, the pole bending problem no longer an issue [3].



Fig. 2 : E-cutter structure

This paper focuses on the design of the E-cutter's actuator. Of the various types of linear motor, the slot type moving permanent magnet linear motor (PMLM) is seen as best candidate to be implemented on the E-cutter. Despite the high thrust density, this type of linear motor (PMLM) has no flying leads which are a potential source of unreliability and limit the achievable stroke, good thermal dissipation and bidirectional force production [4 -5].

In [6], the force required to harvest oil palm was discussed. Based on the findings, is about 200 N force is required to accomplish the harvesting activity. Therefore, the PMLM

needed to be designed with at least 200 N of thrust. Furthermore, in order to ensure the E-cutter is mobile, the total weight of the PMLM is targeted to be below 2.0 kg. Therefore, in this paper, these design requirements for the PMLM are discussed.

## 2 Basic PMLM structure.

In [7], several magnetization arrangements for the PMLM permanent magnet have been compared. The structure topology used for the PMLM was a 6 slot 8 pole configuration. Based on comparisons, it was found that the halbach magnetization arrangement could be applied to the PMLM design for the E-Cutter actuator. Even though it lagged by about 4% when compared to the best model, it provides a simple permanent magnet design compared to its nearest rival.

Therefore, the basic structure of the PMLM is as shown in Fig. 3. The initial design of the PMLM for the E-Cutter actuator has been discussed in [8]. Even though its thrust characteristics are about 26% lower compared to aimed thrust, through structural optimization, incremental thrust is achievable since the total weight of the actuator is far lower when compared to the restricted value.

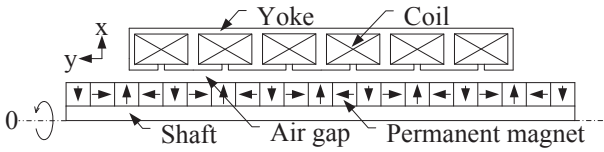


Fig. 3 : Basic structure of PMLM

## 3 PMLM Structure optimization.

Optimization of the PMLM's structure was focused on the PM and coil height. At the same time, the total radius,  $r_{total}$  of the PMLM also was varied. The other structural parameters such as coil pitch,  $\tau_c$ , magnetization pitch,  $\tau_{pm}$  and yoke thickness,  $t_y$  were left fixed. The aim of the structural optimization was to obtained high thrust within a restricted weight. Fig. 4 shows the design parameters of the PMLM.

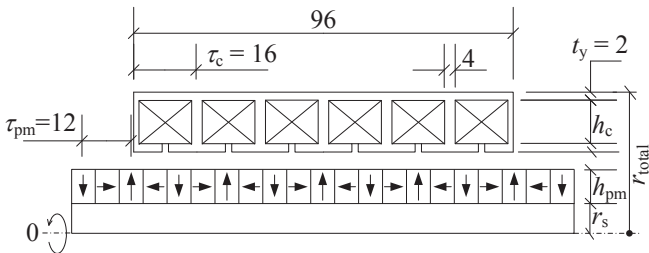


Fig. 4 : Design parameter of PMLM (unit in mm)

The total radius,  $r_{total}$  of PMLM was set to 20 mm, 25 mm and 30 mm. Initially, the shaft radius,  $r_s$  had been set to 1 mm.

The height of the PM,  $h_{pm}$  and the height of the coil  $h_c$  were varied accordingly within the fixed total radius,  $r_{total}$ . Changes to the height of the coil,  $h_c$  made other structural parameters such as coil turns,  $N$ , phase resistance,  $R$  and total weight,  $W$  variable. These parameters was calculated using (1) – (3).

$$N = \frac{1}{\xi} \left( \frac{W_c}{\phi_C} \times \frac{h_c}{\phi_C} \right) \quad (1)$$

$$R = N^2 \frac{\rho l}{a} = \frac{1}{\xi^2} \left( \frac{W_c}{\phi_C} \times \frac{h_c}{\phi_C} \right)^2 \frac{8\pi\rho \left( r_s + h_{pm} + \delta + t_y + \frac{h_c}{2} \right)}{\pi\phi_C^2} \quad (2)$$

$$W = \rho_{copper} v_{coil} + \rho_{NdFeB} v_{pm} + \rho_{SS400} v_{yoke} + \rho_{SUS304} v_{shaft} \quad (3)$$

Where  $W_c$  is the coil width in [m],  $\xi$  is the space factor equal to 0.6,  $\phi_c$  is the copper wire diameter in [m],  $\rho$  is the copper resistivity equal to  $1.67 \times 10^{-6} \Omega \cdot m$ ,  $l$  is the copper wire length in [m],  $a$  is the copper wire cross sectional area in [m<sup>2</sup>],  $\delta$  is the air gap length in [m],  $\rho_{material}$  is the material density in [kg/m<sup>3</sup>] and  $v_{part}$  is the volume of PMLM part in [m<sup>3</sup>].

### 3.1 Optimized PM and coil height.

A sample of the thrust characteristics of the PMLM can be seen in Fig. 5. Based on the thrust characteristics, the average thrust,  $F_{ave}$  of all PMLM models was calculated. Furthermore, the total weight,  $W$  of all PMLM models has also been estimated.

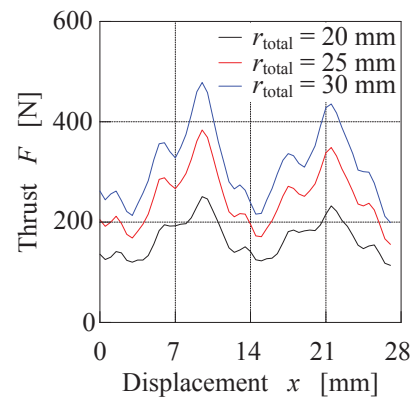


Fig. 5 : Thrust characteristics of PMLM with different of total radius,  $r_{total}$ .

Fig. 6 shows the effect of the PM outer radius,  $r_{pm}$  to the average thrust,  $F_{ave}$  and total weight,  $W$  of the PMLM. Based on Fig. 6 (a), by increasing the PM outer radius,  $r_{pm}$  of the PMLM, the average thrust,  $F_{ave}$  will increase until it reaches a maximum. This is due to incremental size of the PM which

contributes more magnetic energy to the PMLM, producing higher thrust. However, beyond the maximum point, the average thrusts,  $F_{ave}$  is reducing despite the larger size of the PM. The smaller size of the coil used results in a lower magnetomotive force produced by the PMLM.

On the other hand, the total weight,  $W$  of the PMLM is only influenced by the total radius,  $r_{total}$  as shown in Fig. 6 (b). This is because the higher the total radius,  $r_{total}$ , the greater the volume,  $v$  of the PMLM. This will influence the total weight,  $W$  of PMLM as clearly shown in (3).

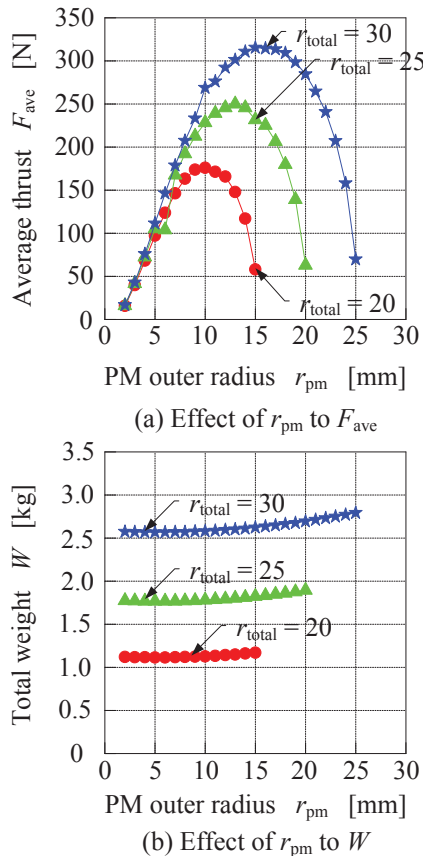


Fig. 6 : Average thrust  $F_{ave}$  and total weight,  $W$  of PMLM

The PMLM models that have the highest average thrust,  $F_{ave}$  for each total radius,  $r_{total}$  are identified and summarized in Table 1 and as shown, the PMLM with an  $r_{total}$  of 25 mm and 30 mm satisfy the average thrust requirement,  $F_{ave}$  with values of 250 N and 316 N respectively. On the other hand, the PMLM with a total radius,  $r_{total}$  of 20 mm and 25 mm satisfy the total weight requirement,  $W$  with limits of 1.13 kg and 1.80 kg respectively. From these results, the PMLM structure with a total radius,  $r_{total}$  of 25.0 mm was selected as the initial model. It has an average thrust,  $F_{ave}$  of 250 N and a total weight,  $W$  of 1.8 kg. This model has an outer radius of the PM,  $r_{pm}$  of 13 mm and the height of the coil,  $h_c$  is 7.5 mm.

No.	Total radius, $r_{total}$ (mm)	PM outer radius, $r_{pm}$ (mm)	Average thrust, $F_{ave}$ (N)	Total weight, $W$ (kg)
1	20.0	10	178	1.13
2	25.0	13	250	1.80
3	30.0	15	316	2.62

Table 1 : Average thrust,  $F_{ave}$  and total weight,  $W$  of optimized model of each  $r_{total}$ .

### 3.2 Optimized shaft radius.

Since the PM of the PMLM is ring shaped, the inner diameter of PM is a crucial factor to determine if the PM could be magnetized or not. Furthermore, a smaller inner diameter of the PM ring increases its manufacturing costs.

On the other hand, for a higher inner PM diameter, a higher shaft radius,  $r_s$  needed. A higher shaft radius,  $r_s$  will strengthen the PMLM structure but at the same time it will reduce the thrust of the PMLM due to a reduced PM size. Therefore, the effect of shaft radius,  $r_s$  on PMLM thrust needed to be established.

Fig. 7 shows the effect of shaft radius,  $r_s$  to average thrust,  $F_{ave}$  of a PMLM at several excitation currents,  $I$ . Based on Fig. 7, the reduction of the average thrust,  $F_{ave}$  is not significant for a shaft radius,  $r_s$  below 6 mm while for a shaft radius,  $r_s$  higher that 6 mm, the average thrust,  $F_{ave}$  was significantly reduced. Therefore, a shaft radius,  $r_s$  of 6 mm is considered as optimal.

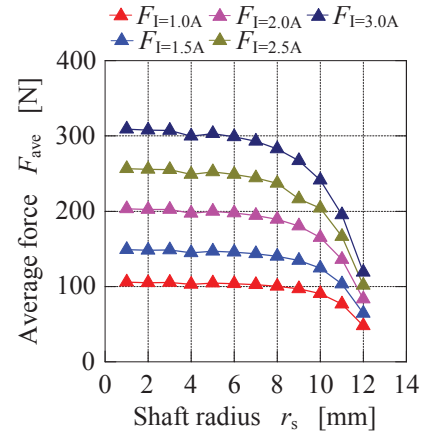


Fig. 7 : Effect of shaft radius,  $r_s$  to average thrust,  $F_{ave}$  of PMLM.

The final structural dimensions of the PMLM are as shown in Fig. 8. The final structure of PMLM has 462 coil turns with  $14.2 \Omega$  of winding resistance for each coil and about a similar total weight,  $W$ , as the initial structure. The PMLM produces about 218 N of average thrust,  $F_{ave}$  and has a total weight,  $W$  of 1.8 kg.

Fig. 9 shows the effect of the excitation current,  $I$  on the thrust characteristics. Since there is a reduction in terms of the permanent magnet size, the thrust characteristics of the final PMLM structure are lower as compared to the initial structure. It needs about 125W supplied in each phase in order to achieve the targeted average thrust,  $F_{ave}$ .

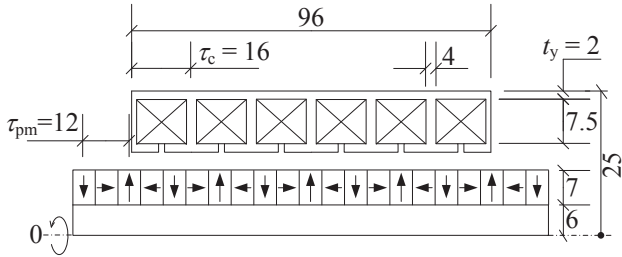


Fig. 8 : Final structure dimension of PMLM (unit in mm)

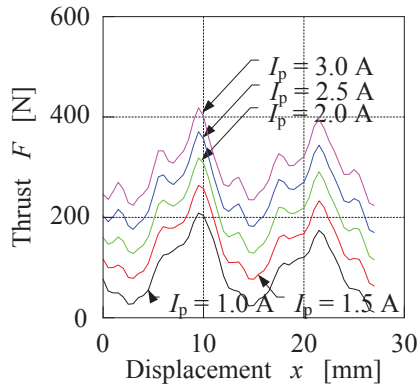


Fig. 9 : Effect of excitation current to thrust characteristics of PMLM

#### 4 Comparison of this PMLM with commercial PMLM performance.

The optimized PMLM performance was then compared with a commercial PMLM. There are about 200 commercial PMLMs from several linear motor manufacturer companies that could be compared to this PMLM. Three type of PMLM were selected: a slot type PMLMs, a slot-less type PMLM and a shaft motor.

Four performance characteristics were used for comparison:

- Thrust,  $F$ .
- Thrust constant,  $k_f$ .
- Motor constant,  $k_m$ .
- Motor constant square density,  $G$ .

All these performance characteristics were calculated using (4) – (6).

$$k_f = \frac{F_{ave}}{I} \quad (4)$$

$$k_m = \frac{F_{ave}}{\sqrt{P_{in}}} \quad (5)$$

$$G = \frac{F^2}{P_{in}v} \quad (6)$$

Fig. 10 shows the performance comparison between this PMLM and the commercial PMLM. Based on the Fig. 10, it is shown that, this PMLM is capable of producing higher performance at a similar volume,  $v$  compared to the commercial PMLM. Additionally, this PMLM is also capable of producing a higher thrust,  $F$  at a smaller size and lower input power,  $P$  as shown in Fig. 10 (d). Because the thrust produced by a linear motor depends on the input power supplied, based on the motor constant square density,  $G$  the capability of the PMLM to produce higher thrust at same input power compared to the commercial PMLM is also shown.

#### 5 Conclusion.

In this paper, a 6 slot 8 pole PMLM was designed in order to be implemented as an E-Cutter actuator. The structure of the PMLM has been optimized in order to produce targeted thrust within a restricted weight. The optimization involved the height of the coil,  $h_c$ , the height of the permanent magnet,  $h_{pm}$  and the shaft radius,  $r_s$ . The performance of the PMLM was then compared to commercial PMLMs. In the end, it was found that the PMLM not only achieved the desired thrust, it also has better performance compared to commercial PMLMs.

#### Acknowledgements

F. Azhar wishes to acknowledge the Universiti Teknikal Malaysia Melaka (UTeM), and Ministry of Higher Education of Malaysia, for giving him the opportunity to pursue his PhD study and for their financial support in Shinshu University.

#### References

- [1] Abdul Razak J., Abdul Rahim S., Ahmad H., Johari J. and M. Mohd Noor, "High Reach Oil Palm Motorized Cutter", *MPOB Information Series*, **MPOB TT No 349**, ISSN 1511-7871, (2007).
- [2] Abdul Razak J., Ahmad H., Johari J., M. Noor, Yosri Gono and Omar Ariffin, "Cantas<sup>TM</sup> - A tool for the efficient harvesting of oil palm fresh fruit bunches", *Journal of Oil Palm Research*, **Vol. 20**, pp. 548 - 558, (2008).
- [3] F. Azhar, "Design of a linear oscillatory actuator for oil palm mechanical cutter", *MSc. Thesis*, University Putra Malaysia, Selangor, Malaysia, (2009).
- [4] Bong Jang K., Heoung Kim T., Do Chun Y., and Lee J., "Iron Loss Calculation in a Flux-Concentration-Type LOA", *IEEE Transactions On Magnetics*, **Vol. 41**, pp. 4024-4026, (2005).

[5] Heoung K.T., Woo L.H., Hyun K.Y., Lee Y, and Boldea I., "Development of a Flux Concentration-Type Linear Oscillatory Actuator", *IEEE Transactions On Magnetics*, **Vol. 40, No. 4**, pp. 2092-2094, (2004).

[6] Abdul Razak J., Desa A., Ahmad H., Azmi Y. and Johari J., "Reaction force and energy requirements for cutting oil palm fronds by spring powered sickle cutter", *Journal of Oil Palm Research*, **11(2)**, pp. 114-122, (1999).

[7] F. Azhar, M. Norhisam, H. Wakiwaka, K. Tashiro, M. Nirei, "Evaluation of Various Permanent Magnet Arrangements on Linear Actuator", *Asia-Pacific Symposium on Applied Electromagnetic and Mechanics 2012, APSAEM 2012*, Ho Chi Minh City, Vietnam, (25 – 27 July 2012), pp. 50 - 55, (2012).

[8] F. Azhar, M. Norhisam, H. Wakiwaka, K. Tashiro, M. Nirei, "Initial Progress and Possible Improvement of E-Cutter Linear Actuator Development", *2012 IEEE International Conference on Power and Energy (PECon 2012)*, Kota Kinabalu, Sabah, Malaysia, (2 – 5 December 2012), pp. 933-938, (2012).

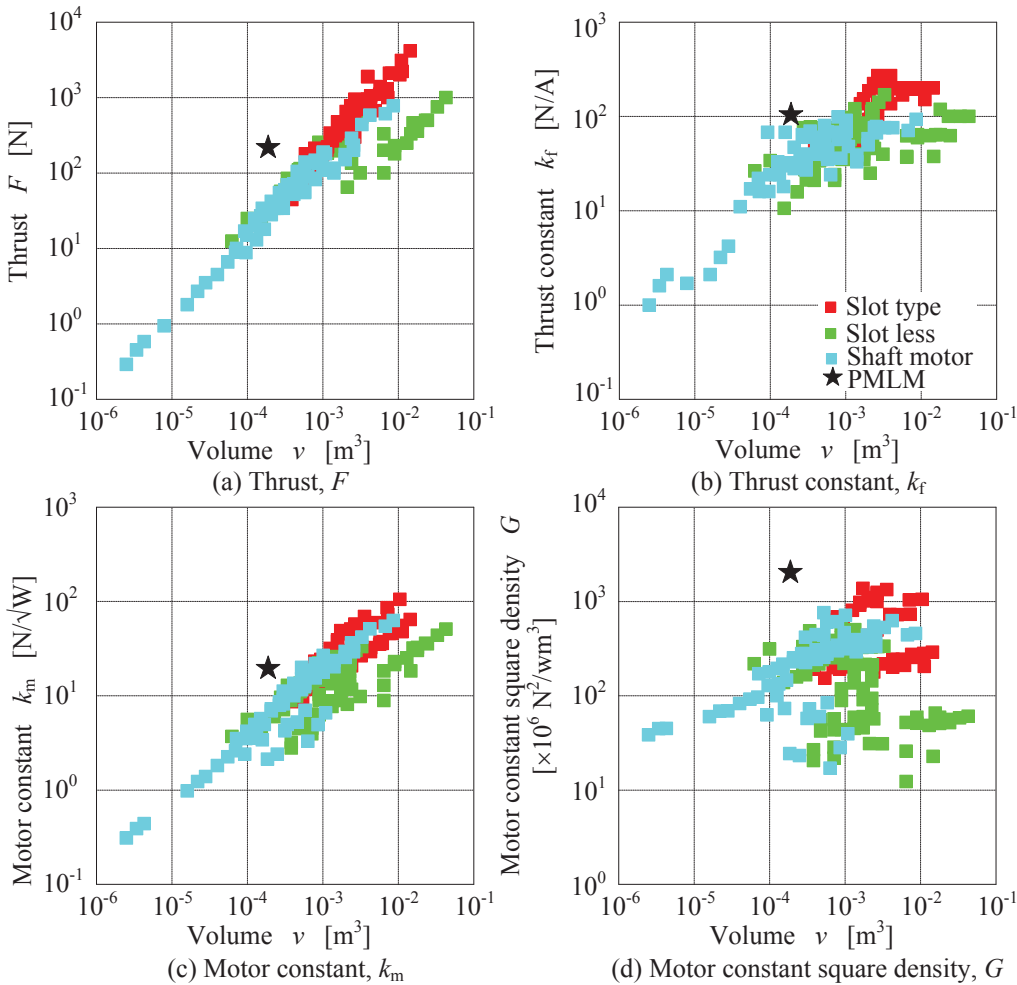


Fig. 10 : Comparison between PMLM and commercialized PMLM performance